GEORG-AUGUST-UNIVERSITÄT GÖTTINGEN

GGNB

Targeting JAK/STAT signalling for sensitization of colorectal cancer cells to chemoradiotherapy

Dissertation

For the award of the degree

"*doctor rerum naturalium*"

Of the Georg-August-Universität Göttingen

Within the doctoral program: Molecular Medicine

Of the Georg-August University School of Science (GAUSS)

submitted by Kristin Kördel

from Kassel, Germany

Göttingen 2021

The thesis entitles “Targeting JAK/STAT signalling for sensitization of colorectal cancer cells to chemoradiotherapy” was conducted from September 2017 until May 2021 in the Institute of Cellular and Molecular Immunology at the Medical Faculty of the Georg-August University Göttingen under supervision of Prof. Dr. Jürgen Wienands. The publication “NOTCH Activation via gp130/STAT3 Signalling Confers Resistance to Chemoradiotherapy “which was published at *Cancers* on the 26 January (doi: 10.3390/cancers13030455) was created on the basis of the data sets generated and presented in this thesis. In detail, the manuscript contains data from figures 3.1 B, 4.1, 4.2, 4.3 B, 4.4, 4.6, 4.8, 4,9, 4.10 D, 4.11 A, 4.12, 4.14 , 4.15, 4.16, 4.17 A, 4.18, 4.21 D, 4.22, 4.23, 4.24 B, 4.25, 4.26 *middle panel*, 4.27, 5.2 A, 6.1.

Members of the thesis committee:

Prof. Dr. Jürgen Wienands (Thesis supervisor & 1st Reviewer)

Institute of Cellular and Molecular Immunology

University Medical Center, Göttingen

Prof. Dr. Matthias Dobbelstein (2nd Reviewer)

Institute of Molecular Oncology

University Medical Center, Göttingen

PD Dr. Marian Grade

Department of General, Visceral and Pediatric Surgery

University Medical Center, Göttingen

Extended examination Board Members:

Prof. Dr. Dieter Kube

Department of Hematology and Oncology

University Medical Center, Göttingen

Prof. Dr. Thomas Meyer

German Centre for Cardiovascular Research, Department of Psychosomatic Medicine and Psychotherapy

University Medical Center Göttingen

Prof. Dr. Markus Bohnsack

Department of Molecular Biology

University Medical Center, Göttingen

Date of submission of thesis: 31.05.2021

Date of oral examination: 06.07.2021

Affidavit

I hereby declare that the thesis “Targeting JAK/STAT signalling for sensitization of colorectal cancer cells to chemoradiotherapy” is my own work. All sources and aids are acknowledged as references.

_____ Göttingen, May 31th, 2021

Kristin Kördel

Acknowledgements

First, I want to thank my supervisor Prof. Wienands for giving me the chance to conduct my Ph.D. thesis in his lab. I am grateful for his time and effort to come up with new ideas and for the many scientific discussions we had together. Prof. Wienands helped me to grow as a scientist, to think critically, and at the same time he gave me the opportunity to bring my own ideas and imagination into our project. Furthermore, he has always supported me and always included and challenged me in processes such as paper writing. In this context I also want to thank Prof. Dobbelstein and Dr. Grade for being members of my thesis committee with exciting discussions and helpful advice during the meetings.

In addition, I want to thank all current and former members of the Institute for Cellular and Molecular Immunology. Special thanks to Anika and Gabi for your help regarding organizational issues and for helping me a lot in the first month of my thesis. Whether bowling or hiking, it was always fun!

Furthermore, I want to thank Prof. Dr. Ghadimi and Dr. Grade for giving me the opportunity to work in the Department of General, Visceral and Pediatric Surgery. I never felt like a guest, but rather as part of the group. Many thanks to Dr. Grade for the project-related meetings, which were always interesting and significantly improved my knowledge of the clinical perspective. Besides Prof. Wienands, Dr. Grade was always a contact person for me who helped me with any questions I had.

I would like to thank all the members of the lab of the Department of General, Visceral and Pediatric Surgery, especially Melanie, Johanna, Jessica, Patricia, Rong and Tiago for the great time we spent together in the lab or on the red sofa. In particular, I thank Melanie and Johanna for the fact that we were/are a united team (Team STAT3 or Team Serpin). We overcame many hurdles together and motivated and supported each other. Even if our "red card" was pulled from time to time. I would like to thank Melanie for her constant support, for her unshakeable trust in me and for her positive manner, which always made me feel part of the team. Many thanks to Gigi and Florian, for helping in the project but more important for our time as the “Gucci gang”. The red sofa was usually a place where we laughed a lot, ate, and drank well and sometimes discussed critical topics. In the mornings it was always nice to have breakfast with Jessica and Johanna and discuss the latest celebrity news. I have happy memories of the Wutball, who had to go through a lot with us. Some train rides with you outside working hours were not always "quiet" ;) and sometimes even ended with the purchase of a notebook. I would especially like to thank Jessica, Johanna and Patricia for the trip to the housewives' fair. It was an excursion that we will probably all do not forget in a hurry. What I will also not forget are the spontaneous conversations with Patricia at the Real freezers. Furthermore, the Monday evenings with Jessica at Havana were always nice and left us with

belly laughs. Johanna, thank you for your open ear and the support I had throughout the work. I was happy to burn myself on the kettle for you.

I thank Tiago for his kind and lovely nature and for his advice not only in the lab but also in private. You have always been an inspiration and a friend to me.

Next, I want to thank the Deutsche Forschungsgemeinschaft (DFG) for funding of my project. Thanks to the graduate program “Molecular Medicine” within the GGNB for excellent coordination and for the large range of courses.

The biggest thanks go to my family, who have supported me in every endeavour in my life. I thank them for their unconditional trust in me. Thanks to carina for the greatest possible support, I could imagine. You are like a rock in the surf or rather like a cherry in the surf. A big thank to Melli, she supported me not only with her great scientific knowledge, but also with her big heart. Thanks to Anna for being my best friend for 20 years and for always being reliable! Hannah for your support no matter when and where- I miss our time in Gießen. Thanks to Naddin for her incredibly positive nature, which always cheered me up. Furthermore, I want to thank Luca, Lena, Stella, Micha, Jana, Nicole, Hanna, Sabrina, Alicia, Janine, Mareike, Lu, Birte, Katrin and Claudio for all the fun apart from work. I look forward to concerts, festivals, or just quiet evenings with you.

Table of Contents

1. Abstract

Despite ever-evolving treatment and screening procedures, Colorectal cancer (CRC) remains a major cause of cancer-related deaths worldwide. Preoperative chemoradiotherapy (CRT), followed by standardized surgical resection of the tumor, represents the standard treatment for locally advanced rectal cancers. However, tumor cells can possess or acquire resistance to CRT, so that affected patients do not benefit from treatment but are afflicted with potential negative side-effects of anti-cancer treatment without any clinical benefit. Therefore, the resistance of tumor cells to CRT represents a fundamental problem in oncology and requires the elucidation of the molecular mechanisms underlying this issue. It is already known that the dysregulation of signalling pathways can cause serious diseases such as cancer and this dysregulation is significantly involved in the development of therapy resistance. Inflammatory cytokines have a key role in cancer progression by regulating many pathways in both, tumor cells and tumor microenvironment. Hence, it is important to understand the tumor intrinsic mechanisms by which CRT resistance is controlled. In this thesis the importance of active STAT3 signalling in mediating CRT resistance in CRC cell lines was evaluated. The requirement of active STAT3 signalling was demonstrated by mutational analysis of STAT3 and subsequent reconstitution studies in the presence and in the absence of cytokine receptor activation. Nevertheless, when combined with chemoradiotherapy, inhibition of STAT3 signalling using Napabucasin completely abolished tumor growth in a xenograft mouse model. Using a RNA-Seq-based screening approach, several STAT3 target genes were identified, such as the RBPJ, that are dually influenced by inflammation induced STAT3 activation and STAT3 knockdown. Strikingly, genetic inhibition of RBPJ, a key transcriptional regulator of the NOTCH cascade, re-sensitized colorectal cancer cells to chemoradiotherapy. Additionally, genetic and pharmaceutical inhibition of the entire NOTCH signalling also re-sensitized chemoradiotherapy resistant cells. Interestingly, inhibition of NOTCH signalling phenocopied the effect of blocking STAT3 signalling. Genetic profiling of rectal cancer patients revealed the importance of the NOTCH signalling axis by correlating NOTCH expression with clinical outcome.

This thesis uncovered, that treatment resistance is orchestrated by a poorly understood signal axis that combines two classical intracellular pathways, inflammatory cell signalling mediated by STAT3, and cell fate decision NOTCH axis controlled by RBPJ. The identification of this crosstalk serves the molecular basis for chemoradiotherapy resistance and paves the way for a personalized, multimodal treatment of patients with rectal cancers that are positive for STAT3/NOTCH-related markers.

2. Introduction

2.1 Cancer

Cancer is one of the major public health problems worldwide and an important barrier to increasing life expectancy in every country [1-3]. In 2020, 19.3 million new cases of cancer raised with 9.9 million deaths [1] and cancer burden is expected to increase about 60% from 2018 to 2040 [3]. Unfortunately, cancer is a diverse disease, and tumor heterogeneity is a major challenge for its diagnosis and the efficacy of treatment [4-6]. The Heterogeneity refers to the existence of cancer cell subpopulations, with distinct genotypes and phenotypes that harbor divergent biological activities, within the tumor and its metastasis [6]. Over the past decades, significant progress has been achieved in understanding the molecular basis of cancer. However, we are far from reaching the point of a cure for all types of cancer.

2.1.1 Colorectal Cancer

2.1.1.1 Epidemiology

Colorectal cancer (CRC) represents a major cause of cancer-related deaths in Europe and the United States [2]. There has been a dramatic increase in our understanding of the epidemiology, molecular mechanisms, and clinical aspects of CRC over the past decades [7] . Nevertheless, CRC continues to account for approximately 10% of all annual diagnosed cancers worldwide and thus ranks among the third most common malignant tumor entity in the Western society, with about 1.88 million cases (1.148,515 cases of colon and 732,210 cases of rectal cancer) and 918,880 deaths (576,858 colon cancer and 339,022 rectal cancer) in 2020 [1,3,8-10] (**Fig 2.1 A**). Importantly, the incidence and mortality rate of CRC are steadily rising in developed nations [10,11]. It is hypothesized, that the global CRC burden is projected to increase by 60% until 2030, reaching more than 2.2 million new CRC cases and 1.1 million more deaths [12,13]. The distribution of CRC burden varies widely, for colon cancer Southern Europe, Australia, New Zealand, and Northern Europe are the regions with the highest incidence, while for rectal cancer, these regions are Eastern Europe, Australia, New Zealand and Eastern Asian [10].

Generally, several risk factors are associated with an increased risk of developing CRC [14]. It is possible to distinguish between (i) modifiable and (ii) non-modifiable risk factors. Modifiable factors are dietary factors like low intake of vegetables and fruits but high intake of red and processed meat, obesity, smoking, alcohol intake, and lack of physical activity (**Fig 2.1 B**, *left panel*). Obesity is a worldwide issue and a well-known modifiable cancer risk factor [15]. Indexes related to obesity like BMI were in a strong correlation with raised CRC risk in males and was reported to increase it even by 30-70%. Furthermore, around 11% of CRC cases have been related to obesity in Europe [16]. Conversely, higher intake of vegetables, fruits, dietary fibre, folate, and calcium have been reported to be protective against CRC [14]. The probability of

being diagnosed with CRC is also related to personal non-modifiable characteristics and habits that cannot be changed, such as age, gender, race/ethnicity, chronic disease history and familial history (**Fig 2.1 B**, *right panel*) [11,17-19]. Since cancer is a disease of ageing, the rate of CRC development and mortality increase rapidly after the age of 50 [7]. This corresponds to a comparatively high median age of 76 (women) and 72 (men). Relative 5-year survival rates with CRC are around 63 % and 62 % for women and men, respectively [20].

2.1.1.2 CRC development, early detection, and staging

In simplistic terms, carcinogenesis describes a multistep process caused by a sequence of mutations in oncogenes, tumor suppressor genes or by epigenetic changes in DNA for instance methylation [21]. About 90% of CRC cases are described as adenocarcinomas, that develops from epithelia cells of the colon and rectum [22]. The distinction between colon and rectum is largely anatomical but impacts further treatment and prognosis [3,23]. CRCs represents a very heterogeneous disease driven by a variety of mutations and mutagens [10]

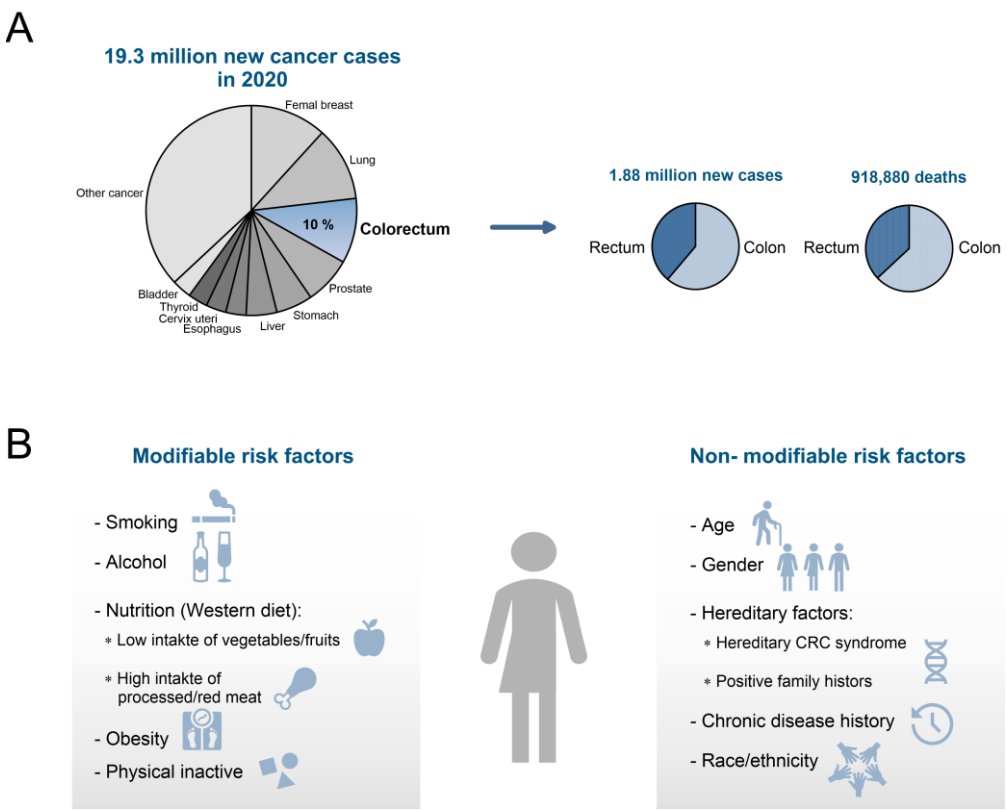

Figure 2.1 Overview of colorectal cancer statistics and risk factors.
A| In 2020 19.3 million new cases of cancer raised of which 10% are colorectal cancer (CRC) (*left panel*). This 10% percent corresponds to 1.88 million new cases (38.9% are localized in the rectum and 61.1% in the colon) and 918,880 deaths in 2020 of which [1] *(right panel*). **B|** Several risk factors are associated with an increased risk for the development of CRC. In general, a distinction is made between modifiable risk factors (left) and non-modifiable risk factors(right).

Unfortunately, not all CRCs share the same driving mutations, which makes consistent treatment almost impossible [10,24]. In the majority of cases, CRC occur sporadically (approx. 95%) and only 2% to 5% of CRC cases are due to hereditary cancer syndromes [25-27]. In

hereditary cancer, important tumor suppressors or DNA repair genes are inactivated by monoallelic gene expression in the germ line. Subsequently, a somatic event “second hit” abrogate the functionality of the remaining wild-type allele and lead to tumor formation [26]. The two most common forms are hereditary nonpolyposis CRC (Lynch syndrome) or familial adenomatous polyposis (FAP) [25,26]. Lynch syndrome is a consequence of various germline mutations in DNA mismatch repair genes [25,28], whereas FAP is characterized by a germline mutation in the adenomatous polyposis coli (*APC*) [25].

Conventionally, CRC arises as a consequence of changes in the cell morphology of normal mucosal epithelium in the colon or rectum, which proliferates uncontrollably to form benign polyps. The multistage progression of the most sporadic colorectal adenocarcinomas is explained in the adenoma-carcinoma sequence model proposed by Vogelstein *et al*. [29,30] (**Fig 2.2 A**). This model has been used a long time as an example for the development of an invasive tumor by multiple genetic alterations. One of the early events in the adenoma-carcinoma sequence is associated with inactivation of the *APC* tumor suppressor gene. *APC* acts as a negative regulator of the β-catenin mediated Wnt signalling, through degradation of β-catenin which thereby limit the transcription of Wnt target genes that are involved in cell cycle regulation [31-33]. The Wnt pathway is critical to CRC tumorigenesis, and more than 90% of patients have alterations, within this pathway [34]. Not surprisingly, given the frequency of changes, neither *APC* nor β-catenin is a useful prognostic marker capable of differentiating between patients [32]. Subsequent malignant transformation is driven by additional mutations occurring in later stages, include activation of the oncogene small GTPase Kirsten Rat Sarcoma Viral Oncogene Homolog (*KRAS*) followed by loss of chromosome 18q with SMAD Family Member 4 (*SMAD4*), which is downstream of transforming growth factor-beta (*TGFβ*), and inactivation of the tumor suppressor Tumor Protein p53 (*p53*) lead to adenocarcinoma formation [35]. This model predicts that at least 7 distinct mutations are required for CRC development [35]. Recently, Wood *et al*. had demonstrated that CRC contains ≤ 80 mutations, of which < 15 mutations are the driving force of tumorigenesis [11,36,37]. However, Smith *et al*., reported that only 7% of CRCs showed mutations in all three oncogenes (*APC*, *KRAS* and *p53*). The most common mutation combination was *p53* and *APC* in 27% of CRC patients studied, whereas mutations in *p53* and *KRAS* were exceedingly rare [21]. These results suggested that tumor mutations arise as heterogeneous pattern and that multiple genetic pathways exist, which contribute to CRC development [21]. In accordance with that, it has been suggested that least three distinct evolutional routes lead to sporadic CRCs [27]. The first traditional pathway is described above, starting from normal mucosa via tubular adenomas to carcinomas (**Fig 2.2 A**). Another well-described but less frequent (10%-20%) developmental pathway of sporadic CRC describes the rise of adenocarcinomas from serrated lesions [27]. The so-called serrated neoplasia pathway is not characterized by a key mutation, but in early

stages by inactivation of various genes via hypermethylation of genomic regions with increase CpG islands density and often by activating *BRAF* mutations [28,38]. The third alternative pathway led to sporadic CRC with poor prognosis, originates from the normal mucosa via villous, partly serrated adenomas (mutations in *KRAS*, *BRAF*, and *APC*) [27].

Furthermore, the acquisition of genomic instability is a fundamental process in cancer development. The most common type of genomic instability occurs in around 85% of sporadic CRC which is called chromosomal instability (CIN) [35,39]. CIN is a process that generates changes in chromosome number and structure, such as somatic copy number alterations (SCNA), or loss of chromosome 17p and 18q, leading to aneuploidy [35,39,40]. These changes are often detectable as a high frequency of SCNA, which are found in 90% of solid tumors and which is associated with most of tumors that arise by the adenoma-carcinoma sequence [41,42]. The second group, occurring in around 13-16% of sporadic CRC are hypermutated and feature microsatellite instability (MSI) due to DNA mismatch repair (MMR)defects [40]. MSI is observed in nearly all CRC tumors that develop in patients with Lynch syndrome by inactivation of various DNA mismatch repair genes (*hMLH1*, *hMSH2*, *hMSH6*, and *hPMS2*) [43,44]. Sporadic tumors with the MSI phenotype usually show high levels of methylation at regulatory regions throughout the genome, including the methylation of CpG-rich promotor sequence of the *hMLH1* gene [39,44]. However, microsatellite-stable (MSS) tumors represent the majority of sporadic tumors [23]. The CpG island methylator phenotype (CIMP) has also been characterized as an epigenetic instability that impacts CRC pathogenesis [45]. CIMP influences CRC development via promotor hypermethylation and silencing of a range of tumor suppressor genes as well as DNA MMR genes, including *hMLH1* [40,46]. Typically, one type of molecular signature dominates, suggesting that the three pathways are rarely overlapping [43]. In some tumors, a complex interplay occurs whereby one signalling pathway is a consequence of another [43]. However, not all adenomas advance to cancer, the accumulation of specific mutations in a particular order is essential for progression towards malignancy. The timeline depends upon the specific pathway of tumorigenesis. Tumorigenesis via the CIN pathway can take a minimum of 10 years, whereas tumor development via the MSI pathway can occur in a few years [44].

One of the key strategies for reducing the global CRC burden focus on prevention and early detection. CRC grows slowly and exposure its symptoms at a late stage [26]. The 5-year survival for patients, diagnosed with early-stage, localized CRC approach 90%, whereas the survival rate of patients diagnosed with late-stage, metastatic CRC, is only 13,1% [14]. Therefore, the regular screening for CRC allows detection of this disease at an early stage when treatments are more successful and the chance for survival is high [3,26]. In addition, screening can significantly reduce treatment costs, as most screening strategies are less expensive and more

important less harmful than chemotherapy for advanced CRC [47]. At a size of several centimeters, the tumor may block the passage of feces and can lead to cramping, pain, bleeding from the rectum [14]. Therefore, for the early detection of CRC, a faecal occult blood test can be performed, in case of a conspicuous finding, colonoscopy is usually recommended. Coloscopy is the preferred screening tool because it allows direct examination of the colorectal mucosa and removal of polyps with malignant potential [48-50]. From the age of 50 (men) and 55 (women), the statutory screening program provides for a routinely colonoscopy [20].

In order to develop the best possible therapy strategy, tumor staging is commonly used to classify the extend of cancer spread, the degree of tumor progression and invasion. The American Joint Committee on Cancer (AJCC) provides the tumor-node-metastatic (TNM) system, which is the current and most used staging system that classify cancer according to three characteristics: 1. The local deep infiltration of the primary tumor (T), 2. The extent of lymph node metastasis (N), and 3. The presence and number of distant metastasis (M) (**Fig 2.2 B**, *left panel*). Based on these criteria the overall stage of the tumor is assigned ranging from 0 to IV according to the Union Internationale Contre le Cancer (UICC) classification [51,52] (**Fig 2.2 B**, *right panel*). However, the TME system also has some limitations. Significantly different clinical outcomes were observed in patients with the same histological TME stage. Therefore, some attempts have been made to integrate additional parameters to the staging of tumors, including immunohistochemistry for tumor biomarkers, molecular signatures, and genetic features [51].

A

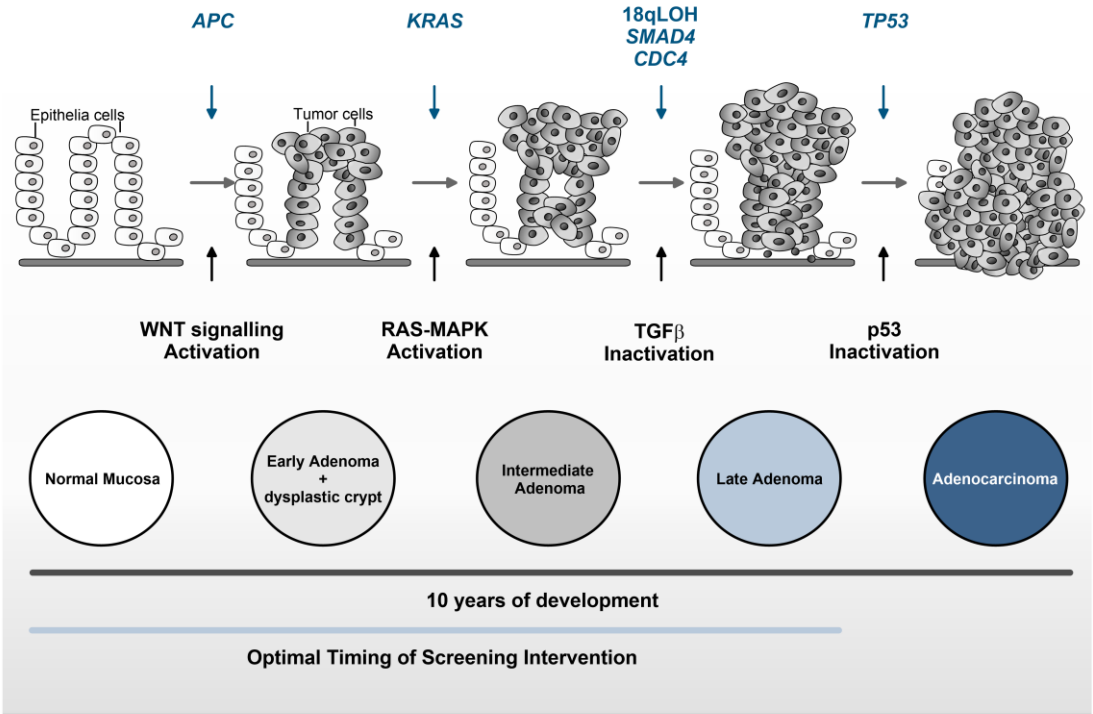

B

TNM staging

TNM stage	Description Cancer growth/spread
TX	No information about the primary tumor
T0	No primary tumor detectable
Tis	Earliest stage; carcinoma in situ
T1	Grow through submucosa
T2	Grow into the muscularis propria
T3	Grow into the outermost layers of the colon/rectum
T4a	Grow through the wall of colon/rectum
T4b	Grow through the wall of colon/rectum and is attached to or has grown into other nearby tissue organs
N0	No spread to nearby lymph nodes
N1	Spread to 1 to 3 nearby lymph nodes
N1c	Spread into areas near the lymph node
N2a	Spread to 4 to 6 near lymph nodes
N2b	Spread to 7 or more nearby lymph nodes
M0	No spread to distant sites
M1a	Spread to 1 distant organ or distant set of lymph nodes
M1b	Spread to more than 1 distant organs or lymph nodes
M1c	Spread to distant parts of peritoneum

UICC classification

Stage	TNM stage T	N	M
0	Tis	N0	M0
I	T1/T2		
IIA	T3		
IIB	T4a		
IIC	T4b		
IIIA	T1/T2 T1	N1/N1c N2a	
IIIB	T3/T4 T2/T3 T1/T2	N1/N1c N2a N2b	
IIIC	T4a T3/T4a T4b	N2a N2b N1/N2	
IVA	Any T	Any N	M1a
IVB			M1b
IVC			M1c

Figure 2.2 Simplified representation of the adenoma-carcinoma sequence in colorectal carcinoma and cancer staging according to the AJCC.
A| The adenoma-carcinoma sequence in colorectal carcinoma shows typical genetic and morphologic alterations (blue) and their effects on the corresponding signalling pathways (black). Modified according to [29,32,53]. **B|** Cancer staging according to the American Joint Committee on cancer (AJCC) TNM system [54] (*left*) and the Union Internationale Contre le Cancer (UICC) classification (*right*) .

2.1.1.3 Treatment

Over the past decades, a growing number of treatment options for CRC raised, which strongly depend on the stage of the tumor, its location, the patient's overall health and various other patient characteristics [55]. At present, surgery, chemotherapy, radiotherapy, antiangiogenic therapy, and novel immunotherapies have been evaluated in clinical trials for the treatment of cancers [56]. The ideal cancer treatment should achieve complete removal of

the tumor and the associated metastasis [57]. Therefore, for early-stage and localized CRC lesions, surgical approaches that range from locally treatment to more invasive methods are used, depending on tumor location and disease invasion [55]. The surgical management of rectal cancer has evolved over the past 100 years and continues to progress to optimize the treatment. Historically, rectal cancer was a not survivable disease, with a lack of standardizes surgical techniques [58]. The most significant contribution in advancing surgical rectal cancer treatment may be the standardization and implementation of a total mesorectal excision (TME) [58]. Nowadays, for early-stage rectal cancers surgical treatment usually involves TME, which is the removal of the entire rectum and mesorectum, including mesorectal fascia [59]. Adjuvant therapy is not indicated for patients with resected (R0 resection) stage I colon cancers [59]. However, nearly a quarter of CRCs are diagnosed at an advanced stage together with metastasis [55,57]. Unfortunately, for these patients, surgical resection alone does not provide effective treatment [55,57].

Consequently, chemotherapy was therefore implemented as a neoadjuvant or adjuvant treatment approach, to minimize the tumor before surgery and to hamper tumor recurrence after surgery, respectively [55]. 5-fluorouracil (5-FU) is one of the first chemotherapeutic drugs with proven anticancer activity, which was first synthesized by Heidelberger *et al*. [60]. 5-FU is a synthetic fluorinated pyrimidine analogue that requires intracellular conversion into active metabolites [61]. In the early 1990s, neoadjuvant treatment with 5-FU, combined with leucovorin became standard of care for patients with stage III and selected stage II colon cancer [62,63]. 5-FU is an essential backbone of chemotherapy treatments for patients with CRC and other gastrointestinal cancers, both in neoadjuvant and adjuvant settings [64]. 5-FU formed the basis for the additional use of oxaliplatin, which has been shown to further improve disease-free survival (DFS) and overall survival (OS) in stage III CRC patients [63,65,66]. Despite progress in novel cancer therapies, 5-FU has been widely used for almost 50 years in treatment of solid malignancies and still represents the most effective and most used agent [64]. Common chemotherapy regimens used in clinics include, FOLFOX (5-FU/leucovorin/oxaliplatin) and FOLFIRI (5-FU/leucovorin/irinotecan) [55,67]. Regarding cancers of the rectum, locally advanced stages of this disease are treated with neoadjuvant chemoradiotherapy (CRT) followed by radical surgical resection [68-71]. Adjuvant chemotherapy is recommended after curative tumor resection for all patients with stage III colon cancer, as well as for patients having stage II colon cancer with high-risk features [72]. For patients with stage I or low-risk stage II CRC after radical surgical resection, adjuvant therapy is not recommended, as it is theoretically possible that surgery alone could achieve a complete cure and ensure long-term survival for the patients [73]. Over the past decades, several strategies including the implementation of 5-FU based combination therapies (combination with radiation) and 5-FU pro-drugs have been developed to enhance tumor sensitivity [56,74].

2.2 Cancer treatment resistance

A tumor is a heterogenous population of cells, harboring cells with different molecular features, that can develop resistance to various therapies including anti-cancer drugs and radiation [75]. Despite the various treatment options available, the resistance of cancer cells is a major clinical challenge and one of the main limiting factors to achieve cure in patients [76].

The appearance of treatment resistance has been observed since the first treatment of patients with chemotherapy [77,78]. A large number of patients either did not respond to a treatment strategy or initially responded but after a period of time suffered a relapse and progression of the disease [55]. One essential reason explaining treatment failures is the presence of innate or acquired resistance. In the simplest case, treatment can lead to the death of a large portion of drug-sensitive cells resulting in a good prognosis for the patient [75,79] (**Fig 2.3 A**). Nevertheless, tumor cells may have molecular features that make them resistant to a treatment, resulting in a partial response and rapid progression [79]. This intrinsic resistance is defined as pre-existing resistance without prior exposure to anti-cancer drugs (**Fig 2.3 A**). However, upon exposure to chemotherapy/radiotherapy, the therapeutic pressure combined with a range of extracellular signals, can trigger cells to acquired resistance [75,76]. This type of resistance can emerge after contact with anti-cancer drugs, which changes cancer cells' properties (**Fig 2.3 B**). Therefore, tumors that initially showed to be sensitive to therapy, later become unresponsive due to the development of resistance [80-82]. Importantly, many descriptions of treatment resistance, especially drug resistance have focused on the differences between intrinsic and acquired resistance, however, in practice many tumors are becoming resistant owing both intrinsic and acquired resistance [76].

The initial idea to fight the resistance of cancer cells against single-agent chemotherapies was the combined administration of chemotherapeutic agents targeting well-defined cancer-driving pathways that had no overlapping mechanisms of action [76]. This approach showed remarkably well results in different types of cancers, including advanced Hodgkin's lymphoma [83] and breast cancer [84]. These successful results made combined chemotherapy a new standard in oncology. Unfortunately, after around 50 years of treating patients with combined chemotherapy, its success had also reached a plateau. Conventional methods such as surgery, radiotherapy and combined chemotherapy are no longer sufficient to successfully treat all tumors [76]. Fortunately, the gain of understanding about the molecular mechanisms that drive cancer progression has also increased and resulted in more effective therapies against tyrosine kinases, nuclear receptors, and other specific molecular targets. More recently, oncological therapy has advanced again by using immunological approaches, including immune checkpoint inhibitors, to attack cancer [85]. In CRC patients with MSI/MMR tumors immune checkpoint inhibitors has shown promising efficacy [85]. Another strategy to circumvent

therapy resistance is to combine drugs that target different signalling pathways [55]. The aim here is to inhibit signalling pathways that run in parallel to each other. There are already pre-clinical studies and clinical trials investigating the safety of such combination approaches. For example, EGFR inhibitors are used together with VEGF/MEK/BRAF inhibitors to treat patients with RAS wild type metastatic CRC [55,86].Currently, the invention of targeted therapy led to significant advances in cancer treatment, because the more specific a drug is, the lower the probability to elicit drug resistance [82,87]. Nevertheless, acquired resistance to several target therapies has already been reported [82].

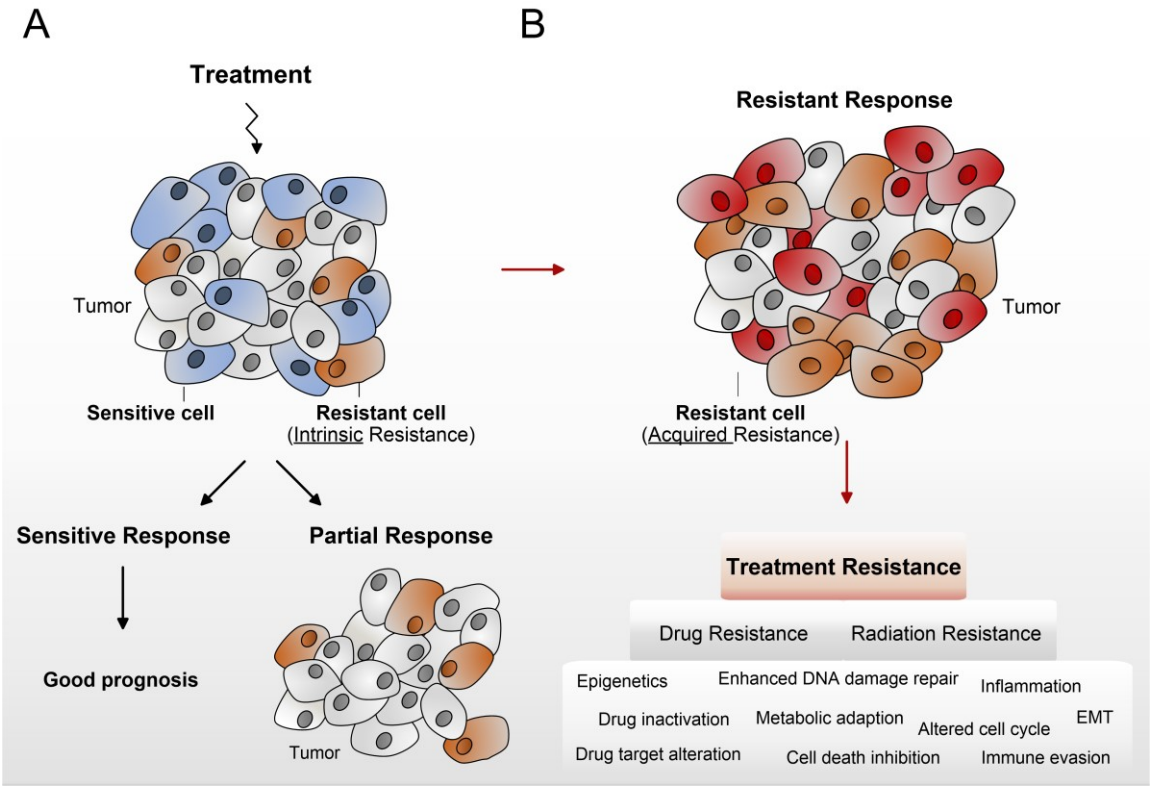

Figure 2.3 Acquired and intrinsic treatment resistance.
A| The tumor is heterogenous, harboring cells with different molecular features, which make them sensitive (blue cells) or resistant to different types of treatments [75]. After treatment, a complete sensitive response to anti-cancer treatment is ideal but rare [79]. Pre-existing subpopulations within a tumor can mediate intrinsic resistance (orange cells). These subpopulations often harbor resistance mediating mutations, which become the predominant populations, resulting in a partial response and rapid progression. **B**| Upon exposure to chemotherapy / radiotherapy, therapeutic pressure combined with extracellular signals, malignant cells develop acquired chemoresistance (red cells) leading to a resistant response [75,76] (*upper panel*). Selected molecular mechanisms that directly or indirectly contribute to a resistant phenotype in human cancer cells [56,87].

There are already countless publications dealing with the causes of therapy resistance. While some mechanisms of drug resistance are disease-specific, others, such as drug efflux, are evolutionarily conserved, as it has already been demonstrated in microbes and human resistant cancer [87]. In addition, many types of cancer may be initially sensitive to a particular chemotherapy and only develop resistance over time due to DNA mutations and metabolic changes that promote drug inhibition and degradation [87]. Note, that these resistance

mechanisms can occur independently or in combination [87]. A selection of mechanisms that have already been associated with treatment resistance in human cancer cell lines are provided in **Figure 2.3 B**.

2.2.1 Treatment resistance in CRC

To date, approximately 50% of all patients with cancer will receive multimodal treatment containing radiotherapy of some form, either alone or along with other treatment modalities such as surgery or chemotherapy [88,89]. About one-third of CRC patients will have no or little response to preoperative CRT [68,70,71,90]. Furthermore, patients with stage 4 CRC have less than a 10% 5-year survival rate owing the ineffectiveness of the current treatment regime [45]. Thus, patients with resistant tumors fail to show benefit from treatment but face potential acute and long-term side effects of chemotherapy and radiation, which include hematologic, gastrointestinal, genitourinary, and dermatological toxicity [68,70,71,90-92]. In rectal adenocarcinoma, approx. 70% of patients do not achieve a pathological complete response (pCR) to neoadjuvant therapy [56,93,94]. In metastatic diseases a treatment failure was observed in approx. 90% of patients. It is hypothesized that in this case the tumor become cross-resistant to a range of chemotherapy [95]. Since 5-FU is one of the most widely used chemotherapeutic agents, it is not surprising that resistance mechanisms have also developed against it. In 5-FU resistant SNU-C1 colon cancer cells, mRNA levels of one of the fundamental 5-FU metabolism enzymes, thymidylate synthase (TS) were found to be increased, leading to enhanced TS catalytic activity [96]. Furthermore, high intrinsic levels of TS were related to 5-FU resistance in *in vitro*, *in vivo* models and in patients [61,97]. Therefore, re-sensitization of tumor cells partially or even fully refractory to treatment represents an attractive solution to this clinical and socioeconomic problem [70,88,98]. Despite the many new discoveries, the molecular basis of ever-evolving treatment resistance remains complex and multifaceted. Consequently, there is an emerging need for therapeutic strategies to defeat treatment resistance.

2.3 Inflammatory gp130 signalling in promoting treatment resistance

As a hallmark of cancer, inflammation is associated with development and progression of tumors [99-101]. Inflammation was originally described according to the four cardinal signs: calor (heat), pallor/dolor (pain), rubor (redness), and tumor (swelling), as the body's response to tissue damage, caused by multiple different injury's [101,102]. The cardinal signs thereby reflect the pro-tumorigenic activity of cytokines and immune cells in the tumor microenvironment (TME) [102,103]. The inflammatory response causes cellular changes that result in repair of the damaged tissue and cellular proliferation at the site of the tumor, which is self-limited in healthy individuals [102]. Cancer is considered as a "wound that does not heal" and therefore attracts similar cell types and mechanisms like wound healing or tissue regeneration [104]. Unfortunately, the dysregulation of inflammatory processes can lead to chronic inflammation, which in turn

leads to the disruption of tissue homeostasis, cell mutations and uncontrolled proliferation providing a pro-tumorigenic environment [101,105].

Already in the 19th century Rudolf Virchow described the role of inflammation in the development of cancer [106]. During his studies, he observed the presence of leukocytes within neoplastic tissue leading to his suggestion that “lymphoreticular inflammation” reflect the origin of cancer at sites of chronic inflammation [106-108]. In accordance with Virchow’s findings, Jass first proposed that infiltration of immune cells represents a novel independent prognostic factor in rectal cancer [109]. Virchow's hypothesis has been supported in recent decades by a wealth of evidence demonstrating that various cancers are triggered by infections and chronic inflammatory disease [108]. An example for this is the link between inflammatory bowel disease (IBD) and development of CRC. Many studies have reported high frequencies of CRC among patients with IBD [110]. IBD patients with family history of CRC have >2-fold higher risk for colon cancer development [111]. Furthermore, chronic intestinal inflammation has become a known risk factor for developing of CRC [112]. Through a multitude of studies, CRC has long been seen as one of the best examples of a tumor that is tightly associated with chronic inflammation, which is present even in the earliest stages of tumor appearance [113].

During the past decades, it has become increasingly clear that within the TME, a complex, coordinated network of cells communicate to form the local immune response [73]. Cytokines, chemokines, and other small inflammatory proteins derived from either malignant or host cells including stroma, endothelia, and immune cells coordinate the intracellular communication in the TME [114] (**Fig 2.4 A**). According to this, there is recently growing evidence that especially inflammatory mediators, including cytokines and their specific receptors are major components in regulating CRC growth, angiogenesis, metastasis, and treatment resistance [56,115] (**Fig 2.4 A**). Inflammatory cytokines have a key role in cancer progression via many pathways, including a direct effect on tumor cells, interaction with the chemokine system, stimulation of epithelial-to-mesenchymal transition (EMT), and augmentation of metastasis [114,116]. Cytokines and immune mediators secreted in the TME affect both myeloid progenitors and mature myeloid cells by stimulating different signalling pathway, which regulate the activity of several transcription factors [117]. These transcription factors, in turn, regulate the synthesis of their target proteins and thus influence the function of myeloid cells [117]. Pro-inflammatory tumor and TME-derived soluble factors, including interleukin 1β (IL-1β), interleukin 6 (IL-6), S100A9 and transforming growth factor β (TGFβ) and cytokines released by activated T cells, including interferon γ (IFNγ), interleukin-4 (IL-4), interleukin 10 (IL-10) and interleukin 13 (IL-13) initiate immunosuppressive pathways and further promote myeloid derived suppressor cells (MDSC) differentiation into immunosuppressive macrophages and dendritic cells [114]. Therefore, the TME and its pro-tumoral features emerge increasingly as an attractive therapeutic target

because it provides the pro-tumorigenic, chronic inflammatory environment that triggered thereby tumor growth, development and may mediate the resistance of cancer cells to treatment. Many of the limitations of current treatments, including chemotherapy, radiotherapy, and emerging targeted therapies, are that the interaction between the anti-cancer drug and the TME is complex and not fully understood.

2.3.1 Interleukin-6

A clear pro-tumoral role of IL-6 has already been shown in 1989 by Klein *et al*. They reported about both an autocrine loop of IL-6 production as well as a paracrine loop induced by bone marrow stroma cells in multiple melanoma (MM) [118]. Accordingly, substantial research has focused on IL-6 as a multifunctional pro-inflammatory cytokine which is produced by several cells within the TME, including tumor infiltrating immune cells, fibroblasts, endothelial cells, keratinocytes and tumor cells themselves [115,119-121] (**Fig 2.4 A**). The IL-6 protein is 21-28 kDa in size, depending on the extent of glycosylation [119]. IL-6 is a major mediator of inflammation and is highly expressed in various cancers. In CRC, high IL-6 expression has been suggested to be associated with cancer progression and metastasis by inducing signalling cascades and thereby triggering proliferation and pro-angiogenetic mechanisms [122-124]. Moreover, elevated levels of serum IL-6 and sIL-6R were detected in patients with i.e., CRC [125,126] and were associated with surgery, chemo- and radiotherapy [127]. The IL-6 family consists of various cytokines, including, IL-6, interleukin-11 (IL-11), Ciliary neurotrophic factor (CNTF), cardiotrophin-1 (CT-1), cardiotrophinlike cytokine (CLC), leukaemia inhibitory factor (LIF), onostatin M(OSM), and IL-27 that share the common glycoprotein 130 (gp13) receptor unit [128,129].

The IL-6 induced signalling is mediated by two different pathways, the classic signalling and the trans-signalling pathway [130]. On target cells, IL-6 induces the classic signalling by binding to membrane-bound IL-6 receptors (IL-6R), whereas during trans-signalling IL-6 binds to a soluble IL-6R (sIL-6R) [130] (**Fig 2.4 B**). Subsequently, the non-signalling IL-6/IL-6R or IL6/sIL-6R complexes bind to the signal-transducing membrane protein gp130, thereby promoting its homodimerization and subsequent initiation of intracellular signalling [129,131,132]. Gp130 is ubiquitously expressed, whereas the expression of IL-6R is restricted to hepatocytes, neutrophils, monocytes, macrophages, and some lymphocytes [129,133]. However, the membrane bound IL-6R can be cleaved by the metalloprotease a disintegrin and metalloprotease 17 (ADAM17) to generate sIL-6R, that in turn promote IL-6 trans-signalling even in cells that are not capable of IL-6R [128,134]. A major difference regarding the receptor formation of the IL-6 family members is that the signalling complex of IL-6 and IL-11 contains a gp130 homodimer, while other family members need a heterodimeric receptor complex containing gp130 and an alternative signalling subunit to activate their signalling cascade [135]. IL-6 classic and trans-

signalling regulate distinct biological effects. The classic signalling is especially important for acute-phase immunological response and central homeostatic processes [136,137]. In contrast, trans-signalling plays a role mainly in the pathophysiology of chronic inflammatory disorders and within the TME of some types of cancer [138]. IL-6-induced signal initiation leads to multiple downstream events that are triggered by activation of receptor-associated cytoplasmic tyrosine kinases, including Janus kinase 1 (JAK1), JAK2 and non-receptor tyrosine-protein kinase 2 (TYK2) [133,135]. Activation of these kinases leads to different patterns of tyrosine phosphorylation and subsequent activation of transcription factors signal transducer and activator of transcription 1,3,5 (STAT1,3,5) [135]. IL-6 also induce the following main signalling mechanisms: 1) The RAS-RAF cascade that regulates several downstream modifiers, including mitogen-activated protein kinases (MAPKs), 2) The SRC-YAP-NOTCH pathway and 3) The RAC serin/threonine-protein kinase (AKT) pathway [135] (**Fig 2.4 B**).

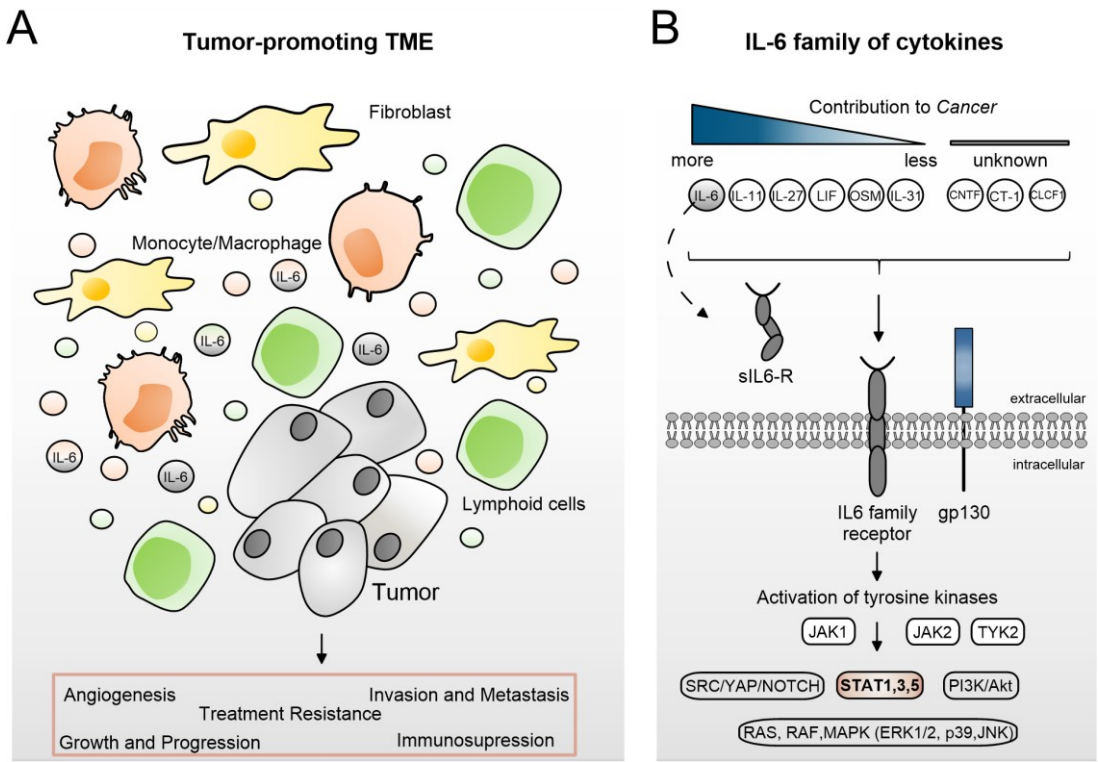

Figure 2.4 Interleukin-6 within a tumor-promoting tumor microenvironment.
A| The communication within a tumor microenvironment (TME) is, besides others, mediated by secreted factors (yellow, green, orange, and grey circles), including chemokines, cytokines, and growth factors from tumor cells, infiltrating immune cells, and stroma cells. Interleukin-6 (IL-6) is secreted by both tumor cells and the tumor surrounding cells and leads to an inflammatory TME which in turn increases treatment resistance, invasion and metastasis, angiogenesis, tumor growth and progression as well as it mediates tumor induced immunosuppression [114]. **B|** IL-6 cytokine family members have different importance within cancer [135]. An important feature of the IL-6 family is that they use common cytokine receptor units. These receptor complexes consist of the common gp130 domain, together with a ligand-binding non-signalling receptor (IL-6 family receptor) [135].

There is increasing evidence for a main role of IL-6 in the progression of cancer, particularly CRC, and relationships with local and systemic inflammatory responses [110,114]. Consistent with

this, IL-6 and IL-11 play a prominent role in the progression of sporadic and inflammation-associated colon and gastric cancer [114]. Pharmacologic inhibition of the IL-11/STAT3 axis in mouse models of gastrointestinal cancer and human tumor cell line xenografts suppressed cell invasion ability and reduced tumor growth [139].

2.3.2 STAT3

The link between chronic inflammation and cancer is clearly illustrated by the fact that a large portion of CRC tumors and cell lines exhibit a constitutive activity of the key pro-inflammatory transcription factors nuclear factor -κB (NF-κB) and STAT3 [111,140].

STAT3 belongs to a family of transcription factors that were first discovered in 1994 during the evaluation of interferon (IFN)- triggered gene regulation [141]. In 1994, Zhong *et al.*, described a DNA-binding protein, which becomes activated through phosphorylation on tyrosine in response to epidermal growth factor (EGF) and IL-6 [142]. At the same time Akira *et al.*, discovered a protein that gets activated in response to IL-6 in hepatocytes, which they called acute phase response factor (APFR) [143]. It was subsequently found to be the same protein, which was henceforth named STAT3. STAT3 belongs to the STAT family of proteins, consisting of seven members (STAT1, STAT2, STAT3, STAT4, STAT6, STAT5a, STAT5b), that have similar protein length, slightly varying from 750 to 850 amino acids [141,144]. STAT proteins comprise of structural and functional conserved domains: 1) amino-terminal domain (NTD), 2) coiled-coil domain (CCD), 3) DNA-binding domain (DBD), 4) linker domain (Linker), 5) Scr-homology 2 domain (SH2), and 6) carboxyl-terminal transactivation domain (TAD) [145] (**Fig 2.5 A**). The particular functions of the domains can be found in **Fig. 2.5 A** (blue). STAT3 is a protein with dual roles - it transduces signals from growth factors and hormones from the cell membrane through the cytoplasm and function as a transcription factor in the nucleus, where it regulates gene expression of its target genes [144,146,147]. STAT3 is known to regulate normal cellular processes, including cell development, differentiation, proliferation, survival, angiogenesis, and immune functions [146,147]. Moreover, STAT3 is activated by signalling induced by the entire IL-6 family of cytokines and growth factors such as EGF, colony stimulating factor 1(CSF-1), and platelet derived growth factor (PDGF), IFNγ, IL-10 and IL-2 [148].

In response to IL-6, STAT3 signalling leads to activation of JAK proteins that activate STAT3 mainly by direct phosphorylation at tyrosine (705) [119,127,135,149-151]. Following activation, phosphorylated STATs homo- or hetero-dimerize through reciprocal phosphotyrosine-SH2 domain interactions and subsequently translocate from the cytosol into the nucleus [141,144]. The STAT3 dimer can then bind to a 9-base-pair consensus sequence (TTCCGGAA – GAS sequence), located in the promotor regions of STAT3 target genes [152] to regulate the transcription of specific target genes [141,144] (**Fig 2.5 B**). An additional phosphorylation site within

the TAD region, serin 727, maximizes transcriptional activity of STAT3 [153] (**Fig. 2.5 B**). Under physiological conditions, the JAK/STAT3 pathway is transient and tightly regulated, by activation of protein phosphatases, by inhibitors of phosphorylation, by nuclear inhibitory factors or by negative regulators (suppressors of cytokine signalling -SOCS proteins) [147]. However, in many cancers, STAT proteins are aberrantly activated [154].

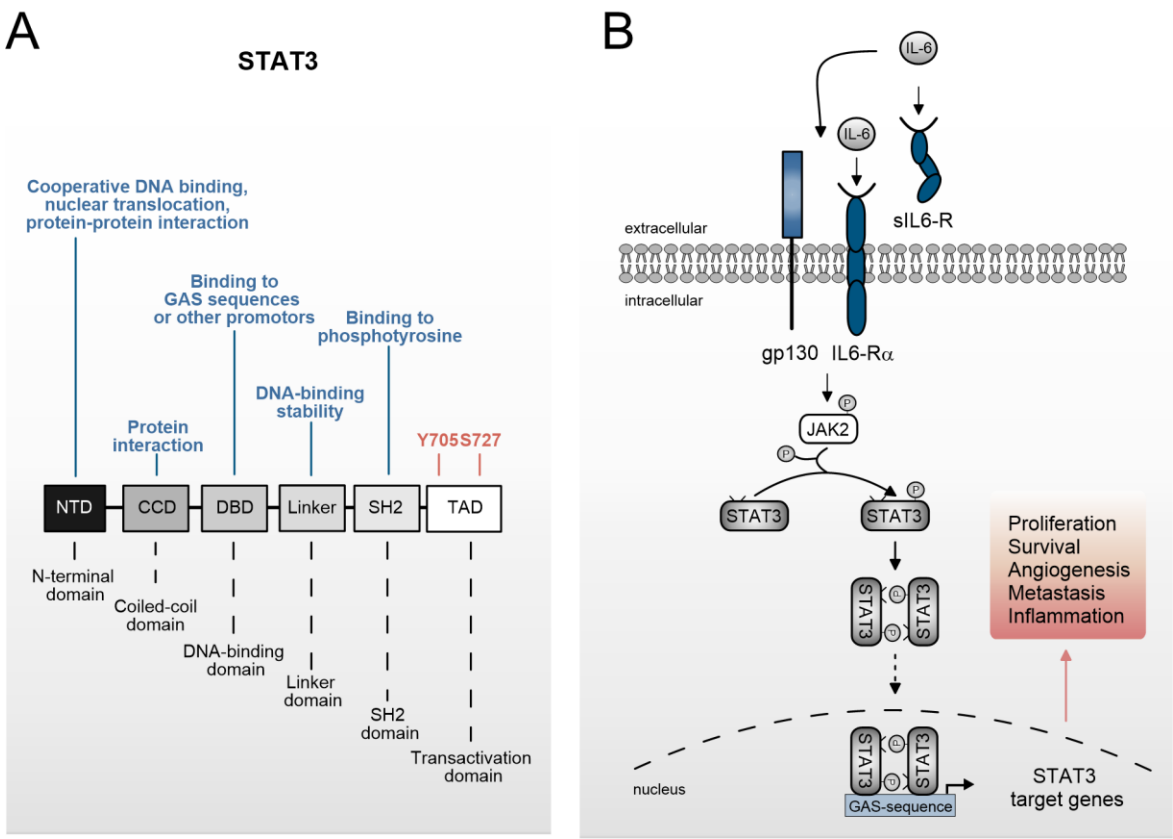

Figure 2.5 IL-6 induced STAT3 signalling.
A| Amino acid sequence of STAT3(α) as an example of the STAT3 protein family. Structurally, STAT3 comprises the N-terminal domain (NTD), coiled-coil domain (CCD), DNA-binding domain (DBD), linker domain (LD), Scr homology (SH2) domain and transcriptional activation domain (TAD) [145]. The functions of the domains are highlighted in blue, important phosphorylation sites are highlighted in orange. **B|** Highly simplified representation of IL-6 induced STAT3 signalling with the major steps of the intracellular signalling cascade. Following receptor ligation, induced by IL-6 binding, JAK2 gets activated to phosphorylate STAT3 that in turn dimerizes and translocated into the nucleus to regulated expression of STAT3 target genes by binding to specific docking sites called interferon-gamma activated sequences (GAS) [119,127,135,149-152].

2.3.2.1 The IL-6/JAK/STAT3 axis in CRC treatment resistance

Aberrant STAT3 activation is associated with various human cancers and is implicated in increased synthesis of key inflammatory mediators, cytokines, and chemokines [146]. This results in amplification of recruited immune cells and modulation of the function of these cells in the TME. Cancer cells harboring increased pSTAT3 activity demonstrate high tumor malignancy and its expression is an indicator of poor prognosis [119,145]. In addition to STAT3 itself, some of

its target genes also play a tumorigenic role. IL-6, C-X-C Motif Chemokine Ligand 12 (CXCL12) and Mitochondrially Encoded Cytochrome C Oxidase II (COX2) are responsible for inflammation while BCL2 Apoptosis Regulator (BCL-2) and BCL2 Like 1 (BCL-XL) are important for cell survival. The invasion characteristics of tumor cells can be enhanced by the expression of Mucin 1 (MUC1) and the induction of metastasis by proteins such as Matrix Metallopeptidase 1,2 and 9 (MMP-1,2 and 9) [145,155]. Furthermore, activation of STAT3 by IL-6 prevents apoptosis and enhances proliferation of malignant cells through upregulation of anti-apoptotic and proliferative factors [114]. STAT3 signalling is frequently activated in both primary tumors as well as cell lines and phosphorylated STAT3 can be detected in 25-40% of rectal cancers [156]. Of note, constitutively activated STAT3 as a result of mutations at the STAT3 protein or the *STAT3* gene is extremely rare. Rather, this protein is abnormally activated by autocrine and paracrine mechanisms such as aberrant activity of cell surface receptors by TME- associated cytokines, amplified or mutated receptors or by a loss of negative endogenous STAT3 regulators such as protein inhibitors of activated STATs (PIAS) [145]. Thus, it is not surprising that STAT3 has been studied as a tumor therapeutic target excessively, owning to its role in tumor formation, metastasis, and drug resistance [157]. Direct inhibition of the JAK/STAT3 pathway appears to be highly effective and has been approved by the Food and Drug Administration (FDA). Unfortunately, clinical studies revealed that direct inhibition of STAT3 does not result in satisfactory results due to high sequence similarity with the other STAT members [158,159]. Moreover, other issues such as high toxicity and poor bioavailability have become significant obstacles to the clinical development of direct STAT3 inhibitors [158]. These findings lead to increased research focused on indirect inhibition of the signalling pathway, by targeting its upstream and downstream signalling components [157]. Therefore, JAK inhibitors, including Ruxolitinib showed positive clinical outcomes and have been approved by FDA for cancer therapy [119,127,150].

Importantly, abundant evidence has indicated that STAT3 is important for mediating treatment resistance, such as targeted therapy, chemotherapy, radiotherapy, and immunotherapy [160,161]. In 2010, my host research group established an *in vitro* model for testing cell lines regarding their sensitivity to CRT. Therefore, 12 human CRC cell lines were pre-treated with 3 µM 5-FU and subsequently irradiated with 2 Gy. In parallel, pretherapeutic gene expression profiles were generated and compared with the corresponding surviving fractions. The analysis revealed a significantly STAT3- expression in cell lines with comparatively high CRT resistance [162]. It has also been demonstrated that the treatment with the STAT3 inhibitor STATTIC significant sensitized CRC cells to CRT both *in vitro* and *in vivo* [147]. In accordance with this, a direct contribution of STAT3 inhibition and CRT sensitization was made in CRC cells *in vitro* [163]. Furthermore, Ebbing *et al.* showed that stroma cell-derived IL-6 mediates CRT resistance of esophageal adenocarcinomas, which could be reverted by inhibition of IL-6 [164].

2.4 Aims of the thesis

The aim of the currently work was to further investigate the role of STAT3 as a driver of CRT resistance in CRC cells and to uncover possible molecular mechanisms underlying STAT3-mediated CRT resistance. Thus, I wanted (i) to get a clear understanding of the influence of the JAK/STAT signalling on CRT resistance, testing novel JAK/STAT inhibitors as CRT-sensitizer in human CRC cell lines in vitro. (ii) To investigate, whether the use of a pharmacological STAT3 inhibitor has an impact on CRC cells *in vivo*. (iii) To understand the STAT3 mediated CRT resistance using an RNA-Sequencing (RNA-Seq) based approach to analyze the consequences of STAT3 perturbation on a global transcriptome level. (iv) To identify respective STAT3 downstream targets that may functionally mediate the resistance phenotype.

3. Materials and Methods

3.1 Materials

3.1.1 Chemicals

Table 1 Chemicals

Substances	Company
2-Mercaptoethanol	Carl Roth GmbH & Co. KG
4-(2-hydroxyethyl)-1-piperazineethanesulfonic acid (HEPES)	Carl Roth GmbH & Co. KG
5-fluorouracil (5-FU)	Sigma
Acetic acid	Carl Roth GmbH & Co. KG
Agarose	Sigma
Ammonium persulfate (APS)	AppliChem
Bovine serum albumin (BSA)	Sigma
Brilliant blue R 250	Carl Roth GmbH & Co. KG
Bromophenol blue	Sigma
Deoxynucleotide triphosphates (dNTP)	Carl Roth GmbH & Co. KG
Desoxy-ATP (adenosine triphosphate) [33P]-labelled	Hartmann Analytic
Disodium hydrogen phosphate dihydrate (Na_2HPO4)	Merck
Dithiothreitol (DTT)	AppliChem
ECL Advance Western Blot detection kit	Amersham Bioscience
Egtazic acid (EGTA)	Merck
Ethanol, 99.8%	Carl Roth GmbH & Co. KG
Ethylenediaminetetraacetic acid (EDTA solution pH 8.0)	QualityBiological
Ficoll	Amersham Bioscience
Formaldehyde solution, 37%	AppliChem
GelRed® Nucleic Acid Gel Stain	Biotium
Glycerol, UltraPure™	Invitrogen
Glycine	AppliChem
hemalum solution	Merck
Hydrogen chloride (HCL) solution	Merck
IGEPAL-CA-360	Sigma
Immobilion® Forte western Blot HRP Substrate	Millipore Cooperation
Klenow fragment	New England Biolabs
Magnesium chloride (MgCl)	Merck
Methanol, 99%	Carl Roth GmbH & Co. KG
Milk powder, blotting grade	Carl Roth GmbH & Co. KG
N, N, N', N' – Tetramethylethylendiamin (TEMED)	AppliChem
Nonident P-40 (NP-40)	AppliChem
Pefabloc® SC-Protease Inhibitor	Carl Roth GmbH & Co. KG
PhosSTOP	Roche
Potassium chloride (KCL)	Merck
Potassium dihydrogen phosphate trihydrate (KH_2PO_4)	Merck
Prestained protein ladder (10-180 kDa)	BioFroxx
Proteo Block, Protease inhibitor	Fermentas
Resazurin Solution	PromoKine
Roti®phorese Gel30 solution	Carl Roth GmbH & Co. KG
Roti®Quant	Carl Roth GmbH & Co. KG
Sodium Chloride (NaCl)	Carl Roth GmbH & Co. KG
Sodium Dodecyl Sulfate (SDS) salt	Merck
Sodium Hydroxide (NaOH)	Merck
Sodium orthovanadate (Na_3VO_4)	Acros Organics
Sucrose (saccharose)	Merck
Tris ultrapure	AppliChem
Triton X-100	Serva
Tween20	AppliChem

3.1.2 Disposables and laboratory equipment

Laboratory equipment and solutions that needed to be sterile were sterilized using HST32/3 autoclave (Zirbus technology GmbH,Bad Grund/Harz,Germany). Pasteur pipets used in cell culture or other sensitive settings were sterilized using ST6060 Hot air sterilizer (Thermo Fisher Scientific Inc., Waltham, MA, USA).

Note that only disposables and laboratory equipment that were used in the group of PD Dr. Marian Grade and Prof. Dr. Jürgen Wienands were listed in **Tab. 2**. Other equipment's and solutions that were used in cooperating institutes and departments were not listed.

3.1.2.1 Disposables

Table 2 Disposables

Supplies	Company
12-well plate	Sarstedt
15- and 50-ml tubes	Sarstedt
175 cm^2	Sarstedt
25 cm^2 and 75 cm^2 flask	Sarstedt
384-well plate, FrameStar®, skirted PCR plate	4titude
6-well plate	Sarstedt
96-well plate, black, for photometry	Corning
96-well plate, Cyto One®	STARLAB GmbH
96-well plate, white, for luminescence	Thermo Scientific
Biosphere safe seal tubes 1.5 ml and 2 ml	Sarstedt
Cell scraper M, length 300 mm	TPP
Cell spatula, length 195 mm	TPP
Chromatography paper 3 mm	Whatman™ GE Healthcare UM Limited
Cryovials	Sarstedt
Disposable reagent reservoirs, PS, white	Carl Roth GmbH & Co. KG
Falcon tubes, 15 ml, 50 ml	Sarstedt
Illustra-MicroSpin-G-25 columns	GE Healthcare
Pasteur pipettes, glas, 150 mm	Th. Geyer
Pasteur pipettes, glas, 230 mm	Th. Geyer
PVDF membrane Hybond-P	Amersham Biosciences
QIAshredder	Qiagen Sciences
Reaction tubes 1.5 ml	Carl Roth GmbH & Co. KG
Reaction tubes 2 ml and 5 ml	STARLAB international GmbH
Rotilabo®-liquid reservoirs, PVC (unsterile)	Carl Roth GmbH & Co. KG
Serological pipette 2 ml, 5 ml, 10 ml, 25 ml, 50 ml	STARLAB international GmbH
Stericup® Quick Release	Merck Millipore
Tip One® filtertips sterile,10/20 µl, 100 µl, 200 µl, 1000 µl	STARLAB international GmbH
Tip One® tips 10/20 µl, 200 µl, 300 ml, 1000 µl, 1250 µl	STARLAB international GmbH

3.1.2.2 Laboratory equipment

Table 3 Laboratory equipment

Equipment	Company
Autoclave, HST32/35	Zirbus technology GmbH
Biomolecular imager Typhoon FLA900	GE Healthcare
Caunting chamber	Brand GmbH & Co. KG
Cell culture incubator CO_2	Labotect

Cell culture incubator O_2	Labotect
Centrifuge 5415 D	Eppendorf
Centrifuge Allegra X-30R	Beckman Coulter GmbH
Centrifuge Heraeus Fresco 17	Thermo Scientific Open Biosystems
Centrifuge mini Rotilabo®	Carl Roth GmbH & Co. KG
ImageQuant LAS 4000 mini	GE Healthcare Life Sciences
Colony Counter, eCount™	Heathrow Scientific® LLC
Digital-Control Water Baths, Isotemp®	Fisher Scientific
Elektrophorese plates	Ochs Laborbedarf
Eppendorf® Research®, multichannel pipette (12), 5-100 µl	Eppendorf
Eppendorf® Research®, multichannel pipette (8), 50-1200 µl	Eppendorf
Eppendorf® Research®, multistepper pipette 20-300 µl	Eppendorf
Eppendorf® Research®, single channel pipette, 0.5-10 µl	Eppendorf
Fluid aspiration system BVC professional	Vacuubrand
Freezer MDF U537 (-20 °C)	Sanyo
Freezer ultra-low (-150 °C)	Sanyo
Freezer VIP Series MDF U74V (-80 °C)	Sanyo
Freezing Container, 5100 Cryo 1°C	Thermo Fisher Scientific Inc.
Fridge (4 °C, - 20 °C) premium	Liebherr
Hera Safe (sterile bench)	Heraeus
Homogeniser in Ultrasonic Technology, BANDELIN SONOPULS HD 3100	BANDELINE electronic GmbH & Co. KG
Hot air sterilizer, Heraeus ST6060	Thermo Fisher Scientific Inc.
Magnetic stirrer	IKA®- Werke GmbH & Co. KG
Microscope, EC3	Leica AG
Microscope, Leica DM IL	Leica AG
Microscope, Leica LED2500	Leica AG
Mini-Transilluminator	BioRad
Mithras LB943 microplate reader	Berthold Technologies GmbH
NucleofectorTM 2b Device	Lonza
pH-meter, PB-11	Sartorius AG
Phosphoimaging system, Typhoon FLA 9500	GE Healthcare
Pipette controller, accu-jet®	Brand GmbH & Co. KG
Pipettes, Eppendorf Research® plus, 2,5 µl, 10 µl, 20 µl, 100 µl, 200 µl, 1000 µl	Eppendorf
PowerPac 3000	BioRad
Real time PCR, C1000 Thermocycler	BioRad
Semi dry blotting aperture	Peqlab
Stainless Steel Beads, 5mm (200)	QIAGEN GmbH
Thermomixe	Eppendorf
Tilting shaker, WS42	A. Hartenstein GmbH
TissueLyser LT	QIAGEN GmbH
Vaporiser, Vapor 2000	Dräger
Victor X4 light multilabel reader	PerkinElmer
Vortexer, RS-VA 10	Phoenix Instruments
Water Purification System, Milli-Q Reference Ultrapure	Merck Millipore
Weight scale, BD ED 100	Sartorius AG
Weight scale, BP 610	Sartorius AG
Weight scale, ED224S	Sartorius AG
Xstrahl RS225 molecular research system	Gulmay Medical Ltd.

3.1.3 Water

Most solutions and buffers that referred to this thesis were prepared with double-distilled H_2O (quality reached using Mili-Q ultrapure Water System, Merck Millipore). For RNA studies DNase-, RNAse-, protease-, calcium-, and magnesium-free water was used (Water for Molecular Biology, Merck Millipore).

3.1.4 Kits

Table 4 Ready-to-use kits

Kit	Company
Amaxa™ Cell Line Nucleofector™ Kit V and L Kit (25 RCT)	Lonza
Cignal Reporter Assay Kit STAT3, CCS-9028L	QIAGEN GmbH
Dual-Luciferase Reporter Assay System	Promega
MycoAlertVR, Mycoplasma Detection Kit	Lonza
Pierce® Bicinchoninic Acid Assay (BSA) protein Assay Kit	Thermo Fisher Scientific Inc.
RNase-Free DNase Set	QIAGEN GmbH
RNeasy Mini Kit	QIAGEN GmbH
SensiFAST™ Probe No-ROX One-Step Kit	Bioline

3.1.5 Software

3.1.5.1 Computer software

Table 5 Software

Software	Version	Company
EndNote 20	0.1	Cleverbridge AG
Grapher	8	Apple Inc
GraphPad Prism	9	GraphPad Software
ImageJ (Public domain)	1.52a	developed at NIH by Wayne Rasband
ImageQuant™ LAS 4000 mini-1.2		GE Healthcare UK Limited
ImageQuant™ TL 7.0		GE Healthcare UK Limited
KaleidaGraph	4.1.0	Synergy Software Systems
Microsoft Office 2016	2016MSO	Microsoft
ND-1000		PEQLAB Biotechnologie GmbH
Toolkit for Interactive Network Analysis (TINA)	2	DesignSoft
Wallac 1420 Workstation 3.00.0.53		PerkinElmer

Note that only software's that were used in the group of PD Dr. Marian Grade and Prof. Dr. Jürgen Wienands were listed in **Tab. 6** and **7**. Software's that were used for sequencing and analyzing the RNA-Seq experiment were named in section 3.2.6 but originally belongs to the corresponding institutes and departments.

3.1.5.2 Online platforms

Table 6 Online platforms

Online platform	Link	Company
Bioinformatics & Evolutionary Genomics (Venn diagrams)	http://bioinformatics.psb.ugent.be/webtools/Venn/	VIB-UGENT Center For Plant Systems Biology
COSMIC database	https://cancer.sanger.ac.uk/cosmic	Sanger institute
GeneCards, The human gene database	https://www.genecards.org/	Weizmann Institute of Science, Life Map Science

Heatmapper	http://www.heatmapper.ca/	Wishart Research Group at the University of Alberta
Morpheus	https://software.broadinstitute.org/morpheus/	Broad Institute
NCBI Blast	https://blast.ncbi.nlm.nih.gov/Blast.cgi	National Centre for Biotechnology Information
Cancer Cell Line Encyclopedia (CCLE)	https://portals.broadinstitute.org/ccle	Broad Institute
PrimerBank	https://pga.mgh.harvard.edu/primerbank/	The Massachusetts General Hospital

3.1.6 Stimulants and Inhibitors / Drugs

3.1.6.1 Stimulants

Table 7 Stimulants

Stimulants	Solvent	Company
Hyper-IL-6	Cell culture medium	Kindly provided by Prof. Rose John Institute of Biochemistry (Kiel)
IFN-γ	Cell culture medium	Biomol
rIL-6	Cell culture medium	Merck

3.1.6.2 Inhibitors

Table 8 Inhibitors

Inhibitors / inhibitory antibodies	Solvent	Company
DAPT	DMSO	Sigma
Napabucasin (Napa)	DMSO	Sellckchem
Ruxolitinib (Ruxo)	DMSO	Sellckchem
Tocilizumab (Toci)	PBS	Kindly provided by Prof. Rose John Institute of Biochemistry (Kiel)

3.1.7 Buffers and solutions

3.1.7.1 Cell lysis buffer

NP-40 lysis buffer

Table 9 NP-40 lysis buffer

Substances	Stock	Final concentration	For 100 ml
NaCL	5 M	150 mM	3 ml
NP-40	100%	1%	1 ml
Tris	1 M	50 mM	5 ml

All components were diluted, add to 100 ml ddH_2O and pH adjusted to 7.8. For cell lysis, following components (**Tab. 10**) were added to the required volume of buffer before use.

Table 10 Freshly added components for NP-40 based cell lysis

Substances	Dilution
DTT	1:10 (stock: 1 M)
Phosphatase Inhibitor	1:10 (stock: 1 tablet in 10 ml ddH_2O)
Protease Inhibitor	1:25 (stock: 1 tablet in 10 ml ddH_2O)

Ripa buffer

Table 11 Ripa buffer

Substances	Stock	Final concentration	For 100 ml
EDTA	0.5 M	2 mM	400 µl
NaCL	5 M	150 mM	3 ml
Na-Deoxycholate		0.5%	500 mg
NP-40	100%	1%	1 ml
NP-40		1%	1 ml
Tris	1 M	50 mM	5 ml

All components were diluted, add to 100 ml ddH_2O and pH adjusted to 8. For cell lysis, following components (**Tab. 12**) were added to the required volume of buffer before use.

Table 12 Freshly added components for Ripa buffer-based cell

Substances	Dilution
Protease Inhibitor	1:25 (stock: 1 tablet in 10 ml ddH_2O)
Phosphatase Inhibitor	1:10 (stock: 1 tablet in 10 ml ddH2O)

Chromatin fractionation buffer Buffer- A

Table 13 Chromatin fractionation buffer Buffer- A

Substances	Stock	Final concentration	For 100 ml
KCL	250 mM	10 mM	4 ml
$MgCl_2$	2 M	1,5 mM	75 µl
Saccharose		0.34 M	11.638 g
Glycerol		10%	10 ml, 12.6 g
TritonX-100		0.1%	100 µl
HEPES (pH 7.9)	100 mM	10 mM	10 ml

Chromatin fractionation buffer Buffer- B

Table 14 Chromatin fractionation buffer Buffer- B

Substances	Stock	Final concentration	For 100 ml
EDTA	0.5 M	3 mM	600 µl
EGTA	20 mM	0.2 mM	1 ml

All components were diluted, add to 100 ml ddH_2O. Before use, components provided in **Tab. 10** were added.

3.1.7.2 Buffer for EMSA

Cytoplasmic extraction buffer

Table 15 Cytoplasmic extraction buffer

Substances	Stock	Final concentration	For 100 ml	pH value
EDTA	0.5 M	1 mM	200 µl	
Glycerin (v/v)		10%	10 ml	
HEPES	100 mM	20 mM	20 ml	7.4
KCL	250 mM	10 mM	4 ml	
Na_3VO_4	1 M	0.1 mM	10 µl	

All components were diluted, add to 100 ml ddH_2O. Before use, the following components (**Tab. 16**) were added.

Table 16 Freshly added components for the cytoplasmic extraction buffer

Substances	Dilution/ final concentration
DTT	3 mM (stock 1 M)
IGEPAL	0.1%
Pefabloc	0.4 M
Protease Inhibitor	1:10 (stock: 1 tablet in 10 ml ddH_2O)

Nuclear extraction buffer

Table 17 Nuclear extraction buffer

Substances	Stock	Final concentration	For 100 ml	pH value
EDTA	0.5 M	1 mM	200 µl	
Glycerin (v/v)		20%	20 ml	
HEPES	100 mM	20 mM	20 ml	7.4
KCL	10 M	420 mM	4,2 ml	
Na_3VO_4	1 M	0.1 mM	10 µl	

All components were diluted, add to 100 ml ddH_2O. Before use, the following components (**Tab. 18**) were added.

Table 18 Freshly added components for the nuclear extraction buffer

Substances	Dilution/ final concentration
DTT	3 mM (stock 1 M)
Pefabloc	0.4 M
Protease Inhibitor	1:10 (stock: 1 tablet in 10 ml ddH_2O)

3.1.7.3 Additional buffers and solutions

Table 19 Additional Buffers and solutions

Buffers	Substances	Final concentration	For 1000 ml	pH value
Coomassie decolorizing solution	Methanol (v/v) Acetic acid (v/v) ddH_2O	5% 7% 88%	50 ml 70 ml 880 ml	
Coomassie fixing solution (for gels)	Methanol (v/v) Acetic acid (v/v) ddH_2O	50% 10% 40%	500 ml 100 ml 400 ml	
Coomassie staining solution	Methanol (v/v) Coomassie Brilliant Blue (w/v) Acetic acid (v/v) ddH_2O	50% 0.05% 10% 40%	500 ml 500 mg 100 ml 400 ml	
EMSA loading buffer	HEPES KCl MgCl2 EDTA EGTA Ficoll	100 mM 200 mM 5 mM 2.5 mM 0.5 mM 20%		
Freezing media (cell culture)	L15 Media/RPMI media FBS L-Glutamin DMSO	20% 1% 10%		
Sample buffer (Protein, 6x)	SDS Mercaptoethanol Glycerin Bromphenol blue	6% 30% 40%	3 ml 3 ml 4 ml Spatula tip (for 10 ml final volume)	
SDS-PAGE loading gel (4x) buffer	Tris	1000 nM	121.16 g	6.8
SDS-PAGE running (10x) buffer	Tris Glycine SDS	250 mM 1920 mM 1%	30.29 g 144.13 g 10 ml	8.3
SDS-PAGE running (1x) buffer	SDS-PAGE running (10x) buffer ddH_2O	1x	100 ml 900 ml	
SDS-PAGE separating gel (4x) buffer	Tris	1500 nM	181.72 g	8.8
TAE (50 x)	Tris Glacial acetic acid	40 mM 20 mM	242 g 57.1 ml	7.6

	EDTA	1 mM	100 ml of 0.5 M	8.0
TAE (1x)	TAE (50 x) ddH_2O	1x	20 ml 980 ml	
TBE (10x)	Tris base Boric acid EDTA	1 M 1 M 0.02 M	121.1 g 61.8 g 7.4 g	
TBE (2.4 x)	TBE (10x) ddH_2O	2.4 x	416.6 ml 583,4 ml	
TBS (10x)	NaCL Tris	150 nM 50 nM	87.66 g 60.57 g	7.5
TBS (1x)	TBS (10x) ddH_2O	1x	100 ml 900 ml	
TBST (1x)	TBS (10x) Tween20 ddH_2O	1x 0.1%	100 ml 1 ml 899 ml	
Western Blot blocking buffer	Milk powder TBST (1x)	5%	50 g 1000 ml	
Western Blot transfer (10x) buffer	Tris Glycine SDS solution	48 nM 39 nM 0.037%	58 g 29 g 37 ml	
Western Blot transfer (1x) buffer	Western Blot transfer (10x) buffer Methanol ddH_2O	1 x	100 ml 200 ml 700 ml	

All components were diluted, add to 1000 ml ddH_2O, and were adjusted to their respective pH value.

3.1.8 Equipment and Substances for SDS- Polyacrylamide gel electrophoresis

Table 20 Electrophoresis supplies

Equipment	Company
Glass plate, straight cut	Biometra GmbH
Glass plate, fix spacer	Biometra GmbH
Combs for electrophoresis	Biometra GmbH
Silicone seals, 1.0 mm	Biometra GmbH

Table 21 Composition of loading and separating gels

Substances	Loading gel (7.5%)	Loading gel (10%)	Separating gel (5%)
10% APS	200 µl	200 µl	100 µl
10% SDS solution	200 µl	200 µl	50 µl
30% Roti®phorese	5 ml	6.7 ml	0.83 ml
4x Loading gel buffer (pH 6.8)	-	-	0.63 ml
4x Loading gel buffer (pH 8.8)	5 ml	5 ml	-
ddH_2O	9.6 ml	7.9 ml	3.4 ml
TEMED	20 µl	20 µl	10 µl

Additionally, 75 µl bromphenol-blue solution were added to the gel to make loading easier. The listed values are enough for 2 mini gels

3.1.9 Antibodies for Western Blot analysis

3.1.9.1 Primary Antibodies

All primary antibodies (species: rabbit) were diluted according to the manufacturer's recommendations in either 5% Milk-TBST or 5% BSA-TBST and were incubated over night at 4 °C under gently shaking.

Table 22 Primary Antibodies used for Western Blot analysis

Antibodies (clone)	Dilution	Company
Actin (Polyclonal)	1: 10,000	Sigma
ADAM9 (D64B5)	1: 1,000	Cell Signalling
Cleaved Notch-1 (NICD) (D3B8)	1: 1,000	Cell Signalling
DLL4 (Polyclonal)	1: 1,000	Cell Signalling
GP130 (Polyclonal)	1: 1,000	Cell Signalling
HA-tag (C29F4)	1: 10,000	Cell Signalling
HDAC1 (Polyclonal)	1: 1,000	Cell Signalling
HES1 (D6P2U)	1: 1,000	Cell Signalling
Jagged1 (28H8)	1: 1,000	Cell Signalling
Jagged2 (C23D2)	1: 1,000	Cell Signalling
Nicastrin (D38F9)	1: 1,000	Cell Signalling
NOTCH1 (D1E11)	1: 1,000	Cell Signalling
NOTCH2 (D76A6)	1: 3,000	Cell Signalling
NOTCH3 (D11B8)	1:1,000	Cell Signalling
NUMB (C29G11)	1: 1,000	Cell Signalling
PEN2 (D6G8)	1: 1,000	Cell Signalling
Presenilin 1 (D29D1)	1: 2,000	Cell Signalling
Presenilin 2 (D30G3)	1: 2,000	Cell Signalling
$pSTAT3^{Ser727}$ (Polyclonal)	1: 1,000	Cell Signalling
$pSTAT3^{Tyr705}$ (D3A7)	1: 1,500	Cell Signalling
RBPSUH (RBPJ) (D10A4)	1: 2,000	Cell Signalling
TACE (D22H4)	1: 1,000	Cell Signalling

3.1.9.2 Secondary Antibody

Secondary antibody (species: goat) was diluted in 5% Milk-TBST and were incubated 2 hours at RT under gently shaking.

Table 23 Secondary Antibody used for Western Blot analysis

Protein	Dilution	Company
Anti-rabbit IgG-HRP conjugated	1: 30,000	Acris

IgG = immunoglobulin G, HRP = horseradish peroxidase

3.1.10 Olignonucleotides

3.1.10.1 siRNA

siRNA pools were obtained from Dharmacon, the AllStarsNEG as well as the STAT3 siRNAs (#7 and #8) were obtained from QIAGEN GmbH.

Table 24 siRNAS

Gene	Target Sequence	Accession Number
Negative control (ON-TARGETplus)	UGGUUUACAUGUCGACUAA UGGUUUACAUGUUGUGUGA UGGUUUACAUGUUUUCUGA UGGUUUACAUGUUUUCCUA	n.a.
STAT3 (Pool)	GAGAUUGACCAGCAGUAUA CAACAUGUCAUUUGCUGAA CCAACAAUCCCAAGAAUGU CAACAGAUUGCCUGCAUUG	NM_003150
RBPJ (Pool)	GUAGAGAGCCUUCAGUUGA CUCCCAAGAUUGAUAAUUA CCAGAUACUUGCAUGUAGA GGUCCGAAAUGAUGGAAUC	NM_203283
BCL6 (Pool)	CCUUAAUCGUCUCCGGAGU GUAUAUACCCGUACAACGU GUUAUAACUACUCCGGAGA CAUCAAGCCUCCUCGUGAA	NM_001706
DPYD (Pool)	AAAGAGAGGCGUACCCUUA CGUAUGAUGUAGUGAAUUU CUACCAGGCUAUACAGUUU GUGUUAAGGUGAUUUGUGA	NM_000110
DUOX2 (Pool)	GAGGAUAAGUCCCGUCUAA CAUCUGUGUUGGCGUGUUU GAACUGGAGUGAUCUCAAC GGAGUGACCUACCUGCAAU	NM_014080
ELF3 (Pool)	GAACUGAGGGUUGGAACUA GGAGCUGCGUCUGGUCUUU GCCAUUGACUUCUCACGAU GAACAAGUACGACGCAAGC	NM_004433
HIF1A (Pool)	GAACAAAUACAUGGGAUUA AGAAUGAAGUGUACCCUAA GAUGGAAGCACUAGACAAA CAAGUAGCCUCUUUGACAA	NM_181054
MUC1 (Pool)	GCCGAAAGAACUACGGGCA CGAUAUAACCUGACGAUCU CCACCAAUUUCUCGGACAC CCGAGAAGGUACCAUCAAU	NM_182790
NAMPT (Pool)	GGUAAGAAGUUUCCUGUUA CAAAUUGGAUUGAGACUAU UAACUUAGAUGGUCUGGAA CAAGCAAAGUUUAUUCCUA	NM_001018021
S100A9 (Pool)	GGUCAUAGAACACAUCAUG GCAGCUGGAACGCAACAUA CCAAUACUCUGUGAAGCUG ACACAAAUGCAGACAAGCA	NM_002965
SERPINB3 (Pool)	GAUCUAAGCAUGAUUGUGU	NM_006919

	GUUCAUCACCAGUUUCAAA UAAUCACCCUUUCCUAUUC CACAACAGAUUAAGAAGGU	
SERPINB4 (Pool)	UGUAGUAGUAGUCGAAUUA CAACACUGCACAACAAAUU GUUCAUCACCAGUUUCAAA CGACACUGGUUCUUGUGAA	NM_002974
TRIB2 (Pool)	UCGAAGAGUUGUCGUCUAU CGGCUGACCUCGCAGGAAA CAUAGUAACAUCAACCAAA UGUGCAAGGUGUUUGAUAU	NM_021643
Negative control (AllStarsNEG)	CAGGGTATCGACGATTACAAA	n.a.
STAT3 (#7) *	CAGCCTCTCTGCAGAATTCAA	NM_003150
STAT3 (#8) *	CAGGCTGGTAATTTATATAAT	NM_003150

* siRNA STAT3 (#7) and siSTAT3 (#8) were pooled for RNA-Seq experiments, bp = base pair, n.a. = not applicable

3.1.10.2 Primer for semi-quantitative RT-PCR

For primer design the online platforms PrimerBank and NCBI blast were used. All Primers were dissolved in DNase-, RNase-, proteinase-free water and stored at -20°C. HPRT1 was ordered from Eurofins all other primers are ordered from IDT (Integrated DNA Technologies).

Table 25 Primer for semi-quantitative RT-PCR

Gene	Primer sequence (5’ -> 3’)	Product size (bp)	Accession Number
BCL-6	CAGCCAACCTGAAAACCCAC	92	NM_001706
DPYD	GGCGGACATCGAGAGTATCCT	78	NM_000110
DUOX2	AGGATACCGTCCTTTCCTAGAC	194	NM_014080
ELF3	TCTTCCCCAGCGATGGTTTT	122	NM_004433
HIF1A	TGCTTACACACAGAAATGGCCT	161	NM_001530
HPRT1	TGACACTGGCAAAACAATGCA	93	NM_000194.2
MUC1	ACGACGTGGAGACACAGTTC	93	NM_002456
NAMPT	AATGTTCTCTTCACGGTGGAAAA	98	NM_005746
RBPJ	CTGACTCAGACAAGCGAAAGC	79	NM_015874
S100A9	GGTCATAGAACACATCATGGAGG	155	NM_002965
SERPINB3	CGCGGTCTCGTGCTATCTG	100	NM_006919
SERPINB4	ACTCAGTGAAGCCAACACCA	174	NM_175041
TRIB2	GACTCCGAACTTGTCGCATTG	85	NM_021643

bp = base pair

3.1.9 Vectors and Plasmids

3.1.9.1 Vectors for dual luciferase assay

Table 26 Vectors used for dual luciferase assay

Vector	Company
CignalTM Reporter Assay Kit STAT3	QIAGEN GmbH
pGL4.14[luc2/Hygro] Vector	Promega
pGL4.47[luc2P/SIE/Hygro] Vector	Promega
pRL_CMV Vector	Promega

3.1.9.2 Plasmids used for STAT3 expression

Table 27 Plasmids used for bacterial HA-tagged fusion protein expression

Insert	Backbone	Source
STAT3 WT	pmaxKS	Doctoral thesis Florian Krause, CALL, *
STAT3 Y705F	pmaxKS	Doctoral thesis Florian Krause, CALL, *
STAT3 S727A	pmaxKS	Doctoral thesis Florian Krause, CALL, *
STAT3 Y705F/S727A	pmaxKS	Doctoral thesis Florian Krause, CALL, *

* unpublished data

3.1.10 Probe Sequences for electrophoretic mobility shift assay

Table 28 Sequences for electrophoretic mobility shift assay

Probe	Probe sequence	Company
M67	5’ -> 3’: CGACATTTCCCGTAAATCTG 3’ -> 5’: CAGATTTACGGGAAATGTCG	Sigma
RBPJ (mutated)	5’ -> 3’: CGGGGGCCCTTGGTAGCAGGCC 3’ -> 5’: GGCCTGCTACCAAGGGCCCCCG	Sigma
RBPJ (native)	5’ -> 3’: CGGGGGCTTCCGGGATCAGGCC 3’ -> 5’: GGCCTGATCCCGGAAGCCCCCG	Sigma

bp = base pair, red = mutation site

3.1.11 Human cell lines and cell culture reagents

3.1.11.1 Human cell lines

Human colorectal cancer cell lines, LS411N, SW837 and SW1463, were obtained from the American Type Culture Collection (ATCC, Manassas, VA) and cultured in recommended medium, supplemented with 10% fetal bovine serum and 2 mM L-glutamine. All additional adherent cell lines including culturing details were listed in **Tab. 29**.

Table 29 Human cell lines and culture conditions

Cell line	Origin	Medium	Incubator	Split growth ratio
FLO-1*	Human esophagus	RMPI + 10% FBS and 1% L-glutamine	37 °C, humidified, 5% CO_2	n.a.
HeLa*	Cervix epithelial adenocarcinoma	EMEM + 10% FBS and 1% L-glutamine	37 °C, humidified, 5% CO_2	n.a.
LS411N	Colorectal carcinoma	RMPI + 10% FBS and 1% L-glutamine	37 °C, humidified, 5% CO_2	1:5
MCF7*	Breast adenocarcinoma	EMEM + 0.01 mg/ml human recombinant Insulin, 10% FBS and L-glutamine	37 °C, humidified, 5% CO_2	n.a.
SW1463	Rectal adenocarcinoma	L15 + 10% FBS and 1% L-glutamine	37°C, humidified,0% CO2	1:5
SW837	Rectal adenocarcinoma	L15 + 10% FBS and 1% L-glutamine	37°C, humidified, 0% CO_2	1:3

* This cell lines were not cultivated for this study. We used/ received protein lysates.

3.1.11.2 Cell culture reagents

Table 30 Cell culture reagents for cultivation of human cell lines.

Substances	Company
Dimethyl sulfoxide (DMSO)	Sigma
Fetal bovine serum (FBS)	Pan
Leibovitz's L-15 medium	Invitrogen
L-Glutamine	BioWhittaker
Lipofectamine RNAiMAX	Thermo Fisher Scientific
Lipofectamin: SiLentFect	BioRad
RPMI-1640 medium	Invitrogen
Lipofectamin: X-tremeGENE™	(Roche) now Merck
Trypan blue 33.3%	Merck
Phosphate buffered saline PBS pH 7.2	Invitrogen
0.25% Trypsin-EDTA	Invitrogen

3.1.12 Animal Studies

Athymic nude Naval Medical Research Institute (NMRI) Foxn1nu/Foxn1nu mice were obtained from Janvier (Janvier-Labs, Le Genest-Saint-Isle, France).

Table 31 Chemicals and Equipment used for animal studies

Chemicals/ Equipment	Company
Digital caliper, RS PRO, 0-150 mm	RS Components GmbH
Disposable hypodermic needle, 100 Sterican	B.Braun Melsungen AG
Glucose 5% (G-5)	B.Braun Melsungen AG
Hypromellose	Sigma
Injekt®-F Tuberculin, Luer Solo	B.Braun Melsungen AG
Kodan® Tinktur forte	Schülke & Mayr GmbH
Scalpel blade, Bayha 22	C. Bruno Bayha GmbH
Sevorane (Sevofluran)	Abbvie
Sterofundin® ISO	B.Braun Melsungen AG
Tissue culture dish, 100 * 20 mm	Sarstedt
Tween-80	AppliChem
Weight scale, Scout Pro	Indivumed

Table 32 Substances used for animal studies

Solution	Substances	Final concentration	For 100 ml
DMSO for mice	DMSO Hypromellose solution	-	60 µl 740 µl (for 1 ml)
Formalin (4%)	Formaldehyde (37%) PBS	4%	10.8 ml 89.2 ml
Hypromellose solution	Hypromellose Tween-80 ddH_2O	0.5% 0.1%	0.5 ml 0.1 ml 100 ml
Napabucasin for mice	Napabucasin (10 mg/ml in DMSO) Hypromellose solution	0.8 mg/ml	60 µl 740 µl (for 1 ml)

Hypromellose solution should be filter-sterilized using Stericup® quick release, Vacuum driven disposable filtration system (Millipore). The volume of Napabucasin to be injected was determined individually for each mouse depending on weight (weight * 6.666 = µl to be injected). The final concentration to be injected is 5 mg/kg.

3.2 Methods

3.2.1 *In vivo* experiments

3.2.1.1 Mice strain, housing conditions and documentation

Female NMRI-Foxn1$_{nu}$/Foxn1$_{nu}$ mice used for the experiments were purchased from Janvier Breeding Center (Le Genest St. Isle, France). Mice were housed in the animal facility of the University Medical Center Göttingen in sterile cages, under standard conditions (22°C, 50% relative humidity, 12-h light/dark cycles) and provided with food and water *ad libitum*. The animal experiments were approved by the German Animal Welfare Act (reference number: 33.9-42502-04-17/2383).

3.2.1.2 Pharmacokinetics of Napabucasin

3.2.1.2.1 Determination of Napabucasin concentration

Firstly, to determine the Napabucasin concentration mice were randomly divided into three treatment groups: DMSO, Napabucasin (5 mg/kg) and Napabucasin (20 mg/kg). For xenograft transplantation, 2x10^6 SW1463 cells (logarithmic growth phase), were suspended in 100 µl L-15 containing 20% FBS, and subcutaneously injected into the right flank of 8 till 10 weeks old female nude mice (**Figure 3.1 C**, upper left picture). When the tumor reached a volume of about 150 mm³ (approximately 3 weeks after SW1463 cell injection) the mice were treated like indicated in **Figure 3.1 A**. After 14 days of treatment (oral application of either DMSO or Napabucasin once a day), the mice were euthanized and the primary tumors were excised, weighed, and frozen at -80 °C for following protein and RNA studies. One portion was fixed by formalin (37%) and afterwards embedded in paraffin for immunohistochemical analysis (**Figure 3.1 C**, lower pictures).

3.2.1.2.2 Testing Napabucasin as a treatment option

5 mg/kg Napabucasin was chosen to be the best working dose in this mouse model using SW1463 to form a tumor. In analogy to section 3.2.1.2.2 experimental tumors were induced by subcutaneous injection of 2x10^6 SW1463 cells in the right flank of 8 till 10 weeks old NMRI-Foxn1$_{nu}$/Foxn1$_{nu}$ mice. Mice were randomly assigned into five different treatment groups: DMSO (n=15), Napabucasin (n=15), Napabucasin + RT (n=15), Napabucasin + CRT (n=13) and DMSO+ CRT groups(n=14). The treatment protocol recapitulates clinical conditions described in Spitzner *et al.*,2014, i.e., fractionated doses of chemotherapy and irradiation, and included intraperitoneal injections of 5-FU (50 mg/kg) [147] and oral application of either DMSO or Napabucasin (5 mg/kg), each one hour before irradiation (**Fig. 3.1 B**). Irradiation was performed under permanent sevoflurane inhalation narcosis. Non-tumor parts were shielded with a lead block for vital organ protection, and tumors were irradiated daily with 1.8 Gy for 14 days (total dose of 25.2 Gy) using an X-ray irradiator (**Tab. 33**) (**Fig. 3.1 C**, upper pictures). After irradiation, a depot of G-15 and sterofundin was injected into the left and right flank of the

mice. Pictures at day 1, 5, 9 and 14 after start of treatment were taken to document the tumor development during the experiment. The treatment phase was followed by an observational period in which the re-growth of the tumor was studied.

Table 33 Parameters for irradiation

Parameter	Settings
Dose	1.8 Gy
KV	70
mA	25
Filter	3
Table high	315 mm
Irradiation time	1 min, 25 sec

3.2.1.3 Health status, documentation survival and tumor regrowth analysis

SW1463 tumor-bearing mice were monitored three times a week for health status, tumor size, body weight and movement abnormalities (large tumors could restrict the mobility of mice). Tumor volume (volume = (width² x length) / 2) was measured thrice weekly after tumor cell inoculation. According to the legal termination criterion, mice must be sacrificed when the tumor volume reached approximately 1,500 mm³ in size, when the animals show an onset of symptoms, including 20% weight loss within three measurements, destruction of the tumor, both self-induced and externally caused, general health abnormalities or after 3 months of observation period. The complete dissection of each animal was documented in a protocol together with representative pictures of different organs. For sample collection, tumors were excised, weighed, and stored at -80°C for further analysis. One part of the tumor tissue was collected and processed for RNA, DNA, and protein isolation. The other part was fixed by formaldehyde and paraffin-embedded for immunohistochemical analyses (**Fig. 3.1**, lower pictures). The Kaplan-Meier method was used to estimate the tumor regrowth and the overall survival between the experimental groups. In this study, full tumor regrowth was defined as a tripling in tumor size (450 mm^3).

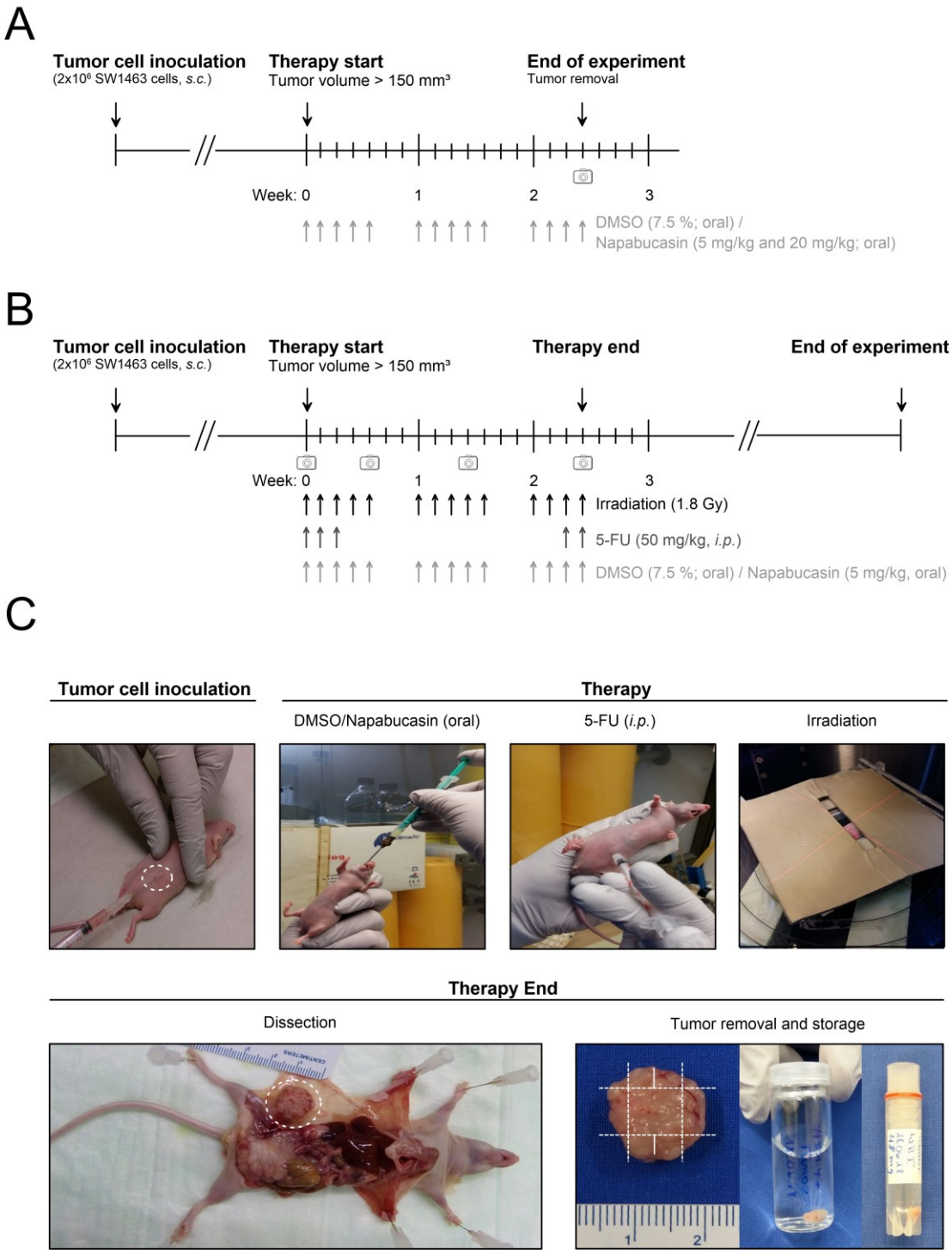

Figure 3.1 Treatment protocol for testing Napabucasin in a xenograft nude mice model.
A| and B| Schematic treatment protocol or **C|** Photographically visualized treatment protocol. SW1463 cells were injected subcutaneously into NMRI-Foxn1 nude mice. At a tumor volume of approximately 150 mm³, mice received their treatment which depend on the treatment group: group 1 (control): DMSO; group 2 (control): 5 mg/kg Napabucasin; group 3 (CRT): DMSO, 50mg/kg 5-FU, 14x irradiation at 1.8 Gy; group 4 (CRT): 5 mg/kg Napa, 50mg/kg 5-FU, 14x irradiation at 1.8 Gy; group 5 (RT): 5 mg/kg Napabucasin, 14 x irradiation at 1.8 Gy. Mice will be sacrificed when tumor volumes reached approximately 1500 mm³, when they show serious physically impairing symptoms or if they reach the end of the experiment which is defined as an observation period of 3 months.

3.2.2 Human studies

In this thesis, existing data sets were used and re-analyzed according to the experimental approaches. Therefore, biopsy collection, preparation, and gene expression profiling were performed as described [165,166]. This project was conducted by the Clinical Research Unit 179 (KFO179). It was approved by the Ethics Committee of the University Medical Center Goettingen together with informed consent obtained from all patients.

Summarized, biopsies (tumor and mucosa) were obtained from 207 patients with locally advanced rectal cancer during clinical staging procedure prior to any therapy. These pretherapeutic biopsies were collected between 2001 and 2014 at the Department of General, Visceral and Pediatric Surgery at the University Medical Center Goettingen as well as in 10 cooperating hospitals throughout Germany. All patients were treated with preoperative chemoradiotherapy, either within or according to the CAO/ARO/AIO-94 and -04 trials [68,90]. All analysis concerning these data were carried out by the institute of Medical Bioinformatics, University Medical Center Goettingen, 37073 Goettingen, Germany. The patients' characteristics were exported from the internal database (SecuTrial, iAS, Berlin, Germany) (**Tab. 34)**. Survival rates were conducted using the R package survival, computed using Kaplan-Meier analysis and tested with the Cox proportional hazards model.

Table 34 Clinical characteristics of rectal cancer patients

Characteristics	Cohort (n = 207)
Age	
Years, median (range)	63 (36 – 82)
Sex	
Male, *n* (%)	144 (69.6)
Female, *n* (%)	63 (30.4)
DFS	
Follow-up time, month, median (range)	37 (0 – 188)
Reported events, *n* (%)	52 (25.1)
UICC Staging (2010)	
ypUICC 0, *n* (%)	35 (16.9)
ypUICC I, *n* (%)	56 (27.1)
ypUICC II, *n* (%)	48 (23.3)
ypUICC III, *n* (%)	49 (23.7)
ypUICC IV, *n* (%)	19 (9.2)

DFS = disease-free survival, UICC = Union International Contre le Cancer, ypUICC refers to histopathologic assessment of the resected specimens after completion of preoperative chemoradiotherapy.

3.2.3 Cell culture

The Human colorectal cancer cell lines, LS411N, SW837, and SW1463 (ATCC, Manassas, VA) were cultured in their recommended medium, supplemented with 10% FBS and 2 mM L-glutamine. Mycoplasma contamination was routinely tested using MycoAlertVR Mycoplasma Detection Kit, and cross-contamination was surveyed by short tandem repeat (STR) profiling (Leibniz Institute DSMZ, Braunschweig, Germany). All used cell lines and their conditions are listed in **Tab. 29.** Generally, the recommended cell culture medium and all other substances needed for cultivation of the cells should be pre-heated at 37°C prior usage.

3.2.3.1 Unfreezing

Frozen cells were thawed at 37°C in a water bath. After defrosting, cells were resuspended in 10 ml of their recommended pre-heated cell culture medium and centrifuged for 5 min at 800 rpm. The supernatant was discarded, the cell pellet was resuspended in fresh medium and cells were transferred into a T25 flask. To remove dead and detached cells, the medium was exchanged after 24 hours.

3.2.3.2 Freezing

To freeze cells, the medium was discarded, and cells were washed with PBS. Afterward, cells were harvested using 0.25% Trypsin-EDTA (37 °C, 5 min) to digest cell-cell junctions. The detached cells were transferred in 15 ml tubes and centrifuged for 5 min at 800 rpm. The supernatant was discarded, the cell pellet was resuspended in the respective freezing medium (cell medium with an additional amount of 10% DMSO and 20% FBS) and transferred to cryotubes. Afterward, the cryotubes were stored in freezing containers by -80°C to allow gradual cooling (1 degree per minute). After at least 100 min, cryotubes were transferred -150°C for long time storage.

3.2.3.3 Maintenance, subculture and seeding of adherent cells

Cells growing in log-phase were subcultured at 70 - 80% confluence by washing with PBS, followed by treatment with 0.25% Trypsin-EDTA (37 °C, 5 min). The detached cells were resuspended in their respective medium and centrifuged at 800 rpm for 5 min. The cell pellet was resuspended in fresh medium, and cells were counted using a counting chamber. Before counting, a portion of the cell suspension was diluted with trypan blue solution (1:10) to make dead cells visible (dead cells - stained blue, living cells - white/transparent). 10 µl of this solution was filled in the counting chamber, and white/transparent cells inside the four large corner squares were counted. To calculate the cell number per ml the average of cells in the four squares was estimated and multiply with 10^4 and the dilution factor from trypan blue (1:10 dilution = 10). After cell counting, cells were seeded in their recommended growth ratio (**Tab. 29**) or for experiments in the appropriated cell numbers (**Tab. 36**). If the cells did not reach 70% confluence, the used medium was exchanged by new medium.

3.2.3.4 Treatment

Before RNA or protein extraction and during various assays cells were treated with different stimuli or inhibitors (**Tab. 35**). The respective reagent was diluted in pre-heated medium at the established concentration for each cell line (**Tab. 29**).

Table 35 Established concentrations and incubation times for each reagent

Substance	Cell line	Concentration	Incubation time
DAPT	LS411N SW837 SW1463	2.5 µM 5 µM 5 µM	48 h 72 h 72 h
Hyper-IL-6*	LS411N SW837 SW1463	20 ng/ml	16 h
Napa	LS411N SW837 SW1463	1000 nM 500 nM 1000 nM	1 h
rhIL-6**	LS411N SW837 SW1463	100 ng/ml 100 ng/ml 50 ng/ml	10 min 20 min 10 min
Ruxo	LS411N SW837 SW1463	250 nM 250 nM 100 nM	16 h
Tocilizumab*	LS411N SW837 SW1463	20 ng/ml 20 ng/ml 10 ng/ml	16 h

*Concentrations and timepoints were previously established[167]; ** For DLR assay= incubation time 16 h

3.2.4 Transfection methods

3.2.4.1 Nucleofection (Amaxa)

Upon nucleofection, cells were temporarily permeabilized by an electric field to absorb nucleic acids [168]. Cells were transfected using Nucelofactor™ 2b device and respective Amaxa™ Cell Line Nucleofector™ kits according to the manufacturer's recommendation. Briefly, cells were washed with PBS, detached using 0.25% Trypsin-EDTA and the cell number was calculated using a counting chamber. For one transfection approach, 1* 10^6 cells were resuspended in 100 µl of their appropriate cell-type-specific Nucleofector® solution. Afterwards, 1.25 µl siRNA was mixed with this cell solution and the mixture was then transferred into a cuvette (each sample should be prepared separately, to avoid storing cells longer than 15 min in Nucleofector® solution). The cuvette was inserted into the Nucleofector® device and the cell-type-specific program was used to achieve the nucleofection (**Tab. 36**). Immediately after transfection, the cells were removed from the cuvette using a transfer pipette and 1 ml of pre-warmed RPMI medium was added. After 15 min incubation at 37°C, cells were

centrifuged at 700 rpm for 5 min, the cell pellet was resuspended in recommended medium and cell solution was finally transferred into a culture dish or flask. 24 h after transfection medium was exchanged.

3.2.4.2 Lipid-based transfection

For RNA interference studies the desired siRNA was incorporated into the cells using lipid-based transfection. This transfection method is based on positively charged liposomes that form complexes with the negatively charged phosphate backbone of nucleic acids. These Lipid-DNA complexes enter the cells through endocytosis [169].

One transfection consisted of 100 µl serum-free medium (M0 medium) per well, in which first 0.5 µl siRNA (corresponding to 10 ng) was diluted and then 6 µl lipid was pipetted. This reaction mix was incubated for 5 min at room temperature to enable the binding of siRNA to the liposomes. In the meantime, cells were washed with PBS, detached using 0.25% Trypsin-EDTA and the cell number was calculated using a counting chamber (for details see **Tab. 36**) The siRNA/lipid solution was pipetted dropwise to the cells.

Table 36 Transfection details for different assays

Assay	Cell line	Cell number	Transfection method/ program
Colony formation assay	LS411N SW837 SW1463	2,000,000	Amaxa,L-Kit, T-20 Amaxa, V-Kit, T-30 RNAiMAX
Cellular viability assays	LS411N SW837 SW1463	5,000 6,000 5,000	BioRad SiLentFect RNAiMAX RNAiMAX
Dual luciferase assay	LS411N SW837 SW1463	200,000 500,000 100,000	X-tremeGENE HP Amaxa, V-Kit; T-30 X-tremeGENE HP

3.2.5 Molecular biology

3.2.5.1 Total RNA isolation from human cell lines and animal tissue

The RNeasy® Mini Kit was used for purification of total RNA from human CRC cell lines and animal tissue (mice tumors) according to the manufacturer instructions. Briefly, for cell lysis, the medium was discarded, and cells were washed with PBS. Subsequently, 350 µl RLT buffer was added to the cell culture flask/dish (< $5*10^6$ cells = 350 µl RLT buffer, $5*10^6$ - $1*10^7$ cells = 600 µl RLT buffer) and cells were harvested using a cell scraper. The resulting lysate was pipetted directly into a QIAshredder spin column placed in a 2 ml collection tube, and centrifuged for 2 min at full speed and at RT. For animal tissue, the tumor sample was mixed with the appropriated amount of RLT buffer (350 µl) put directly into the QIAshredder spin column and were centrifuged, too.

The homogenized lysate (flow-through into the 2 ml tube) was mixed with 1 volume (350 µl) of 70% ethanol by pipetting. This solution was transferred into a RNeasy spin column placed in a 2 ml collection tube and centrifuged for 30 s at 10,000 rpm (in this step, the RNA binds to the membrane in the column). The flow-through was discarded and 350 µl of RW1 buffer was added to the column before re-centrifugation for 20 s at 10,000 rpm. To remove unwanted DNA, 80 µl of DNase solution (10 µl DNase mixed with 70 µl buffer) was added to the membrane and was incubated for 15 min at RT. Afterwards, 350 µl of RW1 buffer was added to the column before centrifugation for 30 sec at 10,000 rpm. The flow-through was discarded and the membrane was washed two times using 500 µl of RPE buffer and centrifugation for 30 sec (first washing step) or 2 min (second washing step) followed by discarding the flow-through. After the collection tube has replaced the column was centrifuged for 1 min at full speed. For elution of the RNA, 25 µl of RNAse-free water was added directly to the membrane. The column was centrifuged for 1 min at 10,000 rpm. Note that the RNA was contained in the eluate. The total RNA amount was measured using a Nanodrop and RNA stock concentration was diluted to 100 ng/µl. For qPCR analysis, the RNA was further diluted to a concentration of 10 ng/µl. RNA samples were stored at -80 °C.

3.2.5.2 RT-qPCR

A RT-qPCR was performed to analyze the relative expression of target genes using the SensiFAST™ SYBR® No-ROX One-Step PCR System according to the manufacturer's instructions. All steps were done on ice. RT-qPCR was performed in triplicates in a reaction volume of 10 µl as well as a non-template control (NTC) to exclude contaminations.

For each well a reaction mix of the following reaction components was prepared:

Table 37 Composition of RT-qPCR reaction mix

Substances	1 x reaction mix
PCR water	2.9 µl
Reverse Transcriptase	0.1 µl
RiboSafe RNase Inhibitor	0.2 µl
RNA template (10 ng/µl)	1 µl
Sensifast (2x)	5 µl

Subsequently, 9.2 µl of the reaction mix was pipetted into each well. For the primer-working solution (final concentration: 400 mM) 10 µl of the forward primer and 10 µl of the reverse primer were mixed with 80 µl of PCR water. All primers used in this study are listed in **Tab. 25**. The 96-well plate was covered with an adhesive film and was centrifuged for 1 min at 3000 rpm before placing it into the C100 Thermocycler.

Table 38 3-step-cycling for RT-qPCR

Cycles	Temperature	Time	Notes
1	45 °C	10 min	Reverse transcription
1	95 °C	2 min	Polymerase activation
40	95 °C	5 s	Denaturation
	60 °C	10 s	Annealing/Extension
	72 °C	5 s	

The resulting CT values were used to calculate the relative expression of the evaluated gene. Therefore, the CT values were normalized to the house-keeping gene *Hprt* and were afterwards analyzed using the ΔΔCt method (Livak and Schmittgen, 2001).

3.2.5.2.1 Optimization of new primers

To establish new RT-qPCR primes the model of relative quantification [170] was used. A standard RT-qPCR was conducted as described before (see section 3.2.5.2). As RNA templates, RNA samples from different CRC cell lines were pooled (SW837, SW1463, LS411N, SW480). To generate a standard curve, different RNA template concentrations (100 ng, 10 ng, 1 ng and 0.1 ng) for each reaction mix were used. For determination of the primer efficiencies *Cq cycles* versus the *log of starting quantity* were automatically plotted to calculate the slope. The corresponding primer efficiencies were calculated according to the equation $E= 10^{[-1/slope]}$ [171]. The optimal primer efficiency was defined between approx. 90 and 110%.

Melting curve analysis has to result in a single product-specific melting temperature without any additional peaks. Additional peaks can be a hint for primer-dimers that were generated during amplification cycles. The specificity of the primers was additionally checked using agarose gel electrophoresis (see section 3.2.5.2.2). If electrophoresis results in a single product (single band) with the desired length, the primes were used for further experiments.

3.2.5.2.2 Agarose gel electrophoresis

To separate DNA fragments by size agarose gel electrophoresis was used. For this 1% agarose gels were prepared in 1x TAE buffer. The agarose mix was heated to dissolve the agarose in the buffer. When the solution has cooled to 50-60 °C it was mixed with 4 µl gelRed® (nucleic acid dye) and poured it into the gel tray. Samples were mixed with one fifth of 6x DNA loading buffer and loaded onto the gel as well as a 100 bp DNA ladder to determine the size of the DNA Fragments. DNA fragments were separated at 120 V for 30 min. Afterwards, the dyed nucleic acids were visualized using a transilluminator.

3.2.6 RNA sequencing analysis of CRC cells with or without Hy-IL-6 stimulation

To silence the STAT3 expression, SW837 and SW1463 cells were transfected with either siRNA targeting STAT3 or a scrambled siRNA as negative control (siCtrl.) (see **Tab. 24** for siRNA sequences), with three independent biological replicates. To rule out that siRNAs

obtained from different companies generate different experimental outcome and to minimize the possible variance between the replicate's siRNAs obtained from two companies (Dharmacon and Qiagen) were used. The samples were treated either without further stimulation or incubation with 20 ng/ml Hy-IL-6 for 16 hours (for detailed transfection and stimulation protocol see section 3.2.4). After incubation, cells were washed with PBS and harvested for RNA analysis and Western blot analysis.

The sequencing of total RNA samples was conducted at the NGS-Integrative Genomics Core Unit (NIG), University Medical Center Goettingen. Briefly, the quality and integrity of RNA were assessed with the Fragment Analyzer from Advanced Analytical by using the standard sensitivity RNA Analysis Kit (DNF-471). All samples selected for sequencing exhibited an RNA integrity number > 8. RNA-Seq libraries were generated using the TruSeq RNA library kit. Libraries were pooled and sequenced on the Illumina HiSeq 4000 (SE; 1 x 50 bp; 30-35 Mio reads/sample).

RNA-Seq data were analyzed at the Core Facility, Medical Biometry and Statistical Bioinformatics, Department of Medical Statistics, University Medical Center Goettingen.
There initial quality control steps (using FastQC; [172]) the alignment of the reads to the human reference genome (assembly GRCh38) (using STAR version 2.5.2b; [173]) and quality control on the input data and the alignment statistics (using Multiqc version v1.6. dev0; [174]) were performed. In addition, they generated the transcription level quantifications (using ensemble annotation release 93 and the software RSEM version 1.2.19; [175]) and edgeR (version 3.26.6; [176]) was used to model gene expression with transfection kit and the experimental conditions: stimulation, knockdown (KD), combined treatment (stimulation and KD) as factors.

All results were summarized in tables displaying genes with effect size and significance annotation. The resulting *P*-values were adjusted for multiple testing using Benjamini-Hochberg to control for the false discovery rate (FDR).
Differentially expressed genes were identified for three conditions (siCtrl. vs. siCtrl. + Hy-IL-6; siCtrl. vs. siSTAT3; siCtrl. + Hy-IL-6 vs. siSTAT3 + Hy-IL-6) according to the FDR cut-off of 0.01. The number of differentially up- and down-regulated genes was calculated and depicted as volcano plots.

Venn diagram analysis and heatmaps were generated using web-based tools (**Tab. 6**). The sequencing data and abundance measurement files have been submitted to the NCBI Gene Expression Omnibus (GEO) under the accession number GSE139455.

3.2.6.1 Opposite Direction analysis

To filter the resulting gene lists more stringently a new way to analyze these lists was established in this study. The Opposite Direction analysis (ODA) identified genes that were significantly upregulated (FDR cut-off 0.01) upon Hy-IL-6 stimulation of cells and, inversely, downregulated upon STAT3 silencing or *vice versa*.

3.2.7 Protein biochemistry

3.2.7.1 Preparation of total cell extracts for Western blot analysis

Total cell extracts were prepared from CRC cells to investigate the expression of various proteins by Western blotting. Before lysis, the medium was discarded, and cells were washed once with ice-cold PBS. Afterward, 150 µl of NP-40 lysis buffer (for detailed composition see section 3.1.7.1 and **Tab. 9 -10**) were used per 1 x 10^6 million cells. For lysis, the cells were scraped, and the cell lysate was transferred to a 1.5 ml reaction tube which was incubated for 45 min on ice. The lysate was centrifuged at 10,000 rpm at 4°C for 10 min to eliminate cell debris (cell debris = pellet). The total cell extracts (supernatant) used for Western blot analysis were subsequently mixed with one fourth of 5x sample buffer (for detailed composition see **Tab. 19**) and boiled for 5 min at 95 °C. The samples were either stored at -20°C or were directly used for SDS-PAGE.

3.2.7.2 Isolation of purified proteins from three cellular fractions: cytosol, nucleus, and chromatin

Protein extracts from cytosol, nucleus and chromatin were prepared from CRC cells to investigate the expression of various proteins in different cellular compartments by western blotting. Before lysis, the medium was discarded, and cells were washed once with ice-cold PBS. Afterwards, 500 µl per well (6-well plate) of buffer A (for detailed composition see section 3.1.7.1 and **Tab. 13**) were added directly to the cells. After 5 min incubation on ice, cells were scraped and transferred to a 1.5 ml reaction tube. Cells were subsequently centrifuged at 1,500 g for 5 min at 4°C. The supernatant (contains the cytoplasmic protein fraction) was transferred into a new 1.5 ml reaction tube. The pellet (contains nuclei) was washed with buffer A by light tapping. Subsequently, 200 µl of buffer B (for detailed composition see 3.1.7.1 and **Tab. 14**) was added to the pellet, the lysate was incubated for 30 min on ice following centrifugation at 2,000 g for 5 min at 4º C. The supernatant (containing the soluble nuclear fraction) was transferred into a new 1.5 ml reaction tube. The pellet (containing the insoluble chromatin fraction) was mixed with additional 200 µl of buffer B and sonicated (time: 10 sec., Amplitude 42%, pulse 000.5 s/000.5 s). All lysates (cytoplasmic, soluble nuclear and insoluble chromatin fraction) used for Western blot analysis were subsequently mixed with one fourth of 5x sample buffer (for detailed composition see **Tab. 19**) and boiled for 5 min at 95 °C. The samples were either stored at -20°C or were directly used for SDS-PAGE.

3.2.7.3 Preparation of total cell extracts for EMSA experiments

Preparation of total cell extracts was required for EMSA experiments. Before lysis, the medium was discarded, and cells were washed once with ice-cold PBS. Afterward, cells were incubated with 50 µl cytoplasmic extraction buffer per well (6-well plate) (for detailed composition see section 3.1.7.2 and **Tab. 15-16**) on ice for 5 min. Afterwards, they were

harvested using a cell scraper and transferred to a 1.5 reaction tube. The extracts were centrifuged at 16,000 g for 15 sec at 4°C. The supernatant (containing the cytosolic protein fraction) was transferred into a new 1.5 reaction rube and centrifuged again for 15 sec at 4°C and 16,000 g. The resulting supernatant was collected and placed on ice. Subsequently, the pellet was incubated with 50 µl nuclear extraction buffer (for detailed composition see 3.1.7.2 and **Tab. 17-18**) on ice for 30 min following centrifugation for 15 min at 4°C at 16,000 g. The supernatant (containing the nucleic protein fraction) was transferred to a 1.5 ml reaction tube. Finally, the cytosolic protein fraction was mixed with the same amount of nucleic protein extraction. The protein extracts were stored at -80°C until further use.

3.2.7.4 Protein extraction of tumor samples

Protein extracts of tumor samples were prepared to investigate the expression of various proteins by Western blotting. Depending on the weight of the tumors, the amount of RIPA buffer (for detailed composition see section 3.1.7.1 and **Tab. 11-12**) was determined: 20 µl RIPA buffer per 1 mg tumor. For lysis, the calculated amount of RIPA buffer was added together with one stainless steel bead to each sample. Tissues were lysed using a Tissuelyser (program: 3’ 50 Hz, 2’ 40 Hz). Thereafter, beads were removed, and the samples were incubated for 10 min on ice before they were sonicated (time: 10 sec., amplitude 42%, pulse 000.5 s/000.5 s). After sonication, lysates were incubated on ice for 10 min following centrifugation for 20 min at 10.000 g. The supernatant was transferred into a new 1.5 ml reaction tube and was subsequently mixed with one fourth of 5x sample buffer (for detailed composition see **Tab. 19**) and boiled for 5 min at 95 °C. The samples were either stored at -20°C or were directly used for SDS-PAGE.

3.2.7.5 Protein concentration determination

3.2.7.5.1 Protein determination according to Bradford

The binding of the Bradford dye to proteins causes a shift in the absorption maximum of the dye from 465 to 595 nm. This increased absorption at 595 nm could be measured spectroscopically and used to determine the protein concentration of samples [177].

First, a BSA standard series was prepared with concentrations ranging from 0 to100 µg/ml BSA. This series was used to quantify the amount of protein in each sample and to subtract any background. The protein samples were diluted 1:50 in ddH_2O before measurement. 50 µl of each standard dilution and the dilution solutions of the samples were pipetted into a 96-well microtiter plate as technical replicates. Subsequently, 200 µl Roti®-Quant (2:5.5) was added to each well. After 5 min incubation at RT the optical density of the protein solution at an absorbance of 595 nm was measured using Victor™ X4 Multilabel Plate Reader. The Protein concentrations of the unknown samples were calculated using the slope of the regression line.

3.2.7.5.2 Protein determination according to the Bicinchoninic acid assay

The Bicinchonic acid assay (BCA) was developed by Paul K. Smith (Measurement of Protein Using Bicinchoninic Acid, 1985). It is based on the conversion of Cu^{2+} to Cu^{+} under alkaline conditions. The Cu^{+} is then detected by reaction with BCA (The Bicinchoninic Acid (BCA) Assay for Protein Quantitation John M. Walker). By adding bicinchoninic acid it chelates with the Cu^{+} ion, forming a purple-coloured product that strongly absorbs light at a wavelength of 562 nm, which is proportional to the amount of protein in each sample.

The assay is suitable to determine the protein concentration after RIPA buffer-based Protein lysis. The Pierce® Bicinchoninic Acid Assay (BSA) protein Assay Kit was used according to the manufacturer's instructions. Briefly, a BCA standard series was prepared with concentrations ranging from 0 to 2,000 µg/ml BSA. This series was used to quantify the amount of protein in each sample and to subtract any background. The protein samples were diluted 1:20 in ddH_2O before measurement. 25 µl of each standard dilution and the dilution solutions of the samples were pipetted into a 96-well microtiter plate as technical replicates. Subsequently, 200 µl of premixed working reagent (1:5) was added to each well. The plate was incubated for at least 30 min, at 37°C in the dark. Afterward, the optical density of purple-coloured product at an absorbance of 562 nm was measured using Victor™ X4 Multilabel Plate Reader. The protein concentrations of the unknown samples were calculated using the slope of the regression line.

3.2.7.6 Sodium dodecyl sulfate polyacrylamide gel electrophoresis

Sodium dodecyl sulfate polyacrylamide gel electrophoresis (SDS-PAGE) was used to separate denatured and reduced proteins according to their molecular weight due to a polyacrylamide gel. Large proteins move slower through the electric field than small proteins. Samples were loaded onto a (10% or 7.5%) polyacrylamide stacking gel and were afterwards separated in a 10% polyacrylamide resolving gel (preparation and composition of gels see **Tab. 21**). In addition, 2 µl of prestained protein ladder was added to each gel to estimate the size of each band. The separation was performed using gel chambers filled with 1 x SDS-PAGE running buffer (for detailed composition see section 3.1.7.3) at 20 mA/gel for approximately 2 hrs.

3.2.7.7 Semi-dry Western Blot

For identification of proteins with specific antibodies, separated proteins were transferred onto a PVDF membrane using a semi-dry western blot system. The PVDF membrane was activated using 100% methanol. The membrane together with the gel and six Whatman paper were equilibrated in 1x Western blot transfer buffer (for detailed composition see section 3.1.7.3). The membrane was placed on top of three Whatman papers. The gel was placed on the membrane and three Whatman paper were put on top of the gel. The transfer was conducted at 1 mA per cm^2 of membrane for 1 h.

3.2.7.8 Immunostaining

Following protein transfer, membranes were incubated for 1 h in blocking solution (for composition see **Tab. 19**) to block unspecific protein binding sites for antibodies. Afterwards, membranes were washed three times (in total 15 min) with TBST buffer (for detailed composition see section **Tab. 19**) and incubated with the respective primary antibody (for details see **Tab. 22**) over night at 4 °C continuously shaking.

On the next day, membranes were washed thrice in TBST buffer for 5 min each to eliminate any unbound antibodies. Afterwards, membranes were incubated with horse-radish peroxidase (HRP) conjugated secondary antibodies, that detect the constant region (Fc region) of the respective primary antibodies (for details see **Tab. 23**) for 2 h at RT. The antibody-tagged protein bands were detected by addition of 100 µl HRP Substrate (ECL solution), which was converted by HRP on secondary antibodies in proportion to the number of bound antibodies. The detection was performed by the CCD camera ImageQuant LAS4000 mini.

3.2.8 Functional *in vitro* assays

3.2.8.1 Electrophoretic mobility shift assay

Electrophoretic mobility shift assay (EMSA) was used to assess the DNA binding ability of STAT3 and was performed, as described in [178]. Note that the EMSA experiment was performed in close cooperation with Prof. Dr. mult. Thomas Meier (Department of Psychosomatic Medicine and Psychotherapy, German Centre for Cardiovascular Research, Georg-August University, 37073 Goettingen, Germany). Briefly, SW837 cells grown on 10 cm dishes were either stimulated with 20 ng/ml Hy-IL-6 for 30 min or left untreated. Whole-cell extracts were prepared as described in section 3.2.7.3. Lysates of unstimulated or IFNγ stimulated HeLa cells were used as positive control for GAS binding (stimulated with 50 ng/ml for 30 min). For The sequences of the control probe M67, the native and the mutated RBPJ fragment were listed in **Tab. 28**. [33P]-labelled duplex oligonucleotide probes with 5 bp T overhangs at their 5' end, were generated by an end-filling reaction catalyzed by the Klenow fragment. For the end-filling reaction the following substances were mixed and were incubated for 25 min at RT.

Table 39 Composition of the end-filling reaction for EMSA

Substances	Concentration/amount
Klenow fragment	5 units
10 x Eco-Pol buffer	5 µl
Annealed oligonucleotides	0.1 ng
[33P]-labelled ATP	8 µl

After incubation, an excess of non-radioactive dNTPs (6.5 mM od each dNTP) was added, and the reaction mix was incubated for 5 min at RT. The reaction was stopped by addition of 1 µl of 0.5 mM EDTA solution. Free nucleotides were removed by centrifugation at 700 xg for 3 min at RT using an Illustra-MicroSpin-G-25 column. For competition experiments, a 750-fold molar excess of unlabeled native RBPJ was added to the reaction and incubated for 15 min at room temperature. 4 µl of cellular extracts were incubated with 8 µl of EMSA reaction buffer containing 1 ng of the [^{33}P]-labelled probes. Afterwards the samples were loaded onto equilibrated non-denaturing 8% TBE- acrylamide: bisacrylamide gels (29:1) which consists of: 12% Rotiphorese, 2.4% TBE buffer, 2% APS and 0.2% TEMED. Electrophoretic separation was conducted at 400 V in 0.25x TBE buffer. Later, the DNA-binding activity was visualized on vacuum-dried gels (gel was pressed against Whatman paper and was than vacuum-dried) using a laser phosphoimaging system (Typhoon FLA 9500) including the TINA software.

3.2.8.2 Colony Formation Assay

The effect of diverse pathway perturbations on sensitivity to RT and/or CRT was tested using a colony formation assay (CFA), as standard in the field [147,179]. The colony formation assay was specifically used to determine the capacity of cells to form colonies under different treatments. A colony is defined as an accumulation of at least 50 cells [179]. In general, cells were seeded and allowed to adhere for approximately 8 hrs. For CRT experiments, cells were pre-incubated with 3 µM of 5-FU overnight and subsequently irradiated at 1, 2, 4, 6, and 8 Gy of X-rays. For RT, cells were subsequently irradiated (0, 1, 2, 4, 6, 8 Gy) 24 h after seeding.

For pre-treatments Napabucasin was administered for 1 h, Hy-IL-6, Tocilizumab or Ruxolitinib for 16 h and DAPT for 24-72 h (**Figure 3.2 A**) prior irradiation. For RNA Interference studies the cells were transfected with either control siRNA or siRNA targeting the respective protein. After cell line specific incubation time (**Tab. 35**) cells were treated with or without 5-FU prior to irradiation (**Figure 3.2 B**). In combination experiments, the cells are first transfected with respective siRNA and then treated with the appropriate inhibitor (**Figure 3.2 C**).

Followed irradiation, the medium was replaced with fresh medium to eliminate 5-FU, and all other substances. After cell line-specific incubation times (12-19 days), colonies were stained with Mayer's hemalum solution, counted, and analyzed according to Franken *et al.* [179]. Only colonies consisting of at least 50 cells were included into the evaluation. For determinationthe colony forming capacity, all fractions were normalized to the plating efficiency (PE) of the 0 Gy control plate. The PE is the ratio of number of counted colonies to the number of seeded cells [179].

$$PE\ [\%] = \frac{number\ of\ colonies\ formed\ (0\ Gy)}{number\ of\ seeded\ cells\ (0\ Gy)} * \ 100\ \%$$

After determination of the plating efficiency, surviving fractions (SF) were calculated by using following equation [179]:

$$SF\ [\%] = \frac{counted\ colonies\ after\ treatment\ (x\ Gy)}{seeded\ cells\ (x\ Gy) * PE}$$

For analysis, SF data were viewed dependent on the irradiation dose and additionally fit by linear regression [179]. Confidence intervals and R^2 change are included in the regression.

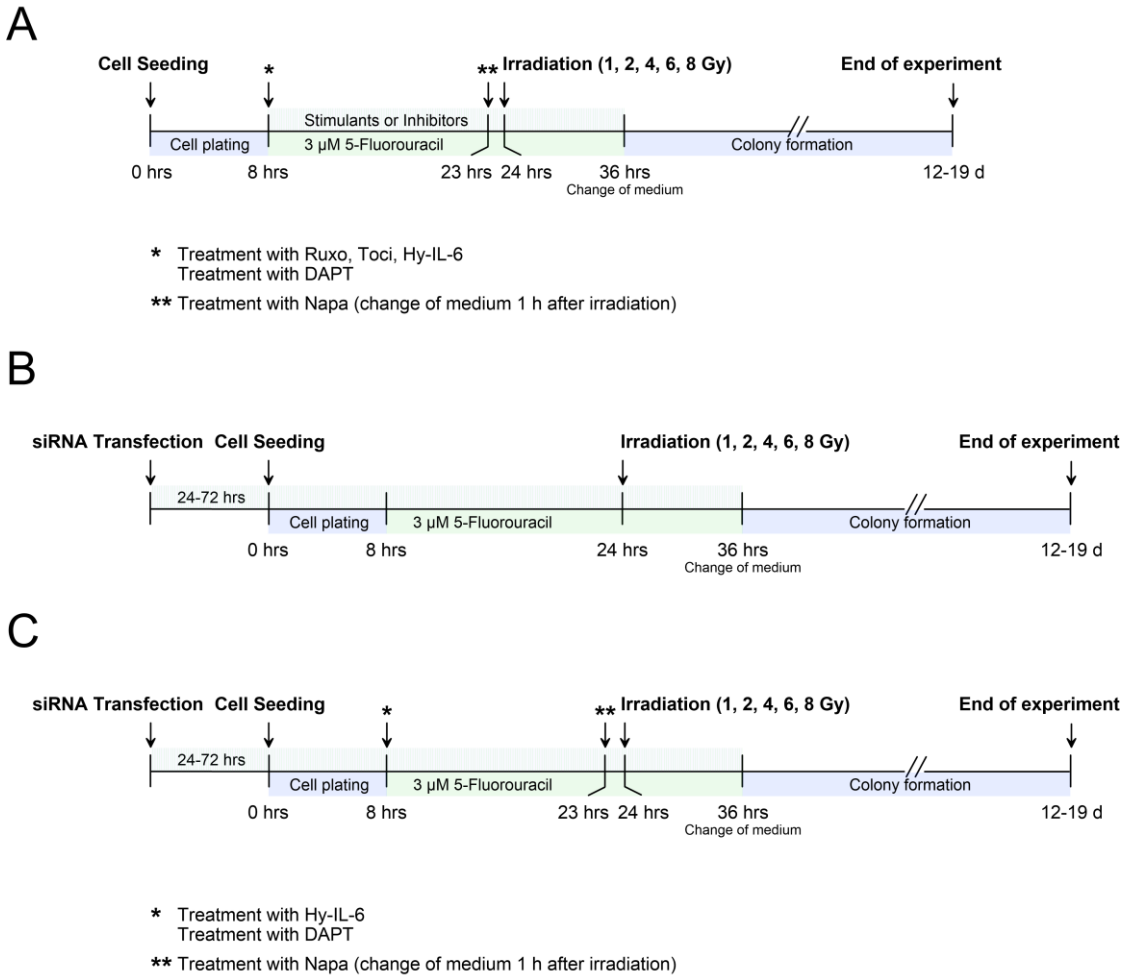

Figure 3.2 Experimental flow for CFA experiments after different treatments.
A| - C| Schematic treatment protocol for CFAs with indicated substances and incubation times either for stimulants and inhibitors (A), siRNAs (B) or a combination of both (C).

Details for transfection are listed in **Tab. 36** and described in section 3.2.4. In addition, detailed experimental conditions for each CFA experiment are shown in **Tab. 40**.

Table 40 Detailed conditions for CFA experiments

Cell line	Treatment	Incubation time	Cell number			
			0, 1, 2 Gy	4 Gy	6 Gy	8 Gy
LS411N	siCtrl. / siSTAT3	72 h*	500	1,000	1,500	2,000
	DMSO / Napa	1 h	500	1,000	1,500	2,000
	Hy-IL-6	16 h	500	1,000	1,500	2,000
	Toci	16 h	500	1,000	1,500	2,000
	DMSO/ Ruxo	16 h	500	1,000	1,500	2,000
	STAT3-WT	24 h*	500	1,000	1,500	2,000
	STAT3-Y705F	24 h*	500	1,000	1,500	2,000
	STAT3-S705A	24 h*	500	1,000	1,500	2,000
	STAT3-Y705F/S727A	24 h*	500	1,000	1,500	2,000
	siRBP + DMSO	48 h*	500	1,000	1,500	2,000
	siCtrl. + DAPT	48 h*	500	1,000	1,500	2,000
	DMSO / DAPT	48 h*	500	1,000	1,500	2,000
	siRBPJ + DAPT	48 h*	500	1,000	1,500	2,000
SW837	siCtrl. / siSTAT3	96 h*	750	1,500	2,250	3,000
	siCtrl. / siRBPJ	72 h*	750	1,500	2,250	3,000
	siCtrl. / siSTAT3 + siRBPJ	96 h*	750	1,500	2,250	3,000
	DMSO / Napa	1 h	750 / 1,500	1,500 / 3,000	2,250 / 4,500	3,000 / 6,000
	siCtrl. + DMSO	96 h* / 1 h*	750	1,500	2,250	3,000
	siSTAT3+ DMSO	96 h* / 1 h*	750	1,500	2,250	3,000
	siCtrl. + Napa	96 h / 1 h	1,500	3,000	4,500	6,000
	siSTAT3 + Napa	96 h / 1 h	1,500	3,000	4,500	6,000
	Hy-IL-6	16 h	750	1,500	2,250	3,000
	Toci	16 h	750	1,500	2,250	3,000
	DMSO / Ruxo	16 h	+750	1,500	2,250	3,000
	DMSO / DAPT	72 h	750	1,500	2,250	3,000
	siRBPJ + DMSO	72 h*	750	1,500	2,250	3,000
	siCtrl. + DAPT	72 h*	750	1,500	2,250	3,000
	siRBPJ + DAPT	72 h*	750	1,500	2,250	3,000
SW1463	siCtrl. / siSTAT3	72 h†	750	1,500	2,250	3,000
	DMSO / Napa	1 h	750 / 1,500	1,500 / 3,000	2,250 / 4,500	3,000 / 6,000
	Hy-IL-6	16 h	750	1,500	2,250	3,000
	Toci	16 h	750	1,500	2,250	3,000
	DMSO / Ruxo	16 h	750	1,500	2,250	3,000
	siCtrl. / DMSO	72 h†	750	1,500	2,250	3,000
	siRBPJ + DMSO	72 h†	750	1,500	2,250	3,000
	siCtrl. + DAPT	72 h†	750	1,500	2,250	3,000
	siRBPJ + DAPT	72 h†	750	1,500	2,250	3,000

STAT3-WT = expression vector for wild-type STAT3, STAT3-Y705F = expression vector for mutated STAT3 (mutated at tyrosine 705), STAT3-S727A = expression vector for mutated STAT3 (mutated at serine 727), STAT3-Y705F/S727A = expression vector for mutated STAT3 (mutated at tyrosine 705 and serine 727), * = Nucleofection, † = lipid-based transfection

3.2.8.3 Using Dual luciferase reporter assay to determine STAT3 transcriptional activity after different treatments.

For determination of the STAT3 transcription factor activity under different pathway perturbation, a dual luciferase reporter assay (DLR) was performed. Therefore, the Cignal Reporter Assay Kit (used for SW837 cells) and the Dual-LuciferaseVR Reporter Assay System (used for LS411N and SW1463 cells) were used according to the manufacturers' instructions and as described in [147].

In the DLR assay, the activities of Firefly and *Renilla* luciferase were measured. The used DLR system contains two reporter plasmids each coding for a luciferase to measure transcriptional activity. One of those plasmids' drives the expression of *Renilla* luciferase (Ren-Luc), fused to a constitutive active promoter (**Fig. 3.3 A**, *left panel*), which cause *Renilla* luciferase to be expressed in all cells unregulated. Moreover, the expression of *Renilla* luciferase served as a transfection efficiency control and for normalization (Farr and Roman, 1992). The other plasmids allow for the expression of Firefly-luciferase driven in the presence (**Fig. 3.3 A**, *middle panel*) or absence (**Fig. 3.3 A**, *right panel*) of the STAT3 transcriptional response element (Ctrl. -Luc or STAT3-Luc, respectively). Ctrl. -Luc allows for further normalization of STAT3-regulated expression of Firefly-luciferase. Ren-Luc was co-transfected with either Ctrl. -Luc or STAT3-Luc into untreated or previously treated STAT3-wild-type (WT) cells (**Fig. 3.3 B**).

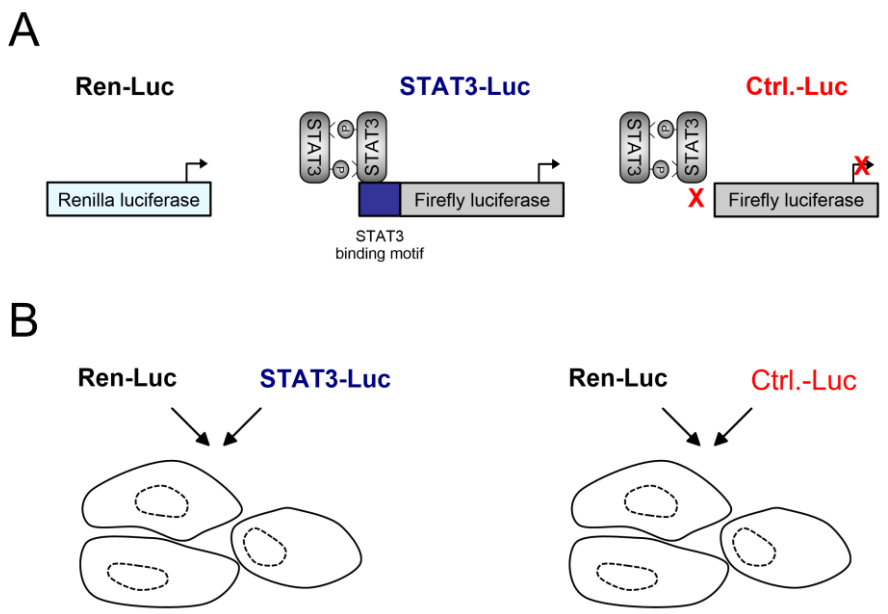

Figure 3.3 Principle of DLR assays.
A| DLR assays based on two different luciferase reporter plasmids. One of those plasmids' codes for *Renilla* luciferase (Ren-Luc), fused to a constitutive active promotor (*left panel*). Whereas the other plasmid codes for Firefly luciferase either under the control of an STAT3 binding domain (STAT3-Luc) or as a control without expression regulating binding domain (Ctrl. -Luc). **B|** Cells were co-transfected with Ren-Luc reporter plasmid together with either STAT3-Luc (*left panel*) or Ctrl. -Luc (*right panel*).

The standard DLR protocol was adapted individually for each CRC cell line (LS411N, SW1463 and SW837) (**Figure 3.4)**. All details including inhibitor incubation times, individual cell numbers per well, transfection methods and amount of transfected DNA were listed in **Tab. 41**. A detailed description of the different transfection methods is provided in section 3.2.4.

To determine the impact of different treatments on STAT3 transcriptional activity, WT LS411N was washed with PBS, detached using 0.5% Trypsin-EDTA solution, counted, and seeded into 12-well plates. After serum starvation, cells were co-transfected with the reporter plasmids (Ren-Luc + STAT3-Luc or Ren-Luc + Ctrl. -Luc, respectively). 24 h after lipid-based transfection cells were stimulated with indicated substances (**Tab. 35**) (**Figure 3.4 A**, *upper panel*). SW837 cells were co-transfected with reporter plasmids using nucleofection and seeded into 12-well plates. 24 h after transfection medium was exchanged. After additional 48 h, cells were treated with indicated substances (**Tab. 35**) (**Figure 3.4 A**, *middle panel*). SW1463 WT cells were seeded into 12-well plates. 24 h after seeding, cells were transfected with reporter plasmids. After additional 24 h cells were treated as indicated (**Tab. 35**) (**Figure 3.4 A**, *lower panel*).
For Ruxolitinib, Tocilizumab and Napabucasin studies cells were additionally stimulated with rhIL-6 for 16 h before lysis.

To analyze the STAT3 transcriptional activity after siRNA treatment, LS411N cells were firstly transfected with the indicated siRNAs. After 24 h of serum starvation, cells were co-transfected with reporter plasmids (**Figure 3.3 B**, *upper panel*). SW837 cells were co-transfected with respective siRNAs and reporter plasmids (**Figure 3.3 B**, *middle panel*). 24 h after transfection, the medium was changed. SW1463 cells were transfected with the indicated siRNAs using a lipid-based transfection system (**Figure 3.3 B**, *lower panel*). 24 h after first lipid-based transfection, cells are transfected again with the reporter plasmids. 24 h after transfection, all cells were stimulated with rhIL-6 for 16 h before lysis.

Afterwards, cell lysis was performed using a passive lysis buffer. Samples were frozen in nitrogen and subsequently stored at -80°C until further use. The light units of firefly luciferase reporter were first measured by adding 100 µl Luciferase Assay Substrat (LARII) to each well (96-well plate) with 20 µl of each sample. After the firefly luminescence was quantified, the reaction was quenched, and at the same time the *Renilla* luciferase reaction was simultaneously initiated by adding 100 µl Stop&Glo Reagent (1:50, included in the kit) to each well.

Since each sample was measured in technical triplicates, mean values were calculated, and the blank value (only medium) was deducted from all measured samples to eliminate any background. For normalization, the ration of the Firefly light units to *Renilla* light units was calculated for each sample ("Firefly- light units / *Renilla*- light units"). Based on these

normalized values, the Hyper-IL-6-induced STAT3 activity of otherwise untreated cells was calculated as the ratio of STAT3-Luc to Ctrl. -Luc ("Ratio STAT3-Luc/Ctrl. -Luc"). The specific STAT3 transcriptional reporter activities of siRNA-treated cells or cells treated with Ruxolitinib, Tocilizumab and Napabucasin were calculated by further normalization to Ctrl. -Luc values of untreated and treated cells resulting in the ratio termed "normalized STAT3 activity“.

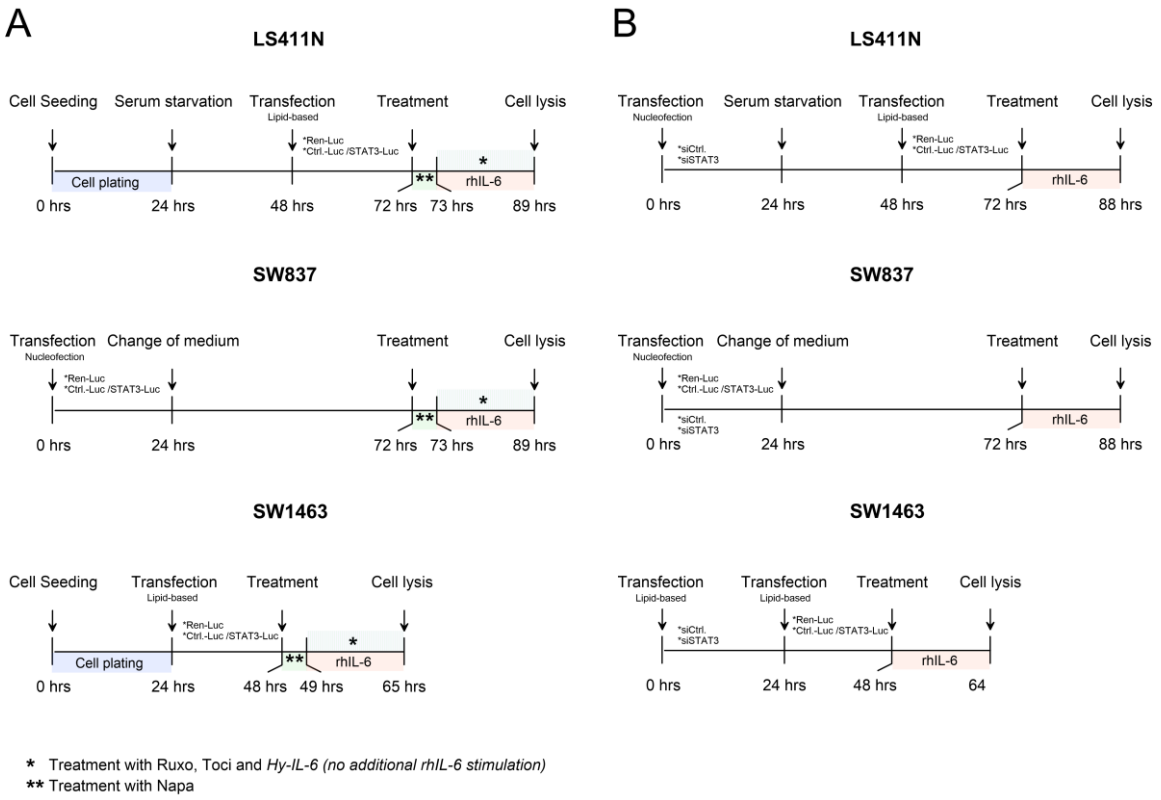

Figure 3.4 Experimental flow for DLR experiments after different treatment.
A| and **B|** Schematic treatment protocol for DLR assays with indicated substances and incubation times either for LS411N cells (*upper panels*), SW837 cells (*middle panels*) and SW1463 cells (*lower panels*) either after stimulation (A) or after siRNA treatment (B).

Table 41 Detailed conditions for DLR assay

Cell line	Treatment	Incubation time	Cell number	Reporter DNA
LS411N	siCtrl. vs. siSTAT3 *	96 h	200,000	1 µg / 1 µg / 0.1 ng
	DMSO vs. Napa	1 h		
	Hy-IL-6	16 h		
	Toci	16 h		
	DMSO vs. Rux0	16 h		
SW837	siCtrl. vs. siSTAT3 †	96 h	500,000	0.5 µg / 0.5 µg / 12.5 ng
	DMSO vs. Napa	1 h		0.25 µg / 0.25 µg / 6.25 ng
	Hy-IL-6	16 h		0.5 µg / 0.5 µg / 12.5 ng
	Toci	16 h		0.25 µg / 0.25 µg / 6.25 ng
	DMSO vs. Ruxo	16 h		0.25 µg / 0.25 µg / 6.25 ng
SW1463	siCtrl. vs. siSTAT3	72 h	100,000	0.5 µg / 0.5 µl / 5 ng
	DMSO vs. Napa	1 h		
	Hy-IL-6	16 h		
	Toci	16 h		
	DMSO vs. Ruxo	16 h		

Reporter DNA: Ctrl. -firefly luciferase / STAT-firefly luciferase / Renilla luciferase; * Transfection with X-tremeGENE HP, 2 µl lipid; † Transfection with Nucleofection (Amaxa), V-Kit, T-30; § Transfection with X-tremeGENE HP, 0.5 µl lipid.

3.2.8.4 Cellular viability assay

Cellular viability was determined using CellTiter-Blue® (CTB) assay. This assay is based on the ability of living cells to reduce resazurin (redox dye) to resorufin (fluorescent end product). Resazurin is a redox indicator used to monitor viable cells with active metabolism. Non-viable cells lose their metabolic capacity and do not reduce resazurin into resorufin. The amount of resorufin is proportional to the number of viable cells [180].

For details (experiment, treatment, incubation time, cell number, transfection reagent and amount of lipid) see **Tab. 42**. In this study the cellular viability of CRC cells following inhibitor treatment or genetic modification using siRNAs was measured. For inhibitor treatment, cells were cultivated in their respective medium and were seeded as triplicates into 96-well plates. 24 h after seeding cells were treated with respective inhibitors. For RNA interference studies cells were transfected with siCtrl. or siSTAT3 (detailed description of lipid-based transfection is provided in section 3.2.4.2) and were seeded afterward as triplicate into 96-well plates. After specific incubation times 11 µl of resazurin (1:10) was added to each well. The 96-well plate was covered and incubated for 1 h at 37°C prior measurement. The reduction of resazurin to resorufin was measured at 595 nm emission wavelength using a plate reader according to the manufacturer's instructions. The signal intensity of treated cells was calculated relative to the untreated control cells. A viability of at least 80% was required to continue working with the tested substances.

Table 42 Detailed conditions for CTB assay

Cell line	Treatment	Incubation time	Cell number
LS411N	siCtrl. vs. siSTAT3*	24 h / 48 h / 72 h / 96 h	5,000
	DMSO vs. Napa	1 h / 8 h / 24 h / 48 h	5,000
	Toci	1 h / 24 h / 48 h / 72 h	5,000
	DMSO vs. Ruxo	1 h / 24 h / 48 h / 72 h	5,000
	DMSO vs. DAPT	24 h / 48 h / 72 h	5,000
SW837	siCtrl. vs. siSTAT3†	24 h / 48 h / 72 h / 96 h	6,000
	DMSO vs. Napa	1 h / 8 h / 24 h / 48 h	6,000
	Toci	1 h / 24 h / 48 h / 72 h	6,000
	DMSO vs. Ruxo	1 h / 24 h / 48 h / 72 h	6,000
	DMSO vs. DAPT	1 h / 24 h / 48 h / 72 h	6,000
	DMSO vs. DAPT	24 h / 48 h / 72 h	6,000
SW1463	siCtrl. vs. siSTAT3§	24 h / 48 h / 72 h / 96 h	5,000
	DMSO vs. Napa	1 h / 8 h / 24 h / 48 h	5,000
	Toci	1 h / 24 h / 48 h / 72 h	5,000
	DMSO vs. Ruxo	1 h / 24 h / 48 h / 72 h	5,000
	DMSO vs. DAPT	24 h / 48 h / 72 h	5,000

* Transfection with BioRad SiLentFect, 0.2 µl lipid; † Transfection with RNAiMAX, 0.2 µl lipid; § Transfection with RNAiMAX, 0.1 µl lipid

3.2.9 Statistics

P-values and FRD-values < 0.05 were considered significant. The significance was depicted as: n.s.; *P < 0.05; **P < 0.01; ***P < 0.001. Statistical analysis was performed using Microsoft Excel software Add-in “Data Analysis” and GraphPad Prism software. For data analysis of CFA experiments, analysis of variance (ANOVA) was used to calculate significant differences between control and treatment groups with the use of ANOVA: Two-Factor with Replication. For visualization, data were presented as mean and standard error of the mean (s.e.m.) from at least three independent experiments using the software KaleidaGraph. Statistical analyses of DLR activity and CTB measurements were performed using an unpaired two-tailed Student's t-test in Microsoft Excel and visualized in Grapher. For qPCR analysis the medians of the resulting cycle threshold (Ct) values were normalized to the housekeeping gene *HPRT1* and relative gene expression changes were calculated according to the $2^{-\Delta\Delta CT}$ algorithm. *P*-values were calculated using an unpaired two-tailed Student's t-test in Microsoft Excel and visualized in Grapher. Pearson's correlation was used to calculate *P*-values for correlation of qPCR and RNA-Seq data. Statistical tests of tumor volume were performed in GraphPad Prism (version 8), mixed-effects analysis using Tukey's multiple comparisons test. A Log-rank (Mantel-Cox) test was performed to generate *P*-values of Kaplan-Meier curves.

4. Results

This study is focused on the molecular mechanisms of STAT3-controlled CRT resistance of CRC cells to obtain a better understanding of the intrinsic therapy resistance. One of the major obstacles for a successful treatment response is due to the appearance of tumor cell resistance to CRT. This resistance is a fundamental problem because affected patients do not benefit from this treatment but nonetheless are afflicted with adverse side effects of cytotoxic therapies and irradiation. Therefore, from a clinical perspective, one goal is to improve sensitivity to CRT and thereby reduce unnecessary side effects. Unfortunately, the molecular mechanisms underlying CRT resistance remain complex and have not yet been sufficiently clarified. In recent studies, my host research group suggested a potential role of STAT3 in mediating CRT resistance in CRC cell lines. They described variable sensitivity of CRC cells treated with 5-FU-based CRT and 2 Gy irradiation as well as a positive correlation between CRC cell-intrinsic expression of STAT3 and CRT unresponsiveness [162].

4.1 CRT resistance is controlled by active gp130 signalling and susceptible to pathway perturbations

In order to check if STAT3 protein levels are functionally relevant for mediating CRT resistance, we have subsequently inhibited or activated STAT3 itself or STAT3 pathway components. Direct inhibition of STAT3 was induced by genetic inhibition using RNAi or by using direct STAT3 inhibitors. Indirect inhibition was achieved on STAT3 pathway components using various inhibitors, some of which are already in clinical application. In addition, experiments were performed in which STAT3 activity was either induced by using a fusion protein or reconstituted in STAT3-deficient cells.

The experiments were conducted in collaboration with Melanie Spitzner (CALL, University Medical Center Göttingen) assisted by Florian Krause and Gigi Ton (CALL, University Medical Center Göttingen). Since we were most interested in the role of STAT3 in mediating CRT resistance we choose three MSS (Cancer genome atlas 2020) cell lines based on their STAT3 expression as appropriate model cell lines. We used LS411N cells as negative control because of their STAT3-deficiency and their described sensitivity to CRT [162]. Furthermore, SW1463 and SW837 cells were used as rectal cancer cell lines with STAT3 expression and high resistance to CRT [162].

4.1.1 Transcriptionally active STAT3 drives CRT resistance

To achieve a temporal STAT3 KD in LS411N, SW837 and SW1463 cells, we used siRNAs targeting *STAT3*. To determine the optimal STAT3 KD time points after RNAi treatment, we performed time series in the range of 24 - 96 hours. The assessment of whether the transfection and STAT3 KD was successful was performed by Western blot comparing the

expression levels of STAT3 and pSTAT3^{Y705} in the siRNA-treated cells with a control (siCtrl.) (*Appendix*, **Fig 8.1**). In addition, alteration of the cellular viability of the cells after RNAi treatment were excluded using CTB assay (*Appendix*, **Fig 8.3**).

To test whether STAT3 protein levels are functionally relevant for CRT-resistance, STAT3 was silenced in LS411N, SW837 and SW1463 cell lines using RNAi for 96 h, and 72 h, respectively. RNAi-mediated silencing of STAT3 was analyzed using Western blot analysis with antibodies detecting STAT3, pSTAT3^{Y705} and Actin as loading control (**Fig. 4.1,** upper *left panels*). Reduced STAT3 reporter activity was measured using DLR assay (**Fig. 4.1**, upper *right panels*). Additionally, cells were CFA-cultured to measure their survival following irradiation in the presence of 5-FU. Silencing of STAT3 significantly increased the sensitivity of SW1463 and SW837 cells to CRT whereas the sensitivity of LS411N was not changed (**Fig. 4.1,** *lower panels*).

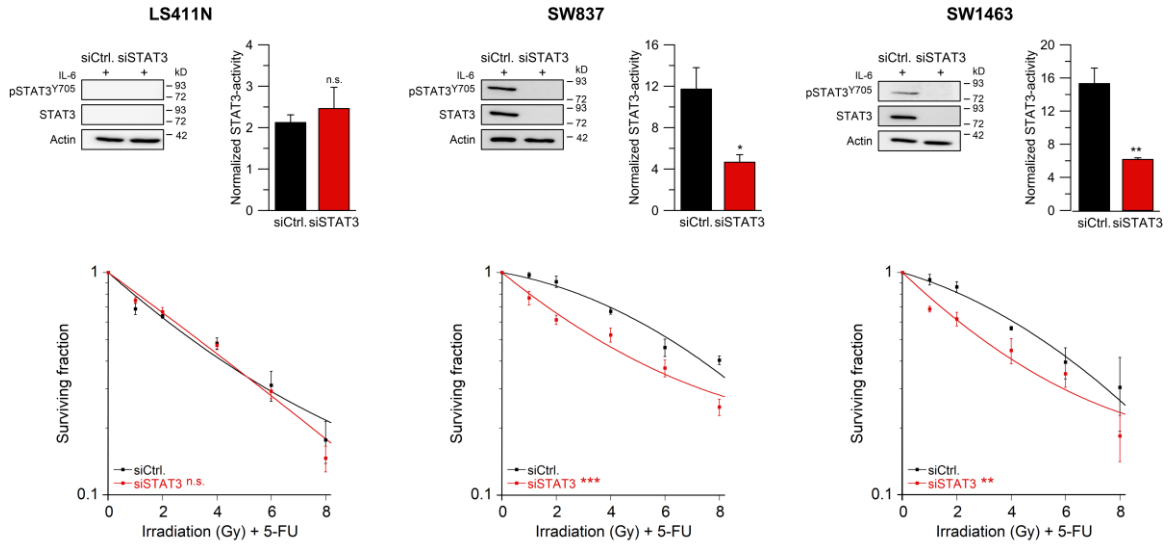

Figure 4.1 siRNA-mediated silencing of STAT3 results in a sensitization to CRT in STAT3 expressing cells.
Indicated cells treated with siRNA against STAT3 or control siRNA (siCtrl.) were analyzed for inducible phosphorylation or expression of STAT3 by immunoblotting (*upper left*)[71] or monitored for inducible STAT3 transcriptional activity (*upper right*) or were colony formation assay (CFA)-cultured to measure their survival following irradiation in the presence of 5-FU (*lower graph*) [71]. Data presented as mean ± s.e.m. from at least n=3 independent biological replicates. *P < 0.05, **P < 0.01, ***P < 0.001, unpaired two-sample Student's t-test or two-way analysis of variance (ANOVA).

Next, we tested whether the gain of STAT3 activity converts CRT-sensitive LS411N cells into CRT-resistant cells. LS411N cells were reconstituted with either WT STAT3, or signalling-inactive versions of STAT3 in which critical tyrosine and/or serine phosphorylation sites were inactivated by replacement with phenylalanine or alanine, respectively (S727A, Y705F, Y705F/S727A). The exchange with alanine and phenylalanine mimicked a constitutive dephosphorylation [181] of the STAT3 protein and allows to study the necessity of individual

phosphorylation sites. The expression of the different STAT3 versions was analyzed via immunoblotting (**Fig. 4.2**, upper *left panel*). Expression of WT and S727A-STAT3 version, but not Y705F- and Y705F/S727A-STAT3 variants, restored STAT3 transcriptional activity measured using DLR assay (**Fig. 4.2**, upper *middle panel*). Importantly, the presence of WT STAT3 increased clonogenic survival after 5-FU-based CRT (**Fig. 4.2**, upper *right panel*), while expression of all signalling-inactive mutants did not (**Fig. 4.2**, *lower panels*).

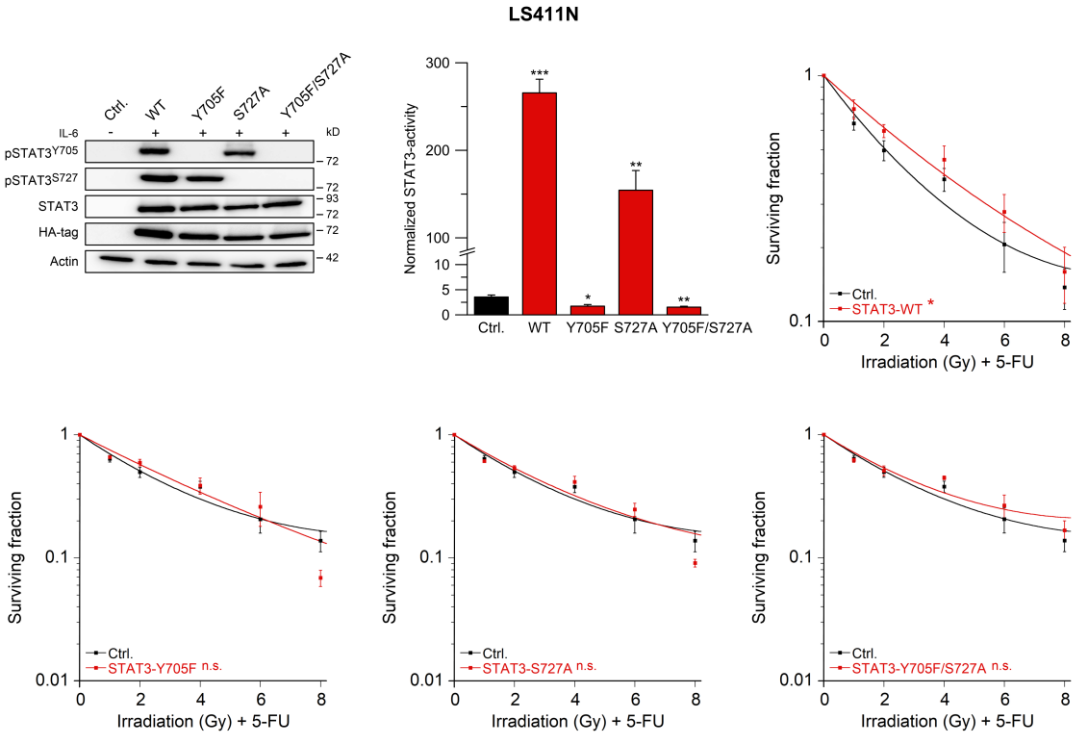

Figure 4.2 Expression of wild-type STAT3 increases the CRT resistance in STAT3-negative LS411N cells.
LS411N cells were transfected with empty control vector (Ctrl.) or constructs encoding HA-tagged versions of wild-type STAT3 or STAT3 variants harboring indicated amino acid exchanges. Expression and phosphorylation of STAT3 proteins (*upper left*), their transcriptional activity (*upper middle*), or CFA survival of wild-type-reconstituted cells (*upper left*) as well as CFA survival of STAT3 variants (*lower panels*) compared to control cells were monitored after irradiation with the indicated doses (Gy) in the presence of 5-FU (CRT) [71]. Data presented as mean ± s.e.m. from at least n=3 independent biological replicates. Experiments were performed by Florian Krause (medical student), CALL, under permanent supervision. *P < 0.05, **P < 0.01, ***P < 0.001, unpaired two-sample Student's t-test or two-way analysis of variance (ANOVA).

These data revealed a direct contribution of signalling active STAT3 to CRT resistance and underlines the necessity of a functional Y705 phosphorylation site. In order to elucidate the impact of STAT3 in the resistance of CRC cells, Spitzner *et al*. initially examined the expression of STAT3 and pSTAT3^{Y705} in human CRC cell lines. However, there was no phosphorylation of STAT3 at the activating tyrosine residue 705 in 10 out of 12 CRC cell lines. Hence, STAT3 was not constitutively active *in vitro* [147]. This strongly indicated an input of upstream regulatory signals that activated the JAK/STAT signalling pathway.

In the next section we focused on potent activators of STAT3, like inflammatory cytokine receptors such as the receptor for IL-6. Elevated levels of serum IL-6 and sIL-6R were detected in patients with i.e., CRC [125] that coincide with surgery, chemo- and radiotherapy [127]. Moreover, IL-6 is known to play various roles in cancer including metastasis of CRC [124]. IL-6 binds to membrane bound IL-6R or to soluble sIL-6R. Subsequently, the non-signalling IL-6/IL-6R or IL6/sIL-6R complexes bind to the ubiquitously expressed gp130 domain (**Fig. 4.3 A**) (**Fig. 2.4 B)**, leading to gp130-homodimer formation and finally to the signal initiation [129]. Signal initiation leads to the activation of JAK that phosphorylates STAT3 [119,127,135,149-151].

Expanding on this, we aimed to explore the possible effect of gp130/JAK/STAT3 axis activation on CRT resistance. To this end, we used the designer fusion protein Hy-IL-6 which consisting of IL-6 and the soluble IL-6 receptor chain and therefore mimics IL-6 trans-signalling [130,182,183]. To assess the influence of the Hy-IL-6 induced gp130 signalling cascade on CRT resistance, SW837, SW1463 cells as well as LS411N cells were treated with Hy-IL-6. Stimulation resulted in a strong inducible phosphorylation of STAT3 at the critical tyrosine phosphorylation sites (Y705) in SW837 and SW1463 cells but not in STAT3-deficient LS411N cells, compared to unstimulated cells (**Fig. 4.3 B**, upper right, middle, and *left panel*). In addition, total STAT3 levels remain unaffected. Furthermore, the stimulation of SW837 and SW1463 increased STAT3 transcriptional activity measured using DLR assay (**Fig. 4.3 B**, upper *left panels*) that translates into increased CFA survival in the presence of 5-FU and irradiation (**Fig. 4.3 B**, *lower panels*). The stimulation of LS411N cells had no impact on CRT resistance of the cells.

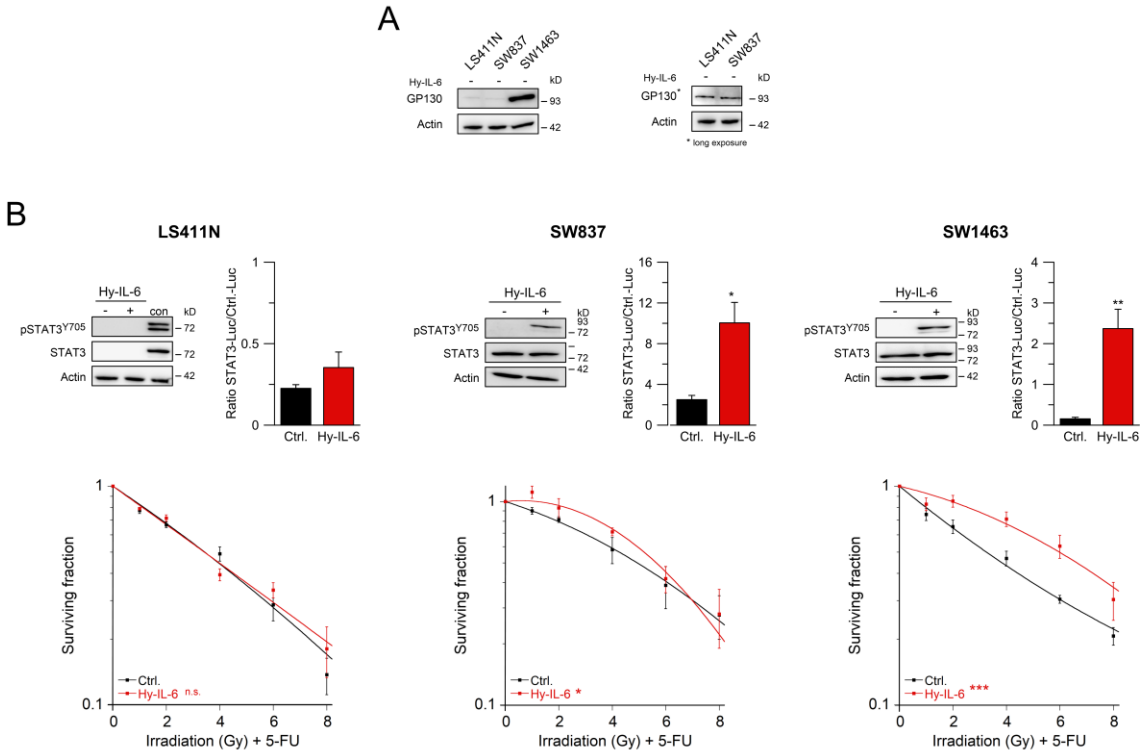

Figure 4.3 Transcriptionally active STAT3 drives CRT resistance.
A| Expression analysis of gp130 by immunoblotting in unstimulated CRC cells. **B|** Hy-IL-6-induced STAT3 phosphorylation and transcriptional activity were analyzed in STAT3-negative LS411N cells (*upper left panel*) and STAT3-positive SW837 or SW1463 cells (*upper middle* and *right panel*), and the impact of that stimulation on sensitivity to CRT was assessed (*lower panels*) [71]. Data presented as mean ± s.e.m. from at least n=3 independent biological replicates. *P < 0.05, **P < 0.01, ***P < 0.001, unpaired two-sample Student's t-test or two-way analysis of variance (ANOVA).

In summary, RNAi against *STAT3* resulted in a clear sensitization against CRT in STAT3 expressing cells (SW1463 and SW837) whereas CFA survival of STAT3 non-expressing LS411N cells are not impaired by RNAi mediated silencing of STAT3. Expression of different STAT3 variants in LS411N cells showed increasing resistance to CRT only after expression of the signalling active wild-type STAT3 version, in which the important phosphorylation sites (Y705 and S727) are active. Further, stimulation with the fusion protein Hy-IL-6 induced strong STAT3 phosphorylation that is associated with increased resistance to CRT. In conclusion, experiments proofed that activated/phosphorylated STAT3, which is transcriptionally active, drives CRT resistance in CRC cells.

4.1.2 Gp130/STAT3 pathway inhibitor mediated perturbation modulates CRT resistance

To further explore the role of IL-6/gp130/STAT3 signalling in mediating CRT resistance, we employed established inhibitors of the gp130/IL-6 receptor signalling cascade to analyze their ability to change the CRT resistance in CRC cells.

4.1.2.1 Treatment with Tocilizumab alter IL-6 signalling in CRC cells

Tocilizumab is a clinically used monoclonal antibody that binds to the IL-6 receptor (sIL-6R and IL-6R) and thereby inhibits the IL-6 classical as well as the trans-signalling pathway and in turn their signal output [119,127,135]. It was previously shown that short time incubation with Tocilizumab dampened the STAT3 phosphorylation of Y705, as well as the transcriptional activity in SW1463 cells [167]. In this present work we used LS411N, SW837 and SW1463 cells and treated them with previous established Tocilizumab concentrations (**Tab. 35**). To ensure that the cells were still viable we measured the cellular viability for LS411N, SW837 and SW1463 cells after incubation with Tocilizumab (*Appendix*, **Fig 8.4**). Treatment of SW837 and SW1463 cells with Tocilizumab dampened STAT3 tyrosine phosphorylation, while total STAT3 levels remained unchanged (**Fig 4.4**, middle and *right panel*). In addition, treatment with Tocilizumab reduced STAT3 transcriptional activity compared to the untreated samples as well as it rendered both cell lines more sensitive to CRT, as revealed by their decreased CFA survival rates (**Fig. 4.4**, left and *right panel*). Importantly, Tocilizumab treatment had no impact on CFA survival of STAT3-deficient LS411N cells.

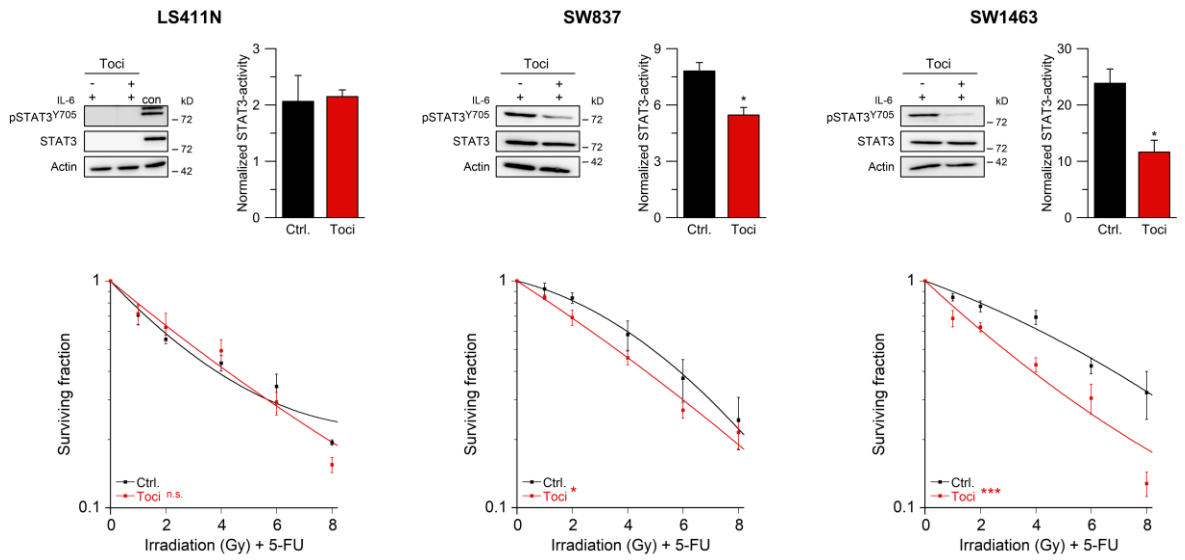

Figure 4.4 Treatment with Tocilizumab render STAT3 expression cells more sensitive against CRT.
Indicated cells were treated with Tocilizumab (Toci) and were analyzed for inducible phosphorylation or expression of STAT3 by immunoblotting (*upper left*) or monitored for inducible STAT3 transcriptional activity (*upper right*) or were colony formation assay (CFA)-cultured to measure their survival following irradiation in the presence of 5-FU (*lower graph*)[71]. Data presented as mean ± s.e.m. from at least n=3 independent biological replicates. *P < 0.05, **P < 0.01, ***P < 0.001, unpaired two-sample Student's t-test or two-way analysis of variance (ANOVA).

4.1.2.2 Treatment with the JAK inhibitor Ruxolitinib

Ruxolitinib is a clinically used small-molecule inhibitor of JAK1 and JAK2 [119], that is not selective for the IL-6/gp130 axis but targets the JAK/STAT axis on an intracellular level. In inactive form STAT3 is predominantly located in the cytoplasm where it gets activated in

response to i.e., cytokine stimulation via tyrosine phosphorylation by JAK proteins [141]. The inhibitory effect of Ruxolitinib is based on its selectivity for JAK1 and JAK2 and therefore on the inhibition of STAT3 activation [184].

To test a potential effect of Ruxolitinib on inhibition of STAT3 phosphorylation we first treated the CRC cell lines SW837 and SW1463 with different Ruxolitinib concentrations (ranging from 10, 50,100, 250 to 500 nM) for 1 and for 24 h to identify reasonable concentrations and time-points (**Fig. 4.5 A**). The inhibitory effect on phosphorylated STAT3 at tyrosine 705 (pSTAT3^{Y705}) was analyzed by Western blotting **(Fig. 4.5 A)**. pSTAT3^{Y705} levels were reduced in SW837 samples treated with a minimum of 100 nM Ruxolitinib for 1 h and 24 h (**Fig. 4.5 A**, *left panels*) and in SW1463 samples treated with 1000 nM Ruxolitinib for 1 h and a minimum of 50 nM Ruxolitinib for 24 h in comparison to the corresponding control samples. While total STAT3 levels remain stable and are not affected by Ruxolitinib treatment (**Fig. 4.5 A**, *right panels*). The cellular viability of LS411N, SW837, and SW1463 was not affected even using the highest Ruxolitinib concentrations (5000 nM). All cellular viability curves resulted in > 80% viability, meaning that Ruxolitinib did not induce a viability loss, confirming that all concentrations were suitable for further experiments (**Fig.4.5 B**). Note that additional time points for Ruxolitinib treatment are shown in *Appendix*, **Fig 8.5**.

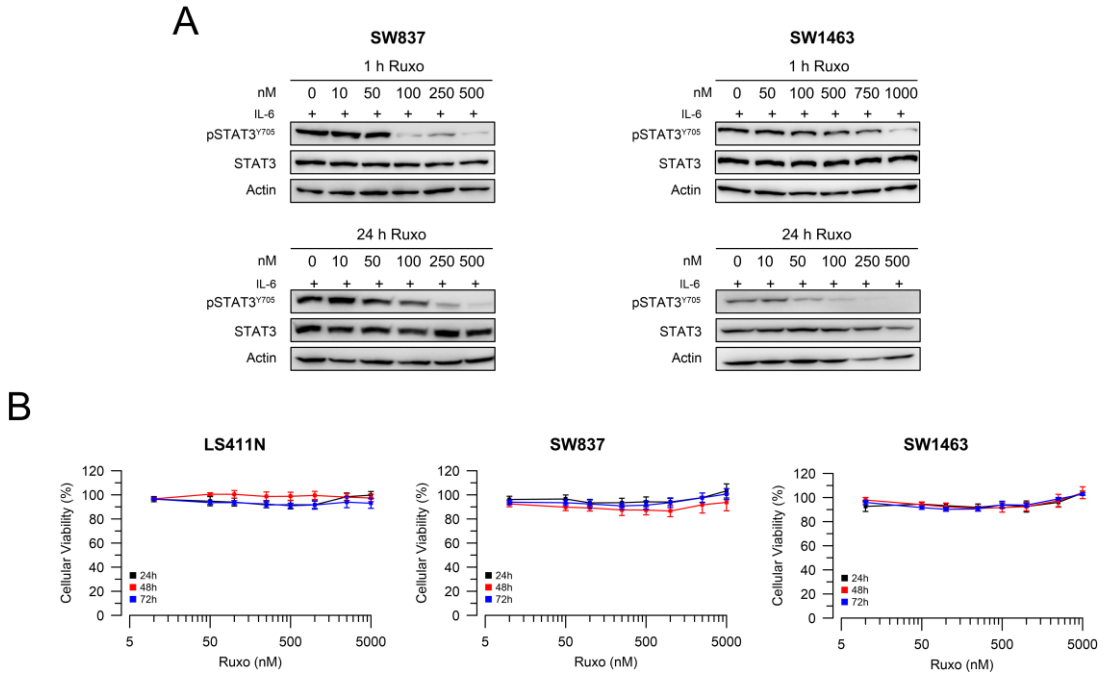

Figure 4.5 Treatment of CRC cells with Ruxolitinib reduces pSTAT3Y705 expression in a dose dependent manner.
A| Western Blot analysis was performed to determine the most effective Ruxolitinib (Ruxo) concentration and treatment timepoint for SW837 and SW1463. For this pSTAT3^{Y705} expression levels were measured using Western Blot after treating the cells for 1 h or 24 h with Ruxolitinib concentrations ranging from 0 to 500 nM. **B|** To test if Ruxolitinib reduce cellular viability LS411N, SW837 and SW1463 were incubated with different concentrations Ruxolitinib ranging from 0 to 5000 nM for 24,48 and 72 h. Cellular viability was measured using a cell titer blue assay and the data are presented as mean ± s.e.m. from at least n=3 independent biological replicates.

To test if the Ruxolitinib-dependent inhibition of STAT3 phosphorylation influences CRT resistance, LS411N, SW837 and SW1463 cells were treated with the previous established concentrations Ruxolitinib for 16 h (**Tab. 35**), incubated with 3 µM 5-FU overnight, followed by irradiation. For the STAT3 negative cell line LS411N the highest possible Ruxolitinib concentration was used (1000 nM). Successful inhibition of STAT3 phosphorylation was confirmed using anti-pSTAT3^{Y705} immunoblotting (**Fig. 4.6**, *upper left panels*), and decreased STAT3 activity was verified using DLR assay (**Fig. 4.6**, *upper right panels*). Treatment of SW837 and SW1463 cells with Ruxolitinib rendered both cell lines more sensitive to CRT, as revealed by their decreased CFA survival rates (**Fig. 4.6**, *lower panels*). Importantly, Ruxolitinib treatment has no impact on CFA survival of STAT3-deficient LS411N cells.

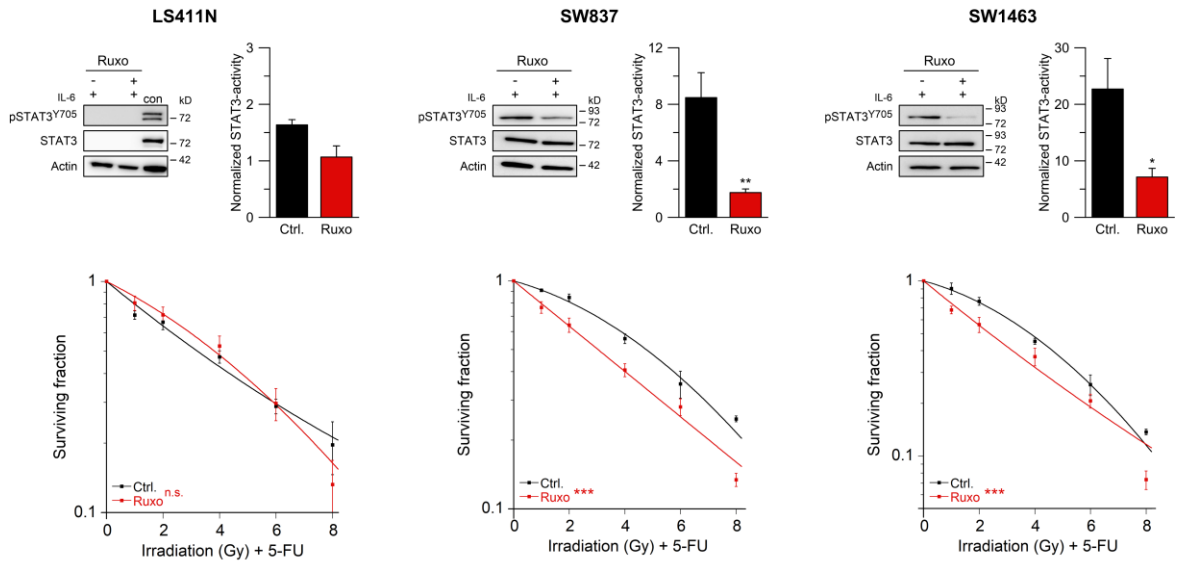

Figure 4.6 Manipulating the JAK/STAT pathway using Ruxolitinib alters STAT3 activation and renders cells more sensitive against CRT.
Indicated cells treated with Ruxolitinib (Ruxo) were analyzed for inducible phosphorylation or expression of STAT3 by immunoblotting (*upper left*) or monitored for inducible STAT3 transcriptional activity (*upper right*) or were colony formation assay (CFA)-cultured to measure their survival following irradiation in the presence of 5-FU (*lower graph*) [71]. Data presented as mean ± s.e.m. from at least n=3 independent biological replicates. *P < 0.05, **P < 0.01, ***P < 0.001, unpaired two-sample Student's t-test or two-way analysis of variance (ANOVA).

Using Tocilizumab and Ruxolitinib we demonstrated that manipulation of gp130/JAK/STAT pathway components at both extracellular and intracellular levels alters STAT3 activation and renders STAT3 expressing cells more sensitive against a 5-FU based CRT. Next, we wanted to analyze the impact of direct STAT3 inhibition.

4.1.2.3 Treatment with the pSTAT3 inhibitor Napabucasin

A promising direct inhibitor of STAT3 is the small-molecule inhibitor Napabucasin (BBI-608) [185]. Napabucasin is less toxic, highly effective in low molecular ranges, orally bioavailable and has already been tested in a phase-III clinical trial for highly advanced, chemotherapy-

refractory CRC [186]. This study resulted in the suggestion that STAT3 might be an important target for the treatment of CRC patients with elevated pSTAT3 expression [186].

To identify reasonable concentrations and time points, we first treated SW837 and SW1463 cells with different Napabucasin concentrations (ranging from 100 to 1000 nM) for 1h (**Fig. 4.7A**). The inhibitory effect on pSTAT3 at tyrosine 705 was analyzed by Western blotting (**Fig. 4.7 A**). pSTAT3^{Y705} levels were reduced in SW837 samples treated with a minimum of 500 nM Napabucasin for 1 h (**Fig, 4.7 A**, *left panels*) and in SW1463 samples treated with 750 nM Ruxolitinib for 1 h in comparison to the corresponding control sample. While total STAT3 levels remain stable and are not affected by Napabucasin treatment (**Fig. 4.7 A**, *right panels*). Furthermore, we tested whether the treatment with Napabucasin affects the cellular viability. The cellular viability decreased from minimal drug concentration to the highest one in all the cases of 24,48 and 72 h of incubation with Napabucasin (**Fig. 4.7 C**). This indicates that all three cell lines were relatively susceptible to Napabucasin-mediated reduction of cellular viability when treating them with high concentrations over a longer period. Based on these results we decided to perform the following experiments with a Napabucasin incubation time of 1 h.

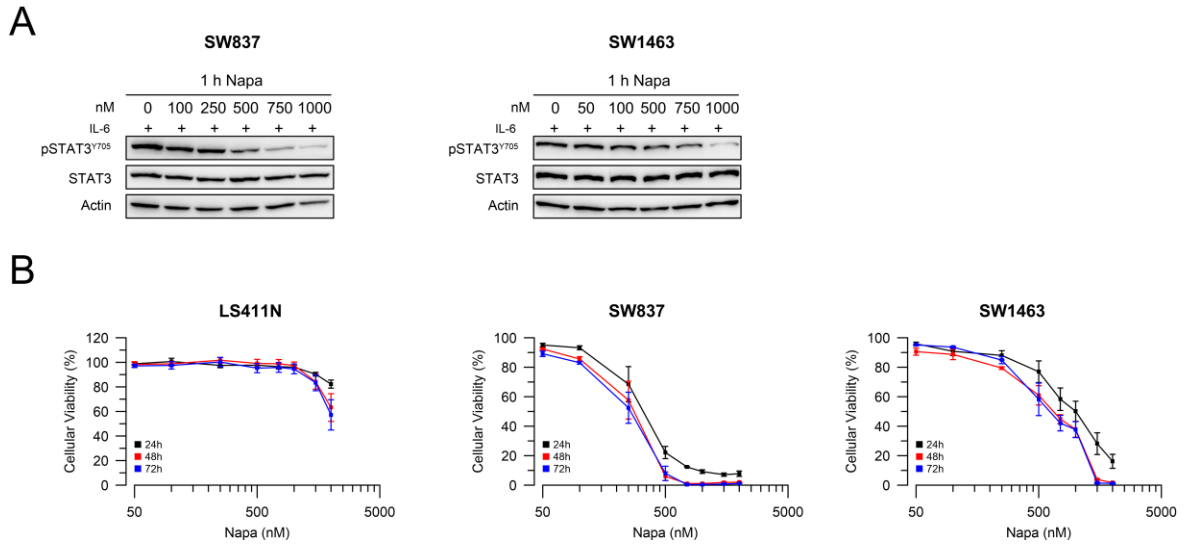

Figure 4.7 Treatment of CRC cells with Napabucasin reduces pSTAT3Y705 expression in a dose dependent manner.
A| Western blot analysis was performed to determine the most effective Napabucasin (Napa) concentration after 1 h of treatment for SW837 and SW1463. STAT3 and pSTAT3^{Y705} expression levels were measured using Western Blot after treating the cells for 1 h with Napabucasin concentrations ranging from 0 to 100 nM. **B|** To test if Napabucasin reduces cellular viability LS411N, SW837 and SW1463 were incubated with different Napabucasin concentrations ranging from 0 to 5000 nM for 24,48 and 72 h. Cellular viability was measured using a cell titer blue assay and the data are presented as mean ± s.e.m. from at least n=3 independent biological replicates.

To analyze the effect of direct STAT3 inhibition on the CRT sensitivity of CRC cells, LS411N, SW837 and SW1463 cells were incubated for 1 h with the respective concentrations

of Napabucasin (**Tab. 35**). The treatment with Napabucasin prevented the phosphorylation of the key activator site, Y705, in STAT3 expressing SW837 and SW1463 cells (**Fig. 4.8**, *upper right*, *middle* and *left panels*) as well as it strongly reduced reporter activity of STAT3 (**Fig. 4.8**, *upper right*, *middle* and *left panels*). Resulting from this it sensitized both cell lines to CRT (**Fig. 4.8**, *lower panels*) without influencing the amount of STAT3 expression (**Fig. 4.8**, *upper right*, *middle* and *left panels*). The CFA survival of LS411N cells remained unaffected following treatment with Napabucasin.

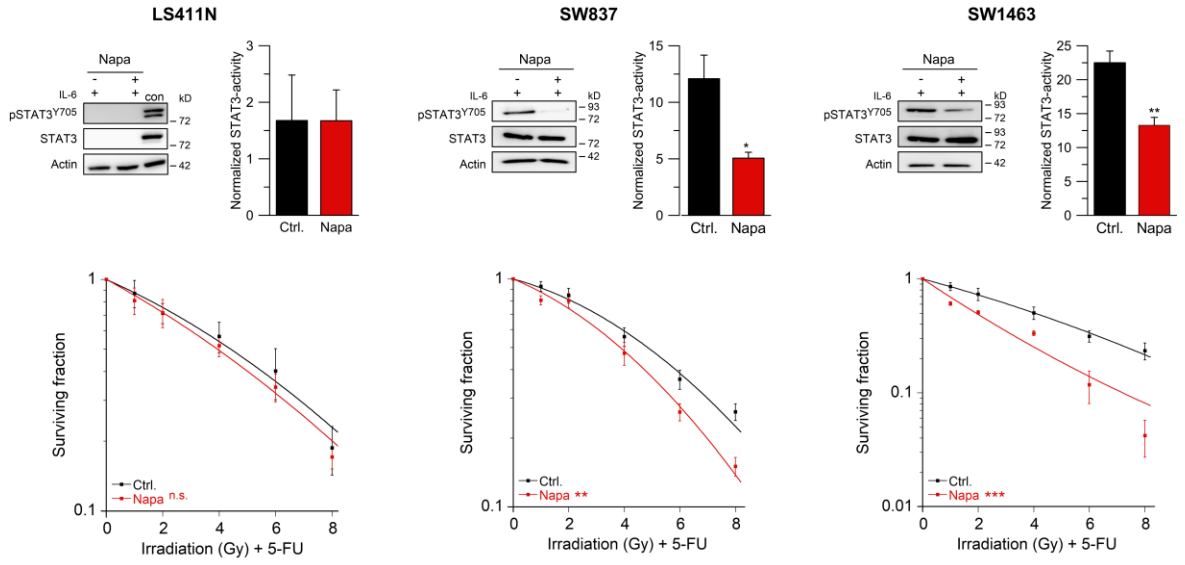

Figure 4.8 Treatment of CRC cells with Napabucasin reduces pSTAT3Y705 expression and renders cells more sensitive to CRT.
LS411N, SW837 or SW1463 cells were left untreated or treated with Napabucasin (Napa) (*left* and *middle panel*) and analyzed for STAT3 functionality (*upper graphs*) or were monitored for CFA survival after CRT (*lower graphs*) [71]. Data presented as mean ± s.e.m. from at least n=3 independent biological replicates. **P* < 0.05, ***P* < 0.01, ****P* < 0.001, unpaired two-sample Student's t-test or two-way analysis of variance (ANOVA).

To evaluate whether treatment with Napabucasin triggers other STAT3 independent mechanisms that lead to a sensitization of CRC cells to CRT, we combined treatment with Napabucasin and RNAi against *STAT3* in SW1463 cells. Successful RNAi mediated STAT3 KD as well as the inhibitory effect of Napabucasin on pSTAT3^{Y705} levels were confirmed using immunoblotting (**Fig. 4.9**, *right panel*). As observed in **Fig. 4.1** and **Fig. 4.8**, both approaches individually affect CRT sensitivity significantly (**Fig. 4.9**, *left panel*). However, when the two treatments are combined, no synergistic effect can be observed in terms of a change in CRT sensitivity (**Fig. 4.9**, *left panel*). Thus, the effect of Napabucasin in our assays can be predominantly ascribed to inhibition of STAT3 tyrosine phosphorylation.

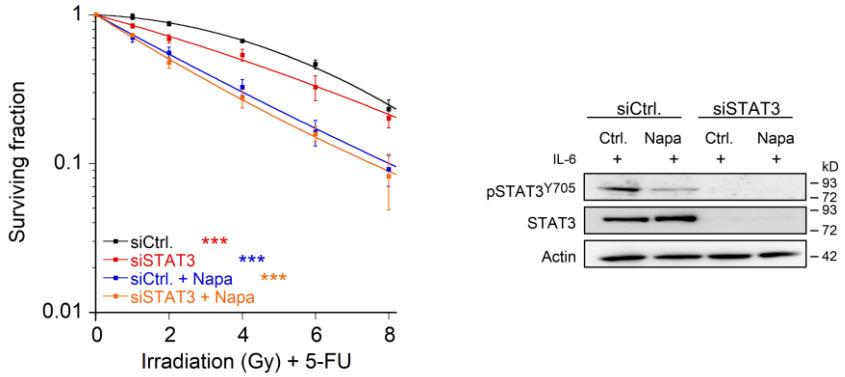

Figure 4.9 Combined treatment of Napabucasin and RNAi targeting STAT3 has no additive effect on CRT resistance.
Following siRNA- mediated STAT3 silencing and treatment with Napabucasin (Napa), SW1463 cells or untreated control cells were subjected to STAT3 immunoblot analysis (*right panel*) or CFA survival after CRT (*left panel*) [71]. Data presented as mean ± s.e.m. from at least n=3 independent biological replicates. *P < 0.05, **P < 0.01, ***P < 0.001, unpaired two-sample Student's t-test or two-way analysis of variance (ANOVA).

In summary, the extent of CRT resistance could be tuned in both directions by manipulating the performance of STAT3 even directly or indirectly through modification of upstream effectors.

4.2 Targeting gp130/STAT3 signalling *in vivo*

The data prompted us to test whether the inhibition of the gp130/STAT3 signalling axis can suppress the growth of tumor transplants under 5-FU based CRT *in vivo*. To assess the effect of STAT3 inhibition on CRT-sensitivity *in vivo* my host research group established a subcutaneous rectal cancer xenograft nude mice model that mirrors clinical conditions i.e., fractionated doses of both radiation and chemotherapy [147]. In previous studies they used the small-molecule inhibitor STATTIC, which inhibits the function of the SH2 domain of STAT3, preventing phosphorylation at Y705 and, subsequently, dimerization and nuclear translocation [187]. In the absence of STATTIC, the tumor volume remained stable during the administration of 5-FU and irradiation whereas the tumor volume of STATTIC-treated mice decreased over time. Therefore, there was a statistically significant effect of the STATTIC treatment on the reduction of tumor volume during the CRT treatment, associated with a significantly delayed tumor re-growth in STATTIC-treated mice compared with control animals as well as a survival benefit for STATTIC- treated mice [147]. These results are limited by the fact that STATTIC was administered locally into the tumor, as STATTIC is not orally bioavailable [187]. Following experiments were performed in collaboration with Melanie Spitzner.

4.2.1 Testing Napabucasin *in vivo*

Accordingly, as STATTIC is not a favorable inhibitor we tested the very promising STAT3 inhibitor Napabucasin because it had a striking impact on CRT re-sensitization in our cell culture models (**Fig. 4.7** and **4.8**).

To assess the effect of a Napabucasin mediated pSTAT3^{Y705} inhibition on CRT-sensitivity *in vivo* we used the subcutaneous rectal cancer xenograft nude mice model that was previously established [147] (see section 3.2.1. and **Fig. 3.1 A** and **B** for details). In a pre-test the effectiveness of two different concentrations Napabucasin (maximum dose:20 mg/kg and reduced dose: 5 mg/kg) were tested [185]. We used the rectal cancer cell line SW1463, which is STAT3 expressing and showed a sensitization against CRT after treatment with Napabucasin (**Fig. 4.8**, *right panel*). Therefore, 2 million SW1463 cells were injected into 8 to 10 weeks old female NMRI-Foxn1$_{nu}$/Foxn1$_{nu}$ mice under sevoflurane inhalation. Once the tumors reached about 150 mm³ in size, mice were randomized into three treatment groups: DMSO (n=2), 5 mg/kg Napabucasin (n=3) and 20 mg/kg Napabucasin (n=2). The mice were treated like indicated in **Fig. 3.1 A**.

We did not notice any obvious sign of toxic side effects or extreme body weight drop of Napabucasin treated mice compared with DMSO treated mice (**Fig. 4.10 A**). Regardless of the treatment the tumor volume of all treatment groups continues to increase (**Fig. 4.10 B**). After 14 days of treatment either with DMSO or with Napabucasin the mice were sacrificed and tumors as well as major organs including stomach, spleen, liver, kidneys, and heart were collected. The appearance as well as the morphology of dissected organs were comparable with those of untreated animals (**Fig. 4.10 C**). These observations indicated that Napabucasin treatment did not lead to visible alterations. The expression of pSTAT3^{Y705} was higher in tumors of DMSO treated mice, as compared to tumors of Napabucasin treated mice indicating a clear Napabucasin effect in SW1463 forming tumors in a dose independent manner (**Fig. 4.10 D**). At the same time, the STAT3 expression level remained unchanged. Therefore, we choose 5 mg/kg Napabucasin for the following experiments.

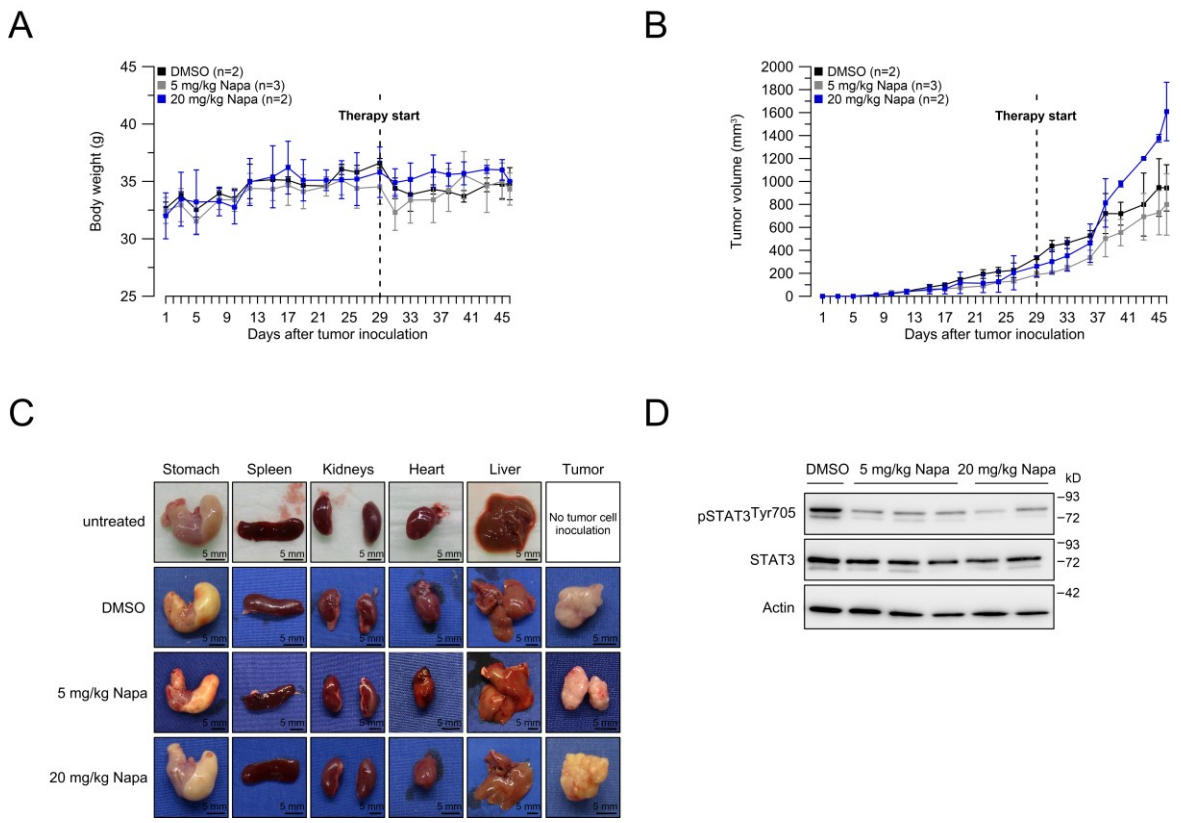

Figure 4.10 Establishment of effective Napabucasin concentrations for further in vivo experiments.
A| Body weight curves of SW1463 bearing mice treated with either DMSO (n=2), 5 mg/kg Napabucasin (n=3) or 20 mg/kg Napabucasin (n=2) for 14 days. **B|** Tumor volumes of mice starting at the first day after tumor cell inoculation. **C|** After three weeks of treatment, tumor-bearing mice were sacrificed 1 hour after oral application of either DMSO or Napabucasin, pictures of different organs were taken to compare treated mice with non-treated mice and **D|** Western blot analysis was performed to confirm inhibition of STAT3 phosphorylation [71].

In analogy to the dose-finding experiments, tumors were induced by subcutaneous injection of 2 million SW1463 in the right flank of 8 to 10 weeks old NMRI-Foxn1$_{nu}$/Foxn1$_{nu}$ mice. The treatment was started when the tumor volume had reached about 150 mm³ in size. All nude mice were randomly assigned into five different treatment groups: DMSO (n=15), Napabucasin (n=15), Napabucasin + RT (n=15), Napabucasin + CRT (n=13) and DMSO + CRT groups(n=14). The mice are treated like indicated in **Fig. 3.1 B** with 5 mg/kg Napabucasin or DMSO orally. For the CRT experiments, 50 mg/kg 5-FU was administered intraperitoneal and 5 mg/kg Napabucasin or DMSO, given orally one hour before irradiation. Irradiation is performed under sevoflurane inhalation narcosis. Nontumor parts were shielded with a lead shield for vital organ protection, and tumors were irradiated daily with 1.8 Gy for 14 days using an X-ray operating at 70 kV, 25 mA and with 0.5-mm Al filtration. To document the tumor development during the treatment period pictures at day 1, 5, 9 and 14 after treatment start were taken. The Tumor and the body weight were measured thrice weekly. The treatment

period is followed by an observational period to investigate the tumor regrowth. We defined the tumor regrowth as a tripling in tumor volume (450 mm^3).

4.2.1.1 Treatment with Napabucasin alone or in combination has no impact on body weight of tumor bearing mice

The body weight of mice remained stable, regardless of the treatment even during the hole administration period (**Fig. 4.11 A**) as well as at the end of treatment (**Fig.4.11 B**).

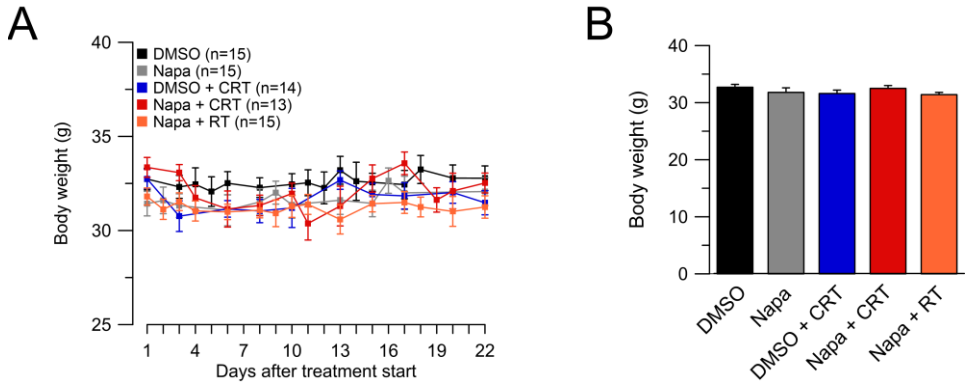

Figure 4.11 Different treatments have no impact on the body weight of the mice.
A|-B| Body weight of mice treated 14 days with either DMSO (n=15), Napabucasin (n=15), DMSO + CRT (n=14), Napabucasin + CRT (n=13) or Napabucasin + RT (n=15) (*left panel*) (A) and at the end of treatment (*right panel*) (B) [71]. Data points consisted of at least seven mice.

4.2.1.2 Treatment with Napabucasin alone did not affect the tumor volume

Both control groups (DMSO and Napabucasin) show a dramatically increasing tumor volume after treatment start (**Fig 4.12 A** and **Fig 4.10 B**). Treatment with Napabucasin alone did not noticeably suppress the growth of tumor transplants compared to treatment with DMSO alone (**Fig 4.12 A-C**).

Importantly, mice in both control groups showed average time to tumor regrowth and life span (**Fig 4.12 D-F**). The time to tumor regrowth was defined as a tripling in tumor size (450 mm^3) and is an important clinical aspect after the end of medical treatment. DMSO treated mice showed 11 days to tumor tripling in comparison to 13 days in Napabucasin treated mice (**Fig. 4.12 E**). All mice included in these treatment groups died within 45 days (**Fig. 4.12 F**). However, tumors in both control groups showed similar growth speed, suggesting that Napabucasin alone without 5-FU and irradiation did not affect tumor development.

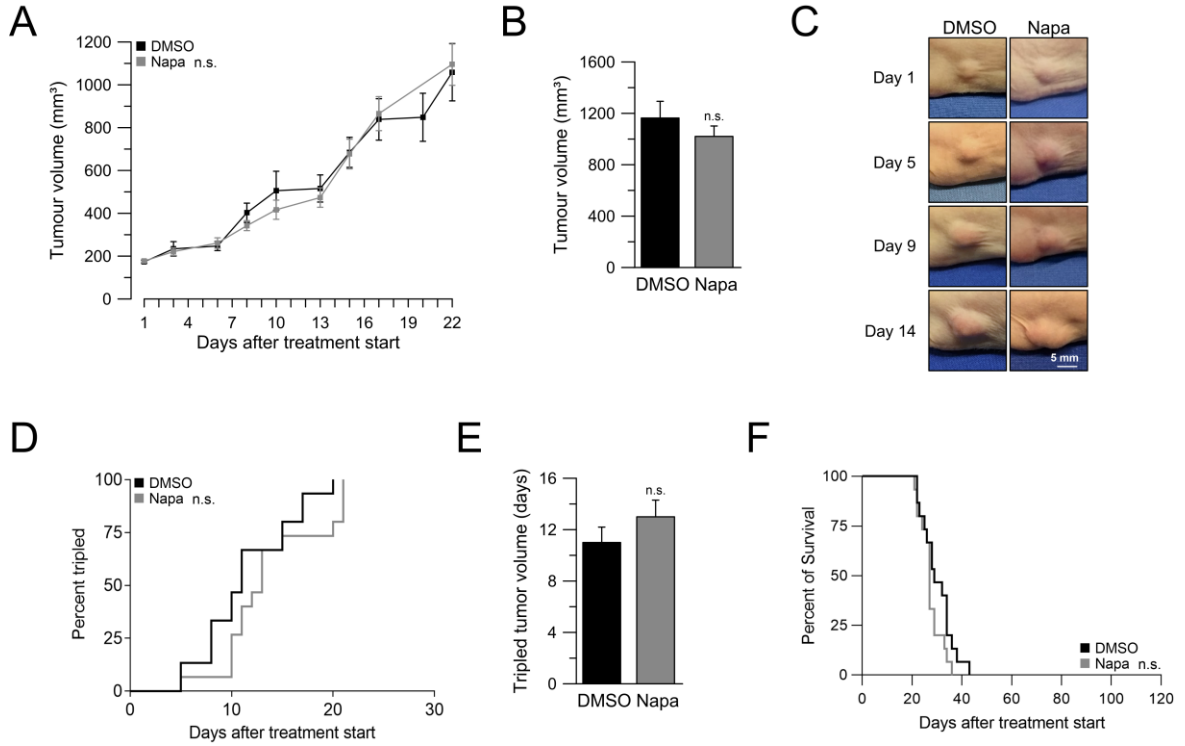

Figure 4.12 Napabucasin alone did not affect the tumor volume.
A| and **B|** Tumor volumes of mice during treatment only with DMSO and Napabucasin without CRT (A), and at the end of treatment (B) [71]. **C|** Pictures of tumors under treatment with DMSO and Napabucasin. Pictures were taken 1 day, 5 days, 9 days, and 14 days after treatment start. **D|** Kaplan-Meier curves were calculated to analyze the time to tumor tripling in the respective groups [71]. **E|** The median tumor tripling time of DMSO treated mice was 11 days, compared to 13 days of Napabucasin treated mice [71]. **F|** Kaplan-Meier curves comparing the survival of DMSO treated mice with Napabucasin treated mice, respectively. Data points (A) consisted of at least seven mice. The significance was verified by unpaired two-sample Student's t-test (B and E) or were calculated by Log-rank (Mantel-Cox) test (A, D and F).

4.2.1.3 Napabucasin reduces tumor volume only in combination with RT and CRT treatment

The use of Napabucasin as monotherapy did not show any effect on tumor volume development (**Fig. 4.12**). Therefore, we treated mice additionally with RT and CRT (for details see section 3.2.1. and **Fig. 3.1 B**). The tumor volume during Napabucasin + RT and Napabucasin + CRT treatment was significantly reduced in both groups compared to the control group. The CRT treatment even more abolished the tumor volume compared to the RT group (**Fig. 4.13 A** and **B**). At the end of treatment, the Napabucasin + CRT treated tumors are the smallest in terms of appearance and calculation. The additional RT reduces the tumor volume compared to Napabucasin monotherapy but not as much as the additional CRT (**Fig. 4.13 A - C**). In the Napabucasin + RT treated but more pronounced in the Napabucasin + CRT treated group the tumor regrowth was time-delayed compared to the Napabucasin only group (**Fig. 4.13 D**). While in the group exposed to Napabucasin + CRT, the mice demonstrated significantly longer median time to tumor tripling (53 days) compared to 27 days in

Napabucasin + RT groups and 13 days in only Napabucasin treated animals (**Fig. 4.13 E**). This resulted in a survival advantage for RT and CRT treated mice. Napabucasin + CRT treated mice also have a survival advantage compared to Napabucasin + RT and Napabucasin only treated animals (**Fig. 4.13 F**).

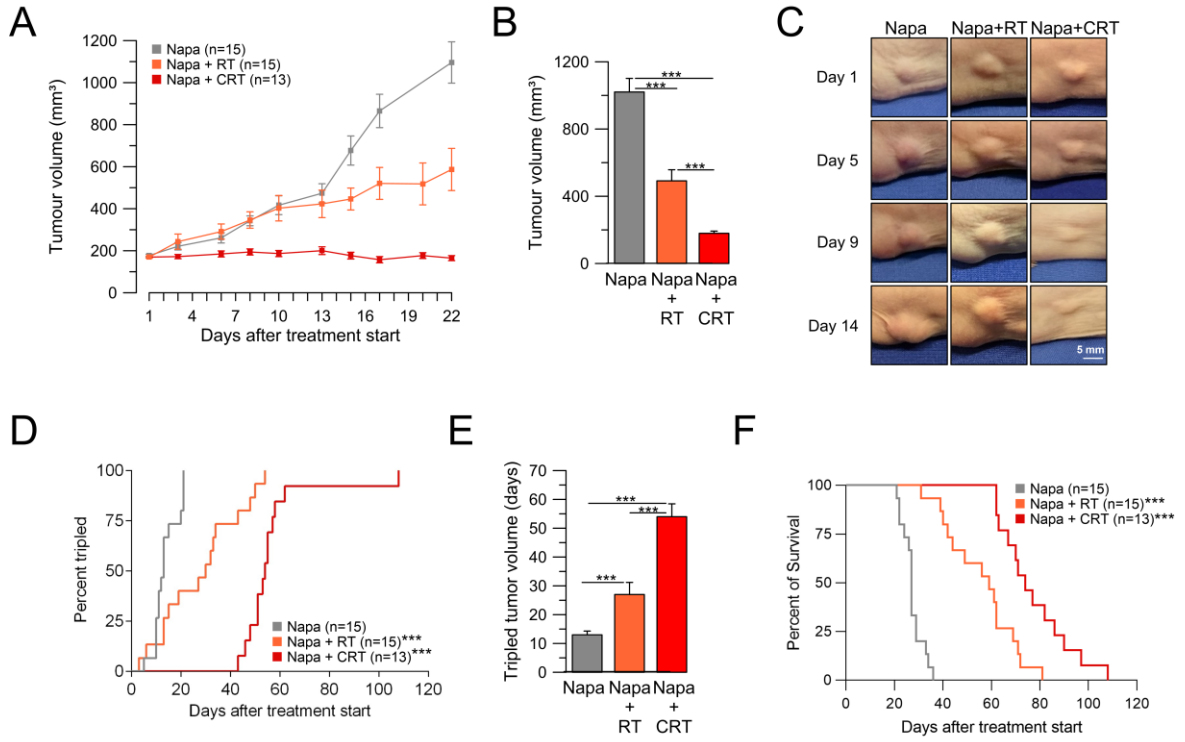

Figure 4.13 Influence of irradiation and chemoradiotherapy on tumor volume.
A| - B| Tumor volumes of mice during treatment only with Napabucasin, with RT or with CRT (A), and at the end of treatment (B.) **C|** Respective pictures of tumors under different treatments during the 14 days treatment period. Pictures were taken 1 day, 5 days, 9 days, and 14 days after treatment start. **D|** Kaplan-Meier curves were calculated to analyze the time to tumor tripling in the respective groups. **E|** The median tumor tripling time of Napabucasin treated mice was 13 days, compared to 27 days of Napabucasin + RT and 54 days of Napabucasin + CRT treated mice. **F|** Kaplan-Meier curves comparing the survival of the three Napabucasin treated groups, respectively. *P*-values were calculated by mixed-effects analysis using Tukey's multiple comparisons test (A), unpaired two-sample Student's t-test (B and E) or Log-rank (Mantel-Cox) test (D and F). Data points consisted of at least seven mice (A).

4.2.1.4 Treatment with Napabucasin in combination with CRT completely abrogated tumor growth during treatment period

To determine whether CRT alone induces the suppression of the tumor volume we compared DMSO + CRT treated mice with Napabucasin + CRT treated mice. However, when combined with CRT, Napabucasin treatment completely abrogated tumor growth (**Fig. 4.14 A-C**).

In addition, Kapla- Meier curves were calculated to compare the tumor regrowth between Napabucasin + CRT and DMSO + CRT groups (**Fig. 4.14 D**). The additional administration of Napabucasin increased the median tumor tripling time from 43 days to 53 days (**Fig. 4.14 E**).

No survival advantage was seen when treating mice with Napabucasin + CRT compared to DMSO + CRT (**Fig. 4.14 F**).

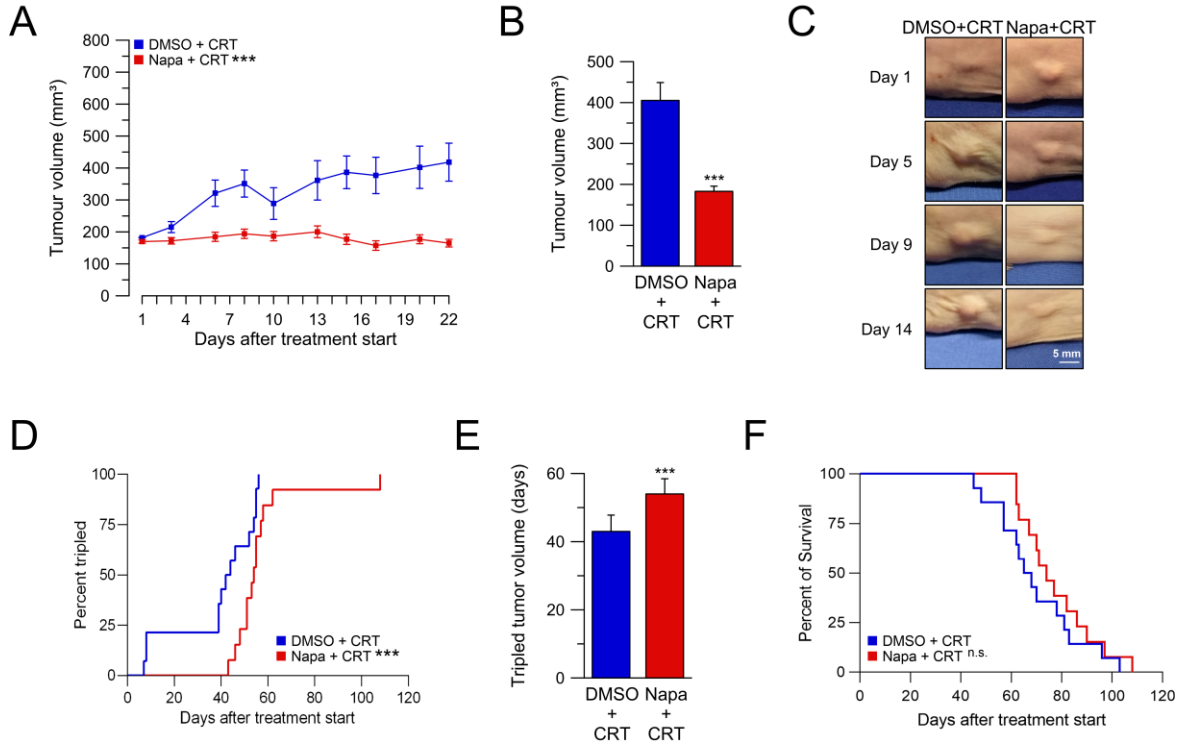

Figure 4.14 The treatment with Napabucasin and CRT diminishes tumor volume.
A| and **B|** Tumor volumes of mice during treatment only with DMSO and Napabucasin with CRT (***P < 0.0001) (A), and at the end of treatment (B) [71], ***P = 6.668E-05. **C|** Respective pictures of tumors under different treatments during the 14 days treatment period. Pictures were taken 1 day, 5 days, 9 days, and 14 days after treatment start. **D|** Kaplan-Meier curves were calculated to analyze the time to tumor tripling in the respective groups [71]. **E|** The median tumor tripling time of DMSO + CRT treated mice was 43 days, compared to 54 days of Napabucasin + CRT treated mice [71], **P = 1.13E-02. **F|** Kaplan-Meier curves comparing the survival of DMSO + CRT treated mice with Napabucasin + CRT treated mice, respectively (n.s). *P*-values were calculated by mixed-effects analysis using Tukey's multiple comparisons test (A), unpaired two-sample Student's t-test (B and E) or Log-rank (Mantel-Cox) test (D and F). Data points consisted of at least seven mice (A).

So far, the results in human CRC cells as well as in xenograft nude mice model led to the conclusion that transcriptionally active STAT3 controls CRT sensitivity *in vitro* and *in vivo*. This CRT sensitivity can be modified by manipulating the gp130/JAK/STAT pathway specifically by manipulating activated STAT3. Alteration of STAT3 activity by direct (RNAi, Napabucasin, or mutation of the phosphorylation site Y705) and indirect (Tocilizumab and Ruxolitinib) inhibition increased CRT sensitivity, whereas activation of STAT3 by gp130/JAK axis-activating Hy-IL-6 decreased CRT sensitivity. The use of Napabucasin demonstrated, both from cell culture data and in the xenograft nude mice model, that inhibition of STAT3 leads to CRT sensitization, an abrogated tumor growth as well as a significant advantage in time of tumor regrowth.

4.3 Target genes of the gp130/STAT3 axis

To gain insights into the STAT3-controlled CRT resistance, I analyzed the consequences of STAT3 perturbation on a global transcriptome level. Therefore, I used RNA-Seq technology to identify respective STAT3 downstream targets that functionally mediate the resistance phenotype. I have demonstrated that siRNA mediated STAT3 knock down resulted in decreased clonogenic survival in CRC cells (**Fig. 4.1**). Likewise, I have demonstrated that stimulation with Hy-IL-6 resulted in remarkably increased clonogenic survival of STAT3-expressing CRC cells (**Fig. 4.3**).

Based on these results, SW837 cells were either transfected with siRNA targeting STAT3 or with a negative control siRNA (siCtrl.). 80 h after transfection, cells were stimulated with Hy-IL-6 for 16 h or were left untreated. After stimulation cells were harvested for further protein or RNA analysis (**Fig. 4.15 A**). RNA-Seq data and abundance measurement files have been submitted to the GEO under the accession number GSE139455. Western blot validation using antibodies against STAT3 and pSTAT3^{Y705} showed a clear STAT3 knock down and a Hy-IL-6 induced phosphorylation of STAT3 in the corresponding samples (**Fig. 4.15 B**).

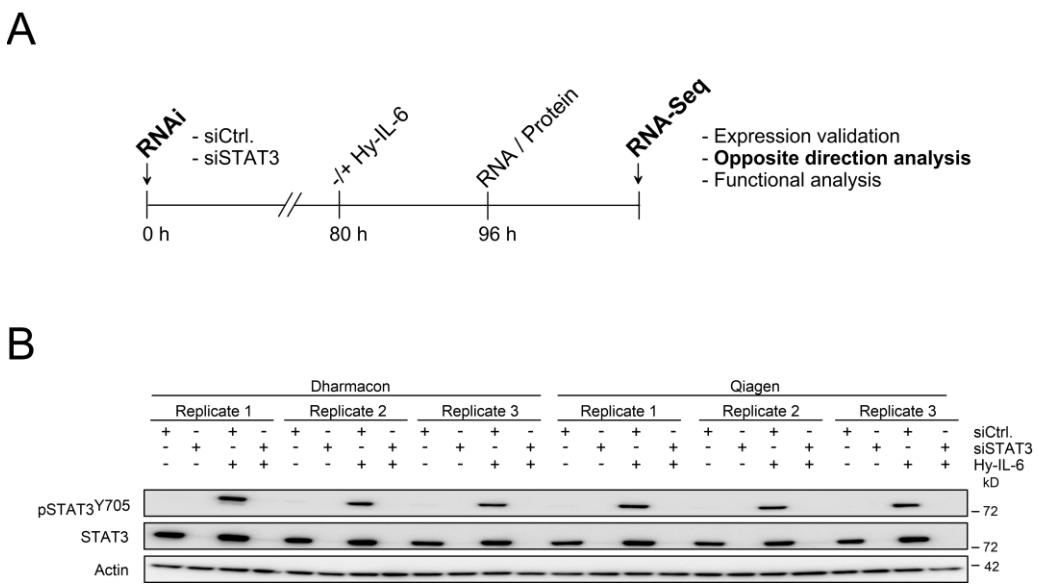

Figure 4.15 Schematic overview of the RNA-Sequencing workflow and expression validation. **A|** RNA-Sequencing-based detection of STAT3 target genes in SW837 cells with basic or silenced STAT3 expression in the presence or absence of Hyper-IL-6. **B|** Immunoblot analysis of siRNA-treated SW837 cells with the indicated antibodies for three experimental conditions: (a) cellular stimulation with Hyper-IL-6 either in the presence of STAT3, or (b) upon siRNA-mediated STAT3 silencing, and (c) targeted STAT3 expression without further stimulation [71].

Next, I determined differential gene expression profiles of SW837 cells under three experimental conditions: (a) cellular stimulation with Hy-IL-6 either in the presence of STAT3 (black), or (b) upon siRNA-mediated STAT3 silencing (blue), and (c) targeted STAT3 expression without further cell stimulation (orange). At a FDR cut-off 5% (FDR < 0.05), the

analysis of individual settings revealed 231 (188 up-regulated and 43 down-regulated, **Fig. 4.16 A**, *left panel*), 2,969 (979 up-regulated and 1,990 down-regulated, **Fig. 4.16 A**, *middle panel*), and 3,738 (1,628 up-regulated and 2,110 down-regulated, **Fig. 4.16 A**, *right panel*) differentially expressed (DE) genes, respectively. Further analysis revealed 71 genes that were significantly deregulated in all three settings, suggesting that their altered transcriptional activity is dually affected by STAT3 expression and cellular stimulation (**Fig. 4.16 B**, yellow).

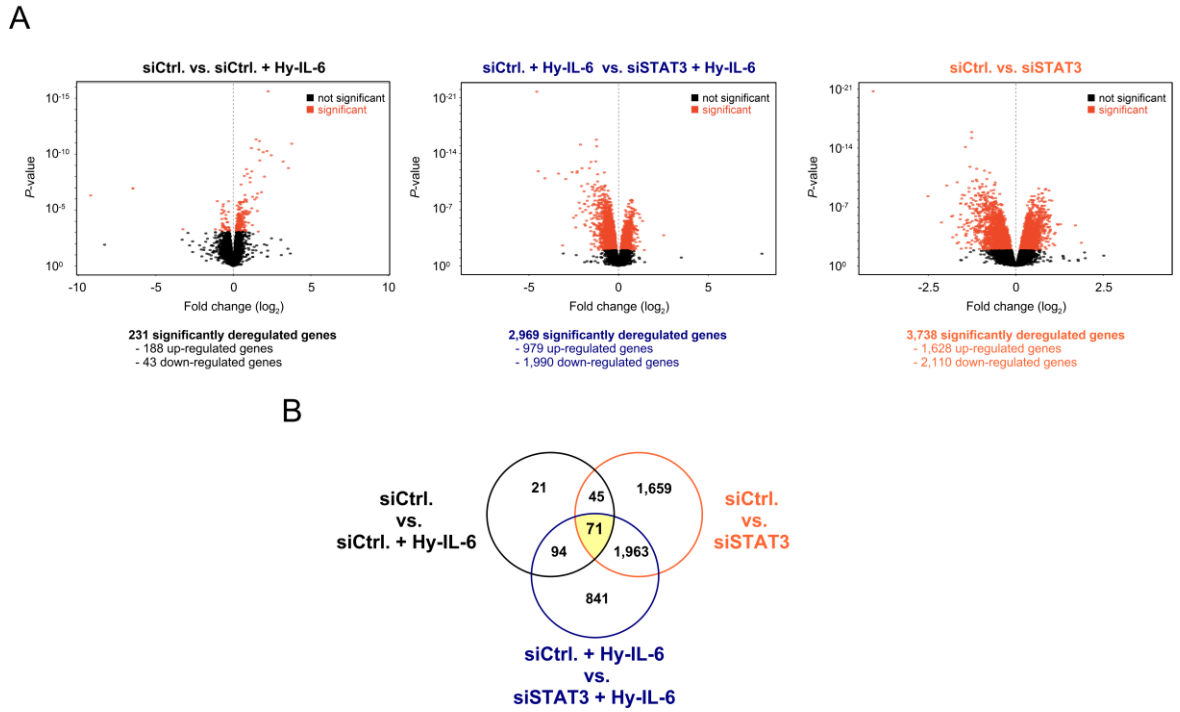

Figure 4.16 Differentially expressed genes after STAT3 pathway alterations.
A| Volcano plots depicting the number and distribution of differentially up- and down-regulated genes. The x-axis shows the $\log_2$ fold changes in expression and the y-axis the *P*-value of a differentially expressed genes. The red dots mark the genes that a significantly deregulated with an FDR cut off 5% [71]. **B|** Venn diagram of differentially expressed genes under indicated conditions (n=3). RNA-Seq revealed 231 (siCtrl. vs. siCtrl. + Hy-IL-6 *left panel*), 2,969 (siCtrl. + Hy-IL-6 vs. siSTAT3 + Hy-IL-6, *middle panel*), and 3,738 (siCtrl. vs. siSTAT3, *right panel*) significant genes (FDR < 0.05), respectively [71].

4.3.1 Opposite Direction Analysis uncovered dual influenced STAT3 target genes

To filter the genes more stringently, I considered only genes that were upregulated or downregulated after pathway stimulation, and simultaneously but inversely, regulated after STAT3 inhibition, for the next experiments. Such Opposite Direction Analysis (ODA) ensured that I only work with genes that were dually influenced by pathway inhibition and activation. The ODA revealed 55 candidate genes probably playing an influential role in STAT3-mediated CRT-resistance (**Fig. 4.17)**. Interestingly, 53 of the 55 genes are upregulated after stimulation

and downregulated after STAT3 silencing and even more downregulated after STAT3 silencing along with Hy-IL-6 stimulation.

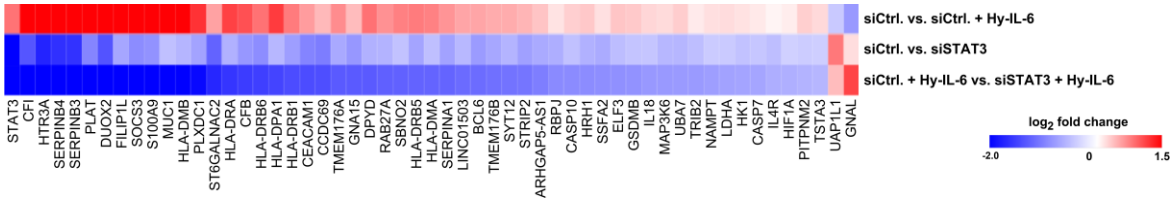

Figure 4.17 Opposite Direction Analysis reveal 55 genes.
A| Expression profiles of genes fulfilling the Opposite Direction Analysis criteria of being upregulated on stimulation with Hy-IL-6, and downregulated on STAT3 inhibition, and *vice versa* [71].

In order to technically validate the results generated so far, I quantified the mRNA expression levels of 12 selected ODA genes for all three conditions using qRT-PCR analysis. Data obtained by RNA-Seq tightly and significantly correlated with those generated by PCR, demonstrating the accuracy of the screening approach (**Fig. 4.18**).

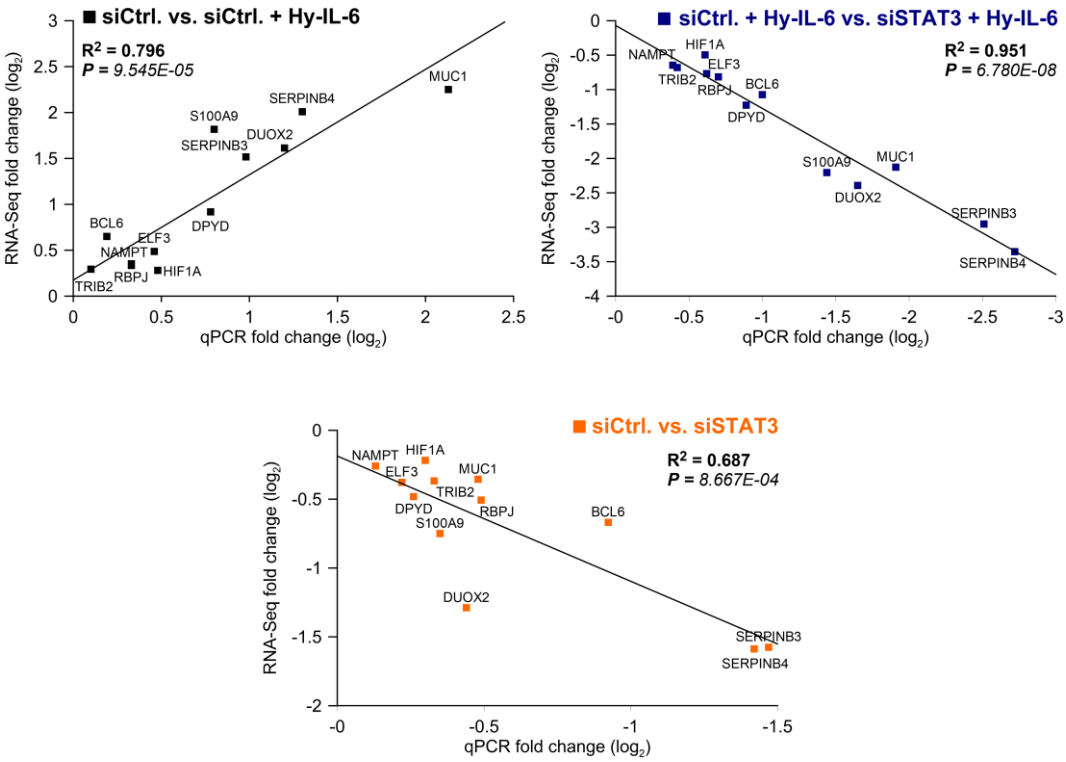

Figure 4.18 qRT-PCR validation of 12 chosen ODA genes.
Linear model analysis correlating mRNA fold changes elucidated by RNA-Seq with qPCR values of 12 chosen ODA genes. *P*-values were calculated using Pearson's correlation [71].

To identify potential STAT3 target genes, that may impact the CRT resistance, I classified the 55 ODA genes into 4 functional categories, respectively (**Fig. 4.19**). Category 1 includes genes that are predominantly related to regulation and functionality of the immune system (**Fig. 4.19**, *upper right*), category 2 includes genes that primarily contribute to signalling transduction

processes (**Fig. 4.19**, *upper left*), category 3 includes genes important in metabolic processes (**Fig. 4.19**, *lower left*) and category 4 includes genes that have functions outside the previous 3 categories (**Fig. 4.19**, *lower right*). However, the function of some genes cannot be assigned to only one category, so affected genes are listed in the crossover areas between categories.

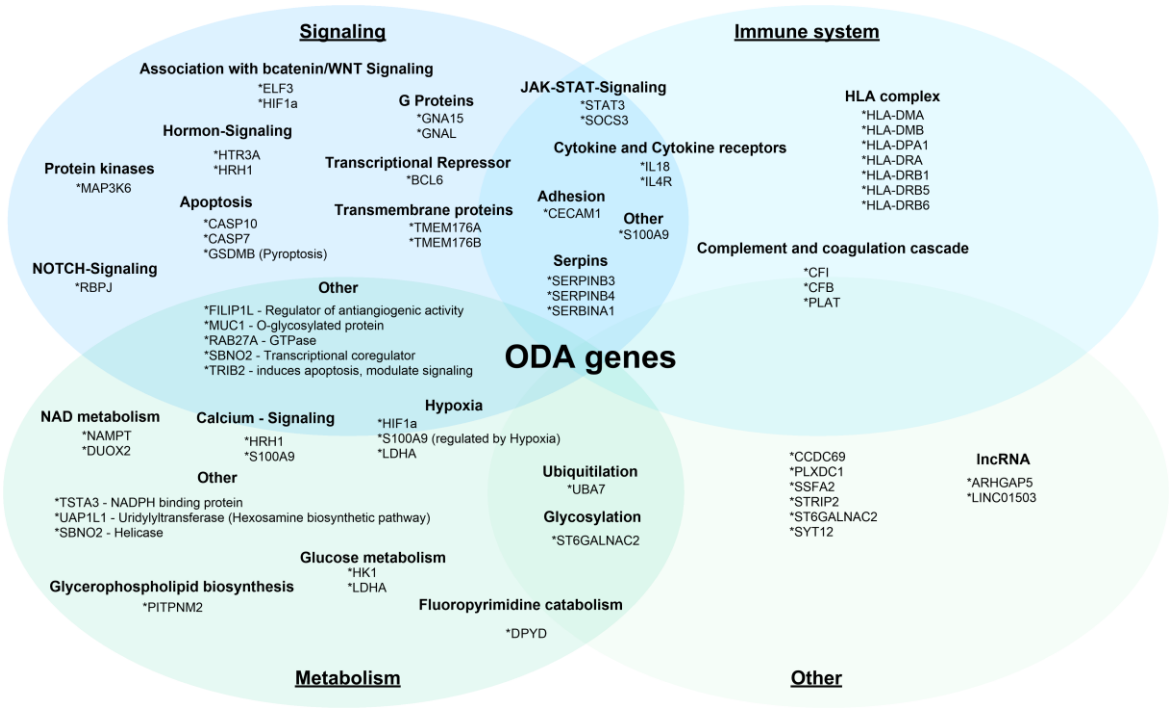

Figure 4.19 ODA genes were classified according to their function.
The 55 ODA genes were filtered according to information found in the human gene database (GeneCards).

The representation in **Figure 4.19** illustrated the wide range of genes that are dually influenced by Hy-IL-6 stimulation and STAT3 silencing. The analysis revealed genes involved in many signalling pathways and regulatory processes. Some of these pathways and processes have been previously linked to CRC and therapy resistance.

To narrow this gene list down, I conducted a literature search that included information's of the genes regarding their importance in CRC. I additionally searched for possible associations between the expression of the genes and a therapy-radio resistance. Based on these results, I selected the following 12 most interesting genes. The WNT/β-catenin signalling represents a key oncogenic pathway previously linked to CRT resistance [33]. E74-like ETS transcription factor 3 (ELF3) is a transcription factor which is overexpressed in CRC and promotes CRC proliferation and invasion by enhancing WNT/β-catenin signalling [188]. Furthermore, it was previously reported that ELF3 expression was associated with disease recurrence of stage II CRC [189]. Hypoxia-inducible factor 1 (HIF1A), is an established target of JAK-STAT signalling and previously reported as a potential determinant of tumor radiosensitivity [190]. In addition, HIF1A overexpression was significantly associated with higher CRC-specific mortality [191].

DPYD, encodes a key 5-FU-metabolizing enzyme dihydropyrimidine dehydrogenase [192]. DPYD is the rate-limiting enzyme, degrading over 80% of 5-FU to its inactive metabolite [193]. Different studies confirmed the predictive value of DPYD expression levels to predict the efficacy of 5-FU based therapy in CRC patients [194,195]. Hexokinase 1 (HK1), an enzyme that catalyzed the first step of glycolysis, has been identified to affect tumorigenesis of CRC and melanoma. shRNA-mediated attenuation of HK1 and HK2 led to decreased cell viability in CRC cells [196]. The transmembrane glycoprotein Mucin 1 (MUC1) impacts the response to radiotherapy in pancreatic cancer [197] and has been demonstrated to participate in maintenance, tumorigenicity, glycosylation and metastasis of colorectal cancer stem cells [198]. Evidence exist that MUC1 has an impact on chemo- and drug resistance in different types of cancer. For example, it mediated chemo-resistance in lung cancer cells [199] as well as it showed to induce drug resistance in pancreatic cancer [200]. The Nicotinamide Phosphoribosyltransferase (NAMPT) is a rate-limiting protein in the NAD salvage pathway [201]. High expression of NAMPT in tumors is associated with decreased patient survival and in mediating the radiation resistance in human glioblastoma stem-like cells [202]. It has also been shown that NAMPT is a potent oncogene in colon cancer progression [203]. B-Cell Lymphoma 6 Protein Transcript (BCL6) is highly expressed in colorectal cancer [204] and its methylation is a prognostic and chemo-sensitive marker in CRC [205]. In addition, I choose the key transcriptional regulator of the NOTCH pathway, Recombination Signal Binding Protein for Immunoglobulin k J-region (RBPJ) [206,207] . In previous studies, inhibition of the NOTCH pathway has been linked to sensitization of glioblastoma or breast cancer cells to radiation [208]. The dual oxidase 2 (DUOX2) may affect the therapeutic effect of gastrointestinal cancer [209,210] and was shown to exhibit a significant higher expression in CRC tumor samples and facilitated the invasion and metastasis ability of CRC cells [211]. Zhou *et al*. found that serum levels of the S100 calcium-binding protein A9 (S100A9) were significantly lower after surgery than before surgery in CRC patients and that S100A9 serum levels served as a diagnostic biomarker in CRC [212] and gastric cancer patients [213]. The upregulation of Serpin Family B Member 3 (SERPINB3) and Serpin Family B Member 4 (SERPINB4) has previously been described as protective in cells exposed to radiation and the suppression of these proteins has been shown to suppress tumor growth [214]. Tribbles pseudokinases 2 (TRIB2) disrupted the p53/MDM2 regulatory axis, which led to resistance to various chemotherapeutic agents [215]. Furthermore, TRIB2 expression was elevated in CRC tissue compared to normal tissues and indicated a poor prognosis of CRC patients [216].

4.3.2 Influence of preselected STAT3 downstream targets on RT resistance

Next, I tested whether the depletion of the 12 preselected ODA genes (*BCL6*, *DPYD*, *DUOX2*, *ELF3*, *HIF1A*, *MUC1*, *NAMPT*, *RBPJ*, *S100A9*, *SERPINB3*, *SERPINB4*, *TRIB2*) had an impact on RT resistance (**Fig. 4.20 A**). Towards this, SW837 cells were transfected with

either siRNAs targeting one of the 12 genes or with a control siRNA (siCtrl.). As a control, SW837 cells were additionally transfected with siRNA targeting STAT3, since it has already been shown that a STAT3 KD led to a sensitization of the cells to CRT (**Fig. 4.1**, *middle panel*). For further analysis, cells were stimulated with Hy-IL-6 (**Fig. 4.20 A**) and were subsequently irradiated with 4 or 6 Gy or were left without any further irradiation. The CFA survival of all samples after 4 Gy irradiation was determined (**Fig. 4.20 B**, *left panel*). The calculated SF of the control samples (black columns) were set to 100% survival. The blue columns represent samples with SF below 100% meaning that a depletion of the respective target gene sensitize SW837 cells against RT. KD of *STAT3* as well as *BCL6*, *DPYD*, *DUOX2*, *HIF1A*, *MUC1*, *NAMPT*, *RBPJ*, *S100A9*, and *SERPINB3* resulted in sensitization of the cells to irradiation with 4 Gy. The SF of these genes were subsequently analyzed after 6 Gy irradiation (**Fig. 4.20 B**, *right panel*). In addition to the KD of STAT3, the depletion of *BCL6*, *DPYD*, *HIF1A*, *MUC1*, *NAMPT* and *RBPJ* also showed a sensitizing effect against irradiation. Based on this screening experiment as well as the literature research, I selected the four most interesting genes (*RBPJ, MUC1*, *BCL6* and *NAMPT*), with which I will conduct further experiments regarding resistance towards RT in SW837 cells.

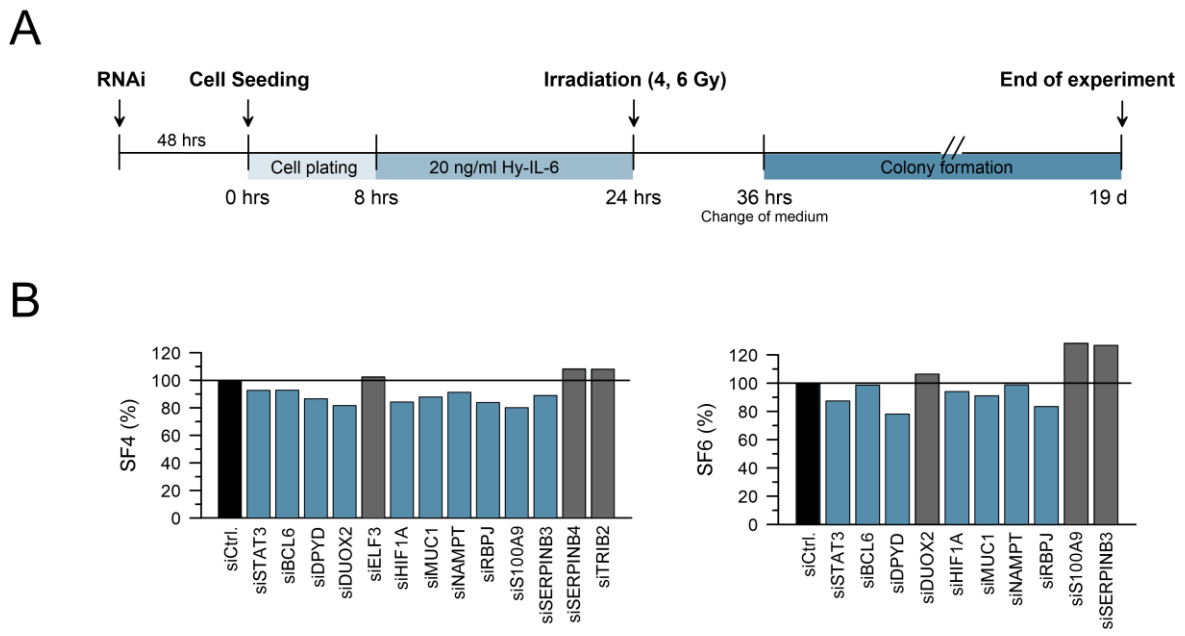

Figure 4.20 Pre-screening of STAT3 target genes in SW837 cells.
A| Schematic overview of the screening experiment. SW837 cells were transfected with control siRNA (siCtrl.) or 12 different siRNA targeting the indicated genes. After cell plating and 16 h stimulation with Hy-IL-6 cells were irradiated with 4 or 6 Gy or were left without irradiation. For CFA analysis the medium was exchanged, and the cells could form colonies for 19 d. **B|** CFA survival of all samples after 4 Gy irradiation (*left panel*). The SF of the control sample (black column) was set to 100% survival. The blue columns represent samples that SF is below 100% and the grey columns represent samples that survival is above 100%. The samples with SF below 100% after 4 Gy irradiation were analyzed for SF after 6 Gy irradiation (*right panel*). Data presented as mean from n=2 independent biological replicates.

To further investigate the selected genes for their ability to modulate RT resistance, *MUC1*, *BCL6* and *NAMPT* were silenced in SW837 cells using RNAi (72 h - *BCL6*, *NAMPT* and *RBPJ*; 96 h- *MUC1*; *Appendix*, **Fig. 8.1,** and **Fig. 8.2**) and additionally stimulated with Hy-IL-6. Successful KD of each gene was determined using qRT-PCR (**Fig. 4.21 A**, *left panel*) or immunoblotting (**Fig. 4.21 B -D**, *left panels*). Additionally, cells were CFA-cultured to measure their survival following irradiation. Silencing of *BCL6*, *NAMPT* and *RBPJ* significantly increased the sensitivity of SW837 cells towards irradiation (**Fig. 4.21 A** and **C**, *right panels*) whereas the sensitivity of SW837 was not changed after *MUC1* KD (**Fig. 4.21 B**, *right panel*).

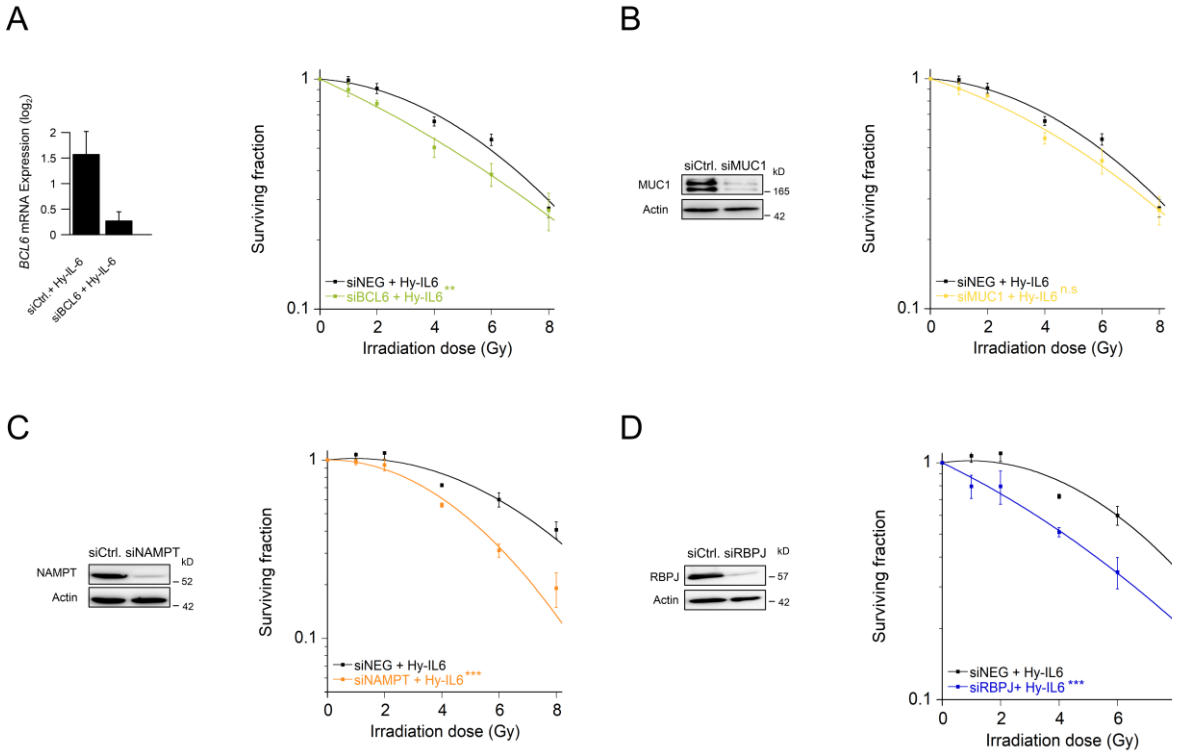

Figure 4.21 siRNA-mediated silencing of *BCL6*, *NAMPT* and *RBPJ* results in a sensitization of SW837 cells to RT.
A| - D| SW837 cells were treated with Hy-IL-6 and siRNA targeting *BCL6* (A, 72 h RNAi treatment), *MUC1* (B, 96 h RNAi treatment), *NAMPT* (C, 72 h RNAi treatment), *RBPJ* (D,72 h RNAi treatment) or with a control siRNA (siCtrl.)[71]. Cells were colony formation assay (CFA)-cultured to measure their survival following irradiation (RT) (*right panel*s). Representative RT-qPCR analysis (A) or Western blot analysis with the indicated antibodies (B, C and D) (*left panel*s). Data presented as mean ± s.e.m. from at least n=3 independent biological replicates. *P < 0.05, **P < 0.01, ***P < 0.001, unpaired two-sample Student's t-test or two-way analysis of variance (ANOVA).

These results indicate that STAT3-mediated CRT resistance in SW837 cells may not be controlled by a single target gene but rather is an interplay of many different proteins and signalling cascades. In order to further elucidate the exact molecular mechanism of STAT3-mediated CRT resistance, further experiments are needed to possibly uncover the network of STAT3 target genes that jointly control CRT resistance. Due to the clear sensitizing effect after

RBPJ KD, I decided in the following section of the thesis to investigate the STAT3 target gene RBPJ in more detail regarding its ability to sensitize CRC cells to CRT.

4.4 RBPJ - a promising STAT3 target gene

I first analyzed whether *RBPJ* is a direct target of STAT3 using EMSA. An *in-silico* search revealed the presence of a canonical docking site for STAT family members, called GAS sequence [217], in the first intron of the *RBPJ* gene approximately 300 bp 3' of the known promotor region and 75 bp downstream of the first exon (**Fig. 4.22 A**).

For identification of STAT1 binding, cellular extracts from unstimulated and IFNγ stimulated HeLa cells [141] were incubated with the [^{33}P]-labelled high-affinity control GAS probe M67. The autoradiograms showed a specific signal that was interpreted to represent binding of STAT1 protein to the M67 probe after IFNγ stimulation (line 2), whereas I could not detect a binding in unstimulated extracts (line 1). Using cellular extracts from Hy-IL-6-stimulated SW837 cells in gel-shift assays, I found that STAT3, which has a slightly slower electrophoretic migration than STAT1 [218], bound to [^{33}P]-labelled duplex oligonucleotides of the native sequence 5´-TTCCGGGAT-´3 (nat) (line 5), but not to a mutated sequence thereof (5´-CCTTGGTAG-´3) (mut) (line 3). In addition, competition experiments using cell lysates incubated with the [^{33}P]-labelled native sequence and subsequently challenged by a 750-fold molar excess of unlabeled DNA of the same sequence resulted in a complete loss of DNA binding activity (line 4) (**Fig. 4.22 B**). These observations demonstrated that STAT proteins are sequence-specifically recruited to the *RBPJ* promoter in SW837 cells.

Figure 4.22 EMSA showing STAT protein binding to GAS elements in the human RBPJ promoter. A| Cut out of the promotor region sequence of RBPJ. Exons 1 and 2 are highlighted in grey, the gamma-interferon-activation sequence (GAS) in turquoise and a GAS-like element in blue [71]. The shown gene sequence was obtained from www.ensembl.org. **B|** Binding of STAT proteins to [^{33}P]-labelled oligonucleotides encompassing prototypic GAS (M67), a mutated GAS (mut) or the native GAS element (nat) from the *RBPJ* promotor, was analyzed by EMSA using unstimulated or IFN-γ-stimulated HeLa cells, or Hy-IL-6-stimulated SW837 cells. As control, the labelled M67 probe was outcompeted (com) by incubating lysates with an excess of unlabeled M67 probe [71].

The EMSA experiment demonstrates that the expression of RBPJ can most likely be directly controlled by STAT3. Upon activation STAT3 can bind to the GAS binding site present in the RBPJ promoter region and thus regulate RBPJ as one of its direct target genes.

4.4.1 The gp130/STAT3 axis connects with the RBPJ-dependent NOTCH signalling pathway

The NOTCH signalling has been known for decades and was originally found during cell fate determination from Drosophila to humans [219-223]. It is a conserved ligand-receptor signalling pathway which can regulate cell differentiation, proliferation, survival, apoptosis, stem cell maintenance as well as the self-renewal of progenitor and stem cells in both adult and embryonic organs [224,225]. At present, four NOTCH receptors have been identified in humans, such as NOTCH 1-4 [224]. Mature NOTCH receptors are heterodimeric proteins consisting of a transmembrane subunit (NTM) and an extracellular subunit (NEC) derived from proteolytic processing of large single-chain precursors by a furin-like protease in the trans-Golgi network (**Fig. 5.1**, *left*) [220,224,226]. NOTCH receptors are activated by interacting with cell membrane-associated ligands designated as either Delta-like (DLL1, DLL3, DLL4) or Serrate-like ligands (JAG1 and JAG2) [223,227]. The ligation of NOTCH receptors to their ligands is followed by a receptor subunit separation and two strictly controlled proteolytic cleavage steps. The first cleavage step is mediated by ADAM/TACE metalloproteases, that cleave the receptor at S2, which initiates a S3 cleavage mediated by the γ-secretase complex (composed of presenilin 1 and 2, nicastrin, presenilin enhancer 2, and anterior pharynx-defective 1) [206,207,225]. This series of cleavages release the active form of NOTCH called NOTCH intracellular domain (NICD), which translocate into the nucleus where it assembles with the conserved DNA-binding protein, RBPJ to drive the expression of NOTCH target genes [206,207]. The initially inactive RBPJ complex binds to a corepressor complex (CoR) which gets exchange after binding of NICD by recruitment of a coactivation complex (CoA) (**Fig. 5.1**, *right*) [207].

4.4.1.1 The NOTCH expression profile in CRC

First, I tested for the presence of NICD as an indicator for constitutive NOTCH signalling as well as for other important NOTCH signalling components. Immunoblot against NICD revealed a strongt NICD expression in unstimulated CRT-resistant SW837 and SW1463 cells (**Fig. 4.23 A**, *left panel*), that, in marked contrast, was almost absent in CRT-sensitive LS411N cells. In accordance, expression of the transcription factor HES1, a main target of active NOTCH signalling [228] was weak in LS411N cells but easily detectable in SW837 and SW1463 cells. Moreover, the signal intensities of HES1 expression are proportional to the NICD positivity and CRT sensitivity of the three cell lines (**Fig. 4.23 A**, *middle panel*). Furthermore, the presence of NICD in the tested cell lines directly correlated with their STAT3 transcriptional activity (**Fig. 4.23 A**, *right panel*).

The cause of constitutive NICD generation in CRT-resistant cells was evaluated by a detailed expression analysis of proteins involved in regulating the NOTCH processing (**Fig. 4.23 B**). SW837, SW1463 and LS411N cells were tested positive for three different NOTCH receptors (NOTCH 1,2,3) (**Fig. 4.23 B**, *left panel*), different patterns of NOTCH ligands (Jagged 1/2 and DELTA-like) (**Fig. 4.23 B**, *middle panel*) and NOTCH cleaving components such as ADAM proteases or γ-secretases complex subunits (presenilin 1, presenilin 2, Nicastrin, PEN2) (**Fig. 4.23 B**, *right panel*). However, a combination of elements capable of NOTCH processing was found only in CRT-resistant SW837 and SW1463 cells, but not in LS411N cells. This uncovered a cell-intrinsic tonic NOTCH signalling activity that is moreover critically relevant for CRT-resistant cells than for CRT-sensitive cells.

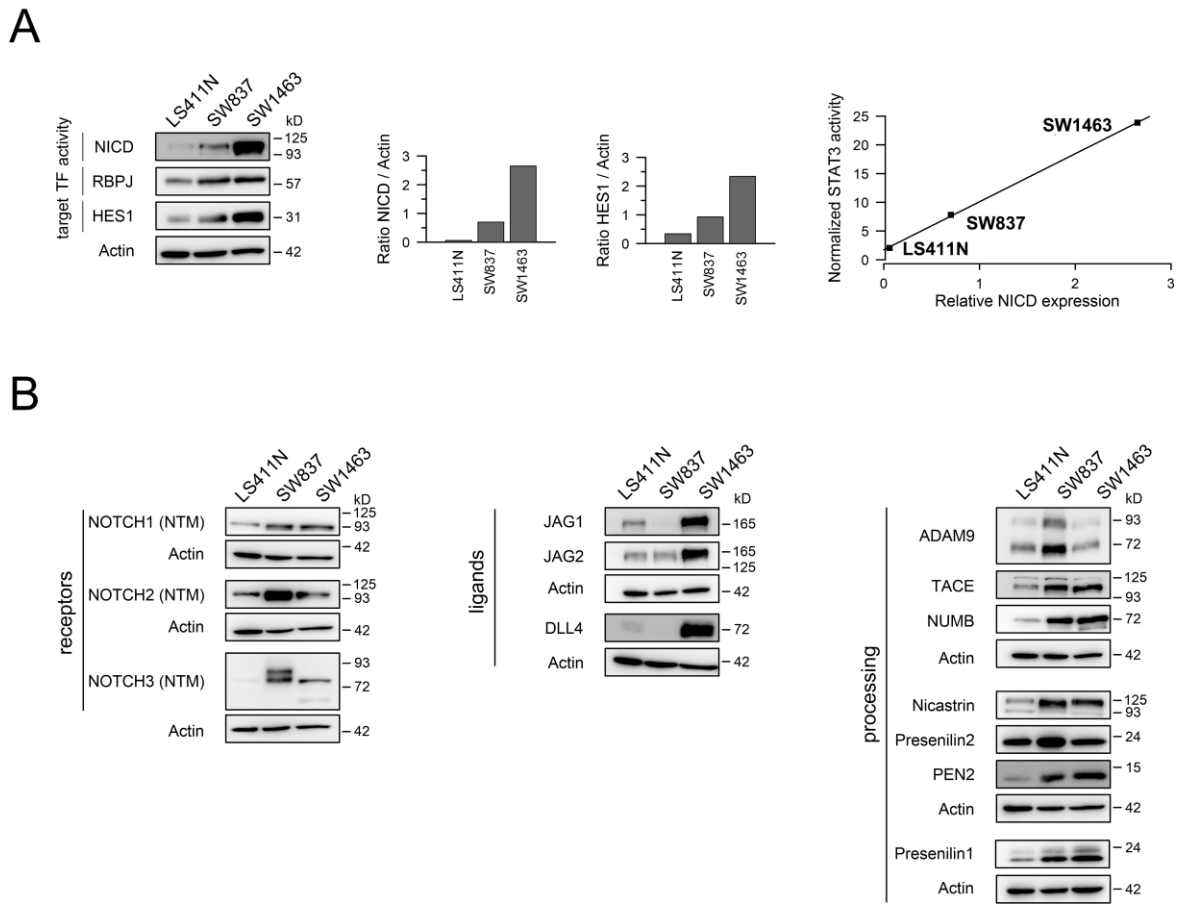

Figure 4.23 NOTCH expression profile in unstimulated CRC cells.
A| Expression analysis of NOTCH pathway components (*upper panel*) and correlation of NICD expression with STAT3 transcriptional activity (*lower panel*) [71]. **B|** Expression analysis NOTCH receptors (*left panel*) and ligands (*middle panel*) as well as γ-secretase complex and additional NOTCH pathway processing proteins (*right panel*) [71].

To investigate the effect of Hy-IL-6 stimulation on the NOTCH expression profile of CRC cells, I stimulated LS411N, SW837 and SW1463 cells with Hy-IL-6 or I left the cells untreated. Western Blot analysis revealed an increased expression of RBPJ in all cell lines (**Fig. 4.24 A**).

Furthermore, I detected increased expression levels of NICD, NOTCH2, NOTCH3 indicating a stronger activation of NOTCH signalling compared to untreated cells in SW837 cells (**Fig. 4.24 A**, *middle panel*). NICD expression was not influenced by stimulation in SW1463 and NOTCH2, NOTCH3 expression is decreased after stimulation (**Fig. 4.24 A**, *right panel*). In stimulated LS411N cells the NICD expression is strongly decreased suggesting a weakened NOTCH1 signalling whereas the NOTCH2 expression is unchanged and the NOTCH3 expression is increased (**Fig. 4.24 A**, *left panel*).

At present, CRT plays an integral part in treatment concepts for various tumor entities [68-70]. Therefore, I analyzed whether irradiation had an impact on the expression of NOTCH signalling components in CRC cells. LS411N, SW837 and SW1463 cells were irradiated with different doses ranging from 0 Gy to 8 Gy, respectively. Increased expression of NICD and NOTCH2 can be detected in irradiated SW837 and SW1463 cells compared to unirradiated cells. In addition, the RBPJ expression in SW1463 cells was increased while it remained unchanged in SW837 (**Fig. 4.24 B,** *middle* and *right panel*). Surprisingly, the protein level of NICD, RBPJ and NOTCH2 decreased following irradiation in LS411N cells (**Fig. 4.24 B***, left panel*).

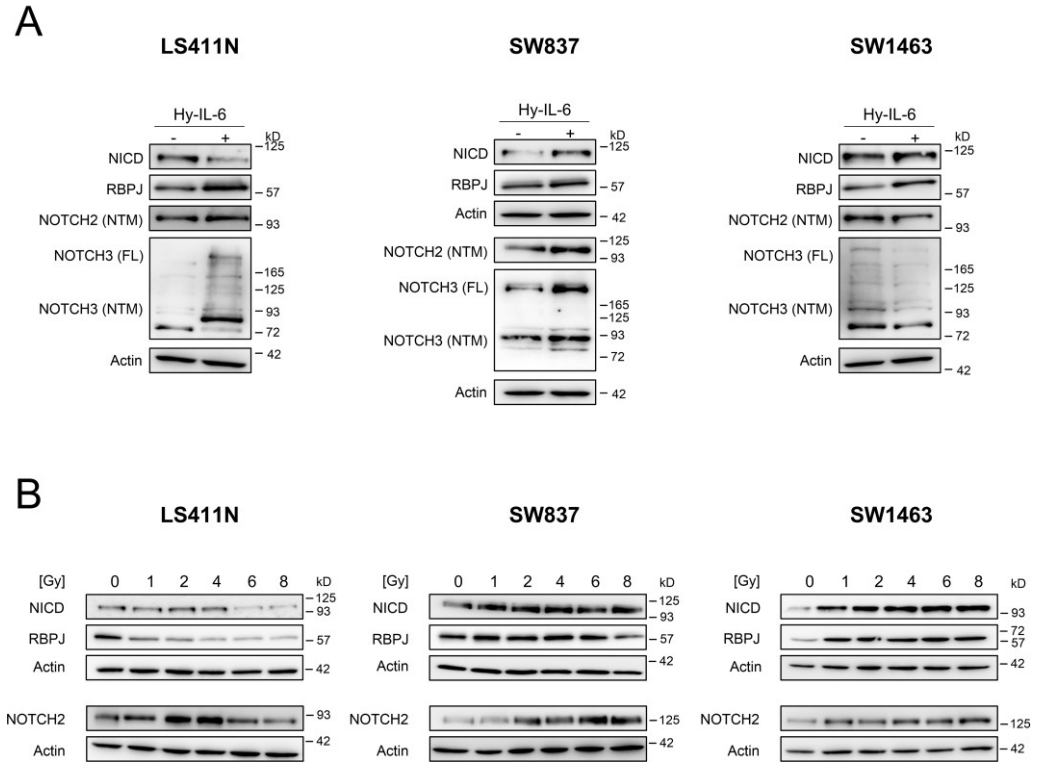

Figure 4.24 The influence of Hy-IL-6 or irradiation on the NOTCH expression profile.
A| CRC cells were stimulated with Hy-IL-6 (20 ng/ml, 16 h) and isolated proteins were analyzed using immunoblot with the indicated antibodies. Data presented as mean ± s.e.m. from at least n=3 independent biological replicates. **B|** CRC cells were irradiated (0-8 Gy) and isolated proteins were analyzed using immunoblot with indicated antibodies [71].

In this section, I demonstrated that SW837, SW1463, and LS411N express selected NOTCH signalling components. I discovered that the CRT-sensitive LS411N cells expressed the

NOTCH components, including NICD, less than the CRT-resistant SW837 and SW1463 cells. Furthermore, I could show that the expression of NOTCH pathway components is a cell line specific, dynamic process and is dependent on stimulation or irradiation. This again reflects the enormous heterogeneity of the individual cell lines.

4.4.2 Perturbations of the NOTCH signalling pathway modulates CRT resistance

Up to this point, I demonstrated that inhibition of RBPJ by RNAi rendered SW837 cells more sensitive to RT (**Fig 4.21 D**) and that LS411N, SW837 and SW1463 cells express important NOTCH signalling components depending on various stimuli (**Fig 4.23** and **4.24**).

Furthermore, I tested to what extent RBPJ contributes to STAT3-mediated CRT resistance by silencing the expression of the two proteins either alone or in combination. Successful RNAi mediated STAT3 and RBPJ KD as well as the inhibitory effect of the STAT3 KD on pSTAT3^{Y705} levels and the RBPJ KD on NICD levels were confirmed using immunoblotting (**Fig. 4.25**, *right panel*). Western Blot analysis of SW837 cells treated with siRNA targeting RBPJ show a decreased expression of the NOTCH intracellular domain NICD compared to the negative control (**Fig 4.25**, *right panel*). In our study NICD serves as a marker for active NOTCH Signalling. Proofing that a depletion of RBPJ damped the NICD expression and at the same time the NOTCH signalling. As observed in **Fig. 4.1** and **Fig. 4.21**, both approaches individually affect CRT sensitivity significantly (**Fig. 4.25**, *left panel*). However, when the two treatments are combined, no synergistic effect can be observed in terms of a change in CRT sensitivity (**Fig. 4.25**, *left panel*). Moreover, RBPJ silencing phenocopied STAT3 silencing as targeting RBPJ alone was as effective as inhibition of STAT3 itself. Indeed, the CFA survival curves of all three experimental settings were nearly identical (**Fig. 4.25**), indicating that RBPJ, similar to STAT3, is a key determinant of CRT resistance.

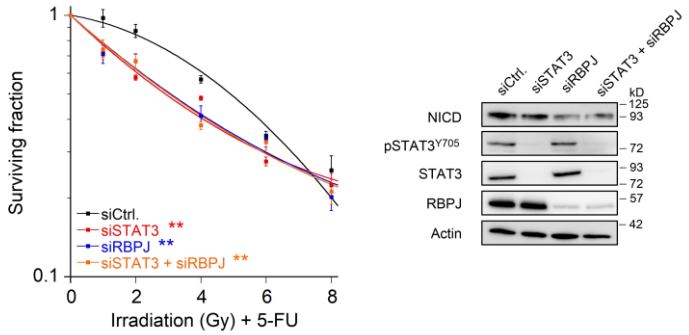

Figure 4.25 Combined silencing of *STAT3* and *RBPJ* has no additive effect on CRT resistance. SW837 cells were treated with siRNA against *STAT3* and *RBPJ*, either alone or in combination and were cultured in colony formation assays (CFA) to measure their survival following irradiation in the presence of 5-FU (CRT) (*left panel*) [71]. Representative Western blot analysis with the indicated antibodies. Data presented as mean ± s.e.m. from at least n=3 independent biological replicates. *P < 0.05, **P < 0.01, ***P < 0.001, unpaired two-sample Student's t-test or two-way analysis of variance (ANOVA).

Since I observed a correlation between RBPJ-dependent NOTCH signalling and CRC resistance, as well as a cell-intrinsic tonic NOTCH processing activity, I wanted to test the impact of pharmacological NOTCH pathway inhibition on CRT resistance.

The γ-secretase complex catalyzed the cleavages of a variety of transmembrane proteins by untethering the cytoplasmic domain from the membrane, that allow the cytoplasmic domains to transduce signals to the nucleus [229,230]. Thus, this enzyme complex is a potent target for many anti-NOTCH therapies because its inhibition abolished further NOTCH activity completely. In recent years, a significant number of clinical trials have also been conducted in which GSI were used as anticancer agents [231]. The chemical compound *N*-[*N*-(3,5-difluorophenacetyl)-L-alanyl] -(*S*)-phenylglycine *t*-butyl ester (DAPT) [232] is a GSI which showed to re-sensitize platinum resistant A2780/CP70 and OV2008/C13 cells to cisplatin treatment [233]. Furthermore, treating human head and neck squamosa cell carcinoma with DAPT increased the sensitivity to cisplatin in vitro [234].

LS411N, SW837 and SW1463 cells were incubated with different DAPT concentrations ranging from 0.1 to 5 µM and for different time points (24, 48 and 72 h) to identify reasonable DAPT concentrations and timepoints (*Appendix*, **Fig 8.5 C**). To verify DAPT-induced NOTCH activity, I analyzed the expression of NICD and HES1 using Western blotting. NICD and HES1 expression was almost absent in LS411N cells treated for 24 h with 5 µM DAPT and SW163 and SW837 cells treated with 5 µM DAPT for 72 h (*Appendix*, **Fig 8.5 C**). To determine a possible DAPT-induced loss of cellular viability, I checked the cellular viability of the cells using CTB assay after 24,48 and 72 h treatment with different DAPT concentrations ranging from 0.1 to 100 µm. Even after treatment with the highest DAPT concentration, no loss of viability was observed in LS411N, SW1463 and SW837 cells (*Appendix*, **Fig 8.4 B)**.

To test the hypothesis, that cell-intrinsic tonic NOTCH signalling might be relevant for CRT resistance, I treated CRT-resistant SW837 and SW1463 as well as CRT-sensitive LS411N cells either with DAPT alone or in combination with RNAi targeting *RBPJ* (**Fig. 4.26**). In each cell line the successful RNAi mediated silencing of *RBPJ* was determined using immunoblotting. Treatment with DAPT resulted in a reduction of NICD expression in all three CRC cell lines, which is more pronounced than the reduction of NICD expression after RBPJ silencing (**Fig. 4.26**, *upper panels*). Moreover, treatment with DAPT resulted in a sensitization to CRT similar to the sensitization after RBPJ silencing in SW837 and SW1463 cells, while the combined blockade of the γ-secretases complex and RBPJ had no additive effect (**Fig. 4.26**, *lower panels*). The CRT-sensitive LS411N cells are not influenced by either RBPJ silencing or treatment with DAPT.

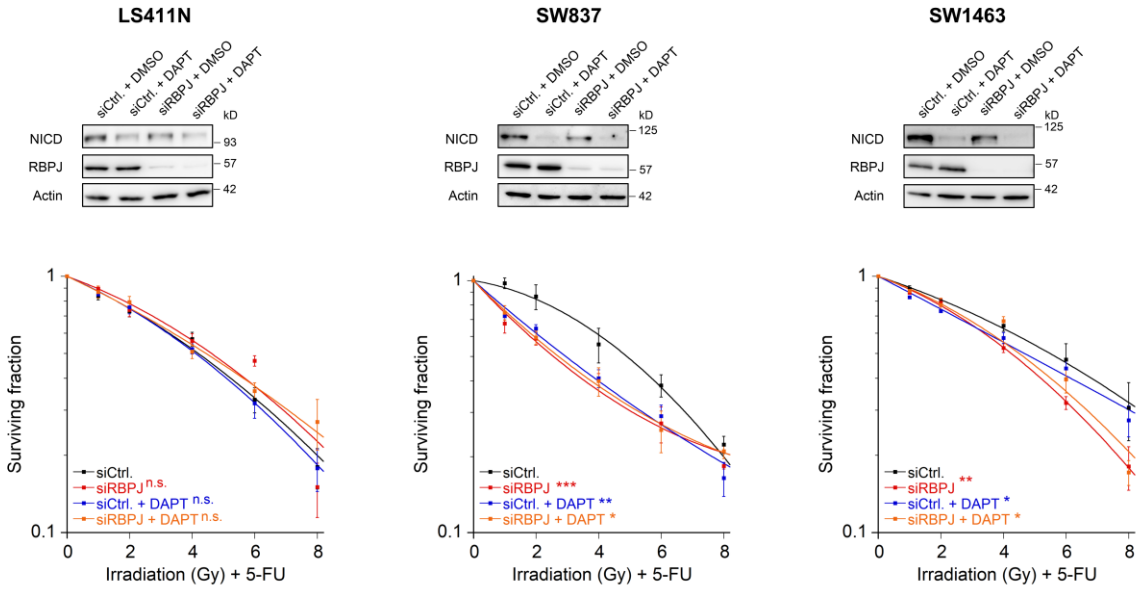

Figure 4.26 Modulation of CRT resistance after RBPJ silencing and treatment with γ-secretases inhibitor DAPT in CRC cells.
A| LS411N (*left panel*), SW837 (*middle panel*)[71], and SW1463 (*right panel*) cells were treated with RNAi against *RBPJ* and after treatment with the γ-secretases inhibitor DAPT, either alone or in combination were analyzed for expression of NICD and RBPJ by immunoblotting (*upper panels*) or were colony formation assay (CFA)-cultured to measure their survival following irradiation in the presence of 5-FU (*lower graphs*). Data presented as mean ± s.e.m. from at least n=3 independent biological replicates. *P < 0.05, **P < 0.01, ***P < 0.001, unpaired two-sample Student's t-test or two-way analysis of variance (ANOVA).

4.4.3 High expression of NOTCH receptors impairs DFS in rectal cancer patients

Finally, to investigate if the RBPJ/NOTCH axis has any prognostic relevance in CRC patients, I analyzed pretherapeutic gene expression profiles obtained from 207 patients with locally advanced rectal cancer who were treated with preoperative CRT. Kaplan-Meier curves were estimated to visualize correlation of gene expression data with clinical parameters. These curves display the DFS which was defined as the time from surgery until detection of locoregional or distant recurrence (**Fig. 4.27**, *left panels*). These curves uncover that high expression of NOTCH2, NOTCH3, and NOTCH4 is associated with impaired DFS, while there was no difference for NOTCH1 (**Fig. 4.27**). Additionally, the number of patients included for the correlation of gene expression (NOTCH1-4) with disease-free survival for each time point (months) and the two groups (high expression vs. low expression) was demonstrated (**Fig. 4.27**, *right panel*).

Furthermore, I examined the expression distribution of the four NOTCH receptors and analyzed in which tissues they are predominantly expressed (tumor or mucosa) (**Fig. 4.28**). NOTCH1 and NOTCH2 do not show clearly distinguishable expression in tumor and mucosa samples (**Fig. 4.28**, *left panels*) while NOTCH3 and NOTCH4 show a clear increased expression in tumor samples (**Fig. 4.28**, *right panels*).

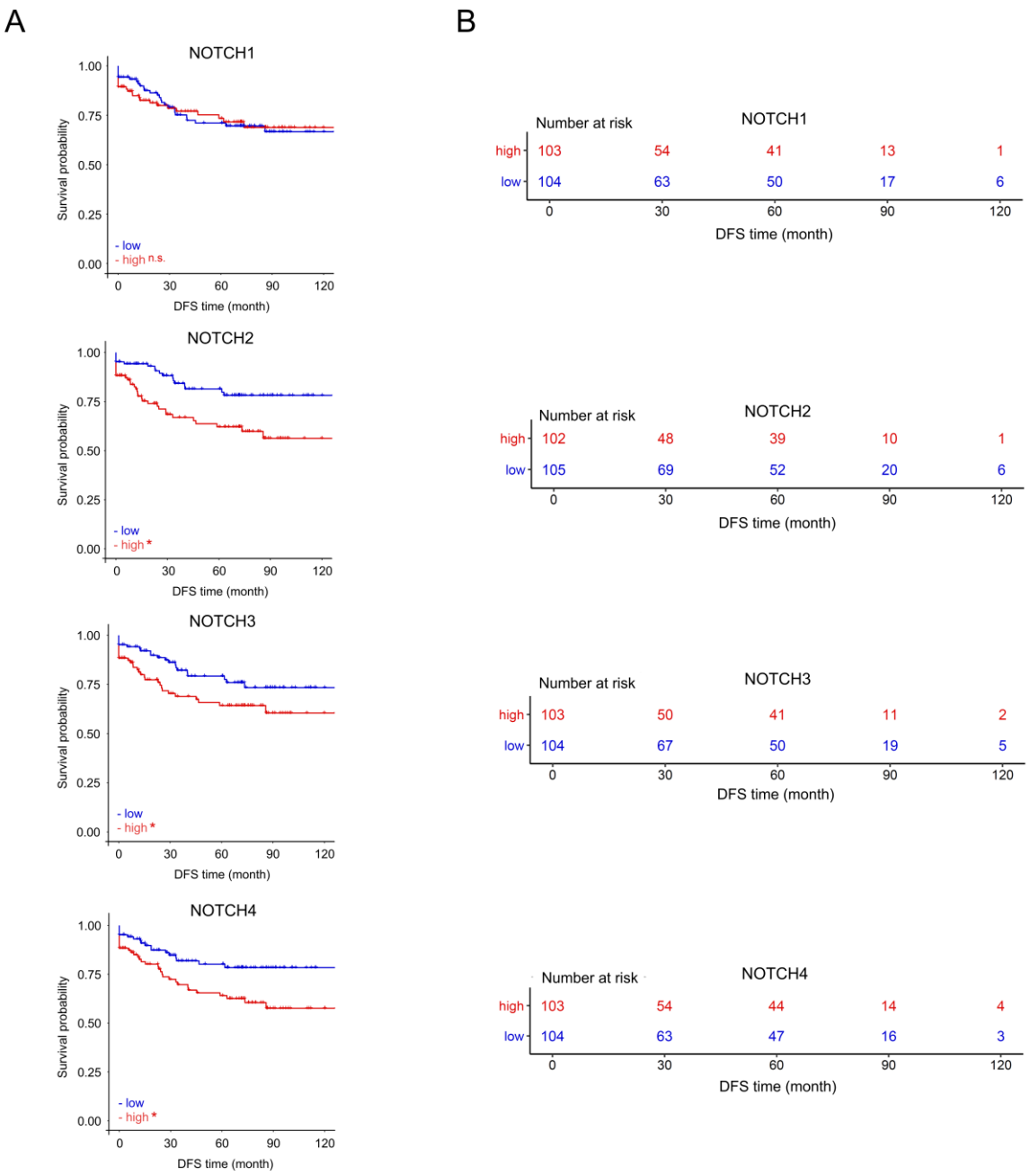

Figure 4.27 High expression of NOTCH2,3 and 4 impairs DFS in rectal cancer patients treated with preoperative CRT.
A| Survival curves of 207 rectal cancer patients who were treated with preoperative CRT. Survival data were plotted against pretherapeutic gene expression levels of NOTCH1-4, respectively [71]. **B|** Number of patients included for the correlation of gene expression (NOTCH1-4) with disease-free survival for each time point (months) and the two groups (high expression vs. low expression) [71].

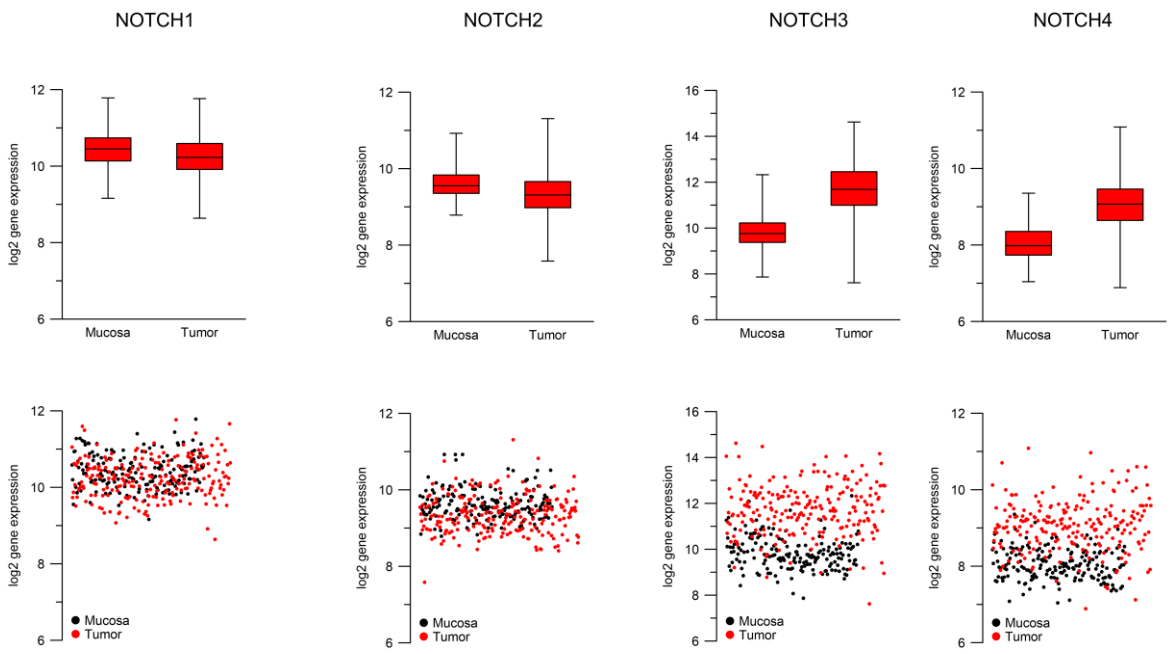

Figure 4.28 NOTCH receptor expression in tumor and mucosa samples from rectal cancer patients treated with preoperative CRT.
A| Box plot shows the expression analysis of NOTCH1-4 in tumor and mucosa samples of 207 rectal cancer patients who were treated with preoperative CRT (*upper panel*s). Distribution of respective gene expression in tumor samples (red dots) or mucosa samples (black dots) (*lower panel*s) Each dot represents one patient.

Summarized, I identified RBPJ as a direct target gene of Hy-IL-6 activated STAT3 signalling. The RBPJ-dependent NOTCH Signalling was modified by STAT3 via regulation of the RBPJ expression. Stimulation of the IL-6/STAT3 pathway via Hy-IL-6 increases the amount of RBPJ, in contrast siRNA mediated silencing of STAT3 resulted in a reduced RBPJ expression. The silencing of RBPJ, the most important binding partner of NICD, provoked in a reduced NOTCH activity and a re- sensitization to irradiation of CRC cells to CRT. Expression analysis of essential NOTCH pathway components showed cell line specific expression patterns that can be related to the respective CRT resistance of the cells. While CRT-sensitive LS411N cells express many NOTCH processing enzymes little or not at all, these are clearly expressed in the CRT-resistant cells. Furthermore, genetic and/or chemical inhibition of the NOTCH pathway shows that CRT-resistant cell lines are re-sensitized after NOTCH inhibition whereas there are no changes in CRT resistance of LS411N cells. Importantly, irradiation further increased the constitutive presence of NICD in CRT-resistant SW837 and SW1463 cells, indicating an alliance between tumor cell-intrinsic and treatment-induced signal responses. Moreover, genetic profiling of rectal cancer patients revealed the importance of the STAT3/NOTCH axis as expression of NOTCH pathway components correlated with clinical outcome. In further experiments we can try to specify the exact NOTCH receptor / ligand combinations that are accountable for the resistance of the cells against CRT.

5. Discussion

Despite ever-improving anti-cancer therapy and screening, CRC remains a major cause of cancer-related deaths globally [1-3,8-10]. Currently, the combined treatment of 5-FU-based chemotherapy, together with radiation followed by radical surgical resection of the tumor is a principal treatment modality for patients with locally advanced rectal cancers [68-70]. However, about one third of patients will have no or only little response to this preoperative CRT [68,70,90]. Thus, the efficiency of cancer treatment is usually limited by acquired and intrinsic resistance, leading to tumor recurrence and consequently poor prognosis [79,235]. Unfortunately, the mechanisms of treatment resistance, both intrinsic and extrinsic, are very complex and were actively debated [236]. The role of STAT3 in mediating CRT resistance in CRC cells was previously presumed [147,162]. This work demonstrated that activated STAT3 mediates the CRT resistance in CRC cells. We showed, that blocking inflammatory gp130/ STAT3 signalling re-sensitized CRT resistant CRC cells. Furthermore, treating SW1463-tumor bearing mice with Napabucasin in combination with CRT abolished tumor growth and serves as a potential clinical treatment strategy. Moreover, we identified STAT3 target genes that were susceptible to STAT3 pathway perturbations. In the context of this, we identified RBPJ as a direct STAT3 target gene that modulates CRT resistance and ensures a tumor cell-intrinsic NOTCH signalling. Finally, we uncovered a disastrous crosstalk between inflammatory STAT3 signalling and the RBPJ-dependent NOTCH signalling in regulating CRC resistance towards CRT. All these findings expand our understanding of the complex processes controlling the CRT resistance in CRC cells and thus may help to improve the therapy of CRC patients in the future [71].

5.1 Inflammation promotes CRT resistance

5.1.1 Activated STAT3 controls CRT resistance

In this study, we explored the role of STAT3 in mediating CRT resistance in CRC cells. We found that the “tonic” activity of STAT3 in CRC cells is the key to their CRT resistance.

In the STAT3-expressing and CRT-resistant cell lines SW837 and SW1463, strong STAT3 phosphorylation at Y705 was detected after IL-6 stimulation, whereas in STAT3-negative and CRT-sensitive LS411N cells, both STAT3 and phosphorylated STAT3 (pSTAT3) were not detected regardless of stimulation. In accordance with this, LS411N cells showed no STAT3-dependent transcriptional activity, whereas SW837 and SW1463 possessed robust basal STAT3 transcriptional activity. Loss of STAT3 expression and concomitant reduced transcriptional activity rendered SW837 and SW1463 cells sensitive to CRT. This effect was not observed in LS411N cells, indicating the importance of STAT3 in mediating CRT resistance. These results confirmed the suggestion of my host research group that attributes STAT3 a primary role in mediating CRC resistance in CRC cells [147]. Furthermore, these results

demonstrate that LS411N cells are a suitable negative control for STAT3-dependent CRT trials. Interestingly, LS411N cells harbor a deletion mutation (pT178fs) in the STAT3 gene, which leads to a frameshift in this protein and may explain the lack of expression [237].

In response to stimuli, STAT3 signalling is activated by phosphorylation of the main phosphorylation site at T705 [119,127,135,149-151]. Following activation, phosphorylated STAT3 dimerize and subsequently translocate from the cytosol into the nucleus, where it regulated the transcription of its target genes [141,144,152]. Furthermore, an additional phosphorylation site S727, maximizes transcriptional activity of STAT3 [153]. Therefore, the phosphorylation of S727 act as a booster that fully activates STAT3. Interestingly, expression of the *STAT3* gene is increased strongly in response to IL-6, and the resulting high levels of unphosphorylated STAT3 (U-STAT3) drive oncogene expression by a mechanism distinct from that used by STAT3 dimers [238,239]. U-STAT3 functions as a transcription factor, binding to unphosphorylated NFκB in competition with inhibitor of NFκB (IκB), driving expression of a small subset of genes that also respond to activated NFκB, such as, *IL6*, and *IL8* [238,240]. However, the U-STAT3 mechanism is not as well characterized as the classical mechanism induced by pSTAT3. Nevertheless, it is important to know whether the CRT resistance of our cells depends on pSTAT3 and/or U-STAT3.

Since LS411N cells do not express STAT3, these cells provide an optimal molecular background for experiments in which both wild-type STAT3 and mutated STAT3 variants were studied. While all STAT3 variants were expressed, they differed in their functionality. Expression of wild-type STAT3, in which both phosphorylation sites are intact, resulted in a huge increase of STAT3 dependent transcriptional activity and thus, to an increased resistance of the cells to CRT. Mutation of the phosphorylation site S727 alone, also led to greatly increased activity, but not to the same extent as in the wild-type variant. Notably, mutation of the major phosphorylation site Y705 showed a loss of function on transcription factor activity level. Furthermore, no increased resistance of the cells to CRT was observed once either of the two phosphorylation sites were mutated. These results clearly demonstrated that the amino acid residues Y705 and S727 are essential for mediating STAT3 induced CRT resistance and that phosphorylation of S727 maximizes the activity of STAT3.

By knocking down STAT3, it was possible to sensitize CRC cells to CRT. We additionally found that phosphorylated and thus transcriptionally active STAT3 can induce CRT resistance. This strongly suggests that CRT resistance is primarily mediated by active STAT3 and not by the alternative U-STAT3 mechanisms. In accordance with that, it has recently been shown that pSTAT3 is present in exosomes from 5-FU resistant CRC cells and to enhance 5-FU resistance in sensitive cells through caspase cleavage cascade [236].

5.1.2 IL-6 trans-signalling promotes CRT resistance

Aberrant activation of STAT3 in cancers is associated with the presence of constitutive activating mutations in upstream tyrosine kinases or tumor-associated oversupply of ligands including cytokines, chemokines, and growth factors that are either expressed by tumor cells themselves or by the surrounding cells of the TME [140]. The TME consists of cancer-associated fibroblasts (CAFs), vascular cells and infiltrating immune cells which plays a crucial role in the mediation of chemoresistance [45]. Cancer-associated fibroblasts (CAFs) are able to reduce drug uptake in tumors and cause resistance during chemotherapy [236,241]. Furthermore, it was shown that Tumor-associated macrophages (TAMs) protected CRC cells from 5-FU based chemotherapy via putrescine [242]. Inflammation affects key cytokine-mediated signalling pathways that control tumor-initiating and tumor promoting processes such as IL-6/gp130-mediated STAT3 signalling [45]. Over the past decades, there is increasing evidence of IL-6 playing a main role in the progression of cancer, particularly CRC [110,114].

Cells lacking expression of IL-6R do not respond to IL-6, but can be stimulated by IL-6, bound to a soluble form of IL-6R [243]. This signalling pathway, termed IL-6 trans-signalling [244], is important for inflammatory diseases and cancer especially within the TME [131]. Leading to the assumption, that the CRT resistance development can be enhanced by components present in a pro-tumorigenic TME. To this end, we stimulated CRC cells with the designed fusion protein Hy-IL-6 which consists of IL-6 and the soluble IL-6 receptor chain and therefore mimics IL-6 trans-signalling [6,130,183]. The aim of the Hy-IL-6 stimulation experiments was first to demonstrate that IL-6 trans-signalling can induce STAT3 activation in CRC cells and second to confirm the CRT resistance-promoting effect of increased STAT3 activity. Treatment with Hy-IL-6 induced STAT3 activation and thus, rendered cells more resistant to CRT. Interestingly, already resistant CRC cell lines even gained an increase in CRT resistance after Hy-IL-6 stimulation, whereas STAT3 negative and CRT-sensitive cells did not. Thereby, the increase in CRT resistance is accompanied by increased transcriptional activity of STAT3 underlining our suggestion that active STAT3 is the driver of CRC resistance.

Patients suffering from colon cancer have been found to produce high levels of IL-6 whereas low levels of IL-6R in inflamed colon and colon cancer have been found [126]. Leading to the suggestion that IL-6 may preferentially activate through trans-signalling rather than via the classical receptor pathway [126]. Additionally, sIL-6R was shown to drive most of the pro-inflammatory activities of IL-6 [137]. Moreover, Schmidt *et al*. demonstrated that IL-6 trans-signalling is required for efficient tumor growth of CRC [243]. These findings underline the importance of the use of Hy-IL-6 in cell culture models because it mimics the IL-6 trans-signalling. To further approve the suggestion that IL-6 trans-signalling is the mediator of CRT resistance in CRC cells the use of the trans-signalling inhibitory protein sgp130Fc [245] would be

a good approach for classic cell culture experiments and *in vivo* studies. Sgp130FC is a recombinant version of soluble gp130, which is generated by the fusion of two soluble gp130 molecules to the Fc region of human IgG1, that differentially inhibits the pro-inflammatory activities of IL-6 without affecting the protective activities of this cytokine [137].

5.1.3 Inhibition of the gp130 /STAT3 axis decreases CRT resistance

Previous results indicate that signalling activity of STAT3 associated with partial CRT resistance can be further potentiated by triggering cytokine receptors of the gp130 family, which may happen in a pro-tumorigenic TME found in solid tumors [45,246]. To further emphasize the importance of the gp130/STAT3 axis in mediating CRT resistance, we inhibited this signalling axis at different molecular levels. We did this by either treating CRC cells with Tocilizumab or Ruxolitinib that block STAT3 upstream components, or by treating cells with the direct STAT3 inhibitor Napabucasin. Tocilizumab is a humanized monoclonal anti- IL-6R antibody, that is FDA approved for the treatment of rheumatic arthritis and Crohn`s disease [247,248]. It competitively binds to both soluble and membrane bound IL-6R and blocks both, the intracellular IL-6 trans-signalling and the classic signalling pathway [247,248]. Ruxolitinib, is a potent and selective oral inhibitor of JAK1 and JAK2 inhibitor and has been approved for treating myelofibrosis and polycythemia vera [249]. It blocks JAK activity by competing with ATP in the catalytic site of the JAK tyrosine kinases [250]. Additionally, the activity of STAT3 was inhibited using the promising small-molecule inhibitor Napabucasin that is less toxic, highly effective in low molecular ranges, and orally bioavailable *in vivo* [185,251]. The use of these inhibitors would suggest that CRC cells, whose CRT resistance mechanisms are particularly dependent on the activity of the gp130/JAK/STAT3 pathway, would respond with sensitization to CRT. Indeed, all three substances inhibited the activation of STAT3, which in turn leads to reduced transcriptional activity of STAT3 as well as a re-sensitization of CRT-resistant cells to 5-FU based CRT. This is the case for both, by blocking STAT3 upstream events and direct STAT3 inhibition. Besides, the basal STAT3 amount was not affected by any treatment which ensures that only STAT3 activation is prevented by the inhibitors. Importantly, our negative control cell line LS411N was not influenced by treatment with these pharmacological inhibitors, underlining that they are not particularly dependent of neither the IL-6 induced gp130 signalling, nor STAT3 signalling itself.

In gastric cancer cells co-cultivated with CAF cells, Ham *et al*. showed that treatment with Tocilizumab with 5-FU resulted in a significant decrease of CAF-mediated chemotherapy resistance [252]. Moreover, Tocilizumab has been tested to sensitize oral squamous cell carcinoma (OSCC) towards radiation, demonstrating that Tocilizumab decreases surviving fractions compared to the control and thus reduced radiation resistance in OSCC [253]. Nevertheless, since monoclonal antibodies can be harmful due to adverse effects such as

immunosuppression, blocking anti-inflammatory activities of IL-6 in general and not specific in tumor cells, its clinical application should be considered more carefully [254,255]. Ruxolitinib is under active clinical investigation for treatment of inflammatory-driven solid tumors [249,256]. In metastatic triple-negative breast cancer, a non-randomized phase II study evaluated the efficacy of Ruxolitinib treatment in patients with pSTAT3-positive tumors [256]. Disappointingly, no objective responses were observed, and the median PFS was only 1.2 months [256]. Therefore, they analyzed patients' biopsies regarding STAT3 signatures. They found, that Ruxolitinib treatment suppressed the JAK/STAT3 pathway in the tumor tissue [256]. Stover *et al*. postulated that the limited anti-tumor activity either occur via incomplete JAK/STAT inhibition or acquired resistance mechanisms that developed after Ruxolitinib treatment [256]. Moreover, the treatment of patients with relapsed/refractory metastatic CRC with Ruxolitinib combined with regorafenib was analyzed in a randomized, double-blind, phase two study [257]. Again, the treatment with regorafenib and Ruxolitinib did not show an increase in PFS/OS compared to regorafenib combined with placebo treatment [257]. Although our results showed that treatment of CRC with Tocilizumab and Ruxolitinib along with a 5-FU based CRT might have a beneficial effect on CRT resistance, their actual use for treating of CRC patients is rather questionable. Additionally, the lack of specificity and the potential side effects are also major disadvantages of indirect STAT3 inhibition [157]. Nevertheless, their use allowed us to further investigate STAT3-mediated resistance mechanisms in our cell culture model and to define the gp130/STAT3 pathway as one of the major signalling pathways in mediating therapy resistance.

To put the focus more on potential clinical treatment strategies, we decided to use the direct STAT3 inhibitor Napabucasin. Napabucasin has already been tested in a phase-III clinical trial for highly advanced, chemotherapy-refractory CRC [186] as well as in studies treating tumor cells from different cancer entities as well as cancer stem cells [185,258,259]. Interestingly, our experiments resulted in a loss of cellular viability after treating STAT3-expressing cells with Napabucasin concentrations above 500 nM. This effect may indicate that due to the massive inhibition of STAT3, the cells are no longer viable. In our negative control cell line LS411N, which has been shown not to "rely" on the STAT3 pathway, the Napabucasin-mediated loss of viability was not observed. Furthermore, we demonstrated that Napabucasin reduced STAT3 activation and thus the transcriptional activity as well as it rendered cells more sensitive to CRT. Our results are consistent with those of Zhang *et al*. They found that treatment with Napabucasin inhibited cell proliferation, cell motility, cell survival, as well as it sensitized prostate cancer cells to docetaxel [259]. Since the exact mechanism of action of Napabucasin is not yet clear, we performed experiments to assess potential molecular off-site effects. Thus, we combined RNAi targeting STAT3 together with Napabucasin. As observed before, both approaches individually re-sensitize CRC cells to CRT and their combination did not have synergistic effects. Thus, the effect of Napabucasin can specifically be ascribed to inhibit the

STAT3 pathway. Of note, an advantage over RNAi mediated STAT3 KD is that the basal STAT3 level is not reduced after Napabucasin treatment. This ensures that only active STAT3 is inhibited, but U-STAT3 is still present in the cellular system. Underlining again the hypothesis that the pSTAT3 mediated STAT3 pathway, and less the U-STAT3 mediated pathway, are the key to CRT resistance. We showed that Napabucasin prevented the activation of STAT3, but not through which mechanisms this inhibition occurs. Froeling *et al*. found that Napabucasin can bind to NAD(P)H Quinone Dehydrogenase 1 (NQO1) leading to the formation of reactive oxygen species (ROS) [260]. ROS causes DNA damage and some other intracellular changes such as the reduction of active STAT3 [260]. We can neither confirm nor deny whether this mechanism of action also takes effect in our cells. Experiments would have to be performed to measure ROS production before and after Napabucasin treatment. In addition, we would have to test our cells for Napabucasin-induced DNA damage, like the upregulation of the stress response genes (*ATF3* and *ATF4*), as well as other members of the AP1 transcription complex (*FOS*, *JUN*) and early response genes that are involved in cell cycle arrest in response to DNA damage (*CDKN1A*, *BTG1*, *BTG2*) [260].

Summarized, our data suggest that there is a “tonic” or “chronic” activation of the IL-6/gp130/STAT3 signalling axis in CRT-resistant CRC cells, which in turn mediates CRT resistance. However, we were not able to detect pSTAT3 in unstimulated cells using both, Western blot, and flow cytometry approaches (data not shown). In addition, we tested whether SW1463 cells secrete IL-6, which then activates the STAT3 signalling pathway via an autocrine loop. However, the use of an Enzyme-linked Immunosorbent Assay (ELISA) showed no IL-6 secretion in cell culture supernatant collected at 0 h, 1 h, 3 h, 6 h, 24 h, 48 h and 72 h intervals (data not shown). Irradiation of the cells with 6 Gy and 15 Gy also did not result in increased IL-6 secretion (data not shown). This could be due to the assay itself, as the sensitivity may not have been sufficient, or the timing of the experiment may have been poor. These results indicated that this “tonic” STAT3 activation may be mediated by signaling events independent of gp130. What points against this suggestion is that the use of Tocilizumab sensitizes CRC cells to CRT. Since Tocilizumab prevents the binding of IL-6 to the gp130 receptor subunit [248], it can be assumed that constant low-level IL-6/gp130 signalling must exist in CRC cells. However, the question remains: Where does this “tonic” STAT3 activation come from? The term “tonic signalling” has already been known in the 1990s, describing a low-level, constitutive signalling in the basal state of B and T lymphocytes [261]. Tonic signalling describes that even in the absence of robust and activating antigen triggers, low-level phosphorylation of signaling intermediates can be observed in resting lymphocytes [261]. It is possible that the amount of pSTAT3 as well as IL-6, in our cells is below a certain detection limit. Zhu *et al*., found that CRC cell lines SW480 and HCT116 secreted IL-6 (SW480= approx. 63.2 pg/ml; HCT116= approx. 57.7 pg/ml) and that LPS stimulations increased IL-6 mRNA transcription as well as

an increase IL-6 secretion (SW480= approx. 247.4 pg/ml; HCT116= approx. 267.2 pg/ml) [262]. Indicating, that CRC cells are capable of secreting IL-6 in general.

Summarized, these effects occurred in the absence of an external pathway activation, suggesting that there is some kind of “tonic” or “chronic” IL-6/gp130/STAT3 signalling in our CRC cells. Nevertheless, we cannot resolve the discrepancy between undetectable STAT3 activity and simultaneous STAT3-mediated CRT resistance. However, we showed really clearly that active STAT3 is critical for mediating CRT resistance in CRC cells.

5.2 Targeting the gp130/STAT3 axis *in vivo*

Altogether, our findings so far prompted us to test whether the inhibition of the gp130/STAT3 signalling axis can suppress the growth of tumor transplants under CRT *in vivo*. Therefore, we choose the STAT3 inhibitor Napabucasin because treatment of CRC cells resulted in a re-sensitization of the cells to CRT *in vitro*. In addition, Napabucasin is gaining increasing importance in clinical trials for CRC patients [186]. The combination of Napabucasin and CRT significantly slows SW1463 xenograft growth compared with the DMSO, and CRT treated group and thus provides a significant advantage in time to tumor regrowth. Hence, we could recapitulate the previously generated results of Napabucasin treatment *in vitro*. Furthermore, we demonstrated that treatment with Napabucasin as a monotherapy did not affect tumor outgrowth, whereas the combination with RT or CRT prevented the tumor growth. In contrast, Zhang *et al*. demonstrated that treatment with Napabucasin alone suppressed tumor growth in a prostate cancer mouse xenograft model [259]. Based on our results, we hypothesized that Napabucasin may act as a RT/CRT sensitizer in CRC cells. This hypothesis is supported by the observation of Nagaraju *et al*, who showed that Napabucasin serves as a CRT sensitizer in HCT116 colon cancer cells, both *in vitro* and *in vivo* [163]. What distinguishes our two studies is that Nagaraju *et al*. used MSI cell lines [163] representing only 13%-15% of the total sporadic CRC tumors [40], whereas we used MSS cells, that represent the majority of sporadic tumors [23]. Additionally, we assessed full tumor regrowth (defined as tripling in tumor size) to measure treatment response, which more closely mirrors the clinical situation as well as the procedure for clinical studies [71].

Currently, there are several *in vivo* models available to study CRC. Besides "classical" methods like AOM-based models and genetically engineered models, there are applications for xenotransplant models and models in which organoids are transplanted into mice [45]. The choice of the appropriate mouse model should be made concerning the intended research question. Our aim was to investigate the tumor intrinsic effect of Napabucasin along with CRT in an immunosuppressed background. However, we used an established mouse model, which is defined as the standard in the field for preclinical xenograft studies investigating inhibitor effects following CRT [263]. This mouse model has the advantages that it mirrors the clinical

setting of fractionated doses of both irradiation and chemotherapy [147]. Noteworthy, for studying tumor-extrinsic factors and the impact of the TME on CRT resistance, other approaches would be to use available techniques like patient-derived xenograft (PDX), tumor organoids or co-cultures of tumor cells with TME associated cells [45,249].

5.3 The STAT3-NOTCH alliance mediating CRT resistance

5.3.1 The STAT3 target gene RBPJ as a new radiosensitizer of CRC cells

The mechanism by which STAT3 mediates CRT resistance is not yet clear. Since STAT3 is a transcription factor, the effect is probably mediated by one or more of its target genes. Therefore, I analyzed the global consequences of STAT3 pathway perturbations on the transcriptome of CRT-resistant SW837 cells. A total number of 71 genes was dually influenced by STAT3 expression and cellular stimulation with Hy-IL-6. According to the self- defined ODA criteria, I identified 55 genes that were upregulated after pathway stimulation, and simultaneously but inversely, downregulated after STAT3 inhibition, and *vice versa* [71]. These genes are involved in many signalling pathways and regulatory processes, that have been partially linked to CRC and therapy resistance before (for details see section 4.3.1 and **Figure 4.19**). In this discussion, however, I will not go further into detail regarding the other 54 target genes. The ODA uncovered the key transcriptional regulator of the canonical NOTCH pathway, RBPJ [206,207]. Closer examination showed that the RBPJ promoter comprised a STAT3 GAS binding site. This suggests that STAT3 can directly regulate RBPJ transcription. Using EMSA, the binding of STAT3 to the GAS sequence of the RBPJ promoter was detected after Hy-IL-6 stimulation. As positive control for GAS-binding, lysates of IFN-γ- stimulated HeLa cells were used. Note, HeLa cells co-express STAT1 and STAT3, which possess distinct electrophoretic mobility, and hence, can distinguish between both STAT proteins when simultaneously detected by EMSA [71]. Therefore, the slower and faster migrated band represents STAT3 and STAT1, respectively [218]. Moreover, RNAi-mediated silencing of RBPJ led to a pronounced re-sensitization of CRC cells to RT, which thereby identifies RBPJ as a new resistance-mediating STAT3 target gene in CRC.

5.3.2 NOTCH expression profile correlates with STAT3 activity

Since RBPJ is the main transcription factor of the NOTCH signalling [206,207], it is obvious that I subsequently focused on the NOTCH signalling in CRC cells and the possible influence of this signalling axis on CRT resistance. The NOTCH signalling has been known for decades and was originally found during cell fate determination from Drosophila to humans [219-223]. NOTCH signalling is a conserved ligand-receptor signalling pathway, which can regulate cell differentiation, proliferation, survival, apoptosis, stem cell maintenance as well as the self-renewal of progenitor and stem cells in both adult and embryonic organs [224,225]. Dysregulated activation of NOTCH signalling in human cancers was first implicated through studies in T cell acute lymphoblastic leukemia (T-All) that uncovered a constitutively active form of NOTCH1

which was detected in more than 50% of patients with T-ALL [264,265]. In recent decades, more evidence has accumulated on the oncogenic activity of NOTCH signalling in a broad spectrum of human cancers, including breast, lung, pancreatic, prostate cancer, glioblastoma, as well as CRC [225]. However, due to its pleiotropic functions, NOTCH signalling was shown to influence both, promoting or suppressing tumor development, dependent on the cellular context [207,266-269]. At present, four NOTCH receptors (NOTCH 1-4) have been identified in humans [224] that derived from proteolytic processing of large single-chain precursors by a furin-like protease in the trans-Golgi network (**Fig. 5.1**, *left*) [220,224,226]. The canonical NOTCH signalling is activated after ligation of NOTCH receptors and ligands (DLL1, DLL3, DLL4, JAG1 and JAG2) (**Figure 5.1**) [220,223,224,226,227] followed by two strictly controlled proteolytic cleavage steps that are necessary to fully activate the NOTCH pathway. The first cleavage step is mediated by ADAM/TACE metalloproteases, which initiates the second cleavage by the γ-secretase complex [206,207,225]. This series of cleavages release the active form NICD, which translocate into the nucleus where it assembles with RBPJ to drive the expression of NOTCH target genes (**Figure 5.1**, *right*) [206,207].

NOTCH signalling components have been shown to be expressed in the normal gastrointestinal tract where they play a critical role in the maintenance of the intestinal epithelia [270,271]. In the human colon, NOTCH1,2 and 3 are expressed at the basal crypt, while JAG1 is present at the top of the crypts [272]. Moreover, NOTCH1,2,3, and the NOTCH target gene HES1 are expressed in the gastric mucosa [272].The expression of NOTCH ligands, receptors and downstream genes has been studied in CRC tissue samples. A study discovered that levels of JAG, NOTCH1 and HES1 are comparable to or partially greater than those found in proliferative intestinal crypts, indicating that the NOTCH pathway is activated in colorectal adenocarcinomas [273,274]. Moreover, numerous gain gain-of-function mutations in *NOTCH1* and *NOTCH2* were found in solid cancers and B/T cell lymphomas, which allow for constitutive proteolytic NICD cleavage or increased stability of NICD, increase the expression of NOTCH target genes [275]. In accordance with this, I observed constitutive NOTCH activity in unstimulated CRC cells. Robust expression of NICD was found in CRT-resistant SW837 and SW1463 cells that was almost absent in CRT-sensitive LS411N cells. The presence of NICD directly correlated with STAT3 transcriptional activity. In accordance, the expression of HES1 was weak in LS411N cells but easily detected in SW837 and SW1463 cells. The signal intensities of HES1 expression are proportional to the NICD positivity and CRT sensitivity of these cells. Additionally, CRC cells were tested positive for three NOTCH receptors (NOTCH 1,2,3), patterns of NOTCH ligands (Jagged 1/2 and DELTA-like) and NOTCH cleaving components (ADAM proteases or γ-secretases complex subunits: presenilin 1, presenilin 2, Nicastrin, PEN2. However, a combination of elements capable of NOTCH processing was found only in CRT-resistant SW837 and SW1463 cells, but not in LS411N cells [71]. This

uncovered a cell-intrinsic tonic NOTCH signalling activity that is moreover relevant for CRT-resistant CRC cells than for CRT-sensitive cells.

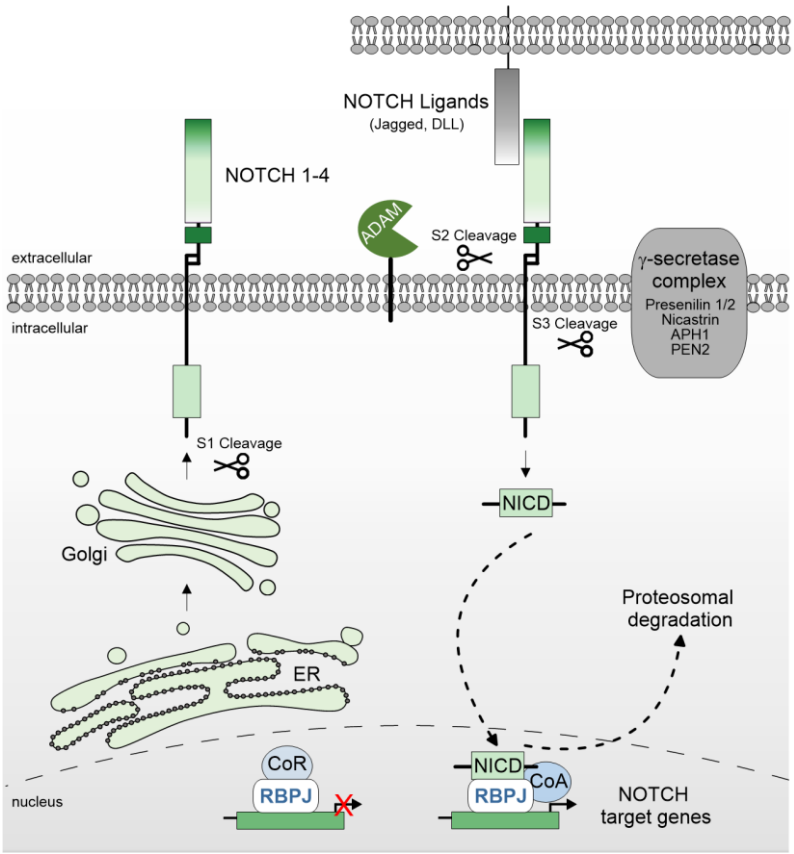

Figure 5. 1 The NOTCH signalling pathway
Mature NOTCH receptors are heterodimeric proteins consisting of a transmembrane subunit (NTM) and an extracellular subunit (NEC) derived from proteolytic processing of large single-chain precursors by a furin-like protease in the trans-Golgi network [220,224,226]. Following ligation of NOTCH receptors on the cell surface by DELTA/Jagged ligands, NICD becomes proteolytically cleaved. The first cleavage step is mediated by ADAM/TACE metalloproteases, that cleave the receptor at S2, which initiates a S3 cleavage mediated by the γ-secretase complex [71,206,207,225]. NICD translocate in the nucleus where it assembles with the transcription factor RBPJ to drive NOTCH target genes expression [206,207].

Stimulation of CRC cells with Hy-IL-6 showed a clear upregulation of NICD in CRT resistant cell lines, while the sensitive cell line showed a downregulation of NICD. RBPJ, on the other hand, was expressed in a higher amount by all three cell lines after Hy-IL-6 stimulation. In the SW837 cells, it is also striking that Hy-IL-6 stimulation increased the expression of the receptors NOTCH2 and 3, which was not the case in the other two cell lines. I have already observed that STAT3 is activated by stimulation with Hy-IL-6 and that CRC cells become more resistant to CRT treatment through STAT3 pathway stimulation. Using genome wide studies, I have identified RBPJ as a STAT3 target, which found to be a direct STAT3 target using EMSA. Here I was able to show that the RBPJ protein is increasingly expressed in CRT-resistant CRC cells after Hy-IL-6 stimulation. Irradiation gradient experiments uncovered that

NICD, RBPJ and NOTCH2 were upregulated in irradiated cells with an increase of irradiation dose compared to non-irradiated CRC cells. Thus, upregulation was observed only in CRT-resistant CRC cells, whereas protein levels of all tested proteins decreased in the CRT-sensitive cell line LS411N. This observation indicates that the irradiation of already CRT-resistant rectal cancer cells even further promotes their radio resistance by inducing the generation of NICD and RBPJ. In Accordance with this, Zhang *et al*., demonstrated an upregulation of NOTCH1 and HES1 after irradiation of HT-29 and LoVo cells [235]. Furthermore, it was demonstrated that radiation therapy promotes inflammatory responses in the tumor tissues, and the upregulation of cytokines such as IL-6 is not only a crucial mediator of inflammation but also conferred a survival advantage to tumor cells [253,276].

RBPJ inhibition re-sensitized CRT-resistant cells to CRT. However, the combination of RBPJ KD and STAT3 KD did not lead to a synergistic effect on CRT resistance. This could be due to the fact that the cells may already be at their maximum sensitization threshold and further inhibition would only lead to cell death. Moreover, RBPJ silencing phenocopied STAT3 silencing as targeting RBPJ alone was as effective as inhibition of STAT3 itself, indicating that RBPJ, similar to STAT3, is a key determinant of CRT resistance.

5.3.3 RBPJ-dependent NOTCH signalling in mediating CRT resistance

In addition to NOTCH- mediated carcinogenic effects, it was reported that NOTCH signalling mediated radio resistance and chemoresistance of several tumors, such as gastric carcinoma and esophageal adenocarcinoma [208,277]. The inhibition of the NOTCH pathway has been linked to sensitize of glioblastoma or breast cancer cells to radiation [208]. However, the NOTCH pathway has not yet been directly linked to CRT responsiveness in CRC. The canonical NOTCH pathway depends on two strictly controlled proteolytic cleavage steps, mediated by ADAM/TACE metalloproteases and the γ-secretase complex [206,207,225].This multitude of activation steps enables the inhibition of the NOTCH pathway at different points. I demonstrated that pharmacological inhibition of the γ-secretase complex as well as RNAi-mediated KD of RBPJ resulted in the sensitization of CRC cells to 5-FU-based CRT.

DAPT belongs to the class of nonspecific γ-secretase inhibitors (GSIs). The γ-secretase complex catalyzed the cleavage of various transmembrane proteins by untethering the cytoplasmic domain from the membrane. This allows the cytoplasmic domains to transduce signals to the nucleus [229,230]. Originally, the γ-secretase was found to be the protease responsible for generating of Amyloid β (Aβ), and thus GSIs were initially developed for treatment of Alzheimer`s disease [278-281]. Recently, a significant number of clinical trials have also been conducted in which GSI were used as anticancer agents [231]. The use of these agents has shown therapeutic activity in numerous preclinical models, but with a few exceptions they have not yet produced satisfactory results in early clinical trials [231,275]. The first trial of a γ-

secretase inhibitor in CRC was conducted by Strosberg and colleagues. In this phase II clinical trial, the γ-secretase inhibitor RO4929097 displayed only little effect in patients with metastatic, refractory CRC [273].

In the performed experiments, the expression of NICD was considered a marker for active NOTCH signalling. Interestingly, the reduction of NICD was more pronounced after DAPT treatment than after RBPJ KD. DAPT treatment completely inhibited canonical NOTCH signalling [231], but GSIs are not completely effective in blocking all tumor-related NOTCH functions [282]. Indeed, besides the more common canonical NOTCH signalling that depends on the proteolytic cleavage steps as well as on binding to RBPJ, NOTCH can signal via a non-canonical pathway that proceeds without RBPJ [283]. For example, NOTCH4 canonical signalling is required for developing of mammary glands, but NOTCH4 non-canonical signalling is related to mammary tumorigenesis [283]. Nevertheless, both approaches individually, as well as in combination re-sensitized CRT resistant cells to CRT without any synergistic effect. Leading to the suggestion that the RBPJ-dependent NOTCH signalling is important in mediating CRT resistance. Alternative RBPJ-independent mechanisms seemed to be not necessary for the maintenance of CRT resistance. Notably, the CRT- sensitive cell line LS411N, was not influenced by neither RBPJ KD nor DAPT treatment. This suggests that the NOTCH pathway, as well as the STAT3 pathway, may not be involved in CRT resistance in these cells.

In addition to DAPT, other GSIs were tested for their potential effect in CRC cells. Meng and colleagues reported about a chemotherapy induced NOTCH1 upregulation in colon cancer cells, which could be reversed by adding a GSI (GSI34) to the cells. Additionally, downregulation of NOTCH1 resulted in enhanced chemo sensitization whereas an overexpression of NICD increased chemoresistance [284]. Meng *et al*. hypothesized that colon cancer cells may upregulate NOTCH1 as a protective mechanism in response to chemotherapy [284]. Recently, a novel ADAM17 inhibitor (ZLDI-8) was described, which sensitized CRC cells to 5-FU or irinotecan by inhibiting NOTCH and reversing EMT *in vivo* and in *vitro* [225,285]. A disadvantage of GSIs is that they block the processing of more than 90 different substrates and are not strictly NOTCH-specific [275,286]. This non-specific inhibition makes it impossible to discriminate between individual NOTCH receptors [287] in order to study their individual impact on CRT resistance. Furthermore, treating patients with GSI caused partially severe side effects like gastrointestinal toxicity including, diarrhea, vomiting, and nausea [275]. Therefore, various research groups focused on direct inhibition of the NOTCH signalling by modulating the expression of single NOTCH components. The direct inhibition allowed specific members of the NOTCH pathway to be targeted, potentially minimizing side effects caused by global inhibition of the pathway [288]. Liu *et al*., observed that the miR-195-5p mediated inhibition of NOTCH1 promoted the chemotherapeutic effects of 5-FU by increasing apoptosis in CRC

cells [289]. Additionally, inhibition of NOTCH2 and RBPJ via miR-195-5p inhibited CRC stemness and 5-FU resistance in human CRC tissue and CRC cells [290]. RNAi mediated inhibition of NOTCH1 in regorafenib-resistant SW480 colon cancer cells partially restored sensitivity to regorafenib treatment *in vitro* [291]. KD of JAG2 sensitized CRC cells to chemotherapy via downregulation of p21 [292]. There have also been attempts to target the NOTCH pathway downstream of the γ-secretase-mediated activation [275]. Moellering *et al.*, designed a peptide named SAHM1 (stabled α-helical peptide derived from MAML1) that mimic a dominant negative form of MAML1 by competitively binding to the NICD-RBPJ complex in T-ALL [286]. However, the development of such agents as therapeutic drugs remains challenging due to manufacturing, stability, and other pharmacokinetic issues [275]. As an important downstream target of the NOTCH signalling pathway, HES1 was shown to promote chemoresistance to 5-FU in CRC *in vitro* and *in vivo* [293]. Therefore, the clinical significance of chemo response of HES1 in stage II and II CRC patients was investigated using a tissue microarray[293]. Stage II CRC patients with higher HES1 expression showed a higher recurrence rate after chemotherapy [293]. Additionally, colon cancer cell lines that overexpressed HES1 were more resistant to 5-FU treatment *in vitro* [293].

To investigate the exact mechanisms of NOTCH-mediated CRT resistance, further experiments need to be conducted. Since there are different NOTCH receptors as well as ligands, a future question would be whether there is a specific receptor/ligand combination in CRC cells that mediates CRT resistance. This finding could allow for protein-specific inhibition of these proteins without disrupting the complete NOTCH signalling.

5.4 What do our data implicate for future clinical strategies?

In this work, I identified a novel crosstalk between IL-6/gp130/STAT3 signalling and the RBPJ/NOTCH pathway mediating the CRT resistance in CRC cells. Blocking the tumor cell-intrinsic gp130/STAT3 axis or the RBPJ/NOTCH axis enhanced the responsiveness to CRT in CRC-resistant cells as well as in an *in vivo* xenograft mouse model. But how can these results now be integrated into a clinical treatment strategy for CRC patients?

5.4.1 Potential use of pSTAT3 and NOTCH receptor expression as prognostic markers in rectal cancer patients

Napabucasin has already been tested in a phase-III clinical trial for highly advanced, chemotherapy-refractory CRC. In this trial Jonker *et al.* demonstrated the first time that pSTAT3 is a poor prognostic factor in patients with metastatic CRC. 22% of the studied patients had pSTAT3 positive tumors, which were associated with a shortened OS [186]. Additionally, patients with pSTAT3-positive disease treated with Napabucasin showed a longer OS than in the placebo group [186]. In contrast, Napabucasin treatment of patients with pSTAT3 negative tumors resulted in negatively impaired OS compared to the placebo group [186] . Based on our

findings and keeping the clinical trial of Jonker *et al*., in mind, I propose a potential model for a personalized treatment strategy for CRC patients with pSTAT3-positive tumors (**Figure 5.2 A**). This treatment strategy includes screening of pre-therapeutic tumor biopsies for the presence of phosphorylated STAT3, followed by a combined treatment with CRT and Napabucasin in case of phospho-STAT3 positivity.

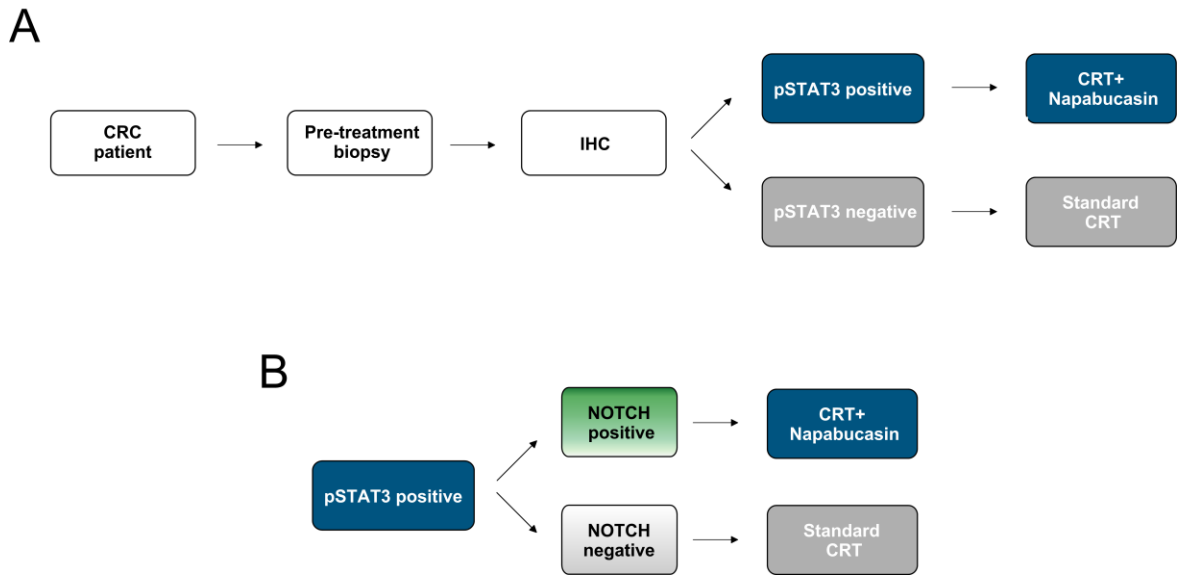

Figure 5. 2 Proposed model for personalized treatment of CRC patients.
A| Pre-therapeutic biopsies of CRC patients were tested for phosphor-STAT3 using immunohistochemistry (IHC). Patients with pSTAT3 negative tumors will be treated with standard CRT, whereas patients with pSTAT3 positive tumors will be treated with standard CRT in combination with Napabucasin [71] . **B|** Based on (A), the phsopho-STAT3 status of the tumours could be determined and then a distinction made between NOTCH positive and NOTCH negative tumours. Based on this, phospho-STAT3 and NOTCH positive tumours could be treated with napabucasin + CRT, while only STAT3 positive tumours would be treated with standardised CRT.

Considering the crosstalk of STAT3 and NOTCH signalling, the model in **Figure 5.2 A** could be further specified. Identical to **Figure 5.2 A**, pSTAT3-positive tumors must be identified. Furthermore, we can determine the NOTCH status of the tumors using markers such as NOTCH receptors (**Figure 5.2 B**).

The common feature of all cancers associated with a dysregulated NOTCH activity is the overexpression of NOTCH receptors and their ligands. In the gastrointestinal tract, NOTCH signalling is critical in cell proliferation control and tumorigenesis [235]. In pretherapeutic gene expression profiles obtained from 207 patients with locally advanced rectal cancer, I uncovered that high expression of NOTCH2, NOTCH3, and NOTCH4 is associated with impaired DFS, while there was no difference for NOTCH1. Indicating that rectal patients with lower NOTCH 2,3 and 4 expression had a better outcome. For NOTCH ligands as well as other pathway components such as cleavage proteins, no expression advantage or disadvantage could be

found. Many studies exist that investigated NOTCH components as possible biomarkers for gastrointestinal cancers. Chu *et al.*, showed that NOTCH1 expression was significantly higher in colorectal tumors than that of normal colorectal epithelial cells [294]. Furthermore, the overall survival rate for patients with NOTCH1-positive tumors was significantly lower than for those with NOTCH1- negative tumors [294]. Additionally, NOTCH3 was associated with poor clinical outcomes in multiple gastric datasets. Inhibiting NOTCH3 expression by RNAi sensitizes gastric cancer cells to cisplatin and 5-FU [295]. It was shown that NOTCH1 and its target gene, HES1 are expressed more in advanced colon tumors than in low-grade tumors [284,296]. All four NOTCH receptors were correlated to worsen OS for all gastric cancer patients [297]. Additionally, overexpression of the NOTCH target gene HEY1 in malignant colorectal tissue from stage II and stage III CRC patients correlates with poor outcome [298]. Considering all these results, it is initially surprising that no effect of NOTCH1 expression was detected in the rectal cancer samples I examined. However, precisely this finding reflects the heterogeneity of cancer in general and reinforces the current efforts to develop a therapy strategy that is individually adapted to each patient.

Defining the pSTAT3 as well as the NOTCH status of the tumors can ensure that only patients in whom both signalling pathways are active are treated with Napabucasin (**Figure 5.2 B**). Nevertheless, further studies of Napabucasin in combination with CRT must be made proofing that our suggested concept could be adapted into clinical treatment settings. Currently, a phase 3 trial including patients with previously treated metastatic CRC treated with Napabucasin in combination with FOLFIRI (5-FU, Leucovorin and Irinotecan) is ongoing (NCT02753127 [299]). This study hopefully gives new insights regarding the clinical importance of Napabucasin in the treatment of CRC. In addition, it would have to be investigated whether pSTAT3-positive tumors, which are NOTCH negative, would also respond to treatment with Napabucasin. This would require preliminary experiments with cell lines that are active in pSTAT3 but lack NOTCH activity. Another consideration would be the use of Napabucasin together with a NOTCH inhibitor. However, I showed that inhibition of both STAT3 and NOTCH resulted in no synergistic effect regarding the CRT re-sensitization. In addition, there is still no applicable NOTCH inhibitor that has been able to show success in clinical trials. However, the overall results provide a basis for future experiments addressing the issue of CRT resistance in CRC cells, which may contribute to an optimized treatment of CRC patients.

6. Conclusion

In this project, I studied the role of STAT3 in the context of CRT resistance in CRC. Here, I identified IL-6/gp130/STAT3 signalling crosstalk's with RBPJ/NOTCH pathway as a CRT resistance mechanism in CRC cells. Blocking the tumor cell-intrinsic gp130/STAT3 axis or the RBPJ/NOTCH axis enhanced the responsiveness to CRT in CRC-resistant cells (**Figure 6.1**). Furthermore, I showed that STAT3 executed treatment resistance by triggering the expression of RBPJ (**Figure 6.1**). Moreover, genetic profiling of rectal cancer patients revealed the importance of the NOTCH receptor expression because it correlated with clinical outcome.

Treatment resistance is associated with many complicated processes, including aberrant activation of multiple signalling pathways. Therefore, it is implausible that only one signalling pathway is responsible for controlling treatment resistance. It is more likely to be a network of many different factors and signalling pathways that are regulated by tumor intrinsic mechanisms (like interaction with other tumor cells) as well as by tumor extrinsic mechanisms (such as the interaction with the TME). There are studies describing the crosstalk of NOTCH and STAT3 in gastrointestinal cancer, but not in the context of tumor-intrinsic CRT resistance development in CRC cells. Both the NOTCH and the JAK/STAT3 pathway exhibit pleiotropic effects on many common processes regulating cell fate [228]. In neuroepithelia cells the suppression of HES1 reduced the induction of STAT3 phosphorylation [228]. In gastric cancer patients, NOTCH1 and JAG1 expression was significantly associated with pSTAT3 [300]. In addition, another group proved that the expression of HES1 correlates with the expression of Matrix Metallopeptidase 14 (MMP14) [301]. Furthermore, they showed that STAT3 overexpression increased expression of MMP14. HES1 depletion decreased STAT3 phosphorylation but did not change the basal expression level of STAT3 in Caco2 and SW480 cells [301]. Ectopic overexpression of HES1 increased MMP14 expression as well as STAT3 phosphorylation in HCT116 cells [301]. This result led to the suggestion that up-regulation of MMP14 by HES1 in colon cells depends on the STAT3 pathway and regulates the invasion ability [301]. Inhibiting the endogenous NOTCH pathway by GSI inhibitor DAPT reduced the IL-6 expression [302]. Simultaneous inhibition of the STAT3 and NOTCH pathway greatly inhibited the malignant behavior of gastric cells and significantly restored sensitivity of the resistant cells to trastuzumab [302]. These findings suggested that sustained activation of JAG1/NOTCH signalling in gastric cancer cells elicits an aberrant release of IL-6, leading to resistance to trastuzumab [302].

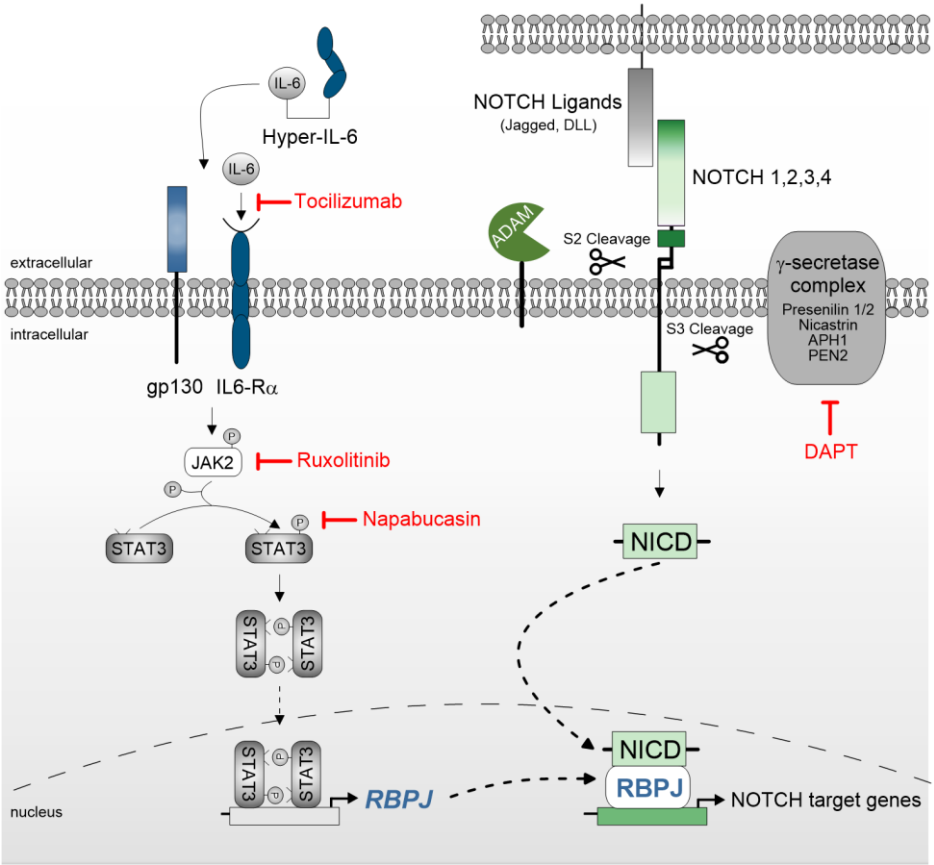

Figure 6. 1 Crosstalk between the gp130/JAK/STAT3 signalling and the RBPJ/NOTCH pathway in mediating CRT resistance in CRC cells.
Schematic overview of inflammatory gp130/STAT3 signalling and the RBPJ/NOTCH axis as well as the identified crosstalk between both pathways [71]. Pharmaceutical inhibitors used in this study are depicted in red. Hyper-IL-6 represents a chimeric fusion protein encompassing IL-6 and the soluble IL-6 receptor chain and therefore mimics IL-6 trans-signalling [182]. Both signalling pathways act together to block the responsiveness to CRT in CRC cells. In response to stimuli, cytokine receptors of the gp130 family activate Janus tyrosine kinases (JAKs) that in turn activate STAT3 via tyrosine phosphorylate. Activated STAT3 dimerizes and translocate into the nucleus to regulate expression of its target genes [119,127,135,149-151], including RBPJ. Following ligation of NOTCH receptors on the cell surface by DLL4/JAG ligands, NICD becomes proteolytically cleaved by ADAM family members translocate in the nucleus where it assembles with the transcription factor RBPJ to drive NOTCH target genes expression [206,207].

In this work, only tumor cell-intrinsic resistance mechanisms were investigated. However, as repeatedly emphasized, tumor extrinsic factors are also of crucial importance in the mediation of CRT resistance. Extrinsic NOTCH activity for example of tumor surrounding cells, showed high importance in CRC. Activated NOTCH1 signalling was observed in CRC and other cancers. This activation could either occur via NOTCH1 ligands on the surface of tumor cells (tumor intrinsic mechanisms) or by NOTCH ligands and components of the TME (tumor extrinsic mechanisms) [303,304]. It was nicely shown that the activation of NOTCH1 signalling in the murine intestinal epithelium led to highly penetrant metastasis in CRC [303]. Interaction between a tumor and its microenvironment is important for tumor initiation and progression. Moreover, extrinsic factors released by TME associated cells can promote treatment resistance. In colorectal tumors, it was shown that myofibroblasts secreted IL-6 and IL-8 have

a critical role in the maintenance and spread of CSCs via the NOTCH/HES1 and STAT3 signalling pathway [305]. These data suggest IL6/IL8 mediated NOTCH/HES1 signalling pathway as a potential target in drug development [305].

In summary, blocking the tumor cell-intrinsic gp130/NOTCH signalling axis could improve responsiveness to CRT. Overall, the discovery of a gp130/NOTCH alliance as the basis of CRT resistance offers a novel treatment concept for patients with rectal cancer. Appropriate clinical trials are needed to validate the suitability of our concepts to reverse CRT resistance and the value of phosphorylated STAT3 and/or NOTCH as prognostic biomarkers for CRC patients.

7. References

1 Sung, H. *et al.* Global cancer statistics 2020: GLOBOCAN estimates of incidence and mortality worldwide for 36 cancers in 185 countries. *CA Cancer J Clin*, doi:10.3322/caac.21660 (2021).

2 Siegel, R. L., Miller, K. D., Fuchs, H. E. & Jemal, A. Cancer Statistics, 2021. *CA Cancer J Clin* **71**, 7-33, doi:10.3322/caac.21654 (2021).

3 *https://canceratlas.cancer.org/*.

4 Hassanpour, S. H. D., M. Review of cancer from perspective of molecular. *Journal of Cancer Research and Practice* **4**, 127-129, doi:https://doi.org/10.1016/j.jcrpr.2017.07.001 (2017).

5 Meacham, C. E. & Morrison, S. J. Tumour heterogeneity and cancer cell plasticity. *Nature* **501**, 328-337, doi:10.1038/nature12624 (2013).

6 Fisher, R., Pusztai, L. & Swanton, C. Cancer heterogeneity: implications for targeted therapeutics. *Br J Cancer* **108**, 479-485, doi:10.1038/bjc.2012.581 (2013).

7 Keum, N. & Giovannucci, E. Global burden of colorectal cancer: emerging trends, risk factors and prevention strategies. *Nat Rev Gastroenterol Hepatol* **16**, 713-732, doi:10.1038/s41575-019-0189-8 (2019).

8 Dekker, E., Tanis, P. J., Vleugels, J. L. A., Kasi, P. M. & Wallace, M. B. Colorectal cancer. *Lancet* **394**, 1467-1480, doi:10.1016/s0140-6736(19)32319-0 (2019).

9 Bray, F. *et al.* Global cancer statistics 2018: GLOBOCAN estimates of incidence and mortality worldwide for 36 cancers in 185 countries. *CA Cancer J Clin* **68**, 394-424, doi:10.3322/caac.21492 (2018).

10 Rawla, P., Sunkara, T. & Barsouk, A. Epidemiology of colorectal cancer: incidence, mortality, survival, and risk factors. *Prz Gastroenterol* **14**, 89-103, doi:10.5114/pg.2018.81072 (2019).

11 Zhu, G. X. *et al.* Wnt/β-catenin signaling: Causes and treatment targets of drug resistance in colorectal cancer (Review). *Mol Med Rep* **23**, 1, doi:10.3892/mmr.2020.11744 (2021).

12 Arnold, M. *et al.* Global patterns and trends in colorectal cancer incidence and mortality. *Gut* **66**, 683-691, doi:10.1136/gutjnl-2015-310912 (2017).

13 Ferlay, J. *et al.* Cancer incidence and mortality worldwide: sources, methods and major patterns in GLOBOCAN 2012. *Int J Cancer* **136**, E359-386, doi:10.1002/ijc.29210 (2015).

14 Simon, K. Colorectal cancer development and advances in screening. *Clin Interv Aging* **11**, 967-976, doi:10.2147/cia.S109285 (2016).

15 Świerczyński, M., Szymaszkiewicz, A., Fichna, J. & Zielińska, M. New insights into molecular pathways in colorectal cancer: Adiponectin, interleukin-6 and opioid signaling. *Biochim Biophys Acta Rev Cancer* **1875**, 188460, doi:10.1016/j.bbcan.2020.188460 (2021).

16 Bardou, M., Barkun, A. N. & Martel, M. Obesity and colorectal cancer. *Gut* **62**, 933-947, doi:10.1136/gutjnl-2013-304701 (2013).

17 Mármol, I., Sánchez-de-Diego, C., Pradilla Dieste, A., Cerrada, E. & Rodriguez Yoldi, M. J. Colorectal Carcinoma: A General Overview and Future Perspectives in Colorectal Cancer. *Int J Mol Sci* **18**, doi:10.3390/ijms18010197 (2017).

18 Dahmus, J. D., Kotler, D. L., Kastenberg, D. M. & Kistler, C. A. The gut microbiome and colorectal cancer: a review of bacterial pathogenesis. *J Gastrointest Oncol* **9**, 769-777, doi:10.21037/jgo.2018.04.07 (2018).

19 Jayasekara, H. *et al.* Associations of alcohol intake, smoking, physical activity and obesity with survival following colorectal cancer diagnosis by stage, anatomic site and tumor molecular subtype. *Int J Cancer* **142**, 238-250, doi:10.1002/ijc.31049 (2018).

20 https://www.krebsdaten.de/Krebs/DE.

21 Smith, G. *et al.* Mutations in APC, Kirsten-ras, and p53--alternative genetic pathways to colorectal cancer. *Proc Natl Acad Sci U S A* **99**, 9433-9438, doi:10.1073/pnas.122612899 (2002).

22 Fleming, M., Ravula, S., Tatishchev, S. F. & Wang, H. L. Colorectal carcinoma: Pathologic aspects. *J Gastrointest Oncol* **3**, 153-173, doi:10.3978/j.issn.2078-6891.2012.030 (2012).

23 Cancer Genome Atlas, N. Comprehensive molecular characterization of human colon and rectal cancer. *Nature* **487**, 330-337, doi:10.1038/nature11252 (2012).

24 Sideris, M. & Papagrigoriadis, S. Molecular biomarkers and classification models in the evaluation of the prognosis of colorectal cancer. *Anticancer Res* **34**, 2061-2068 (2014).

25 Jasperson, K. W., Tuohy, T. M., Neklason, D. W. & Burt, R. W. Hereditary and familial colon cancer. *Gastroenterology* **138**, 2044-2058, doi:10.1053/j.gastro.2010.01.054 (2010).

26 Brenner, H., Kloor, M. & Pox, C. P. Colorectal cancer. *Lancet* **383**, 1490-1502, doi:10.1016/s0140-6736(13)61649-9 (2014).

27 Yamagishi, H., Kuroda, H., Imai, Y. & Hiraishi, H. Molecular pathogenesis of sporadic colorectal cancers. *Chin J Cancer* **35**, 4, doi:10.1186/s40880-015-0066-y (2016).

28 Bettington, M. *et al.* The serrated pathway to colorectal carcinoma: current concepts and challenges. *Histopathology* **62**, 367-386, doi:10.1111/his.12055 (2013).

29 Vogelstein, B. *et al.* Genetic alterations during colorectal-tumor development. *N Engl J Med* **319**, 525-532, doi:10.1056/nejm198809013190901 (1988).

30 Day, D. W. & Morson, B. C. The adenoma-carcinoma sequence. *Major Probl Pathol* **10**, 58-71 (1978).

31 Thorstensen, L. *et al.* Genetic and epigenetic changes of components affecting the WNT pathway in colorectal carcinomas stratified by microsatellite instability. *Neoplasia* **7**, 99-108, doi:10.1593/neo.04448 (2005).

32 Walther, A. *et al.* Genetic prognostic and predictive markers in colorectal cancer. *Nat Rev Cancer* **9**, 489-499, doi:10.1038/nrc2645 (2009).

33 Emons, G. *et al.* Chemoradiotherapy Resistance in Colorectal Cancer Cells is Mediated by Wnt/beta-catenin Signaling. *Mol Cancer Res* **15**, 1481-1490, doi:10.1158/1541-7786.MCR-17-0205 (2017).

34 Giles, R. H., van Es, J. H. & Clevers, H. Caught up in a Wnt storm: Wnt signaling in cancer. *Biochim Biophys Acta* **1653**, 1-24, doi:10.1016/s0304-419x(03)00005-2 (2003).

35 Pino, M. S. & Chung, D. C. The chromosomal instability pathway in colon cancer. *Gastroenterology* **138**, 2059-2072, doi:10.1053/j.gastro.2009.12.065 (2010).

36 Wood, L. D. *et al.* The genomic landscapes of human breast and colorectal cancers. *Science* **318**, 1108-1113, doi:10.1126/science.1145720 (2007).

37 Blank, A., Roberts, D. E., 2nd, Dawson, H., Zlobec, I. & Lugli, A. Tumor Heterogeneity in Primary Colorectal Cancer and Corresponding Metastases. Does the Apple Fall Far From the Tree? *Front Med (Lausanne)* **5**, 234, doi:10.3389/fmed.2018.00234 (2018).

38 Andrew, A. S. *et al.* Hyper-Methylated Loci Persisting from Sessile Serrated Polyps to Serrated Cancers. *Int J Mol Sci* **18**, doi:10.3390/ijms18030535 (2017).

39 Harada, S. & Morlote, D. Molecular Pathology of Colorectal Cancer. *Adv Anat Pathol* **27**, 20-26, doi:10.1097/pap.0000000000000247 (2020).

40 Müller, M. F., Ibrahim, A. E. & Arends, M. J. Molecular pathological classification of colorectal cancer. *Virchows Arch* **469**, 125-134, doi:10.1007/s00428-016-1956-3 (2016).

41 Poulogiannis, G. *et al.* Prognostic relevance of DNA copy number changes in colorectal cancer. *J Pathol* **220**, 338-347, doi:10.1002/path.2640 (2010).

42 Court, C. M. *et al.* Somatic copy number profiling from hepatocellular carcinoma circulating tumor cells. *NPJ Precis Oncol* **4**, 16, doi:10.1038/s41698-020-0123-0 (2020).

43 Pancione, M., Remo, A. & Colantuoni, V. Genetic and epigenetic events generate multiple pathways in colorectal cancer progression. *Patholog Res Int* **2012**, 509348, doi:10.1155/2012/509348 (2012).

44 Nguyen, L. H., Goel, A. & Chung, D. C. Pathways of Colorectal Carcinogenesis. *Gastroenterology* **158**, 291-302, doi:10.1053/j.gastro.2019.08.059 (2020).

45 Schmitt, M. & Greten, F. R. The inflammatory pathogenesis of colorectal cancer. *Nat Rev Immunol*, doi:10.1038/s41577-021-00534-x (2021).

46 Goldstein, N. S. Serrated pathway and APC (conventional)-type colorectal polyps: molecular-morphologic correlations, genetic pathways, and implications for classification. *Am J Clin Pathol* **125**, 146-153 (2006).

47 Lansdorp-Vogelaar, I., van Ballegooijen, M., Zauber, A. G., Habbema, J. D. & Kuipers, E. J. Effect of rising chemotherapy costs on the cost savings of colorectal cancer screening. *J Natl Cancer Inst* **101**, 1412-1422, doi:10.1093/jnci/djp319 (2009).

48 Angarita, F. A., Feinberg, A. E., Feinberg, S. M., Riddell, R. H. & McCart, J. A. Management of complex polyps of the colon and rectum. *Int J Colorectal Dis* **33**, 115-129, doi:10.1007/s00384-017-2950-1 (2018).

49 Rex, D. K. *et al.* American College of Gastroenterology guidelines for colorectal cancer screening 2009 [corrected]. *Am J Gastroenterol* **104**, 739-750, doi:10.1038/ajg.2009.104 (2009).

50 Davila, R. E. *et al.* ASGE guideline: colorectal cancer screening and surveillance. *Gastrointest Endosc* **63**, 546-557, doi:10.1016/j.gie.2006.02.002 (2006).

51 Bruni, D., Angell, H. K. & Galon, J. The immune contexture and Immunoscore in cancer prognosis and therapeutic efficacy. *Nat Rev Cancer* **20**, 662-680, doi:10.1038/s41568-020-0285-7 (2020).

52 Weitz, J. *et al.* Colorectal cancer. *Lancet* **365**, 153-165, doi:10.1016/s0140-6736(05)17706-x (2005).

53 Montminy, E. M., Jang, A., Conner, M. & Karlitz, J. J. Screening for Colorectal Cancer. *Med Clin North Am* **104**, 1023-1036, doi:10.1016/j.mcna.2020.08.004 (2020).

54 Wittekind, C. in *Praxis der Viszeralchirurgie* (Springer, Berlin, Heidelberg, 2001).

55 Fong, W. & To, K. K. W. Drug repurposing to overcome resistance to various therapies for colorectal cancer. *Cell Mol Life Sci* **76**, 3383-3406, doi:10.1007/s00018-019-03134-0 (2019).

56 Buckley, A. M., Lynam-Lennon, N., O'Neill, H. & O'Sullivan, J. Targeting hallmarks of cancer to enhance radiosensitivity in gastrointestinal cancers. *Nat Rev Gastroenterol Hepatol* **17**, 298-313, doi:10.1038/s41575-019-0247-2 (2020).

57 Xie, Y. H., Chen, Y. X. & Fang, J. Y. Comprehensive review of targeted therapy for colorectal cancer. *Signal Transduct Target Ther* **5**, 22, doi:10.1038/s41392-020-0116-z (2020).

58 Knol, J. & Keller, D. S. Total Mesorectal Excision Technique-Past, Present, and Future. *Clin Colon Rectal Surg* **33**, 134-143, doi:10.1055/s-0039-3402776 (2020).

59 Pox, C. *et al.* [S3-guideline colorectal cancer version 1.0]. *Z Gastroenterol* **51**, 753-854, doi:10.1055/s-0033-1350264 (2013).

60 Heidelberger, C. *et al.* Fluorinated pyrimidines, a new class of tumour-inhibitory compounds. *Nature* **179**, 663-666, doi:10.1038/179663a0 (1957).

61 Blondy, S. *et al.* 5-Fluorouracil resistance mechanisms in colorectal cancer: From classical pathways to promising processes. *Cancer Sci* **111**, 3142-3154, doi:10.1111/cas.14532 (2020).

62 Patel, P. A. Evolution of 5-fluorouracil-based chemoradiation in the management of rectal cancer. *Anticancer Drugs* **22**, 311-316, doi:10.1097/CAD.0b013e3283441a63 (2011).

63 Sargent, D. *et al.* Evidence for cure by adjuvant therapy in colon cancer: observations based on individual patient data from 20,898 patients on 18 randomized trials. *J Clin Oncol* **27**, 872-877, doi:10.1200/jco.2008.19.5362 (2009).

64 Capitain, O. *et al.* The influence of fluorouracil outcome parameters on tolerance and efficacy in patients with advanced colorectal cancer. *Pharmacogenomics J* **8**, 256-267, doi:10.1038/sj.tpj.6500476 (2008).

65 André, T. *et al.* Oxaliplatin, fluorouracil, and leucovorin as adjuvant treatment for colon cancer. *N Engl J Med* **350**, 2343-2351, doi:10.1056/NEJMoa032709 (2004).

66 Kuebler, J. P. *et al.* Oxaliplatin combined with weekly bolus fluorouracil and leucovorin as surgical adjuvant chemotherapy for stage II and III colon cancer: results from NSABP C-07. *J Clin Oncol* **25**, 2198-2204, doi:10.1200/jco.2006.08.2974 (2007).

67 Benson, A. B., 3rd *et al.* Colon Cancer, Version 1.2017, NCCN Clinical Practice Guidelines in Oncology. *J Natl Compr Canc Netw* **15**, 370-398, doi:10.6004/jnccn.2017.0036 (2017).

68 Sauer, R. *et al.* Preoperative versus postoperative chemoradiotherapy for rectal cancer. *N Engl J Med* **351**, 1731-1740, doi:10.1056/NEJMoa040694 (2004).

69 Cunningham, D. *et al.* Colorectal cancer. *Lancet* **375**, 1030-1047, doi:10.1016/S0140-6736(10)60353-4 (2010).

70 Smith, J. J. & Garcia-Aguilar, J. Advances and challenges in treatment of locally advanced rectal cancer. *J Clin Oncol* **33**, 1797-1808, doi:10.1200/JCO.2014.60.1054 (2015).

71 Koerdel, K. *et al.* NOTCH Activation via gp130/STAT3 Signaling Confers Resistance to Chemoradiotherapy. *Cancers (Basel)* **13**, doi:10.3390/cancers13030455 (2021).

72 Stintzing, S. Management of colorectal cancer. *F1000Prime Rep* **6**, 108, doi:10.12703/p6-108 (2014).

73 Mei, Z. *et al.* Tumour-infiltrating inflammation and prognosis in colorectal cancer: systematic review and meta-analysis. *Br J Cancer* **110**, 1595-1605, doi:10.1038/bjc.2014.46 (2014).

74 Mierzwa, M. L., Nyati, M. K., Morgan, M. A. & Lawrence, T. S. Recent advances in combined modality therapy. *Oncologist* **15**, 372-381, doi:10.1634/theoncologist.2009-S105 (2010).

75 Shnaider, P. V. *et al.* New Insights into Therapy-Induced Progression of Cancer. *Int J Mol Sci* **21**, doi:10.3390/ijms21217872 (2020).

76 Vasan, N., Baselga, J. & Hyman, D. M. A view on drug resistance in cancer. *Nature* **575**, 299-309, doi:10.1038/s41586-019-1730-1 (2019).

77 Periti, P. & Mini, E. Drug resistance in cancer: an overview of the clinical aspects. *J Chemother* **1**, 5-9, doi:10.1080/1120009x.1989.11738856 (1989).

78 Rhoads, C. P. Nitrogen mustards in the treatment of neoplastic disease; official statement. *J Am Med Assoc* **131**, 656-658, doi:10.1001/jama.1946.02870250010003 (1946).

79 Cui, C. *et al.* Functions and mechanisms of circular RNAs in cancer radiotherapy and chemotherapy resistance. *Mol Cancer* **19**, 58, doi:10.1186/s12943-020-01180-y (2020).

80 Nikolaou, M., Pavlopoulou, A., Georgakilas, A. G. & Kyrodimos, E. The challenge of drug resistance in cancer treatment: a current overview. *Clin Exp Metastasis* **35**, 309-318, doi:10.1007/s10585-018-9903-0 (2018).

81 Lippert, T. H., Ruoff, H. J. & Volm, M. Intrinsic and acquired drug resistance in malignant tumors. The main reason for therapeutic failure. *Arzneimittelforschung* **58**, 261-264, doi:10.1055/s-0031-1296504 (2008).

82 Aleksakhina, S. N., Kashyap, A. & Imyanitov, E. N. Mechanisms of acquired tumor drug resistance. *Biochim Biophys Acta Rev Cancer* **1872**, 188310, doi:10.1016/j.bbcan.2019.188310 (2019).

83 DeVita, V. T., Jr. *et al.* Curability of advanced Hodgkin's disease with chemotherapy. Long-term follow-up of MOPP-treated patients at the National Cancer Institute. *Ann Intern Med* **92**, 587-595, doi:10.7326/0003-4819-92-5-587 (1980).

84 Bonadonna, G. *et al.* Combination chemotherapy as an adjuvant treatment in operable breast cancer. *N Engl J Med* **294**, 405-410, doi:10.1056/nejm197602192940801 (1976).

85 Kalyan, A., Kircher, S., Shah, H., Mulcahy, M. & Benson, A. Updates on immunotherapy for colorectal cancer. *J Gastrointest Oncol* **9**, 160-169, doi:10.21037/jgo.2018.01.17 (2018).

86 Zhao, B. *et al.* Mechanisms of resistance to anti-EGFR therapy in colorectal cancer. *Oncotarget* **8**, 3980-4000, doi:10.18632/oncotarget.14012 (2017).

87 Housman, G. *et al.* Drug resistance in cancer: an overview. *Cancers (Basel)* **6**, 1769-1792, doi:10.3390/cancers6031769 (2014).

88 Begg, A. C., Stewart, F. A. & Vens, C. Strategies to improve radiotherapy with targeted drugs. *Nat Rev Cancer* **11**, 239-253, doi:10.1038/nrc3007 (2011).

89 Delaney, G., Jacob, S., Featherstone, C. & Barton, M. The role of radiotherapy in cancer treatment: estimating optimal utilization from a review of evidence-based clinical guidelines. *Cancer* **104**, 1129-1137, doi:10.1002/cncr.21324 (2005).

90 Rodel, C. *et al.* Preoperative chemoradiotherapy and postoperative chemotherapy with fluorouracil and oxaliplatin versus fluorouracil alone in locally advanced rectal cancer: initial results of the German CAO/ARO/AIO-04 randomised phase 3 trial. *Lancet Oncol* **13**, 679-687, doi:10.1016/S1470-2045(12)70187-0 (2012).

91 Lange, M. M. & van de Velde, C. J. Urinary and sexual dysfunction after rectal cancer treatment. *Nat Rev Urol* **8**, 51-57, doi:10.1038/nrurol.2010.206 (2011).

92 Bryant, C. L., Lunniss, P. J., Knowles, C. H., Thaha, M. A. & Chan, C. L. Anterior resection syndrome. *Lancet Oncol* **13**, e403-408, doi:10.1016/S1470-2045(12)70236-X (2012).

93 Hoendervangers, S., Couwenberg, A. M., Intven, M. P. W., van Grevenstein, W. M. U. & Verkooijen, H. M. Comparison of pathological complete response rates after neoadjuvant short-course radiotherapy or chemoradiation followed by delayed surgery in locally advanced rectal cancer. *Eur J Surg Oncol* **44**, 1013-1017, doi:10.1016/j.ejso.2018.03.014 (2018).

94 Geh, J. I., Crellin, A. M. & Glynne-Jones, R. Preoperative (neoadjuvant) chemoradiotherapy in oesophageal cancer. *Br J Surg* **88**, 338-356, doi:10.1046/j.1365-2168.2001.01670.x (2001).

95 Longley, D. B. & Johnston, P. G. Molecular mechanisms of drug resistance. *J Pathol* **205**, 275-292, doi:10.1002/path.1706 (2005).

96 Shibata, J., Aiba, K., Shibata, H., Minowa, S. & Horikoshi, N. Detection and quantitation of thymidylate synthase mRNA in human colon adenocarcinoma cell line resistant to 5-fluorouracil by competitive PCR. *Anticancer Res* **18**, 1457-1463 (1998).

97 Sobrero, A., Aschele, C., Guglielmi, A., Nobile, M. T. & Rosso, R. Resistance to 5-fluorouracil and 5-fluoro-2'-deoxyuridine mechanisms and clinical implications. *J Chemother* **2 Suppl 1**, 12-16, doi:10.1080/1120009x.1990.11738999 (1990).

98 Seiwert, T. Y., Salama, J. K. & Vokes, E. E. The concurrent chemoradiation paradigm--general principles. *Nat Clin Pract Oncol* **4**, 86-100, doi:10.1038/ncponc0714 (2007).

99 Hanahan, D. & Weinberg, R. A. Hallmarks of cancer: the next generation. *Cell* **144**, 646-674, doi:10.1016/j.cell.2011.02.013 (2011).

100 Dmello, R. S., To, S. Q. & Chand, A. L. Therapeutic Targeting of the Tumour Microenvironment in Metastatic Colorectal Cancer. *Int J Mol Sci* **22**, doi:10.3390/ijms22042067 (2021).

101 Singh, N. *et al.* Inflammation and cancer. *Ann Afr Med* **18**, 121-126, doi:10.4103/aam.aam_56_18 (2019).

102 Fishbein, A., Hammock, B. D., Serhan, C. N. & Panigrahy, D. Carcinogenesis: Failure of resolution of inflammation? *Pharmacol Ther* **218**, 107670, doi:10.1016/j.pharmthera.2020.107670 (2021).

103 Serhan, C. N. Treating inflammation and infection in the 21st century: new hints from decoding resolution mediators and mechanisms. *Faseb J* **31**, 1273-1288 (2017).

104 Dvorak, H. F. Tumors: wounds that do not heal. Similarities between tumor stroma generation and wound healing. *N Engl J Med* **315**, 1650-1659, doi:10.1056/nejm198612253152606 (1986).

105 Medzhitov, R. Origin and physiological roles of inflammation. *Nature* **454**, 428-435, doi:10.1038/nature07201 (2008).

106 Virchow, R. An Address on the Value of Pathological Experiments. *Br Med J* **2**, 198-203, doi:10.1136/bmj.2.1075.198 (1881).

107 Balkwill, F. & Mantovani, A. Inflammation and cancer: back to Virchow? *Lancet* **357**, 539-545, doi:10.1016/s0140-6736(00)04046-0 (2001).

108 Landskron, G., De la Fuente, M., Thuwajit, P., Thuwajit, C. & Hermoso, M. A. Chronic inflammation and cytokines in the tumor microenvironment. *J Immunol Res* **2014**, 149185, doi:10.1155/2014/149185 (2014).

109 Jass, J. R. Lymphocytic infiltration and survival in rectal cancer. *J Clin Pathol* **39**, 585-589, doi:10.1136/jcp.39.6.585 (1986).

110 Guthrie, G. J., Roxburgh, C. S., Horgan, P. G. & McMillan, D. C. Does interleukin-6 link explain the link between tumour necrosis, local and systemic inflammatory responses and outcome in patients with colorectal cancer? *Cancer Treat Rev* **39**, 89-96, doi:10.1016/j.ctrv.2012.07.003 (2013).

111 Terzić, J., Grivennikov, S., Karin, E. & Karin, M. Inflammation and colon cancer. *Gastroenterology* **138**, 2101-2114.e2105, doi:10.1053/j.gastro.2010.01.058 (2010).

112 Jess, T., Rungoe, C. & Peyrin-Biroulet, L. Risk of colorectal cancer in patients with ulcerative colitis: a meta-analysis of population-based cohort studies. *Clin Gastroenterol Hepatol* **10**, 639-645, doi:10.1016/j.cgh.2012.01.010 (2012).

113 Lasry, A., Zinger, A. & Ben-Neriah, Y. Inflammatory networks underlying colorectal cancer. *Nat Immunol* **17**, 230-240, doi:10.1038/ni.3384 (2016).

114 Diakos, C. I., Charles, K. A., McMillan, D. C. & Clarke, S. J. Cancer-related inflammation and treatment effectiveness. *Lancet Oncol* **15**, e493-503, doi:10.1016/s1470-2045(14)70263-3 (2014).

115 Cui, G., Yuan, A., Sun, Z., Zheng, W. & Pang, Z. IL-1β/IL-6 network in the tumor microenvironment of human colorectal cancer. *Pathol Res Pract* **214**, 986-992, doi:10.1016/j.prp.2018.05.011 (2018).

116 Germano, G., Allavena, P. & Mantovani, A. Cytokines as a key component of cancer-related inflammation. *Cytokine* **43**, 374-379, doi:10.1016/j.cyto.2008.07.014 (2008).

117 Gabrilovich, D. I., Ostrand-Rosenberg, S. & Bronte, V. Coordinated regulation of myeloid cells by tumours. *Nat Rev Immunol* **12**, 253-268, doi:10.1038/nri3175 (2012).

118 Klein, B. *et al.* Paracrine rather than autocrine regulation of myeloma-cell growth and differentiation by interleukin-6. *Blood* **73**, 517-526 (1989).

119 Johnson, D. E., O'Keefe, R. A. & Grandis, J. R. Targeting the IL-6/JAK/STAT3 signalling axis in cancer. *Nat Rev Clin Oncol* **15**, 234-248, doi:10.1038/nrclinonc.2018.8 (2018).

120 Nozawa, H., Chiu, C. & Hanahan, D. Infiltrating neutrophils mediate the initial angiogenic switch in a mouse model of multistage carcinogenesis. *Proc Natl Acad Sci U S A* **103**, 12493-12498, doi:10.1073/pnas.0601807103 (2006).

121 Nagasaki, T. *et al.* Interleukin-6 released by colon cancer-associated fibroblasts is critical for tumour angiogenesis: anti-interleukin-6 receptor antibody suppressed angiogenesis and inhibited tumour-stroma interaction. *Br J Cancer* **110**, 469-478, doi:10.1038/bjc.2013.748 (2014).

122 Zhang, N., Zhang, M., Wang, Z., Gao, W. & Sun, Z. G. Activated STAT3 Could Reduce Survival in Patients with Esophageal Squamous Cell Carcinoma by Up-regulating VEGF and Cyclin D1 Expression. *J Cancer* **11**, 1859-1868, doi:10.7150/jca.38798 (2020).

123 Toyoshima, Y. *et al.* IL6 Modulates the Immune Status of the Tumor Microenvironment to Facilitate Metastatic Colonization of Colorectal Cancer Cells. *Cancer Immunol Res* **7**, 1944-1957, doi:10.1158/2326-6066.Cir-18-0766 (2019).

124 Rokavec, M. *et al.* IL-6R/STAT3/miR-34a feedback loop promotes EMT-mediated colorectal cancer invasion and metastasis. *J Clin Invest* **124**, 1853-1867, doi:10.1172/jci73531 (2014).

125 Xu, J. *et al.* Diagnostic and Prognostic Value of Serum Interleukin-6 in Colorectal Cancer. *Medicine (Baltimore)* **95**, e2502, doi:10.1097/md.0000000000002502 (2016).

126 Chung, Y. C. & Chang, Y. F. Serum interleukin-6 levels reflect the disease status of colorectal cancer. *J Surg Oncol* **83**, 222-226, doi:10.1002/jso.10269 (2003).

127 Huynh, J., Chand, A., Gough, D. & Ernst, M. Therapeutically exploiting STAT3 activity in cancer - using tissue repair as a road map. *Nat Rev Cancer* **19**, 82-96, doi:10.1038/s41568-018-0090-8 (2019).

128 Rose-John, S. Interleukin-6 signalling in health and disease. *F1000Res* **9**, doi:10.12688/f1000research.26058.1 (2020).

129 Scheller, J., Ohnesorge, N. & Rose-John, S. Interleukin-6 trans-signalling in chronic inflammation and cancer. *Scand J Immunol* **63**, 321-329, doi:10.1111/j.1365-3083.2006.01750.x (2006).

130 Rose-John, S. Interleukin-6 biology is coordinated by membrane bound and soluble receptors. *Acta Biochim Pol* **50**, 603-611 (2003).

131 Jones, S. A., Scheller, J. & Rose-John, S. Therapeutic strategies for the clinical blockade of IL-6/gp130 signaling. *J Clin Invest* **121**, 3375-3383, doi:10.1172/jci57158 (2011).

132 Taga, T. & Kishimoto, T. Gp130 and the interleukin-6 family of cytokines. *Annu Rev Immunol* **15**, 797-819, doi:10.1146/annurev.immunol.15.1.797 (1997).

133 Hunter, C. A. & Jones, S. A. IL-6 as a keystone cytokine in health and disease. *Nat Immunol* **16**, 448-457, doi:10.1038/ni.3153 (2015).

134 Müllberg, J. *et al.* The soluble interleukin-6 receptor is generated by shedding. *Eur J Immunol* **23**, 473-480, doi:10.1002/eji.1830230226 (1993).

135 Jones, S. A. & Jenkins, B. J. Recent insights into targeting the IL-6 cytokine family in inflammatory diseases and cancer. *Nat Rev Immunol* **18**, 773-789, doi:10.1038/s41577-018-0066-7 (2018).

136 Hoge, J. *et al.* IL-6 controls the innate immune response against Listeria monocytogenes via classical IL-6 signaling. *J Immunol* **190**, 703-711, doi:10.4049/jimmunol.1201044 (2013).

137 Rose-John, S., Winthrop, K. & Calabrese, L. The role of IL-6 in host defence against infections: immunobiology and clinical implications. *Nat Rev Rheumatol* **13**, 399-409, doi:10.1038/nrrheum.2017.83 (2017).

138 Rose-John, S., Mitsuyama, K., Matsumoto, S., Thaiss, W. M. & Scheller, J. Interleukin-6 trans-signaling and colonic cancer associated with inflammatory bowel disease. *Curr Pharm Des* **15**, 2095-2103, doi:10.2174/138161209788489140 (2009).

139 Putoczki, T. L. *et al.* Interleukin-11 is the dominant IL-6 family cytokine during gastrointestinal tumorigenesis and can be targeted therapeutically. *Cancer Cell* **24**, 257-271, doi:10.1016/j.ccr.2013.06.017 (2013).

140 Bollrath, J. *et al.* gp130-mediated Stat3 activation in enterocytes regulates cell survival and cell-cycle progression during colitis-associated tumorigenesis. *Cancer Cell* **15**, 91-102, doi:10.1016/j.ccr.2009.01.002 (2009).

141 Darnell, J. E., Jr. STATs and gene regulation. *Science* **277**, 1630-1635, doi:10.1126/science.277.5332.1630 (1997).

142 Zhong, Z., Wen, Z. & Darnell, J. E., Jr. Stat3: a STAT family member activated by tyrosine phosphorylation in response to epidermal growth factor and interleukin-6. *Science* **264**, 95-98, doi:10.1126/science.8140422 (1994).

143 Akira, S. *et al.* Molecular cloning of APRF, a novel IFN-stimulated gene factor 3 p91-related transcription factor involved in the gp130-mediated signaling pathway. *Cell* **77**, 63-71, doi:10.1016/0092-8674(94)90235-6 (1994).

144 Yu, H., Pardoll, D. & Jove, R. STATs in cancer inflammation and immunity: a leading role for STAT3. *Nat Rev Cancer* **9**, 798-809, doi:10.1038/nrc2734 (2009).

145 Shih, P. C. Revisiting the development of small molecular inhibitors that directly target the signal transducer and activator of transcription 3 (STAT3) domains. *Life Sci* **242**, 117241, doi:10.1016/j.lfs.2019.117241 (2020).

146 Wang, X., Crowe, P. J., Goldstein, D. & Yang, J. L. STAT3 inhibition, a novel approach to enhancing targeted therapy in human cancers (review). *Int J Oncol* **41**, 1181-1191, doi:10.3892/ijo.2012.1568 (2012).

147 Spitzner, M. *et al.* STAT3 inhibition sensitizes colorectal cancer to chemoradiotherapy in vitro and in vivo. *Int J Cancer* **134**, 997-1007, doi:10.1002/ijc.28429 (2014).

148 Takeda, K. & Akira, S. STAT family of transcription factors in cytokine-mediated biological responses. *Cytokine Growth Factor Rev* **11**, 199-207, doi:10.1016/s1359-6101(00)00005-8 (2000).

149 Garbers, C., Aparicio-Siegmund, S. & Rose-John, S. The IL-6/gp130/STAT3 signaling axis: recent advances towards specific inhibition. *Curr Opin Immunol* **34**, 75-82, doi:10.1016/j.coi.2015.02.008 (2015).

150 Yu, H., Lee, H., Herrmann, A., Buettner, R. & Jove, R. Revisiting STAT3 signalling in cancer: new and unexpected biological functions. *Nat Rev Cancer* **14**, 736-746, doi:10.1038/nrc3818 (2014).

151 Kang, S., Narazaki, M., Metwally, H. & Kishimoto, T. Historical overview of the interleukin-6 family cytokine. *J Exp Med* **217**, doi:10.1084/jem.20190347 (2020).

152 Becker, S., Groner, B. & Müller, C. W. Three-dimensional structure of the Stat3beta homodimer bound to DNA. *Nature* **394**, 145-151, doi:10.1038/28101 (1998).

153 Wen, Z., Zhong, Z. & Darnell, J. E., Jr. Maximal activation of transcription by Stat1 and Stat3 requires both tyrosine and serine phosphorylation. *Cell* **82**, 241-250, doi:10.1016/0092-8674(95)90311-9 (1995).

154 Bournazou, E. & Bromberg, J. Targeting the tumor microenvironment: JAK-STAT3 signaling. *Jakstat* **2**, e23828, doi:10.4161/jkst.23828 (2013).

155 Siveen, K. S. *et al.* Targeting the STAT3 signaling pathway in cancer: role of synthetic and natural inhibitors. *Biochim Biophys Acta* **1845**, 136-154, doi:10.1016/j.bbcan.2013.12.005 (2014).

156 Monnien, F. *et al.* Prognostic value of phosphorylated STAT3 in advanced rectal cancer: a study from 104 French patients included in the EORTC 22921 trial. *J Clin Pathol* **63**, 873-878, doi:10.1136/jcp.2010.076414 (2010).

157 Zou, S. *et al.* Targeting STAT3 in Cancer Immunotherapy. *Mol Cancer* **19**, 145, doi:10.1186/s12943-020-01258-7 (2020).

158 Beebe, J. D., Liu, J. Y. & Zhang, J. T. Two decades of research in discovery of anticancer drugs targeting STAT3, how close are we? *Pharmacol Ther* **191**, 74-91, doi:10.1016/j.pharmthera.2018.06.006 (2018).

159 Heppler, L. N. & Frank, D. A. Targeting Oncogenic Transcription Factors: Therapeutic Implications of Endogenous STAT Inhibitors. *Trends Cancer* **3**, 816-827, doi:10.1016/j.trecan.2017.10.004 (2017).

160 Sun, C. Y., Nie, J., Huang, J. P., Zheng, G. J. & Feng, B. Targeting STAT3 inhibition to reverse cisplatin resistance. *Biomed Pharmacother* **117**, 109135, doi:10.1016/j.biopha.2019.109135 (2019).

161 Bosch-Barrera, J., Queralt, B. & Menendez, J. A. Targeting STAT3 with silibinin to improve cancer therapeutics. *Cancer Treat Rev* **58**, 61-69, doi:10.1016/j.ctrv.2017.06.003 (2017).

162 Spitzner, M. *et al.* A gene expression signature for chemoradiosensitivity of colorectal cancer cells. *Int J Radiat Oncol Biol Phys* **78**, 1184-1192, doi:10.1016/j.ijrobp.2010.06.023 (2010).

163 Nagaraju, G. P. *et al.* Napabucasin (BBI 608), a potent chemoradiosensitizer in rectal cancer. *Cancer*, doi:10.1002/cncr.32954 (2020).

164 Ebbing, E. A. *et al.* Stromal-derived interleukin 6 drives epithelial-to-mesenchymal transition and therapy resistance in esophageal adenocarcinoma. *Proc Natl Acad Sci U S A* **116**, 2237-2242, doi:10.1073/pnas.1820459116 (2019).

165 Bremer, S. C. B. *et al.* Enhancer of Zeste Homolog 2 in Colorectal Cancer Development and Progression. *Digestion*, 1-9, doi:10.1159/000504093 (2019).

166 Jo, P. *et al.* Neoadjuvant Therapy in Rectal Cancer - Biobanking of Preoperative Tumor Biopsies. *Sci Rep* **6**, 35589, doi:10.1038/srep35589 (2016).

167 Ton, G. *The role of the IL-6-STAT3 axis for sensitization of colorectal cancer cells to chemoradiotherapy*, Georg-August-University, (2018).

168 Neumann, E., Schaefer-Ridder, M., Wang, Y. & Hofschneider, P. H. Gene transfer into mouse lyoma cells by electroporation in high electric fields. *Embo j* **1**, 841-845 (1982).

169 Felgner, P. L. *et al.* Lipofection: a highly efficient, lipid-mediated DNA-transfection procedure. *Proc Natl Acad Sci U S A* **84**, 7413-7417, doi:10.1073/pnas.84.21.7413 (1987).

170 Pfaffl, M. W. A new mathematical model for relative quantification in real-time RT-PCR. *Nucleic Acids Res* **29**, e45, doi:10.1093/nar/29.9.e45 (2001).

171 Rasmussen, L. D., Ekelund, F., Hansen, L. H., Sørensen, S. J. & Johnsen, K. Group-Specific PCR Primers to Amplify 24S a-Subunit rRNA Genes from Kinetoplastida (Protozoa) Used in Denaturing Gradient Gel Electrophoresis. *Microb Ecol* **42**, 109-115, doi:10.1007/s002480000120 (2001).

172 Andrews, S. *FastQC A Quality Control Tool for High Throughput Sequence Data*, <https://github.com/s-andrews/FastQC> (2014).

173 Dobin, A. *et al.* STAR: ultrafast universal RNA-seq aligner. *Bioinformatics* **29**, 15-21, doi:10.1093/bioinformatics/bts635 (2013).

174 Ewels, P., Magnusson, M., Lundin, S. & Kaller, M. MultiQC: summarize analysis results for multiple tools and samples in a single report. *Bioinformatics* **32**, 3047-3048, doi:10.1093/bioinformatics/btw354 (2016).

175 Li, B. & Dewey, C. N. RSEM: accurate transcript quantification from RNA-Seq data with or without a reference genome. *BMC Bioinformatics* **12**, 323, doi:10.1186/1471-2105-12-323 (2011).

176 Robinson, M. D., McCarthy, D. J. & Smyth, G. K. edgeR: a Bioconductor package for differential expression analysis of digital gene expression data. *Bioinformatics* **26**, 139-140, doi:10.1093/bioinformatics/btp616 (2010).

177 Bradford, M. M. A rapid and sensitive method for the quantitation of microgram quantities of protein utilizing the principle of protein-dye binding. *Anal Biochem* **72**, 248-254, doi:10.1006/abio.1976.9999 (1976).

178 Petersen, J. *et al.* Identification of a distinct subset of disease-associated gain-of-function missense mutations in the STAT1 coiled-coil domain as system mutants. *Mol Immunol* **114**, 30-40, doi:10.1016/j.molimm.2019.07.008 (2019).

179 Franken, N. A., Rodermond, H. M., Stap, J., Haveman, J. & van Bree, C. Clonogenic assay of cells in vitro. *Nat Protoc* **1**, 2315-2319, doi:10.1038/nprot.2006.339 (2006).

180 Riss, T. L. *et al.* in *Assay Guidance Manual* (eds S. Markossian *et al.*) (Eli Lilly & Company and the National Center for Advancing Translational Sciences, 2004).

181 Dissmeyer, N. & Schnittger, A. Use of phospho-site substitutions to analyze the biological relevance of phosphorylation events in regulatory networks. *Methods Mol Biol* **779**, 93-138, doi:10.1007/978-1-61779-264-9_6 (2011).

182 Fischer, M. *et al.* I. A bioactive designer cytokine for human hematopoietic progenitor cell expansion. *Nat Biotechnol* **15**, 142-145, doi:10.1038/nbt0297-142 (1997).

183 Rose-John, S. *et al.* Studies on the structure and regulation of the human hepatic interleukin-6 receptor. *Eur J Biochem* **190**, 79-83, doi:10.1111/j.1432-1033.1990.tb15548.x (1990).

184 Han, E. S. *et al.* Ruxolitinib synergistically enhances the anti-tumor activity of paclitaxel in human ovarian cancer. *Oncotarget* **9**, 24304-24319, doi:10.18632/oncotarget.24368 (2018).

185 Li, Y. *et al.* Suppression of cancer relapse and metastasis by inhibiting cancer stemness. *Proc Natl Acad Sci U S A* **112**, 1839-1844, doi:10.1073/pnas.1424171112 (2015).

186 Jonker, D. J. *et al.* Napabucasin versus placebo in refractory advanced colorectal cancer: a randomised phase 3 trial. *Lancet Gastroenterol Hepatol* **3**, 263-270, doi:10.1016/S2468-1253(18)30009-8 (2018).

187 Schust, J. *Neue Ansätze zur Identifizierung niedermolekularer Inhibitoren der STAT3-Aktivierung und -Homodimerisierung*, Bayerischen Julius-Maximilians-Universität Würzburg, (2006).

188 Wang, J. L. *et al.* Elf3 drives β-catenin transactivation and associates with poor prognosis in colorectal cancer. *Cell Death Dis* **5**, e1263, doi:10.1038/cddis.2014.206 (2014).

189 Takaoka, A. *et al.* ELF3 Overexpression as Prognostic Biomarker for Recurrence of Stage II Colorectal Cancer. *In Vivo* **35**, 191-201, doi:10.21873/invivo.12248 (2021).

190 Moeller, B. J., Cao, Y., Li, C. Y. & Dewhirst, M. W. Radiation activates HIF-1 to regulate vascular radiosensitivity in tumors: role of reoxygenation, free radicals, and stress granules. *Cancer Cell* **5**, 429-441 (2004).

191 Baba, Y. *et al.* HIF1A overexpression is associated with poor prognosis in a cohort of 731 colorectal cancers. *Am J Pathol* **176**, 2292-2301, doi:10.2353/ajpath.2010.090972 (2010).

192 Henricks, L. M. *et al.* DPYD genotype-guided dose individualisation of fluoropyrimidine therapy in patients with cancer: a prospective safety analysis. *Lancet Oncol* **19**, 1459-1467, doi:10.1016/S1470-2045(18)30686-7 (2018).

193 Lunenburg, C., Swen, J. J., Guchelaar, H. J. & Gelderblom, H. Capecitabine-Induced Severe Toxicity Secondary to DPD Deficiency and Successful Treatment with Low Dose 5-Fluorouracil. *J Gastrointest Cancer* **48**, 117-118, doi:10.1007/s12029-016-9908-3 (2017).

194 Vallböhmer, D. *et al.* DPD is a molecular determinant of capecitabine efficacy in colorectal cancer. *Int J Oncol* **31**, 413-418 (2007).

195 Scartozzi, M. *et al.* 5-Fluorouracil pharmacogenomics: still rocking after all these years? *Pharmacogenomics* **12**, 251-265, doi:10.2217/pgs.10.167 (2011).

196 Kudryavtseva, A. V. *et al.* Effect of lentivirus-mediated shRNA inactivation of HK1, HK2, and HK3 genes in colorectal cancer and melanoma cells. *BMC Genet* **17**, 156, doi:10.1186/s12863-016-0459-1 (2016).

197 Gunda, V. *et al.* MUC1-Mediated Metabolic Alterations Regulate Response to Radiotherapy in Pancreatic Cancer. *Clin Cancer Res* **23**, 5881-5891, doi:10.1158/1078-0432.CCR-17-1151 (2017).

198 Guo, M. *et al.* MUC1 plays an essential role in tumor immunity of colorectal cancer stem cell vaccine. *Int Immunopharmacol* **85**, 106631, doi:10.1016/j.intimp.2020.106631 (2020).

199 Ham, S. Y. *et al.* Mucin 1-mediated chemo-resistance in lung cancer cells. *Oncogenesis* **5**, e185, doi:10.1038/oncsis.2015.47 (2016).

200 Nath, S. *et al.* MUC1 induces drug resistance in pancreatic cancer cells via upregulation of multidrug resistance genes. *Oncogenesis* **2**, e51, doi:10.1038/oncsis.2013.16 (2013).

201 Chen, H., Wang, S., Zhang, H., Nice, E. C. & Huang, C. Nicotinamide phosphoribosyltransferase (Nampt) in carcinogenesis: new clinical opportunities. *Expert Rev Anticancer Ther* **16**, 827-838, doi:10.1080/14737140.2016.1190649 (2016).

202 Gujar, A. D. *et al.* An NAD+-dependent transcriptional program governs self-renewal and radiation resistance in glioblastoma. *Proc Natl Acad Sci U S A* **113**, E8247-e8256, doi:10.1073/pnas.1610921114 (2016).

203 Lucena-Cacace, A., Otero-Albiol, D., Jiménez-García, M. P., Muñoz-Galvan, S. & Carnero, A. NAMPT Is a Potent Oncogene in Colon Cancer Progression that Modulates Cancer Stem Cell Properties and Resistance to Therapy through Sirt1 and PARP. *Clin Cancer Res* **24**, 1202-1215, doi:10.1158/1078-0432.Ccr-17-2575 (2018).

204 Sena, P. *et al.* Morphological and quantitative analysis of BCL6 expression in human colorectal carcinogenesis. *Oncol Rep* **31**, 103-110, doi:10.3892/or.2013.2846 (2014).

205 Hu, S. *et al.* Epigenetic silencing BCL6B induced colorectal cancer proliferation and metastasis by inhibiting P53 signaling. *Am J Cancer Res* **5**, 651-662 (2015).

206 Kopan, R. & Ilagan, M. X. The canonical Notch signaling pathway: unfolding the activation mechanism. *Cell* **137**, 216-233, doi:10.1016/j.cell.2009.03.045 (2009).

207 Ntziachristos, P., Lim, J. S., Sage, J. & Aifantis, I. From fly wings to targeted cancer therapies: a centennial for notch signaling. *Cancer Cell* **25**, 318-334, doi:10.1016/j.ccr.2014.02.018 (2014).

208 Yahyanejad, S., Theys, J. & Vooijs, M. Targeting Notch to overcome radiation resistance. *Oncotarget* **7**, 7610-7628, doi:10.18632/oncotarget.6714 (2016).

209 Nguyen, D. M., Parekh, P. R., Chang, E. T., Sharma, N. K. & Carrier, F. Contribution of Dual Oxidase 2 (DUOX2) to Hyper-Radiosensitivity in Human Gastric Cancer Cells. *Radiat Res* **184**, 151-160, doi:10.1667/rr13661.1 (2015).

210 Kang, K. A. *et al.* DUOX2-mediated production of reactive oxygen species induces epithelial mesenchymal transition in 5-fluorouracil resistant human colon cancer cells. *Redox Biol* **17**, 224-235, doi:10.1016/j.redox.2018.04.020 (2018).

211 Zhang, X. *et al.* DUOX2 promotes the progression of colorectal cancer cells by regulating the AKT pathway and interacting with RPL3. *Carcinogenesis* **42**, 105-117, doi:10.1093/carcin/bgaa056 (2021).

212 Zhou, M. *et al.* The Significance of Serum S100A9 and TNC Levels as Biomarkers in Colorectal Cancer. *J Cancer* **10**, 5315-5323, doi:10.7150/jca.31267 (2019).

213 Zhao, Z., Zhang, C. & Zhao, Q. S100A9 as a novel diagnostic and prognostic biomarker in human gastric cancer. *Scand J Gastroenterol* **55**, 338-346, doi:10.1080/00365521.2020.1737883 (2020).

214 Murakami, A. *et al.* Squamous cell carcinoma antigen suppresses radiation-induced cell death. *Br J Cancer* **84**, 851-858, doi:10.1054/bjoc.2000.1683 (2001).

215 Hill, R. *et al.* TRIB2 confers resistance to anti-cancer therapy by activating the serine/threonine protein kinase AKT. *Nat Commun* **8**, 14687, doi:10.1038/ncomms14687 (2017).

216 Hou, Z. *et al.* TRIB2 functions as novel oncogene in colorectal cancer by blocking cellular senescence through AP4/p21 signaling. *Mol Cancer* **17**, 172, doi:10.1186/s12943-018-0922-x (2018).

217 Decker, T., Kovarik, P. & Meinke, A. GAS elements: a few nucleotides with a major impact on cytokine-induced gene expression. *J Interferon Cytokine Res* **17**, 121-134, doi:10.1089/jir.1997.17.121 (1997).

218 Sasse, J. *et al.* Mutational analysis of acute-phase response factor/Stat3 activation and dimerization. *Mol Cell Biol* **17**, 4677-4686, doi:10.1128/mcb.17.8.4677 (1997).

219 Artavanis-Tsakonas, S., Matsuno, K. & Fortini, M. E. Notch signaling. *Science* **268**, 225-232, doi:10.1126/science.7716513 (1995).

220 Blaumueller, C. M., Qi, H., Zagouras, P. & Artavanis-Tsakonas, S. Intracellular cleavage of Notch leads to a heterodimeric receptor on the plasma membrane. *Cell* **90**, 281-291, doi:10.1016/s0092-8674(00)80336-0 (1997).

221 Artavanis-Tsakonas, S., Rand, M. D. & Lake, R. J. Notch signaling: cell fate control and signal integration in development. *Science* **284**, 770-776, doi:10.1126/science.284.5415.770 (1999).

222 Greenwald, I. LIN-12/Notch signaling: lessons from worms and flies. *Genes Dev* **12**, 1751-1762, doi:10.1101/gad.12.12.1751 (1998).

223 Nickoloff, B. J., Osborne, B. A. & Miele, L. Notch signaling as a therapeutic target in cancer: a new approach to the development of cell fate modifying agents. *Oncogene* **22**, 6598-6608, doi:10.1038/sj.onc.1206758 (2003).

224 Miele, L. Notch signaling. *Clin Cancer Res* **12**, 1074-1079, doi:10.1158/1078-0432.Ccr-05-2570 (2006).

225 Majumder, S. *et al.* Targeting Notch in oncology: the path forward. *Nat Rev Drug Discov* **20**, 125-144, doi:10.1038/s41573-020-00091-3 (2021).

226 Logeat, F. *et al.* The Notch1 receptor is cleaved constitutively by a furin-like convertase. *Proc Natl Acad Sci U S A* **95**, 8108-8112, doi:10.1073/pnas.95.14.8108 (1998).

227 Miele, L. & Osborne, B. Arbiter of differentiation and death: Notch signaling meets apoptosis. *J Cell Physiol* **181**, 393-409, doi:10.1002/(sici)1097-4652(199912)181:3<393::Aid-jcp3>3.0.Co;2-6 (1999).

228 Kamakura, S. *et al.* Hes binding to STAT3 mediates crosstalk between Notch and JAK-STAT signalling. *Nat Cell Biol* **6**, 547-554, doi:10.1038/ncb1138 (2004).

229 Schroeter, E. H., Kisslinger, J. A. & Kopan, R. Notch-1 signalling requires ligand-induced proteolytic release of intracellular domain. *Nature* **393**, 382-386, doi:10.1038/30756 (1998).

230 De Strooper, B. *et al.* A presenilin-1-dependent gamma-secretase-like protease mediates release of Notch intracellular domain. *Nature* **398**, 518-522, doi:10.1038/19083 (1999).

231 Espinoza, I., Pochampally, R., Xing, F., Watabe, K. & Miele, L. Notch signaling: targeting cancer stem cells and epithelial-to-mesenchymal transition. *Onco Targets Ther* **6**, 1249-1259 (2013).

232 Dovey, H. F. *et al.* Functional gamma-secretase inhibitors reduce beta-amyloid peptide levels in brain. *J Neurochem* **76**, 173-181, doi:10.1046/j.1471-4159.2001.00012.x (2001).

233 Wang, M., Ma, X., Wang, J., Wang, L. & Wang, Y. Pretreatment with the γ-secretase inhibitor DAPT sensitizes drug-resistant ovarian cancer cells to cisplatin by downregulation of Notch signaling. *Int J Oncol* **44**, 1401-1409, doi:10.3892/ijo.2014.2301 (2014).

234 Gu, F. *et al.* Expression of Stat3 and Notch1 is associated with cisplatin resistance in head and neck squamous cell carcinoma. *Oncol Rep* **23**, 671-676, doi:10.3892/or_00000683 (2010).

235 Zhang, H. *et al.* Inhibition of Notch1/Hes1 signaling pathway improves radiosensitivity of colorectal cancer cells. *Eur J Pharmacol* **818**, 364-370, doi:10.1016/j.ejphar.2017.11.009 (2018).

236 Zhang, Q. *et al.* Exosomal transfer of p-STAT3 promotes acquired 5-FU resistance in colorectal cancer cells. *J Exp Clin Cancer Res* **38**, 320, doi:10.1186/s13046-019-1314-9 (2019).

237 https://portals.broadinstitute.org/ccle/page?cell_line=LS411N_LARGE_INTESTINE>

238 Cheon, H., Yang, J. & Stark, G. R. The functions of signal transducers and activators of transcriptions 1 and 3 as cytokine-inducible proteins. *J Interferon Cytokine Res* **31**, 33-40, doi:10.1089/jir.2010.0100 (2011).

239 Yang, J. *et al.* Novel roles of unphosphorylated STAT3 in oncogenesis and transcriptional regulation. *Cancer Res* **65**, 939-947 (2005).

240 Yang, J. *et al.* Unphosphorylated STAT3 accumulates in response to IL-6 and activates transcription by binding to NFkappaB. *Genes Dev* **21**, 1396-1408, doi:10.1101/gad.1553707 (2007).

241 Loeffler, M., Krüger, J. A., Niethammer, A. G. & Reisfeld, R. A. Targeting tumor-associated fibroblasts improves cancer chemotherapy by increasing intratumoral drug uptake. *J Clin Invest* **116**, 1955-1962, doi:10.1172/jci26532 (2006).

242 Zhang, X. *et al.* Macrophages induce resistance to 5-fluorouracil chemotherapy in colorectal cancer through the release of putrescine. *Cancer Lett* **381**, 305-313, doi:10.1016/j.canlet.2016.08.004 (2016).

243 Schmidt, S. *et al.* ADAM17 is required for EGF-R-induced intestinal tumors via IL-6 trans-signaling. *J Exp Med* **215**, 1205-1225, doi:10.1084/jem.20171696 (2018).

244 Rose-John, S. & Heinrich, P. C. Soluble receptors for cytokines and growth factors: generation and biological function. *Biochem J* **300 (Pt 2)**, 281-290, doi:10.1042/bj3000281 (1994).

245 Jostock, T. *et al.* Soluble gp130 is the natural inhibitor of soluble interleukin-6 receptor transsignaling responses. *Eur J Biochem* **268**, 160-167, doi:10.1046/j.1432-1327.2001.01867.x (2001).

246 Greten, F. R. & Grivennikov, S. I. Inflammation and Cancer: Triggers, Mechanisms, and Consequences. *Immunity* **51**, 27-41, doi:10.1016/j.immuni.2019.06.025 (2019).

247 Tanaka, T. *et al.* Successful treatment of reactive arthritis with a humanized anti-interleukin-6 receptor antibody, tocilizumab. *Arthritis Rheum* **61**, 1762-1764, doi:10.1002/art.24899 (2009).

248 Tanaka, T., Narazaki, M. & Kishimoto, T. Anti-interleukin-6 receptor antibody, tocilizumab, for the treatment of autoimmune diseases. *FEBS Lett* **585**, 3699-3709, doi:10.1016/j.febslet.2011.03.023 (2011).

249 Li, X. *et al.* Ruxolitinib induces apoptosis of human colorectal cancer cells by downregulating the JAK1/2-STAT1-Mcl-1 axis. *Oncol Lett* **21**, 352, doi:10.3892/ol.2021.12613 (2021).

250 Ajayi, S. *et al.* Ruxolitinib. *Recent Results Cancer Res* **212**, 119-132, doi:10.1007/978-3-319-91439-8_6 (2018).

251 Quintás-Cardama, A. & Verstovsek, S. Molecular pathways: Jak/STAT pathway: mutations, inhibitors, and resistance. *Clin Cancer Res* **19**, 1933-1940, doi:10.1158/1078-0432.Ccr-12-0284 (2013).

252 Ham, I. H. *et al.* Targeting interleukin-6 as a strategy to overcome stroma-induced resistance to chemotherapy in gastric cancer. *Mol Cancer* **18**, 68, doi:10.1186/s12943-019-0972-8 (2019).

253 Matsuoka, Y. *et al.* IL-6 controls resistance to radiation by suppressing oxidative stress via the Nrf2-antioxidant pathway in oral squamous cell carcinoma. *Br J Cancer* **115**, 1234-1244, doi:10.1038/bjc.2016.327 (2016).

254 Yamamoto, K. & Rose-John, S. Therapeutic blockade of interleukin-6 in chronic inflammatory disease. *Clin Pharmacol Ther* **91**, 574-576, doi:10.1038/clpt.2012.11 (2012).

255 Guan, M., Zhou, Y. P., Sun, J. L. & Chen, S. C. Adverse events of monoclonal antibodies used for cancer therapy. *Biomed Res Int* **2015**, 428169, doi:10.1155/2015/428169 (2015).

256 Stover, D. G. *et al.* Phase II study of ruxolitinib, a selective JAK1/2 inhibitor, in patients with metastatic triple-negative breast cancer. *NPJ Breast Cancer* **4**, 10, doi:10.1038/s41523-018-0060-z (2018).

257 Fogelman, D. *et al.* Randomized, double-blind, phase two study of ruxolitinib plus regorafenib in patients with relapsed/refractory metastatic colorectal cancer. *Cancer Med* **7**, 5382-5393, doi:10.1002/cam4.1703 (2018).

258 Kawazoe, A. *et al.* Phase 1 study of napabucasin, a cancer stemness inhibitor, in patients with advanced solid tumors. *Cancer Chemother Pharmacol* **85**, 855-862, doi:10.1007/s00280-020-04059-3 (2020).

259 Zhang, Y. *et al.* Suppression of prostate cancer progression by cancer cell stemness inhibitor napabucasin. *Cancer Med* **5**, 1251-1258, doi:10.1002/cam4.675 (2016).

260 Froeling, F. E. M. *et al.* Bioactivation of Napabucasin Triggers Reactive Oxygen Species-Mediated Cancer Cell Death. *Clin Cancer Res* **25**, 7162-7174, doi:10.1158/1078-0432.Ccr-19-0302 (2019).

261 Myers, D. R., Zikherman, J. & Roose, J. P. Tonic Signals: Why Do Lymphocytes Bother? *Trends Immunol* **38**, 844-857, doi:10.1016/j.it.2017.06.010 (2017).

262 Zhu, G. *et al.* TRAF6-Mediated Inflammatory Cytokines Secretion in LPS-induced Colorectal Cancer Cells Is Regulated by miR-140. *Cancer Genomics Proteomics* **17**, 23-33, doi:10.21873/cgp.20164 (2020).

263 Taghian, A. G. & Suit, H. D. Animal systems for translational research in radiation oncology. *Acta Oncol* **38**, 829-838 (1999).

264 Ellisen, L. W. *et al.* TAN-1, the human homolog of the Drosophila notch gene, is broken by chromosomal translocations in T lymphoblastic neoplasms. *Cell* **66**, 649-661, doi:10.1016/0092-8674(91)90111-b (1991).

265 Weng, A. P. *et al.* Activating mutations of NOTCH1 in human T cell acute lymphoblastic leukemia. *Science* **306**, 269-271, doi:10.1126/science.1102160 (2004).

266 Parmigiani, E., Taylor, V. & Giachino, C. Oncogenic and Tumor-Suppressive Functions of NOTCH Signaling in Glioma. *Cells* **9**, doi:10.3390/cells9102304 (2020).

267 Nowell, C. S. & Radtke, F. Notch as a tumour suppressor. *Nat Rev Cancer* **17**, 145-159, doi:10.1038/nrc.2016.145 (2017).

268 Lefort, K. *et al.* Notch1 is a p53 target gene involved in human keratinocyte tumor suppression through negative regulation of ROCK1/2 and MRCKalpha kinases. *Genes Dev* **21**, 562-577, doi:10.1101/gad.1484707 (2007).

269 Nicolas, M. *et al.* Notch1 functions as a tumor suppressor in mouse skin. *Nat Genet* **33**, 416-421, doi:10.1038/ng1099 (2003).

270 Sander, G. R. & Powell, B. C. Expression of notch receptors and ligands in the adult gut. *J Histochem Cytochem* **52**, 509-516, doi:10.1177/002215540405200409 (2004).

271 Radtke, F., Clevers, H. & Riccio, O. From gut homeostasis to cancer. *Curr Mol Med* **6**, 275-289, doi:10.2174/156652406776894527 (2006).

272 Katoh, M. & Katoh, M. Notch signaling in gastrointestinal tract (review). *Int J Oncol* **30**, 247-251 (2007).

273 Strosberg, J. R. *et al.* A phase II study of RO4929097 in metastatic colorectal cancer. *Eur J Cancer* **48**, 997-1003, doi:10.1016/j.ejca.2012.02.056 (2012).

274 Reedijk, M. *et al.* Activation of Notch signaling in human colon adenocarcinoma. *Int J Oncol* **33**, 1223-1229, doi:10.3892/ijo_00000112 (2008).

275 Lehal, R. *et al.* Pharmacological disruption of the Notch transcription factor complex. *Proc Natl Acad Sci U S A* **117**, 16292-16301, doi:10.1073/pnas.1922606117 (2020).

276 Deorukhkar, A. & Krishnan, S. Targeting inflammatory pathways for tumor radiosensitization. *Biochem Pharmacol* **80**, 1904-1914, doi:10.1016/j.bcp.2010.06.039 (2010).

277 Wang, Z. *et al.* Notch signaling drives stemness and tumorigenicity of esophageal adenocarcinoma. *Cancer Res* **74**, 6364-6374, doi:10.1158/0008-5472.Can-14-2051 (2014).

278 Golde, T. E., Koo, E. H., Felsenstein, K. M., Osborne, B. A. & Miele, L. γ-Secretase inhibitors and modulators. *Biochim Biophys Acta* **1828**, 2898-2907, doi:10.1016/j.bbamem.2013.06.005 (2013).

279 Wang, R., Tang, P., Wang, P., Boissy, R. E. & Zheng, H. Regulation of tyrosinase trafficking and processing by presenilins: partial loss of function by familial Alzheimer's disease mutation. *Proc Natl Acad Sci U S A* **103**, 353-358, doi:10.1073/pnas.0509822102 (2006).

280 Shoji, M. *et al.* Production of the Alzheimer amyloid beta protein by normal proteolytic processing. *Science* **258**, 126-129, doi:10.1126/science.1439760 (1992).

281 Haass, C. *et al.* Amyloid beta-peptide is produced by cultured cells during normal metabolism. *Nature* **359**, 322-325, doi:10.1038/359322a0 (1992).

282 Rizzo, P. *et al.* Rational targeting of Notch signaling in cancer. *Oncogene* **27**, 5124-5131, doi:10.1038/onc.2008.226 (2008).

283 Harbuzariu, A., Oprea-Ilies, G. M. & Gonzalez-Perez, R. R. The Role of Notch Signaling and Leptin-Notch Crosstalk in Pancreatic Cancer. *Medicines (Basel)* **5**, doi:10.3390/medicines5030068 (2018).

284 Meng, R. D. *et al.* gamma-Secretase inhibitors abrogate oxaliplatin-induced activation of the Notch-1 signaling pathway in colon cancer cells resulting in enhanced chemosensitivity. *Cancer Res* **69**, 573-582, doi:10.1158/0008-5472.Can-08-2088 (2009).

285 Li, D. D. *et al.* A novel inhibitor of ADAM17 sensitizes colorectal cancer cells to 5-Fluorouracil by reversing Notch and epithelial-mesenchymal transition in vitro and in vivo. *Cell Prolif* **51**, e12480, doi:10.1111/cpr.12480 (2018).

286 Moellering, R. E. *et al.* Direct inhibition of the NOTCH transcription factor complex. *Nature* **462**, 182-188, doi:10.1038/nature08543 (2009).

287 McCaw, T. R. *et al.* Gamma Secretase Inhibitors in Cancer: A Current Perspective on Clinical Performance. *Oncologist* **26**, e608-e621 (2021).

288 Groth, C. & Fortini, M. E. Therapeutic approaches to modulating Notch signaling: current challenges and future prospects. *Semin Cell Dev Biol* **23**, 465-472 (2012).

289 Liu, H. *et al.* miR-139-5p sensitizes colorectal cancer cells to 5-fluorouracil by targeting NOTCH-1. *Pathol Res Pract* **212**, 643-649, doi:10.1016/j.prp.2016.04.011 (2016).

290 Jin, Y. *et al.* Overcoming stemness and chemoresistance in colorectal cancer through miR-195-5p-modulated inhibition of notch signaling. *Int J Biol Macromol* **117**, 445-453, doi:10.1016/j.ijbiomac.2018.05.151 (2018).

291 Mirone, G., Perna, S., Shukla, A. & Marfe, G. Involvement of Notch-1 in Resistance to Regorafenib in Colon Cancer Cells. *J Cell Physiol* **231**, 1097-1105, doi:10.1002/jcp.25206 (2016).

292 Vaish, V., Kim, J. & Shim, M. Jagged-2 (JAG2) enhances tumorigenicity and chemoresistance of colorectal cancer cells. *Oncotarget* **8**, 53262-53275, doi:10.18632/oncotarget.18391 (2017).

293 Sun, L. *et al.* HES1 Promotes Colorectal Cancer Cell Resistance To 5-Fu by Inducing Of EMT and ABC Transporter Proteins. *J Cancer* **8**, 2802-2808, doi:10.7150/jca.19142 (2017).

294 Chu, D. *et al.* High level of Notch1 protein is associated with poor overall survival in colorectal cancer. *Ann Surg Oncol* **17**, 1337-1342, doi:10.1245/s10434-009-0893-7 (2010).

295 Kang, W. *et al.* NOTCH3, a crucial target of miR-491-5p/miR-875-5p, promotes gastric carcinogenesis by upregulating PHLDB2 expression and activating Akt pathway. *Oncogene* **40**, 1578-1594, doi:10.1038/s41388-020-01579-3 (2021).

296 Tyagi, A., Sharma, A. K. & Damodaran, C. A Review on Notch Signaling and Colorectal Cancer. *Cells* **9**, doi:10.3390/cells9061549 (2020).

297 Wu, X. *et al.* Prognostic values of four Notch receptor mRNA expression in gastric cancer. *Sci Rep* **6**, 28044, doi:10.1038/srep28044 (2016).

298 Candy, P. A. *et al.* Notch-induced transcription factors are predictive of survival and 5-fluorouracil response in colorectal cancer patients. *Br J Cancer* **109**, 1023-1030, doi:10.1038/bjc.2013.431 (2013).

299 https://clinicaltrials.gov/ct2/show/NCT02753127

300 Hsu, K. W. *et al.* Activation of the Notch1/STAT3/Twist signaling axis promotes gastric cancer progression. *Carcinogenesis* **33**, 1459-1467, doi:10.1093/carcin/bgs165 (2012).

301 Weng, M. T. *et al.* Hes1 Increases the Invasion Ability of Colorectal Cancer Cells via the STAT3-MMP14 Pathway. *PLoS One* **10**, e0144322, doi:10.1371/journal.pone.0144322 (2015).

302 Yang, Z. *et al.* Acquisition of resistance to trastuzumab in gastric cancer cells is associated with activation of IL-6/STAT3/Jagged-1/Notch positive feedback loop. *Oncotarget* **6**, 5072-5087, doi:10.18632/oncotarget.3241 (2015).

303 Jackstadt, R. *et al.* Epithelial NOTCH Signaling Rewires the Tumor Microenvironment of Colorectal Cancer to Drive Poor-Prognosis Subtypes and Metastasis. *Cancer Cell* **36**, 319-336 e317, doi:10.1016/j.ccell.2019.08.003 (2019).

304 Meurette, O. & Mehlen, P. Notch Signaling in the Tumor Microenvironment. *Cancer Cell* **34**, 536-548, doi:10.1016/j.ccell.2018.07.009 (2018).

305 Kim, B. *et al.* IL-6 and IL-8, secreted by myofibroblasts in the tumor microenvironment, activate HES1 to expand the cancer stem cell population in early colorectal tumor. *Mol Carcinog* **60**, 188-200, doi:10.1002/mc.23283 (2021).

8. Appendix

8.1 Abbreviations

5-FU	5-Fluorouracil
ADAM17	A disintegrin and metalloprotease 17
AJCC	American Joint Committee on Cancer
AKT	RAC serin/threonine-protein kinase
ANOVA	Analysis of variance
APC	Adenomatous polyposis coli
APFR	Acute phase response factor
approx.	approximately
APS	Ammoniumpersulfate
ATCC	American Type Culture Collection
BCA	Bicinchonic acid assay
BCL-2	BCL2 Apoptosis Regulator
BCL6	B-Cell Lymphoma 6 Protein Transcript
BCL-XL	BCL2 Like 1
bp	Base pairs
BSA	Bovine serum albumin
CAFS	Cancer-associated fibroblasts
CCD	Coiled-coil domain
CCSC	Colorectal cancer stem cell
cDNA	Complementary deoxyribonucleic acid
CFA	Colony formation assay
CIMP	CpG island methylation phenotype
CIN	Chromosomal instability
CLC	Cardiotrophin like cytokine
CNTF	Ciliary neutotrophic factor
CoA	Coactivation complex
CoR	Corepressor complex
COX2	Cytochromee C Oxidase II
CRC	Colorectal cancer
CRT	Chemoradiotherapy
CSF-1	Colony stimulating factor 1
Ct	Cycle threshold
CT-1	Cardiotrophin
CTB	Cell titer blue
CXCL12	C-X-C Motif Chemokine Ligand 12
DAPT	*N*-[*N*-(3,5-difluorophenacetyl)-L-alanyl] -(*S*)-phenylglycine *t*-butyl ester
DBD	DNA-binding domain
ddH_2O	Double-distilled water
DE	Differentially expressed
DFS	Disease-free survival
DLL 1,3,4	Delta-like 1,3,4
DLR	Dual luciferase assay
DMSO	Dimethyl sulphoxide
DNA	Deoxyribonucleic acid
DNase	Deoxyribonuclease
dNTP	Deoxynucleotide triphosphates
DPYD	Dihydropyrimidine dehydrogenase
DTT	Dithiothreitol
DUOX2	Dual oxidase 2
EDTA	Ehylenediaminetetraacetic acid
EGF	Epidermal growth factor
EGTA	Ethylene glycol-bis (β-amimoethyl ether)-N,N,N’,N’-tetraacetic acid

ELF3	E74-like ETS transcription factor 3
ELISA	Enzyme-linked Immunosorbent Assay
EMSA	Electrophoretic mobility shift assay
EMT	Epithelial-to-mesenchymal transition
FAP	Familial adenomatous polyposis
FBS	Fetal bovine serum
FDA	Food and Drug Administration
FDR	False discovery rate
G-5	Glucose 5%
GAS	Interferon-γ activated site/sequence
GEO	NCBI Gene Expression Omnibus
GFP	Green fluorescent protein
GO	Gene Ontology
GP130	Glycoprotein!30
GSC	Glioblastom stem-like
GSI	γ-secretase inhibitors
HCL	Hydrogen chloride
HEPES	4-(2-hydroxyethyl)-1-piperazineethanesulphonic acid
HES1	Hairy enhancer-of split 1
HIF	Hypoxia-Inducible Factor
HIF1A	Hypoxia-inducible factor 1
HK1	Hwxokinase 1
HLA	Human Leukocyte Antigen
HPRT1	Hypoxanthine-guanine phosphoribosyltransferase
HRP	Horseradish peroxidase
Hy-IL-6	Hyper-IL-6
IBD	Inflammatory bowel disease
IFN	Interferon
IL	Interleukin
IL-6R	IL-6 receptor
IκB	inhibitor of NFκB
JAG1, 2	Serrate-like
JAK1,2	Janus kinase1,2
KCL	Potassium chloride
KD	knockdown
KH_2PO_4	Potassium dihydrogen phosphate trihydrate
KRAS	Kirsten Rat Sarcoma Viral Oncogene Homolog
LIF	Leukemia inhibitory factor
Linker	Linker domain
MAPK	Mitogen-activated protein kinases
MDSC	Myeloid derived suppressor cell
MgCl	Magnesium chloride
MM	Multiple melanoma
MMP-1,2	Matrix Metallopeptidase 1,2
MMP14	Matrix Metallopeptidase 14
MMR	Mismatch repair
mRNA	Messenger ribonuclein acid
MSI	Microsatellite instability
MSS	Microsatellite stable
MUC1	Mucin 1
n.a.	not applicable
Na_3VO_4	Sodium orthovanadate
NaCl	Sodium chloride
NAMPT	Nicotinamide Phosphoribosyltransferase
NaOH	Sodium Hydroxide
Napa	Napabucasin

NEC	Extracellular subunit
NES	Normalized Enrichment Score
NF-κB	Nuclear factor-κB
NICD	NOTCH intracellular domain
NIG	NGS-Integrative Genomics Core Unit
NMRI	Naval Medical Research Institute
NP-40	Nonident P-40
NQO1	NAD(P)H Quinone Dehydrogenase 1
NTD	Amino-terminal domain
NTM	Transmembrane subunit
ODA	Opposite Direction Analysis
OS	Overall survival
OS	Overall survival
OSCC	Oral squamous cell carcinoma
OSM	Oncostatin
p35	Tumor protein p35
P53	Tumor protein 53
PBS	Phosphate-buffered saline
PCA	Principle Component Analysis
pCR	Pathological complete response
PCR	Polymerase chain reaction
PDGF	Platelet derived growth factor
PDX	Patient-derived xenograft
PE	Plating efficiency
PEN2	Presenilin enhancer 2
PFS	Progression free survival
PIAS	Protein inhibitors of activated STATs
PLB	Passive lysis buffer
p-STAT	Phosphorylated STAT protein
pSTAT3	phosphorylated STAT3
PVDF	Polyvinylidene fluoride
qPCR	Quantitative polymerase chain reaction
RBPJ	Recombination Signal Binding Protein for Immunoglobulin k J-region
RIPA	Radioimmunoprecipitation assay
RNA	Ribonuclein acid
RNAi	RNA-Interference
RNase	Ribonuclease
RNA-Seq	RNA Sequencing
ROS	Reactive oxygen species
RPMI	Roswell Park Memorial Institute medium
RT	Radiotherapy
Ruxo	Ruxolitinib
S100A9	S100 calcium-binding protein A9
SCNA	Somatic copy number alterations
SDS	Sodium dodecyl sulphate
SDS-PAGE	Sodium dodecyl sulphate polyacrylamide gel electrophoresis
SERPINB3	Serpin Family B Member 3
SERPINB4	Serpin Family B Member 4
SF	Surviving fraction
SH2	Src-homology
sIL-6R	Soluble IL-6 receptor
SMAD4	SMAD family member 4
SOCS	Suppressor of cytokine signalling
STAT	Signal transducer and activator of transcription
STR	Short tandem repeat
TAD	Transactivation domain

T-All	T cell acute lymphoblastic leukemia
TAM	Tumor-associated macrophages
TBS(T)	Tris buffered saline (supplemented with Tween-20)
TEMED	Tetramethylethylenediamine
TF	Transcription factor
TGFβ	Transforming growth factor-beta
TME	Tumor microenvironment
TNE	Tumor-node-metastatic
Toci	Tocilizumab
TRIB2	Tribbles pseudokinases 2
TS	Thymidylate synthase
TYK2	Non-receptor tyrosine-protein kinase 2
UICC	Union Internationale Conte le Cancer
U-STAT3	unphosphorylated STAT3
WT	Wild-type

Units

%	Percent
°C	Degree celsius
Da	Dalton
d	Days
g	Gram
h	Hour
l	Liter
m	Meter
M	Mol/l
min	Minute
rpm	Rounds per minute
RT	Room temperature
sec	Second
x g	Times gravity

Amino Acid	**Three letter code**	**One letter code**
Alanine	A	Ala
Arginine	R	Arg
Asparagine	N	Asn
Aspartic acid	D	Asp
Cysteine	C	Cys
Glutamic acid	E	Glu
Glutamine	Q	Gln
Glycine	G	Gly
Histidine	H	His
Isoleucine	I	Ile
Leucine	L	Leu
Lysine	K	Lys
Methionine	M	Met
Phenylalanine	F	Phe
Proline	P	Pro
Serine	S	Ser
Threonine	T	Thr
Tryptophan	W	Trp
Tyrosine	Y	Tyr
Valine	V	Val
Alanine	A	Ala

8.2 Figures

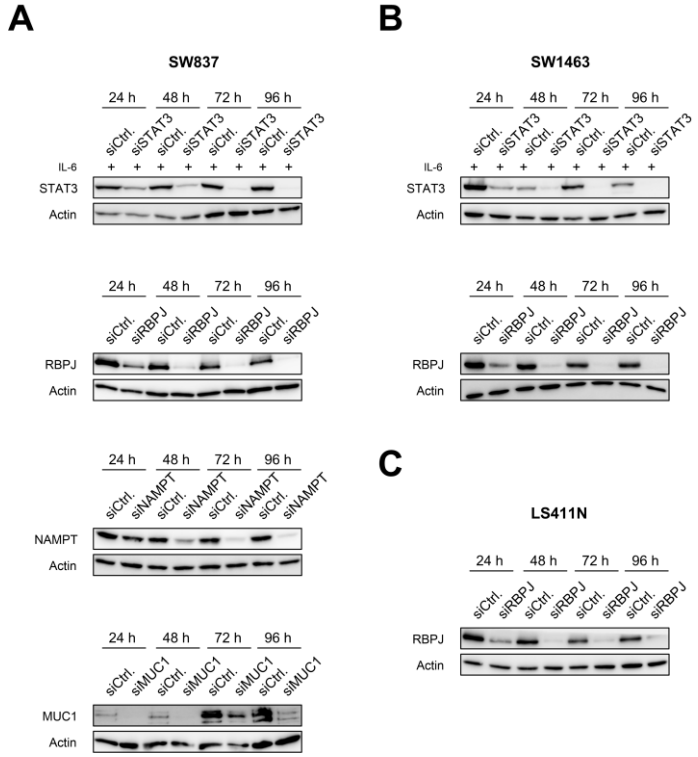

Figure 8. 1 siRNA time series to establish the optimal knockdown time point.
A| SW837 cells were treated with RNAi targeting *STAT3*, *RBPJ*, *NAMPT* and *MUC1* or corresponding control siRNA (siCtrl.) for 24,48,72 and 96 h. expression of the **B|** SW1463 cells were treated with RNAi targeting *STAT3* and *RBPJ* or corresponding control siRNA (siCtrl.) for 24, 48 ,72 and 96 h, respectively. **C|** SW1463 cells were treated with RNAi targeting *RBPJ* or corresponding control siRNA (siCtrl.) for 24, 48 ,72 and 96 h. **A-C|** The expression of the respective proteins was analyzed by immunoblotting using the indicated antibodies. Note that for immunoblot analysis after RNAi against *STAT3* the cells are stimulated with rhIL-6 bevor lysis (**Tab. 35**).

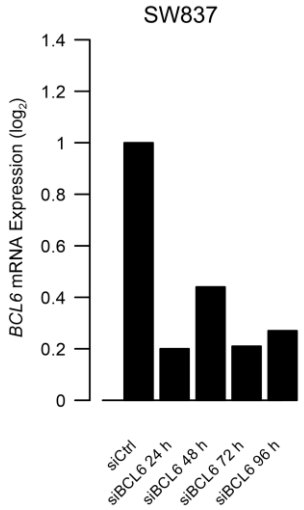

Figure 8. 2 siRNA time series to establish the optimal knockdown time point for BCL6.
SW837 cells were treated with RNAi targeting *BCL6* or corresponding control siRNA (siCtrl.) for 24,48,72 and 96 h, respectively. The mRNA expression of BCL6 was analyzed by qRT-PCR using BCL6 specific primes. The BCL6 expression in the control approach was set to 1. The optimal knockdown is defined as reduction of the expression by 80%, here at a value of at least 0.20.

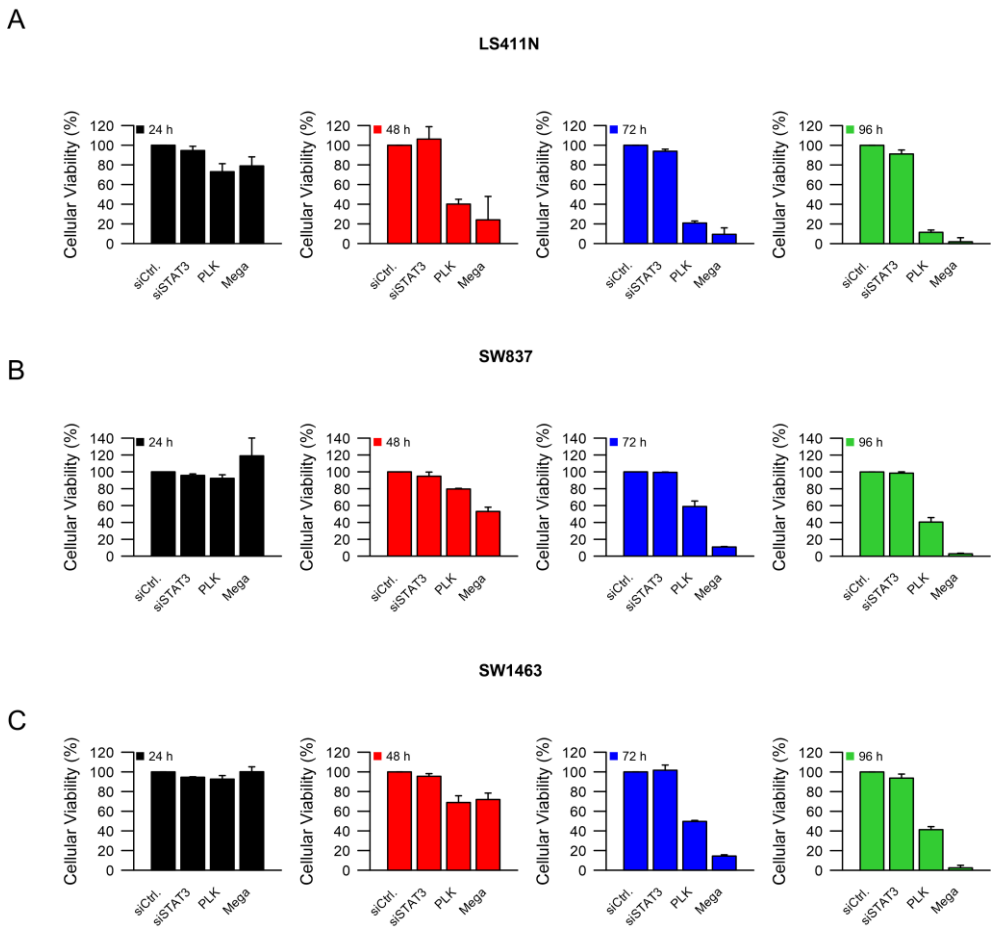

Figure 8. 3 Influence of RNAi induced STAT3 depletion on the cellular viability of CRC cells.
A-C| To test if the depletion of STAT3 using RNAi reduce cellular viability LS411N 8(A), SW837 (B) and SW1463 (C) cells were treated with RNAi targeting STAT3, the corresponding negative control (siCtrl.) or the assay intern controls (PLK and Mega) for 24,48,72 and 96 h, respectively. The cellular viability was measure using a cell titer blue assay and the data are presented as mean ± s.e.m. from at least n=3 independent biological replicates.

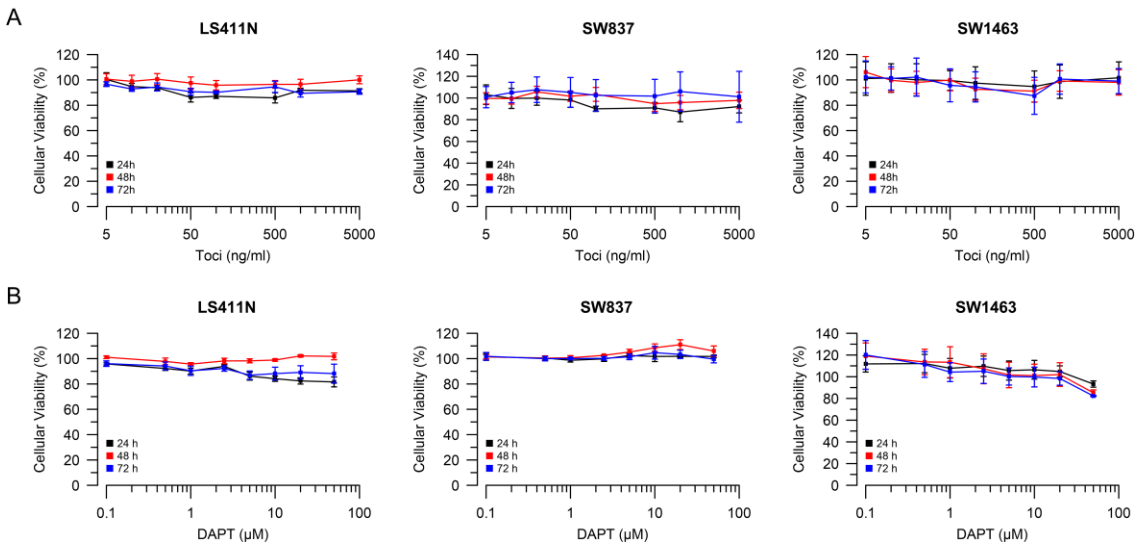

Figure 8. 4 Influence of Tocilizumab and DAPT treatment on the cellular viability of CRC cells. A| and **B|** LS411N, SW837 and SW1463 cells were treated with different Tocilizumab (A) or DAPT (B) concentrations for 24,48 and 72 h, respectively. The cellular viability was measure using a cell titer blue assay and the data are presented as mean ± s.e.m. from at least n=3 independent biological replicates.

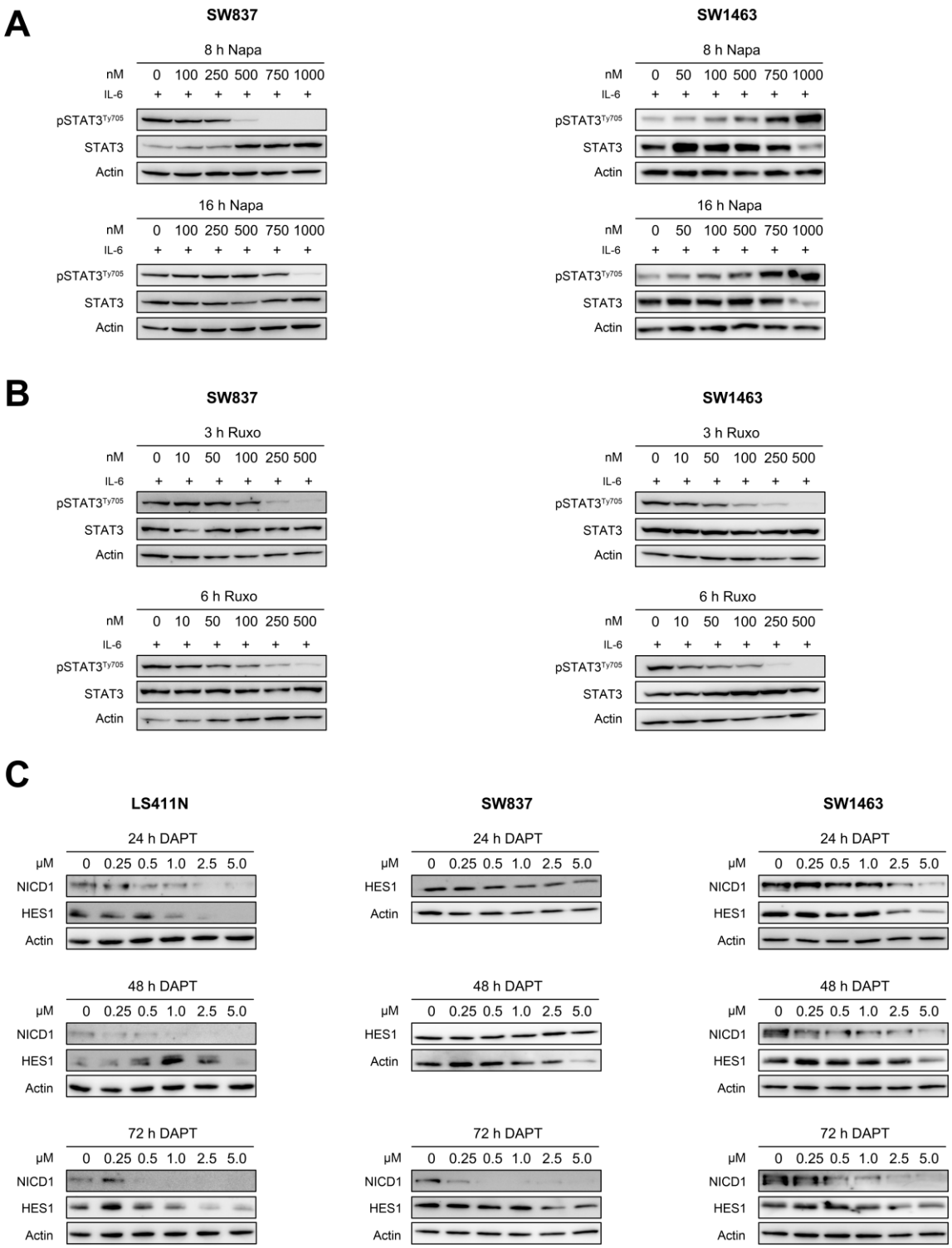

Figure 8. 5 Treatment of CRC cells with Napabucasin, Ruxolitinib and DAPT.
A| pSTAT3^{Y705} expression levels were measured using Western Blot after treating the SW837 and SW1463 cells for 8 h or 16 h with Napa concentrations ranging from 0 to 1000 nM. **B|** To further evaluate the most effective Ruxo concentrations SW837 and SW1463 cells were incubate for 3 h or 6 h with indicated Ruxo concentrations or were left untreated. Proteins were isolated analysed regarding pSTAT3^{Y705} and STAT3 expression. **C|** To test if treatment with DAPT reduce NICD protein levels LS411N, SW837 and SW1463 cells, they were incubated with different DAPT concentrations ranging from 0 to 5000 nM for 24,48 and 72 h.

8.3 List of Tables

8.4 List of Figures

Introduction:

Methods:

Results:

Discussion:

Conclusion:

Appendix:

8.4 Curriculum vitae